THEORETICAL AND EXPERIMENTAL PROCEDURES FOR THE PREDICTION OF THE DYNAMIC BEHAVIOR OF MARINE RISERS

by

NICHOLAS MARINOS PATRIKALAKIS

Diploma in Naval Architecture

National Technical University of Athens

July 1977

Submitted in partial fulfillment
of the requirements for the degree of

DOCTOR OF PHILOSOPHY

IN OCEAN ENGINEERING

at the

MASSACHUSETTS INSTITUTE OF TECHNOLOGY

June 1983

Signature of Author
Department of Ocean Engineering
June 1983

Certified by
Chryssostomos Chryssostomidis
Thesis Supervisor

Accepted by . . . . . .
A. Douglas Carmichael, Chairman
Committee on Graduate Students

THEORETICAL AND EXPERIMENTAL PROCEDURES FOR THE PREDICTION OF THE DYNAMIC BEHAVIOR OF MARINE RISERS

by

NICHOLAS MARINOS PATRIKALAKIS

Submitted to the Department of Ocean Engineering in February 1983 in partial fulfillment of the requirements for the degree of Doctor of Philosophy in Ocean Engineering.

ABSTRACT

The objective of this thesis is the evaluation of our theoretical ability to predict the global dynamic behavior of long flexible cylindrical structures, such as single tube marine risers, using available rigid cylinder experimental results. To achieve this, experiments using a flexible cylindrical model were performed and the experimental results are compared against our theoretical predictions. The scaling procedure governing our experiment is presented. All the non-dimensional parameters of the model were carefully selected to allow us to achieve our main objective under conditions of pronounced violation of the assumptions necessary for the theoretical predictions. In addition, the structural model of the riser necessary for the prediction of the global dynamic behavior of the riser is derived and discussed in detail. The comparison between theory and experiment showed that our theoretical procedure based on rigid cylinder results permitted us to predict the important features of the response of our flexible model with confidence and provided us with estimates of the magnitude of the response. Suggestions for future research geared to provide information for the design of flexible marine cylindrical structures in actual operating conditions are also included.

Thesis Supervisor: Chryssostomos Chryssostomidis, Ph.D.

Title: Professor of Naval Architecture

ACKNOWLEDGEMENTS

I wish to express my deep gratitude to my advisor Professor C. Chryssostomidis for his encouragement at difficult moments, his continuous help, his moderation and for the stimulus of the countless debates we had from which this thesis was shaped. To him I owe more, both intellectually and humanly, than I can ever repay.

I am also indebted to the members of my thesis committee: Professors T. F. Ogilvie, J. G. deOliveira, M. S. Triantafyllou, and R. Van Houten, for their active participation in the execution of this work.

I wish to express my sincere thanks to Professor T. A. Loukakis, who provided expert advice in designing the supporting components that made our experiments possible; and to Professor M. M. Bernitsas who, at the beginning of this work, assisted me in identifying the important literature in this field and provided me with useful suggestions on how to initiate my work; to Mr. P. Erb, Dr. O. Oakley and Mr. C. White, who helped me in selecting the important parameters of our experiments. I wish also to acknowledge the assistance of Mr. C. Grekoussis, Mr. N. Vacassis, Mr. G. Gregoropoulos, Mr. G.

N. Nikolaou, and Mr. E. Vrakas for helping me in the performance of our experiments and the data processing.

I express my deep appreciation to the Department of Ocean Engineering for financial assistance; to the MIT Sea Grant Program, Conoco, Inc., and Gulf Oil Company for funding our experimental work; to the National Technical University of Athens and to Professor T. A. Loukakis personally for letting me use the Laboratory for Hydrodynamics.

I wish to express my sincere thanks to Ms. M. Staruch for her patience in deciphering my manuscripts and expertly editing this work, and to Ms. A. Markowitz and Ms. M. Morey for assisting in editing this thesis.

I am grateful to my wife, Sandy, for her patience, her loving care and encouragement. This dissertation is dedicated to my parents, Marinos and Kleoniki, with gratitude for their love.

TABLE OF CONTENTS

LIST OF TABLES

LIST OF FIGURES

FIGURES FOR EXPERIMENTS 14, 17, 20 AND 23

For experiments 14, 17 and 23, there are two Figures, one for Plane A and one for Plane B. For Experiment 20, there is one Figure of this class for Plane A and three for Plane B.

FIGURE NS: Plots of the Measured Response Strain in Plane A as a Function of the Measured Response Strain in Plane B at Elevation Z and a Certain Time Span in Seconds.

For Each of the Above Experiments, there are two Figures of this class.

FIGURE ND: Plots of the Response Displacement in Plane A as a Function of the Response Displacement in Plane B for Experiment N. The Displacements are calculated from the Experimental Data and are measured in Diameters.

For each of the above experiments there are two figures of this class.

The sequence of presentation of the above Figures follows the experiment order 14, 17, 20 and 23. The sequence shown above is kept for each experiment separately.

FIGURES FOR EXPERIMENTS 2, 1, 3, 4, 9, 10, 8 AND 7

For each of the above experiments there are two Figures: one of the NA class and one of the NB class. The above sequence of Experiments is followed in the presentation.

FIGURES FOR EXPERIMENTS 52, 59, 71, 80, 89, 51, 60, 70, 81, 88

For each of the above experiments, there are two Figures: one of the NB class and one of the NA class. The above sequence of Experiments is followed in the presentation.

The results for Experiment N start on page

Chapter I

INTRODUCTION AND OUTLINE

The problem addressed in this thesis is the evaluation of our theoretical ability to predict the global dynamic behavior of long flexible and tensioned cylindrical structures using available rigid cylinder experimental results. We restricted this investigation to single tube risers because their simple geometry offers us a better chance to understand the dynamic behavior of a flexible cylindrical structure interacting with a real fluid. A schematic representation of an exploration single tube riser and its supporting system is shown in Figure 1, taken from Bernitsas (1979). A brief description of the physical system is included in Appendix A to familiarize the reader with the terminology employed in this work.

The thesis is organized as follows:

Chapter II provides a consistent set of governing equations that can be a starting point for a rational study of the global dynamic behavior of the riser modelled as a thin rod under tension. The equations derived describe coupled flexural, extensional and torsional dynamic oscillations of a thin rod in three dimensions.

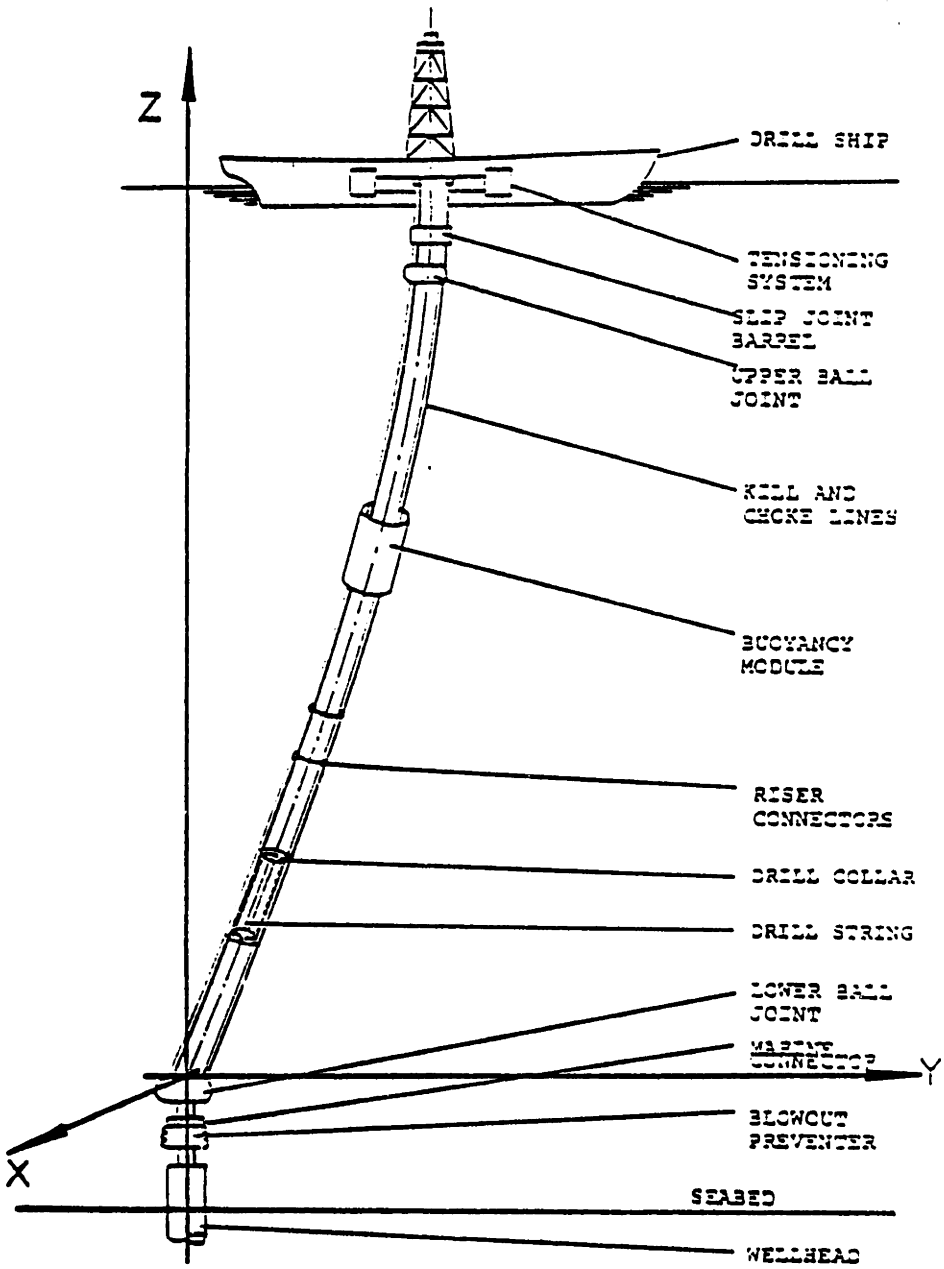

FIGURE 1: A Typical Offshore Drilling System, Bernitsas (1979).

Linear constitutive relations between stresses and strains are assumed. The relations between strains and displacements preserve their non-linearity within the fundamental assumptions of Rayleigh beam theory. The general governing equations derived herein describe the global dynamic behavior of other long flexible cylindrical structures such as conductors, pipelines, tethers, and cables.

A systematic analysis of the general governing equations is the subject of Chapter III. Order of magnitude arguments and the disparity of the time scales of the various modes of a riser's motion are used to elucidate the role of coupling and non-linear terms. The leading order equations for each mode of the riser's motion are derived systematically and some properties of the equations describing flexural oscillations are discussed. The derivation is based on small transverse motions compared to the length and the presence of a slip joint at the upper end of the riser.

Chapter IV describes a theoretical procedure for the prediction of the dynamic response of a marine riser based on available rigid cylinder experimental results. The assumptions necessary for our theoretical procedure are identified and discussed in detail. This Chapter includes a brief review of the main rigid cylinder experimental results from which a model for the local force acting on a flexible cylinder has been derived for a

number of idealized excitation conditions. This review includes an analysis of the usefulness and the limitations of such experiments. Finally, four idealized excitation conditions are employed to illustrate how to use rigid cylinder experimental results to estimate the static and dynamic response of marine risers. These examples also help us identify areas in which the limitations of rigid cylinder experimental results are likely to be magnified.

Chapter V describes a novel experimental procedure which is an attempt to provide a quantitative estimate of the limitations of the theoretical procedure developed in Chapter IV on the global dynamic behavior of long flexible cylinders. This is the principal objective of this work. The model employed in our experiments did not correspond to a specific prototype. However, all its non-dimensional parameters were carefully selected to allow us to achieve our principal objective under conditions of pronounced violation of the assumptions necessary for our theoretical predictions. Chapter V includes the scaling procedure; a description of the model; presentation of experimental results and quantitative comparisons of experimental and theoretical predictions.

Chapter VI summarizes the findings of this work on the basis of which recommendations for future research are made.

Chapter II

THE EQUATIONS OF MOTION OF THE MARINE RISER

II.1 THE MATHEMATICAL MODEL

A mathematical model describing the global behavior of a marine exploration riser was developed by Bernitsas (1979). Based on this study a new model for deep sea marine exploration risers is derived. Whenever possible the same notation used by Bernitsas (1979) has been adopted. The assumptions made in our model, many of which are the same as in Bernitsas (1979), (1980), (1982), are listed below:

1. The riser is modelled as a thin rod rather than as a shell. This is an acceptable assumption because we are only interested in the global behavior of our system and because of the riser's small diameter to length ratio.

2. The material is assumed homogeneous and isotropic which is a good model for steel structures. Small strains permit the use of linear constitutive relations between stresses and strains. Note that strains will remain small even for flexural deformations equal to a few riser diameters because of the large length to diameter ratio of a typical riser.

3. The drill string is neglected, because this leads to small underestimation of the mass and stiffness of the riser.

4. The contribution of the kill and choke lines to the stiffness of the riser is neglected because it is small. This leads to a rotationally uniform structure. Further, any concentrated forces from these lines on the riser through the connectors and flanges are neglected, because their global influence is small.

5. The contribution of the buoyancy modules to the flexural, extensional and torsional rigidity of the riser is neglected. This is justified because the Young's modulus of the buoyancy material is smaller by several orders of magnitude than that of steel.

6. Forces exerted on the riser from the circulating mud as a reaction to centripetal, Coriolis and frictional forces exerted on the mud are neglected because they are small.

7. Shearing deformations are neglected. This is justified because they are of order $(Dn/L)^2$ compared to rotations of riser cross sections after bending, where D, L are the diameter and length of the riser and n the order of the excited flexural mode. For typical deep sea risers

D/L <<1 and n is small (i.e., low frequencies are excited). This assumption implies that plane cross sections remain plane after bending and normal to the neutral axis. (Rayleigh beam theory, see Crandall et al, (1968)).

8. Thermal effects are neglected.

The characteristic features of the model, derived on the basis of the assumptions listed above, are:

a. It models coupled flexural, extensional and torsional dynamic oscillations of thin rods in three dimensions in a consistent manner.

b. The relations between strains and displacements preserve their full non-linearity within the fundamental assumptions of Rayleigh beam theory.

c. Our model is expected to treat accurately:

1. Large flexural deflections of the centerline (of the order of a few riser diameters).

2. Large vertical displacements of any cross section (as long as the centerline extensional strain remains small).

3. Small structural torsion angles (small enough to permit the use of a linear constitutive relation between the torsional restoring moment and the rate of change of the torsion angle with respect to the arc length of the centerline).

4. The impact of the hydrostatic and mud static pressures on the restoring force is properly taken into account (Bernitsas, (1979)).

The purpose of derivation of such a model is the desire to acquire a consistent set of governing equations that can be a reliable starting point for a rational study of the global dynamic behavior of risers.

II.2 BRIEF DEVELOPMENT OF THE EQUATIONS OF MOTION

II.2.1 Analysis of Deformation-Constitutive Relations

Detailed accounts of the equations of equilibrium of thin rods can be found in Love (1944) and Landau and Lifshitz (1959) for the cases of large static deformations. In addition, an extensive analysis of the nature of the strain tensor in a bent, extended and twisted thin rod is given in Love (1944). For the sake of completeness, the

dynamic equations of a riser undergoing flexural, torsional and extensional oscillations are briefly presented below.

The basic cartesian reference frame OXYZ has its center at the lower ball joint, with the positive Z axis directed vertically upwards. The centerline of a deflected riser is a general three-dimensional curve and can be described by three cartesian coordinates with respect to OXYZ in terms of the length s of the curve from the origin O and time t. We will follow the motion of a point A of the centerline being at distance s(0) from O along the curve at time t=0, as it evolves in time. Its coordinates with respect to OXYZ at time t are the components of

$$\underline{r} = (x^1 , x^2 , x^3) \cdot \underline{U} \qquad \text{(II.1)}$$

where

$$\underline{U} = (\hat{i}, \hat{j}, \hat{k})^T \qquad \text{(II.2)}$$

is the right-handed triad of unit vectors of OXYZ, and

$$x^1 = \hat{X}(s,t) = \hat{X}(s(0),0) + u(s,t) \qquad \text{(II.3)}$$

$$x^2 = \hat{Y}(s,t) = \hat{Y}(s(0),0) + v(s,t) \qquad \text{(II.4)}$$

$$x^3 = \hat{Z}(s,t) = \hat{Z}(s(0),0) + w(s,t) \qquad \text{(II.5)}$$

where $\hat{X}(s(0),0)$, $\hat{Y}(s(0),0)$, $\hat{Z}(s(0),0)$ are the coordinates of A at time t=0 and u,v,w are the dynamic displacements of A in the OXYZ axis system and

$$ds = |d\underline{r}| \tag{II.6}$$

The centerline curve is in general tortuous (i.e. non-plane) curve of curvature:

$$K(s,t) = |\underline{r}_{ss}| \tag{II.7}$$

and measure of tortuosity (or geometric torsion):

$$\tau(s,t) = -K^{-2}\det \begin{Bmatrix} x^1_s & x^2_s & x^3_s \\ x^1_{ss} & x^2_{ss} & x^3_{ss} \\ x^1_{sss} & x^2_{sss} & x^3_{sss} \end{Bmatrix} \tag{II.8}$$

(Eisenhart, (1947)). Subscript s denotes partial derivative with respect to the arc length s. From the definition of τ it follows that τ is zero for a plane curve.

To describe flexural, extensional and torsional

deformations of the rod, it is convenient to divide the rod into infinitesimal elements of length ds, each of which is bounded by two adjacent cross sections. To each cross section we attach a coordinate system $A\xi\eta\zeta$, so chosen that all systems are parallel in the state of vertical static equilibrium and further ζ is tangent to the centerline of the rod. When the rod is in vertical static equilibrium OX and $A\xi$, OY and $A\eta$, OZ and $A\zeta$ are parallel. At time t, any two adjacent systems $\xi\eta\zeta$ are rotated through an infinitesimal relative angle. It is known (Crandall et al, (1968)) that an infinitesimal angle of rotation can be regarded as a vector parallel to the axis of rotation. Let $d\underline{\Phi}$ be the vector of the angle of relative rotation of two systems $\xi\eta\zeta$ at distance ds apart along the rod. Its components are the angles of rotation about each of the three coordinate axes. To describe the deformation we define the vector rate of rotation of the coordinate axes along the rod:

$$\underline{\Omega} = \underline{\Phi}_s \qquad \text{(II.9)}$$

The component $\Omega^\zeta = \underline{\Omega} \cdot \hat{t}$ is the rate of change of the structural torsion angle with respect to s, where $\hat{t}$ is the unit tangential vector to the centerline curve at point A defined by:

$$\hat{t} = \underline{r}_s = (\alpha^1, \alpha^2, \alpha^3) \cdot \underline{U} \qquad \text{(II.10)}$$

Let $\hat{n}$, $\hat{b}$ be the normal and binormal unit vectors of the centerline curve at A defined by:

$$\hat{n} = K^{-1} \underline{r}_{ss} = (\beta^1, \beta^2, \beta^3) \cdot \underline{U} \qquad \text{(II.11)}$$

$$\hat{b} = \hat{t} \times \hat{n} = (\gamma^1, \gamma^2, \gamma^3) \cdot \underline{U} \qquad \text{(II.12)}$$

where $$\gamma^i = K^{-1}(x_s^j x_{ss}^k - x_{ss}^j x_s^k) \qquad \text{(II.13)}$$

with the understanding that i,j,k take the values 1,2,3 cyclically. The principal local vectors are connected by the Frenet relations:

$$\hat{t}_s = K \cdot \hat{n} \qquad \text{(II.14)}$$

$$\hat{n}_s = -(K \cdot \hat{t} + \tau \cdot \hat{b}) \qquad \text{(II.15)}$$

$$\hat{b}_s = \tau \cdot \hat{n} \qquad \text{(II.16)}$$

For a fixed time, the change of vector $\hat{t}$ between two neighboring points of the centerline is $d\hat{t} = d\underline{\Phi} \times \hat{t}$ or dividing by ds:

$$\hat{t}_s = \underline{\Omega} \times \hat{t} \qquad \text{(II.17)}$$

Multiplying vectorially by $\hat{t}$ and using (II.12) and (II.14) we find that:

$$\underline{\Omega} = K \hat{b} + \Omega^{\hat{}}\hat{t} \qquad \text{(II.18)}$$

Let f be the angle between $\hat{n}$ and the positive η axis and l,m,n the direction cosines of $\hat{b}$ with respect to $A\hat{\xi}\hat{\eta}\hat{\zeta}$.

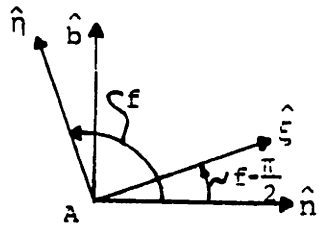

Using (II.16) we obtain that:

$$\tau^2 = l_s^2 + m_s^2 + n_s^2 \qquad \text{(II.19)}$$

The first term of the right hand side of (II.18) is a vector with two components Ω^ξ, Ω^η along $\hat{\xi}$ and $\hat{\eta}$ (since n=0). We may put:

$$l = \underline{\Omega}^\xi K^{-1} = -\cos f \qquad \text{(II.20)}$$

$$m = \underline{\Omega}^\eta K^{-1} = \sin f \qquad \text{(II.21)}$$

with $$K^2 = \underline{\Omega}^{\xi 2} + \underline{\Omega}^{\eta 2} \qquad \text{(II.22)}$$

and $$\tan f = -\underline{\Omega}^\eta / \underline{\Omega}^\xi \qquad \text{(II.23)}$$

Using the fact that (Landau and Lifshitz, (1959)):

$$\hat{b}_s = (\hat{b}_s)_{A\xi\eta\zeta} + \underline{\Omega} \times \hat{b} \qquad \text{(II.24)}$$

and (II.19) we find that:

$$\underline{\Omega}^\zeta = f_s + \tau \qquad \text{(II.25)}$$

Let $\underline{M}$ be the restoring moment at each cross section about the center point, analyzed in its components M^ξ, M^η, M^ζ along the local $A\xi$, $A\eta$, $A\zeta$ axes respectively. The constitutive relations between these and the rate of rotation of the system $A\xi\eta\zeta$ along s are:

$$M^\xi(s,t) = EI(s(0))\underline{\Omega}^\xi(s,t) \qquad \text{(II.26)}$$

$$M^\eta(s,t) = EI(s(0))\underline{\Omega}^\eta(s,t) \qquad \text{(II.27)}$$

$$M^\zeta(s,t) = GI_p(s(0))\underline{\Omega}^\zeta(s,t) \qquad \text{(II.28)}$$

where E, G are the moduli of extension and shear of steel respectively, related by

$$G = E/2(1+\nu) \qquad \text{(II.29)}$$

where ν is the Poisson's ratio and $I(s(0))$ and $I_p(s(0))$ are the moments of inertia of the cross section about a neutral axis and the center respectively. For a complete discussion of the validity of (II.26) - (II.28) see Landau and Lifshitz (1959). The notation of equations (II.26) - (II.28) means that the dimensions and shape of the cross section are assumed unaltered during the dynamic motion of the riser. If this is so:

$$I(s(0)) = \frac{1}{2} I_p(s(0)) = \frac{\pi}{64}[D_o^2(s(0)) - D_i^2(s(0))] \qquad \text{(II.30)}$$

where $D_i(s(0))$, $D_o(s(0))$ are the inner and outer steel pipe diameters at point A and time t=0. The change of shape of the cross section (ovalization) is negligible, because the ratio D_o/δ, where δ is the pipe thickness, is not very large (typical values $D_o/\delta \simeq 25\text{-}30$) and the riser slopes are relatively small, even for large lateral displacements ($\simeq$ a few diameters) for low frequencies (von Kármán, (1911)).

In addition, the approximation of constant riser diameters with time is consistent with a linear constitutive relation for extensional oscillations. If transverse dynamic shrinking and expansion of the riser tubes were

considered, then a material volume conservation in time implies a non-linear constitutive relation connecting tension $T(s,t)$ in the material and the centerline strain $\tilde{\varepsilon}(s,t)$ of the form:

$$T(s,t) = \frac{\tilde{\varepsilon}(s,t)}{1+\tilde{\varepsilon}(s,t)} EA^s(s(0)) + T(s(0),0) \qquad (II.31)$$

where $A^s(s(0))$ is the local steel cross section area and the centerline strain $\tilde{\varepsilon}(s,t)$ is defined by:

$$\tilde{\varepsilon}(s,t) = \frac{ds(t) - ds(0)}{ds(0)} \qquad (II.32)$$

For small values of $\tilde{\varepsilon}(s,t)$ equation (II.31) reduces to:

$$T(s,t) = \tilde{\varepsilon}(s,t)\ EA^s(s(0)) + T(s(0),0) + O(EA^s\tilde{\varepsilon}^2) \qquad (II.33)$$

which is consistent with equations (II.26)-(II.28).

Relations (II.20)-(II.23) and (II.26)-(II.27) imply that the bending moments along the local binormal and normal vectors are respectively:

$$M^b(s,t) = EI(s(0))K(s,t) \qquad (II.34)$$

$$M^n(s,t) = 0 \qquad (II.35)$$

These relations imply that for a tortuous centerline curve, bending takes place in the osculating local plane $(\hat{t}, \hat{n})$ only. This can be also seen from the following geometrical considerations.

The projection of the centerline curve in the neighborhood of point A on the local osculating plane ($\hat{t}$, $\hat{n}$) is a parabola of the form:

$$y^2 = \frac{K(0)}{2} s^2 + O(s^3) \qquad \text{as } s \to 0 \qquad \text{(II.36)}$$

and on the local rectifying plane ($\hat{t}$, $\hat{b}$) a curve exhibiting an inflection point at A of the form:

$$y^3 = - \frac{K(0)\tau(0)}{6} s^3 + O(s^4) \quad \text{as } s \to 0 \qquad \text{(II.37)}$$

where y^2, y^3 are the ordinates of the projected curves along $\hat{n}$ and $\hat{b}$ respectively, the arc length is temporarily measured from point A and $K(0)$, $\tau(0)$ are the values of the curvature and geometric torsion of the centerline curve at point A. These expressions can be shown easily by Taylor expanding $\underline{r}(s)$ (as measured from point A) in the neighborhood of that point and using the Frenet relations (II.14)-(II.16) (Eisenhart, (1947)).

Finally it is convenient to define the following quantities, as shown in Bernitsas, (1979), (1980):

The "effective" tension Pe(s,t) by:

$$Pe(s,t) \equiv T(s,t) + B^*(s(0))[h_w - \hat{Z}(s,t)] - W_m(s(0))[h_m - \hat{Z}(s,t)] \qquad \text{(II.38)}$$

where h_w, h_m are the water and mud elevations above the lower joint and B^*, W_m are defined by:

$$B^*(s(0)) = \rho_w g \frac{\pi}{4} D_o^2(s(0)) \qquad \text{(II.39)}$$

$$W_m(s(0)) = \rho_m g \frac{\pi}{4} D_i^2(s(0)) \qquad \text{(II.40)}$$

where ρ_w, ρ_m are the water and mud densities, g the acceleration of gravity and D_o , D_i the riser tube outer and inner diameters.

Likewise, the "effective weight per unit length" is defined by:

$$W_e(s(0)) \equiv W_m(s(0)) + W_R(s(0)) + W_b(s(0)) - B^*(s(0)) - B_b(s(0)) \qquad \text{(II.41)}$$

where:

$$W_R(s(0)) = \rho^s g \frac{\pi}{4}[D_o^2(s(0)) - D_i^2(s(0))] \qquad \text{(II.42)}$$

$$W_b(s(0)) = \rho_b g \frac{\pi}{4}[D_b^2(s(0)) - D_o^2(s(0))] \qquad \text{(II.43)}$$

$$B_b(s(0)) = \rho_w g \frac{\pi}{4}[D_b^2(s(0)) - D_o^2(s(0))] \qquad \text{(II.44)}$$

where ρ^s, ρ_b are the steel and buoyancy module material densities and $D_b(s(0)$ is the local module outer diameter. The notation of equations (II.38) - (II.44) implies that the diameters at point A are not considered functions of time, which is consistent with the degree of accuracy of (II.26)-(II.28), (II.30), and (II.33) as explained earlier.

The "effective" tension has no real meaning, per se, but it simplifies the notation, since it combines some of the forces acting in the tangential direction at point A (Bernitsas (1979)). A similar comment holds for the term "effective weight per unit length".

II.2.2 Statement of the Equations of Motion

Equilibrium of forces acting on the element ds yields:

$$(Pe\hat{t})_s + (Q^n\hat{n})_s + (Q^b\hat{b})_s + f^t\hat{t} + f^n\hat{n} + f^b\hat{b} + \underline{\Delta} - We(s(0))\hat{k} = [m_e(s(0))]\underline{a} \qquad \text{(II.45)}$$

where $Q^n(s,t)$, $Q^b(s,t)$ are the shearing forces in the $\hat{n}$, $\hat{b}$ directions, f^t, f^n, f^b are the total local hydrodynamic forces per unit length in the $\hat{t}$, $\hat{n}$, $\hat{b}$ directions respectively, $[m_e(s(0))]$ is the structural mass per unit length tensor, $\underline{\Delta}$ the structural damping force per unit length and $\underline{a}$ the acceleration of point A with respect to OXYZ:

$$\underline{a}(s,t) = \underline{r}_{tt} + 2\underline{r}_{st}\, s_t + \underline{r}_{ss}\, s_t^2 + \underline{r}_s\, s_{tt} \qquad \text{(II.46)}$$

where subscript t denotes partial derivative with respect to time t. If the inertial force (right-hand side of (II.45)) is projected to the local $\hat{t}$, $\hat{n}$, $\hat{b}$ vectors, then the mass tensor is diagonal with elements (Bernitsas, (1979)), (1980)):

$$m_e^t(s(0)) = g^{-1}[W_R(s(0)) + W_b(s(0))] \qquad \text{(II.47)}$$

$$m_e^n(s(0)) = m_e^b(s(0)) = g^{-1}[W_R(s(0)) + W_m(s(0)) + W_b(s(0))] \qquad \text{(II.48)}$$

and the resulting three scalar equations of equilibrium of the forces in the $\hat{t},\hat{n},\hat{b}$ directions can be reduced to the following, respectively, after use is made of the Frenet

relations (II.14)-(II.16):

$$Pe_s - K\cdot Q^n + f^t - We(s(0))x_s^3 = m_e^t(s(0)) \cdot [x_{tt}^i + 2x_{st}^i s_t + x_{ss}^i s_t^2 + x_s^i s_{tt}]\, x_s^i - \Delta^t \tag{II.49}$$

$$Q_s^n + K \cdot Pe + \tau \cdot Q^b + f^n - We(s(0))K^{-1}x_{ss}^3 = m_e^n(s(0))[x_{tt}^i + 2x_{st}^i s_t + x_{ss}^i s_t^2 + x_s^i s_{tt}]K^{-1}x_{ss}^i - \Delta^n \tag{II.50}$$

$$Q_e^b - \tau Q^n + f^b - We(s(0))\gamma^3 = m_e^b(s(0)) \cdot [x_{tt}^i + 2x_{st}^i s_t + x_{ss}^i s_t^2 + x_s^i s_{tt}] \cdot \gamma^i - \Delta^b \tag{II.51}$$

where summation notation is implied (over i=1,2,3), if there is repeated upper index i in the terms of a product, and Δ^t, Δ^n, Δ^b are the components of the structural damping force in the $\hat{t}$, $\hat{n}$, $\hat{b}$ directions respectively.

Equilibrium of moments acting on the element ds yields:

$$\underline{M}_s + \hat{t} \times \underline{F} + \underline{M}^H + \underline{\Theta} = \frac{d\underline{H}^A}{dt} \tag{II.52}$$

where

$$\underline{F} = [Q^n, Q^b, Pe]\cdot \underline{U}' \tag{II.53}$$

with

$$\underline{U}' = [\hat{n}, \hat{b}, \hat{t}]^T \tag{II.54}$$

$\underline{M}^H$ denotes the hydrodynamic moment per unit length on the element ds centered at point A and equal to $M^H\zeta\hat{t}$. $\underline{H}^A$ denotes the angular momemtum per unit length of a differential riser element ds with centroid point A, with respect to point A. $\underline{\Theta}$ denotes a structural damping moment.

Let $\underline{\omega}$ be the angular velocity of the body frame $A\hat{\xi}\hat{\eta}\hat{\zeta}$ with respect to OXYZ. Given that axes $A\xi$, $A\eta$, $A\zeta$ are principal axes of inertia of the element ds with centroid point A, then it is convenient to analyze $\underline{H}^A$ with respect to its components in the frame $A\,\xi\eta\zeta$:

$$\underline{H}^A = (H^\xi,\ H^\eta,\ H^\zeta) \cdot \underline{U}'' \qquad \text{(II.55)}$$

where
$$\underline{U}'' = (\hat{\xi},\ \hat{\eta},\hat{\zeta}\ )^T \qquad \text{(II.56)}$$

is the right-handed triad of unit vectors along $A\xi$, $A\eta$, $A\zeta$ and

$$(H^\xi,\ H^\eta,\ H^\zeta)^T = [J_c(s(0))](\omega^\xi,\ \omega^\eta,\ \omega^\zeta)^T \qquad \text{(II.57)}$$

where

$$\underline{\omega} = (\omega^\xi,\omega^\eta,\omega^\zeta)\underline{U}'' \qquad \text{(II.58)}$$

and $[J_c(s(0))]$ is a diagonal inertia per unit length tensor:

$$[J_c(s(0))] = \text{diag}[J^{\xi\xi},\ J^{\eta\eta},\ J^{\zeta\zeta}] \qquad \text{(II.59)}$$

$$J^{\xi\xi}(s(0)) = J^{\eta\eta}(s(0)) = \frac{\pi}{64}[\rho_m D_i^4 + \rho^s(D_o^2-D_i^2)^2 + \rho_b(D_b^2 - D_o^2)^2] \qquad \text{(II.60)}$$

$$J^{\zeta\zeta}(s(0)) = \frac{\pi}{32}[\rho^s(D_o^4-D_i^4) + \rho_b(D_b^4-D_o^4)] \qquad \text{(II.61)}$$

where the dependence of D_o, D_i, D_b from s(0) was neglected from the notation.

Let $\underline{\omega}_o$ be the angular velocity of the frame $A\hat{\xi}\hat{\eta}\hat{\zeta}$ with respect to $A\hat{n}\hat{b}\hat{t}$ and $\underline{\omega}_1$ the angular velocity of the

frame $A\hat{n}\hat{b}\hat{t}$ with respect to OXYZ. Then, using the fact that angular velocities can be considered vectors (Crandall et al, (1968)):

$$\underline{\omega} = \underline{\omega}_o + \underline{\omega}_1 \tag{II.62}$$

The three systems $\underline{U}$, $\underline{U}'$, $\underline{U}''$ are related by the following rotations:

$$\underline{U}' = C(s,t) \cdot \underline{U} \tag{II.63}$$

$$\underline{U}'' = C_1(s,t) \cdot \underline{U}' \tag{II.64}$$

where C, C_1 are 3x3 rotation matrices defined by

$$C(s,t) = \begin{Bmatrix} \beta^1 & \beta^2 & \beta^3 \\ \gamma^1 & \gamma^2 & \gamma^3 \\ \alpha^1 & \alpha^2 & \alpha^3 \end{Bmatrix} \tag{II.65}$$

$$C_1(s,t) = \begin{Bmatrix} \sin f & -\cos f & 0 \\ \cos f & \sin f & 0 \\ 0 & 0 & 1 \end{Bmatrix} \tag{II.66}$$

First, if we let

$$\underline{\omega}_1 = (\omega^n, \omega^b, \omega^t) \cdot \underline{U}' \tag{II.67}$$

the relations (Crandall et al, (1968)):

$$\frac{d\hat{n}}{dt} = \underline{\omega}_1 \times \hat{n}; \quad \frac{d\hat{b}}{dt} = \underline{\omega}_1 \times \hat{b} \; ; \quad \frac{d\hat{t}}{dt} = \underline{\omega}_1 \times \hat{t} \tag{II.68}$$

imply that:

$$\frac{d\underline{U}'}{dt} = [\omega_1]\underline{U}' \tag{II.69}$$

where $[\omega_1]$ is a 3x3 skew-symmetric tensor defined by:

$$[\omega_1] = \begin{Bmatrix} 0 & \omega^t & -\omega^b \\ -\omega^t & 0 & -\omega^n \\ \omega^b & -\omega^n & 0 \end{Bmatrix} \qquad \text{(II.70)}$$

From II.63) we find that:

$$\frac{d\underline{U}'}{dt} = [C_t + C_s\, s_t] \cdot \underline{U} \qquad \text{(II.71)}$$

where derivative of a matrix is the matrix of the derivatives of the elements of the first. Given that C(s,t) is a rotation matrix, then (Crandall et al, (1968)):

$$\underline{U} = C^T \cdot \underline{U}' \qquad \text{(II.72)}$$

which in conjunction with (II.69)-(II.71) imply that:

$$[\omega_1]\underline{U}' = [C_t + C_s\, s_t]C^T\underline{U}' \qquad \text{(II.73)}$$

This relation implies that:

$$\omega^n = -\gamma^i(\alpha_t^i + \alpha_s^i\, s_t) \qquad \text{(II.74)}$$

$$\omega^b = \beta^i(\alpha_t^i + \alpha_s^i\, s_t) \qquad \text{(II.75)}$$

$$\omega^t = \gamma^i(\beta_t^i + \beta_s^i\, s_t) \qquad \text{(II.76)}$$

where the usual summation notation is implied. Relations (II.74)-(II.76) express the components of $\underline{\omega}_1$ in terms of the coordinates x^i of point A with respect to OXYZ.

Finally, from the definition of f (equations (II.20), (II.21)), it is easy to see that:

$$\underline{\omega}_o = (f_t + f_s s_t)\hat{t} \tag{II.77}$$

Since C_1 is a rotation matrix

$$\underline{U}' = C_1^T \cdot \underline{U}'' \tag{II.78}$$

and therefore (II.58), (II.62), (II.67), (II.77), (II.78) imply:

$$[\omega^\xi, \omega^\eta, \omega^\zeta - f_t - f_s s_t]\underline{U}'' = [\omega^n, \omega^b, \omega^t] C_1^T \underline{U}''$$

This implies that:

$$\omega^\xi = \omega^n \sin f - \omega^b \cos f \tag{II.79}$$

$$\omega^\eta = \omega^n \cos f + \omega^b \sin f \tag{II.80}$$

$$\omega^\zeta = f_t + f_s s_t + \omega^t \tag{II.81}$$

It is well known that:

$$\frac{d\underline{H}^A}{dt} = \underline{H}_t^A + \underline{\omega} \times \underline{H}^A \tag{II.82}$$

Using (II.57), (II.60) and (II.82) we find that:

$$\frac{dH^\xi}{dt} = J^{\xi\xi}(\omega_t^\xi + \omega_s^\xi s_t) + \omega^\eta \omega^\zeta (J^{\zeta\zeta} - J^{\eta\eta}) \tag{II.83}$$

$$\frac{dH^\eta}{dt} = J^{\eta\eta}(\omega_t^\eta + \omega_s^\eta s_t) + \omega^\zeta \omega^\xi (J^{\xi\xi} - J^{\zeta\zeta}) \tag{II.84}$$

$$\frac{dH^\zeta}{dt} = J^{\zeta\zeta}(\omega_t^\zeta + \omega_s^\zeta s_t) \tag{II.85}$$

Using (II.78) we find that the projections of the rate of change of angular momentum on $\hat{n}$, $\hat{b}$, $\hat{t}$ are:

$$\frac{dH^n}{dt} = \sin f \frac{dH^\xi}{dt} + \cos f \frac{dH^\eta}{dt} \tag{II.86}$$

$$\frac{dH^b}{dt} = -\cos f \frac{dH^\xi}{dt} + \sin f \frac{dH^\eta}{dt} \qquad \text{(II.87)}$$

$$\frac{dH^t}{dt} = \frac{dH^\zeta}{dt} \qquad \text{(II.88)}$$

Using equations (II.52), (II.53) and (II.14)-(II.16) we obtain three equations of equilibrium of moments in the $\hat{n}$, $\hat{b}$, $\hat{t}$ directions respectively:

$$KM^\zeta + \tau M^b - Q^b + \Theta^n = \frac{dH^n}{dt} \qquad \text{(II.89)}$$

$$M_s^b + Q^n + \Theta^b = \frac{dH^b}{dt} \qquad \text{(II.90)}$$

$$M_s^\zeta + M^{H\zeta} + \Theta^t = \frac{dH^t}{dt} \qquad \text{(II.91)}$$

where $$\underline{\Theta} = [\, \Theta^n, \ \Theta^b, \ \Theta^t]\, \underline{U}' \qquad \text{(II.92)}$$

The above provide a consistent set of governing equations that can be a starting point for a rational study of the dynamic behavior of risers.

II.2.3 Boundary Conditions

At the lower end s=0, due to the presence of the ball joint, which presents negligible stiffness to local bending (at least over a wide range of lower end slopes), we may impose the following boundary conditions:

$$x^i = 0 \quad ; \quad i = 1, 2, 3 \qquad \text{(II.93)}$$

$$x^i_{ss} = 0 \quad ; \quad i = 1, 2, 3 \qquad \text{(II.94)}$$

Equation (II.94) is derived from (II.7) and (II.34). From the definition of geometric torsion (II.8) we find that at s=0:

$$\tau = 0 \qquad \text{(II.95)}$$

Relations (II.36), (II.37), (II.94), (II.95) imply that sufficiently close to s=0 the centerline is a plane curve and can be approximated by a straight line. We further assume that the ball joint exhibits negligible resistance to structural torsion. This implies that at s=0:

$$f_s = 0 \qquad \text{(II.96)}$$

as relations (II.25), (II.28), (II.95) show.

At the upper ball joint, we assume that

$$x^i\,(s(t;L),t) = g^i(t) \qquad i = 1,2 \qquad \text{(II.97)}$$

where g^i (i=1,2) are the deflections of that point in the X, Y directions respectively. Functions g^i may include a constant and a time varying part assumed to be given à priori. This essentially means that the motions of the supporting structure are assumed not to be significantly affected by the upper end horizontal interaction force between riser and structure. This can be verified by comparing this force to the inertial force of a typical oscillating platform.

Assuming nearly perfect function of the upper ball joint,we find that:

$$x^i_{ss} = 0 \qquad i = 1, 2, 3 \qquad \text{(II.98)}$$

to ensure zero curvature at that point.

The final condition expresses the fact that the slip joint eliminates any static or dynamic tension variation at the upper ball joint. This implies using equation (II.33) that

$$\tilde{\varepsilon}(s(t;L),t) = 0 \qquad \text{(II.99)}$$

where, of course, the static term $T(s(0;L),0)$ at the deflected position is assumed to be equal to the tension at s=L in the vertical static equilibrium condition.

Conditions (II.98) imply that $\tau = 0$ at the upper ball joint. If this is assumed to exhibit negligible rigidity in torsion, we find that we may apply a condition similar to (II.96):

$$f_s\,(s(t;L),\ t) = 0 \qquad \text{(II.100)}$$

The above set of boundary conditions is consistent with the order of the differential system (II.49)-(II.51) and (II.89)-(II.91). We may observe that the highest space derivative terms it includes are of the form x^i_{ssss} for i =

1,2,3 and f_{ss}. Therefore four boundary conditions are required for each x^i, i=1,2,3 and two for f. The existence of terms of the form $x^3{}_{ssss}$ indicates a coupling between large amplitude extensional and flexural oscillations.

Chapter III

A SYSTEMATIC ANALYSIS OF THE GENERAL GOVERNING EQUATIONS OF THE RISER

III.1 SIMPLIFICATION AND NON-DIMENSIONALIZATION OF THE GOVERNING EQUATIONS

The purpose of this Chapter is to identify the basic properties of the general differential system describing the riser's dynamic behavior. Qualitative - order of magnitude - arguments and the disparity of the time scales of the various modes of a riser's motion are used to elucidate the role of coupling and non-linear terms. Finally the leading order equations for each mode of the riser's motion are derived systematically from the general differential system described in Chapter II and some properties of the equations describing flexural oscillations are identified and discussed in detail.

The following assumptions are introduced at this point in addition to the assumptions of Chapter II, article 1:

1. The riser pipe diameters D_o, D_i are considered constant along the length which is the usual practice for risers. Variation of the outer diameter due to flanges and

connectors is neglected, because its global influence is very small.

2. The necessary buoyancy is provided by many, short, compared to the length L, buoyancy modules of uniform outer diameter D_b, uniformly distributed along the length. This is a good design practice, leading to small concentrated buoyancy forces from the modules on the riser pipes (Bernitsas, (1980)).

Under these assumptions and because we are interested in the global dynamic behavior of the riser, the effective weight, mass and inertia per unit length tensors can be replaced by their mean values over the length. Let L be the length of the riser between ball joints in its vertical static equilibrium condition and L_b the total length of the modules. We will use the following average quantities instead of their local values:

$$\overline{We} = W_m + W_R - B^* + \frac{L_b}{L}(W_b - B_b) \qquad \text{(III.1)}$$

$$\overline{m^t} = g^{-1}\left(W_R + \frac{L_b}{L} W_b\right) \qquad \text{(III.2)}$$

$$\overline{m^n} = \overline{m^b} = g^{-1}\left(W_R + W_m + \frac{L_b}{L} W_b\right) \qquad \text{(III.3)}$$

$$\overline{J^{\xi\xi}} = \frac{\pi}{32}\left\{\rho^s (D_o^4 - D_i^4) + \rho_b \frac{L_b}{L}(D_b^4 - D_o^4)\right\} \qquad \text{(III.4)}$$

$$\overline{J^{\xi\xi}} = \overline{J^{\eta\eta}} = \frac{\pi}{64}\left\{\rho_m D_i^4 + \rho^s (D_o^2 - D_i^2)^2 + \frac{L_b}{L}\rho_b (D_b^2 - D_o^2)^2\right\} \qquad \text{(III.5)}$$

To simplify the notation we may assume that the time t=0 corresponds to the vertical static equilibrium condition. Therefore:

$$x^1 = \hat{X}(s,t) \equiv u(s,t) \qquad \text{(III.6)}$$

$$x^2 = \hat{Y}(s,t) \equiv v(s,t) \qquad \text{(III.7)}$$

$$x^3 = \hat{Z}(s,t) \equiv Z + w(s,t) \qquad \text{(III.8)}$$

where $(0,0,Z)\cdot \underline{U}$ is the original (t=0) position of point A.

Conversion of the governing equations to a suitable non-dimensional form described below facilitates the purpose of this analysis. All lengths are non-dimensionalized by L, all forces by Pe(0,0), the effective overpull at t=0, Z=0, all moments by LPe(0,0). The following non-dimensional structural parameters are introduced:

$$\varepsilon = \frac{EI}{Pe(0,0)L^2} \qquad \text{(III.9)}$$

$$\mu = \frac{\overline{We}L}{Pe(0,0)} \qquad \text{(III.10)}$$

$$\tilde{\varepsilon}_o = \frac{Pe(0,0)}{EA^s} \qquad \text{(III.11)}$$

where $$A^s = \frac{\pi}{4}(D_o^2 - D_i^2) \qquad \text{(III.12)}$$

$$\varepsilon_T = \frac{GI_p}{Pe(0,0)L^2} \qquad \text{(III.13)}$$

which with the aid of (II.29), (II.30) gives

$$\varepsilon_T = \varepsilon(1 + \nu)^{-1} \tag{III.14}$$

A characteristic time scale of flexural oscillations is:

$$\tau_o = L[\overline{m^n}/Pe(0,0)]^{1/2} \tag{III.15}$$

It is convenient to non-dimensionalize the time by τ_o:

$$t' = t/\tau_o \tag{III.16}$$

as well as all angular velocities. We also define:

$$A = \overline{m^t}/\overline{m^n} \tag{III.17}$$

$$c_1^2 = \frac{\overline{J^{\zeta\zeta}}}{\tau_o^2\, Pe(0,0)} = \frac{\overline{J^{tt}}}{\overline{m^n}\, L^2} \tag{III.18}$$

$$c_2^2 = \frac{\overline{J^{\xi\xi}}}{\tau_o^2\, Pe(0,0)} = \frac{\overline{J^{\eta\eta}}}{\tau_o^2\, Pe(0,0)} = \frac{\overline{J^{\xi\xi}}}{\overline{m^n}\, L^2} \tag{III.19}$$

Using these definitions and denoting non-dimensional variables by the same symbol as corresponding dimensional variables, we obtain the constitutive relations in the form:

$$M^{\zeta}(s,t) = \varepsilon_T\, \Omega^{\zeta}(s,t) \tag{III.20}$$

$$M^{b}(s,t) = \varepsilon\, K(s,t) \tag{III.21}$$

$$T(s,t) = \tilde{\varepsilon}(s,t)/\tilde{\varepsilon}_o + T(Z,0) + O(\tilde{\varepsilon}^2/\tilde{\varepsilon}_o) \tag{III.22}$$

where

$$\tilde{\varepsilon}(s,t) = \frac{ds - dZ}{dZ} \tag{III.23}$$

and $T(s,t)$ is related to the effective tension by:

$$Pe(s,t) = T(s,t) + B^*(h_w - \hat{Z}) - W_m(h_m - \hat{Z}) \tag{III.24}$$

where B^*, W_m, h_m, h_w, Z are, of course, non-dimensional.

The equations of forces (II.49)-(II.51) take the following non-dimensional form respectively:

$$Pe_s - KQ^n + f^t - \mu x_s^3 = A[x^i_{tt} + 2x^i_{st}s_t + x^i_{ss}s_t^2 + x^i_s s_{tt}]x^i_s - \Delta^t \tag{III.25}$$

$$Q^n_s + K\,Pe + \tau Q^b + f^n - \mu K^{-1}x_{ss}^3 = [x^i_{tt} + 2x^i_{st}s_t + x^i_{ss}s_t^2 + x^i_s s_{tt}]\,K^{-1}x^i_{ss} - \Delta^n \tag{III.26}$$

$$Q^b_s - \tau Q^n + f^b - \mu\gamma^3 = [x^i_{tt} + 2x^i_{st}s_t + x^i_{ss}s_t^2 + x^i_s s_{tt}]\,\gamma^i - \Delta^b \tag{III.27}$$

where the usual summation notation is implied.

Using equations (II.83)-(II.88), (III.20), (III.21) and (III.14), the equations of moments (II.89)-(II.91) can be transformed to the following equations respectively:

$$\varepsilon K[(1+\nu)^{-1}\Omega^\zeta + \tau] - Q^b + \Theta^n = \sin f[c_2^2(\omega^\xi_t + \omega^\xi_s s_t) + \omega^\eta\omega^\zeta(c_1^2 - c_2^2)] + \cos f\,[c_2^2(\omega^\eta_t + \omega^\eta_s s_t) + \omega^\xi\omega^\zeta(c_2^2 - c_1^2)] \tag{III.28}$$

$$\varepsilon K_s + Q^n + \Theta^b = -\cos f[c_2^2(\omega^\xi_t + \omega^\xi_s s_t) + \omega^\eta\omega^\zeta(c_1^2 - c_2^2)] + \sin f\,[c_2^2(\omega^\eta_t + \omega^\eta_s s_t) + \omega^\xi\omega^\zeta(c_2^2 - c_1^2)] \tag{III.29}$$

$$\varepsilon_T\,\Omega^\zeta_s + M^{H\zeta} + \Theta^t = c_1^2(\omega^\zeta_t + \omega^\zeta_s s_t) \tag{III.30}$$

Using (II.79)-(II.81), the above three equations can be reduced to the following respectively:

$$\varepsilon K[(1+\nu)^{-1}\Omega^\zeta + \tau] - Q^b + \Theta^n = c_2^2[\omega^n_t + \omega^n_s s_t + \omega^b(f_t + f_s s_t)] + (c_1^2 - c_2^2)\,(\omega^t + f_t + f_s s_t)\,\omega^b \tag{III.31}$$

$$\varepsilon K_s + Q^n + \Theta^b = c_2^2\,[\omega^b_t + \omega^b_s s_t - \omega^n(f_t + f_s s_t)] - (c_1^2 - c_2^2)\,(\omega^t + f_t + f_s s_t)\,\omega^n \tag{III.32}$$

$$\varepsilon_T \Omega_s^{\zeta}+M^{H\zeta}+\theta^t = c_1^2[\omega_t^t+\omega_s^t s_t+f_{tt}+2f_{st}s_t+f_{ss}s_t^2+f_s s_{tt}] \quad \text{(III.33)}$$

The boundary conditions (II.93)-(II.100) are, of course, the same. Using (III.6)-(III.8) and (III.23), the boundary condition (II.99) may be shown to be equivalent to:

$$w_Z = [1 - u_Z^2 - v_Z^2]^{+1/2} - 1 \quad \text{at } Z=1 \quad \text{(III.34)}$$

In the following section, the smallness of a typical flexural deflection of a riser's centerline with respect to the length and the disparity of the time scales of flexural, extensional and torsional oscillations are exploited extensively in an attempt to understand the basic couplings and fundamental properties of the differential system (III.25)-(III.27) and (III.31)-(III.33) under the imposed boundary conditions.

III.2 SYSTEMATIC PERTURBATION EXPANSION OF THE GOVERNING EQUATIONS

The large deflection dynamic equations of the riser are expanded here to a series of equations that can be integrated sequentially. The expansion parameter $\hat{\varepsilon}$ is the ratio of a typical horizontal (static or dynamic) displacement of the riser's centerline over the length L. We assume therefore that Z=O(1), while u,v are of O($\hat{\varepsilon}$) with

$\hat{\varepsilon} << 1$. It is also assumed that D_o/L is of $O(\varepsilon)$. As we will verify a posteriori, it is permitted to assume that for $\hat{\varepsilon} << 1$:

$$w = O(\hat{\varepsilon}^2) \tag{III.35}$$

In this thesis we will be concerned with the leading order consistent equations for each mode of motion.

We may observe from (II.6) and (III.6)-(III.8) that we can consider the coordinates x^i, i=1,2,3 of point A with respect to OXYZ as functions of two independent variables t and Z alone. This is true for the remaining dependent variables. In addition, we may see that the assumption that only the first few flexural modes are excited, effectively implies that space derivatives up to a certain order do not change the order of the quantities themselves. We will need to make this assumption up to the fourth derivative.

Using equations (II.6) and (III.6)-(III.8) we obtain:

$$s_Z(t,Z) = [1 + 2w_Z + w_Z^2 + u_Z^2 + v_Z^2]^{1/2} \tag{III.36}$$

Using the above order of magnitude assumptions we find that:

$$s_Z(t,Z) = 1 + w_Z + \frac{1}{2}(u_Z^2 + v_Z^2) + O(\hat{\varepsilon}^4) \tag{III.37}$$

and integrating:

$$s = s(t,Z) = Z+w(t,Z)+ \frac{1}{2}\int_0^Z [u_Z^2(t,Z')+ v_Z^2(t,Z')]dZ'+ O(\hat{\varepsilon}^4) \qquad \text{(III.38)}$$

Inversely we may consider that

$$Z = Z(t,s) \qquad \text{(III.39)}$$

which implies that:

$$Z_s = s_Z^{-1} = 1 - w_Z - 1/2(u_Z^2 + v_Z^2) + O(\hat{\varepsilon}^4) \qquad \text{(III.40)}$$

and $$Z_{ss} = -w_{ZZ} - u_Z u_{ZZ} - v_Z v_{ZZ} + O(\hat{\varepsilon}^4) \qquad \text{(III.41)}$$

Equation (III.40) and the relations $x^i{}_s = x^i{}_Z Z_s$, i=1,2,3 imply that:

$$\alpha^1 = u_s = u_Z + O(\hat{\varepsilon}^3) \qquad \text{(III.42)}$$

$$\alpha^2 = v_s = v_Z + O(\hat{\varepsilon}^3) \qquad \text{(III.43)}$$

$$\alpha^3 = x^3_s = 1-\frac{1}{2}(u_Z^2+ v_Z^2)+ O(\hat{\varepsilon}^4) \qquad \text{(III.44)}$$

We obtain similarly from $x^i{}_{ss} = x^i{}_{ZZ} Z_s^2 + x^i{}_Z Z_{ss}$, i=1,2,3 that:

$$u_{ss} = u_{ZZ} + O(\hat{\varepsilon}^3) \qquad \text{(III.45)}$$

$$v_{ss} = v_{ZZ} + O(\hat{\varepsilon}^3) \qquad \text{(III.46)}$$

$$x^3{}_{ss} = -u_z u_{zz} - v_z v_{zz} + O(\hat{\varepsilon}^4) \qquad \text{(III.47)}$$

Finally from $x^i{}_{sss} = x^i{}_{zzz} z_s{}^3 + 3x^i{}_{zz} z_s z_{ss} + x^i{}_z z_{sss}$ for i=1,2,3 and:

$$z_{sss} = -[w_{zzz} + u_{zz}^2 + v_{zz}^2 + u_z u_{zzz} + v_z v_{zzz}] + O(\hat{\varepsilon}^4)$$

we find that:

$$u_{sss} = u_{zzz} + O(\hat{\varepsilon}^3) \qquad \text{(III.48)}$$

$$v_{sss} = v_{zzz} + O(\hat{\varepsilon}^3) \qquad \text{(III.49)}$$

$$x^3_{sss} = -u_{zz}^2 - v_{zz}^2 - u_z u_{zzz} - v_z v_{zzz} + O(\hat{\varepsilon}^4) \qquad \text{(III.50)}$$

These relations imply that the curvature and geometric torsion are given by:

$$K(t,z) = (u_{zz}{}^2 + v_{zz}{}^2)^{1/2} + O(\hat{\varepsilon}^3) \qquad \text{(III.51)}$$

$$\tau(t,z) = K^{-2}(u_{zzz} v_{zz} - u_{zz} v_{zzz}) + O(\hat{\varepsilon}^2) \qquad \text{(III.52)}$$

where from now on we denote by K the first term of the right-hand side of (III.51), unless otherwise stated.

Relations (III.37) and (III.23) imply that the

centerline strain is given by:

$$\tilde{\varepsilon}(t,Z) = w_Z + 1/2(u_Z^2 + v_Z^2) + O(\hat{\varepsilon}^4) \qquad \text{(III.53)}$$

From equations (III.45)-(III.47) and (III.51) we obtain:

$$\beta^1 = K^{-1}u_{ZZ} + O(\hat{\varepsilon}^2) \qquad \text{(III.54)}$$

$$\beta^2 = K^{-1}v_{ZZ} + O(\hat{\varepsilon}^2) \qquad \text{(III.55)}$$

$$\beta^3 = K^{-1}(u_Z u_{ZZ} + v_Z v_{ZZ}) + O(\hat{\varepsilon}^3) \qquad \text{(III.56)}$$

$$\gamma^1 = -K^{-1}v_{ZZ} + O(\hat{\varepsilon}^2) \qquad \text{(III.57)}$$

$$\gamma^2 = K^{-1}u_{ZZ} + O(\hat{\varepsilon}^2) \qquad \text{(III.58)}$$

$$\gamma^3 = K^{-1}(u_Z v_{ZZ} - v_Z u_{ZZ}) + O(\hat{\varepsilon}^3) \qquad \text{(III.59)}$$

Next we expand the components of the angular velocity $\underline{\omega}_1$. Using equations (II.74)-(II.76), (III.42)-(III.44) and (III.54)-(III.59) and estimating that both s_t and s_{tt} are of $O(\hat{\varepsilon}^2)$ (see equation (III.38)) we find that:

$$\omega^n = K^{-1}(v_{ZZ}u_{Zt} - u_{ZZ}v_{Zt}) + O(\hat{\varepsilon}^3) \qquad \text{(III.60)}$$

$$\omega^b = K^{-1}(u_{ZZ}u_{Zt} + v_{ZZ}v_{Zt}) + O(\hat{\varepsilon}^3) \qquad \text{(III.61)}$$

$$\omega^t = K^{-2}(u_{ZZ}v_{ZZt} - v_{ZZ}u_{ZZt}) + O(\hat{\varepsilon}^2) \qquad \text{(III.62)}$$

From the last three equations we find that both ω^n, ω^b are of $O(\hat{\varepsilon})$ while ω^t is of $O(1)$. In addition, from equations (III.3)-(III.5) and (III.18)-(III.19) we find that both c_1^2 and c_2^2 are of $O[(D_o/L)^2]$ and therefore of $O(\hat{\varepsilon}^2)$. We assume that f is at most of O(1). These estimates imply that (III.31) and (III.32) may give respectively:

$$Q^b = \varepsilon K[(1+\nu)^{-1}\Omega^\zeta + \tau] + \theta^n + O(\hat{\varepsilon}^3) \qquad \text{(III.63)}$$

$$Q^n = -\varepsilon K_s - \theta^b + O(\hat{\varepsilon}^3) \qquad \text{(III.64)}$$

Using (III.33), (III.14), (III.9), (III.18), (II.29), and (II.30) we obtain:

$$\Omega_s^\zeta + \varepsilon^{-1}(1+\nu)(M^{H\zeta} + \theta^t) = c_3^2(\omega_t^t + \omega_s^t s_t) + c_3^2(f_{tt} + 2f_{st}s_t + f_{ss}s_t^2 + f_s s_{tt}) \qquad \text{(III.65)}$$

where

$$c_3^2 = c_1^2 \varepsilon_T^{-1} = (Pe(0,0)/\overline{m^n})/(GI_p/\overline{J^{tt}}) \qquad \text{(III.66)}$$

c_3 is proportional to the ratio of the velocities of propagation of flexural to torsional waves and it is a very small number for typical risers. In fact, since $c_1^2 = O(\hat{\varepsilon}^2)$, we find that $c_3^2 = O(\hat{\varepsilon}^{2-p})$ where ε is considered quantity of $O(\hat{\varepsilon}^p)$ with $0 \leq p \leq 1$. Values of p close to zero correspond to medium length buoyed risers with typical values of μ (i.e. 4-5). Values of p close to one correspond to long or medium length but highly tensioned risers (e.g. risers with $\mu < 1$). The time scales of the hydrodynamic moment $M^{H\zeta}$ (caused e.g. from an oscillating wake) are typically large enough to coincide with the time scales of resonant flexural oscillations, which are very long compared to the time scales of resonant torsional oscillations. Furthermore, the magnitude of the term $(1+\nu)\varepsilon^{-1}M^{H\zeta} = (1+\nu)L^2M'^{H\zeta}/EI$, where $M'^{H\zeta}$ is the dimensional hydrodynamic moment per unit length about the $\hat{t}$ axis is expected to be small,

because $M'^{H\zeta}$ is small. This discussion shows that torsional oscillations can be treated quasistatically, i.e. equation (III.65) can be effectively replaced by:

$$\Omega_s^{\zeta} \simeq 0 \qquad \text{(III.67)}$$

more precisely by $\Omega_s^{\zeta} = O(\hat{\varepsilon}^{2-p}, \hat{\varepsilon}^{-p} M^{H\zeta})$. Equations (II.25) and (III.67) and boundary condition (II.96) imply that or that

$$f_{ZZ} \simeq -\tau_Z \qquad \text{(III.68)}$$

Therefore, using boundary conditions (II.96) and (II.100), the angle f between $\hat{n}$ and $\hat{n}$ is given by:

$$f(t,Z) \simeq -\int_0^Z \tau(t,Z')dZ' \qquad \text{(III.69)}$$

The errors of equation (III.68) and (III.69) are of the same order as the error of equation (III.67). The fact that $\Omega^{\zeta}\simeq 0$, was verified in the experiment described in Chapter V of this thesis using a riser type flexible model.

Using the fact that $\Omega^{\zeta}\simeq 0$, equation (III.63) reduces to:

$$Q^b = \varepsilon\tau K + \Theta^n \qquad \text{(III.70)}$$

where the errors are of $O(\hat{\varepsilon}^3, \hat{\varepsilon} M^{H\zeta})$. It is interesting to compare this equation with (II.37).

Finally, equation (III.25) contains terms of O(1) expressing equilibrium of the vertical static forces. From equations (III.22), (III.24) we find that:

$$Pe(s,t) = Pe(Z,0) + \tilde{\varepsilon}/\tilde{\varepsilon}_o + w(Z,t)(W_m - B^*) + O(\tilde{\varepsilon}^2/\tilde{\varepsilon}_o) \quad \text{(III.71)}$$

and applying (III.25) in the condition of vertical static equilibrium we find that:

$$Pe(Z,0) = \mu Z + 1 \quad \text{(III.72)}$$

Assuming that $\tilde{\varepsilon}/\tilde{\varepsilon}_o = O(\hat{\varepsilon}^2)$, which we will verify a posteriori as consistent with the solutions of the simplified equations under the imposed boundary conditions, we find that:

$$Pe(s,t) = \mu Z + 1 + O(\hat{\varepsilon}^2) \quad \text{(III.73)}$$

Using equations (III.45)-(III.47), (III.54)-(III.59), (III.70), (III.64), (III.38), (III.26), and (III.27) we find that the leading order equations for the forces in the $\hat{n}$, $\hat{b}$ directions can be reduced to the following respectively:

$$-\varepsilon(K_{ZZ} - K\tau^2) + K(\mu Z + 1) + \mu K^{-1}(u_Z u_{ZZ} + v_Z v_{ZZ}) + f^n = K^{-1}(u_{tt}u_{ZZ} + v_{tt}v_{ZZ}) - \Delta^n \quad \text{(III.74)}$$

$$\varepsilon[(\tau K)_{ZZ} + \tau K_Z] - \mu K^{-1}(u_Z v_{ZZ} - v_Z u_{ZZ}) + f^b = K^{-1}(v_{tt}u_{ZZ} - u_{tt}v_{ZZ}) - \Delta^b \quad \text{(III.75)}$$

with errors of $O(\hat{\varepsilon}^3, \hat{\varepsilon} M^{H\zeta})$, where the structural damping

forces per unit length Δ^n, Δ^b were redefined to include the terms Θ_z^b, Θ_z^n.

Finally, equation (III.25) is also converted to the following leading order dynamic force equation in the $\hat{t}$ direction:

$$w_{zz}+ u_z u_{zz}+ v_z v_{zz}+(W_m-B^*-\mu)\tilde{\varepsilon}_o w_z+ \tilde{f}^t\tilde{\varepsilon}_o + \varepsilon K K_z \tilde{\varepsilon}_o = c_4^2(w_{tt}+ u_{tt}u_z+ v_{tt}v_z) - \Delta^t\tilde{\varepsilon}_o \qquad \text{(III.76)}$$

with errors of $O(\hat{\varepsilon}^4)$, where:

$$c_4^2 = \tilde{\varepsilon}_o A = (Pe(0,0)/\overline{m^n})/(EA^s/\overline{m^t}) \qquad \text{(III.77)}$$

The term c_4 is proportional to the ratio of the velocities of propagation of flexural to extensional waves and it is a very small number for typical risers. In fact, since A=O(1) and $\tilde{\varepsilon}_o$ can be considered as a quantity of $O(\hat{\varepsilon}^2)$ (see (III.11)), we find that $c_4^2 = O(\hat{\varepsilon}^2)$. In addition, the term $f^t\tilde{\varepsilon}_o$ is expected to be very small for typical risers and is assumed to be of $O(\hat{\varepsilon}^4)$. This discussion shows that extensional oscillations can be treated quasistatically compared to flexural oscillations (see also Stoker and Lubkin (1943) and Carrier (1943)) and equation (III.76) can be effectively replaced by :

$$w_{zz}+u_z u_{zz}+v_z v_{zz} = O(\hat{\varepsilon}^4) \qquad \text{(III.78)}$$

This relation in conjunction with boundary condition (III.34) implies that:

$$\tilde{\varepsilon} = w_Z + 1/2(u_Z^2+v_Z^2) = O(\hat{\varepsilon}^4) \qquad \text{(III.79)}$$

This verifies the assumption that $\dot{\tilde{\varepsilon}}/\tilde{\varepsilon}_o = O(\hat{\varepsilon}^2)$ and gives:

$$w(t,Z) = -\frac{1}{2}\int_0^Z [u_Z^2(t,Z')+v_Z^2(t,Z')]dZ' + O(\hat{\varepsilon}^4) \qquad \text{(III.80)}$$

which verifies the original assumption that $w = O(\hat{\varepsilon}^2)$ when $\hat{\varepsilon} << 1$.

Subsequently, equations (III.74) and (III.75) are combined to give the equations of forces in the X,Y directions. The contribution of the tangential dynamic force equation to the equations of forces in the X,Y directions can be shown to be of $O(\hat{\varepsilon}^3)$.

First, using the Frenet relations one may show that for i=1,2,3:

$$x^i_{ssss} = -\frac{3}{2}(K^2)_s\alpha^i+(K_{ss}-K^3-K\tau^2)\beta^i-[(K\tau)_s+\tau K_s]\gamma^i \qquad \text{(III.81)}$$

where K is given by (II.7), (Eisenhart, (1947)).

Using (II.72), we find that for any vector $\underline{\lambda} = (\lambda^X, \lambda^Y, \lambda^Z)\underline{U} = (\lambda^n, \lambda^b, \lambda^t)\underline{U}'$ the following relations are valid:

$$\lambda^X = \beta^1\lambda^n + \gamma^1\lambda^b + \alpha^1\lambda^t \qquad \text{(III.82)}$$

$$\lambda^Y = \beta^2\lambda^n + \gamma^2\lambda^b + \alpha^2\lambda^t \qquad \text{(III.83)}$$

$$\lambda^Z = \beta^3\lambda^n + \gamma^3\lambda^b + \alpha^3\lambda^t \qquad \text{(III.84)}$$

Equation (III.81) implies that

$$u_{ZZZZ} = (K_{ZZ}-K\tau^2)\beta^1 - [(K\tau)_Z+\tau K_Z]\gamma^1+O(\hat{\varepsilon}^3) \qquad \text{(III.85)}$$

$$v_{zzzz} = (K_{zz} - K\tau^2)\beta^2 - [(K\tau)_z + \tau K_z]\gamma^2 + O(\hat{\varepsilon}^3) \quad \text{(III.86)}$$

Using (III.82)-(III.86) and the estimates of α^i, β^i, γ^i (i=1,2,3) given by (III.42)-(III.44), (III.54)-(III.59), equations (III.74) and (III.75) can be combined to give:

$$-\varepsilon u_{zzzz} + [(\mu z+1)u_z]_z + f^X = u_{tt} - \Delta^X \quad \text{(III.87)}$$

$$-\varepsilon v_{zzzz} + [(\mu z+1)v_z]_z + f^Y = v_{tt} - \Delta^Y \quad \text{(III.88)}$$

where the errors are small, more precisely of $O(\hat{\varepsilon}^3, \hat{\varepsilon}M^{H\zeta})$ and f^X, f^Y are the hydrodynamic forces per unit length in the X, Y directions and Δ^X, Δ^Y are structural damping forces. Boundary conditions (II.93), (II.94), (II.97), (II.98) give to the same degree of approximation:

$$u(0,t)=v(0,t)=u_{zz}(0,t)=v_{zz}(0,t)=u_{zz}(1,t)=v_{zz}(1,t)=0 \quad \text{(III.89)}$$

$$u(1,t) = g^1(t), \qquad v(1,t) = g^2(t) \quad \text{(III.90)}$$

The structural dissipation mechanism can be described by an expression which allows variation of the dissipation level as a function of the excited modes and is linear with respect to the velocity of each mode. This simple model is expected to give reliable information about the global influence of the structural dissipation mechanism for relatively small amplitudes of flexural oscillations. The structural dissipation force per unit length in the X

direction can be written as:

$$\Delta^X = \sum_{n=1}^{\infty} c_n \phi_n(Z)\, u_t^n(t) \qquad \text{(III.91)}$$

where c_n is the non-dimensional structural damping coefficient of the nth mode, $\phi_n(Z)$ is the nth eigenfunction defined by:

$$-\varepsilon\phi_n'''' + [(\mu Z+1)\phi_n']' + \sigma_n^2\phi_n = 0 \qquad \text{(III.92)}$$

$$\phi_n(0) = \phi_n(1) = \phi_n''(0) = \phi_n''(1) = 0 \qquad \text{(III.93)}$$

where σ_n is the nth eigenvalue, ()' denotes derivative with respect to Z and $u^n(t)$ is related to the total dynamic response in the X direction $u_d(Z,t)$ by:

$$u_d(Z,t) = Zg_d^1(t) + \sum_{n=1}^{\infty} \phi_n(Z)u^n(t) \qquad \text{(III.94)}$$

where $g_d^1(t)$ is the dynamic part of $g^1(t)$. Similar relations are valid for Δ^Y. The non-dimensional damping coefficient c_n is related to the dimensional structural damping coefficient c_n' by:

$$c_n = c_n' L[\overline{m^n Pe}(0,0)]^{-1/2}\ ,\ n=1,2,.. \qquad \text{(III.95)}$$

It is understood that the structural damping force per unit length is the smaller component of the total damping force per unit length.

III.3 BASIC CHARACTERISTICS OF THE LEADING ORDER EQUATIONS

Equations (III.87), (III.88) under boundary conditions (III.89)-(III.90) are the basic equations used in subsequent parts of this thesis. These equations, even though linear as far as their structural stiffness and inertia terms are concerned, are non-linear coupled partial differential equations due to the non-linear dependence of the exciting hydrodynamic forces f^X, f^Y on both flexural responses. As we have seen in the previous section, the solutions of these leading order equations describing the flexural response can be used to estimate the extensional response to its leading order. The same is true for the torsional response, which as we saw, is very small. It is also important to note that the leading order flexural response is essentially independent of both extensional and torsional responses under the basic assumptions of the previous and present chapter.

Equations (III.87) and (III.88) under boundary conditions (III.89), (III.90) and suitable initial conditions describe forced biharmonic oscillations in two perpendicular planes. For long or medium length but highly tensioned risers, we have seen that ε is typically a small number. For $\varepsilon << 1$, a dominant balance argument, (Carrier

and Pearson, (1968)), reveals that the bending terms are of equal importance as the tension terms only over short edge (or boundary) layers close to Z=0 and Z=1 of width $O(\varepsilon^{1/2})$ from each edge. For this case of localized rapid variation, simple boundary layer theory can be used to construct uniform in Z approximations of the solutions of (III.87), (III.88) for given forces f^X, f^Y. These approximations are expected to work well for a fixed excited wavelength as $\varepsilon \to 0$. They include: a) A component slowly varying in space. b) Two exponentially evanescent parts, when moving away from the ends toward the middle of the rod. These are important within distances of $O(\varepsilon^{1/2})$ from each end.

Approximations of this form are not expected to work well for higher modes, for which the solution has a rapidly oscillatory behavior over the whole space from Z=0 to 1. For this case, bending effects tend to become at least as important as the effects of the effective tension over the whole length of the riser. WKB theory (Bender and Orszag, (1978)) can be effectively used to construct uniform in Z approximations of the solution for the case of a highly oscillatory behavior in space. It is understood that WKB theory requires linearized dependence of the hydrodynamic forces on the response. This is not required by boundary layer theory.

Both methods, if appropriately used, provide simple and useful approximations of the solutions of (III.87) and (III.88) under boundary conditions (III.89) and (III.90) for

given forces f^X and f^Y.

Chapter IV

A THEORETICAL PROCEDURE FOR THE PREDICTION OF THE DYNAMIC RESPONSE OF A MARINE RISER

IV.1 INTRODUCTION

The solution of equations (III.87) and (III.88) requires the explicit modelling of the local hydrodynamic force. For a number of idealized excitation conditions, there exists information from rigid cylinder experiments that allows the formulation of an approximate mathematical model for the local hydrodynamic force. Such experiments may be subdivided into two broad categories. The first category involves measurements of the hydrodynamic force acting on rigid cylinders in an a priori defined flow. A model for the local hydrodynamic force derived from such experiments, even though approximate, provides a useful insight into the dynamic behavior of risers in an efficient manner. However, as it is apparent from the definition of rigid cylinder experiments, such a model implies the following assumptions:

1. Any force component measured in a rigid cylinder experiment which will make a flexible cylinder respond in a different form than the one used to

conduct the rigid cylinder experiment must be neglected.

2. Rigid cylinder experiments cannot provide information on the spanwise correlation of local hydrodynamic forces.

The second category of rigid cylinder experiments involves cylinders which are mounted on elastic springs and dashpots. These experiments attempt to relate force to response of different form than the imposed motion by representing the flexible cylinder with an idealization which has only a small number of degrees of freedom and by allowing the idealized system to respond to the force it experiences. The response in existing spring mounted rigid cylinder experiments is a one degree of freedom translation.

In order to provide a quantitative estimate of the limitations of theoretical estimates of the response of a riser based on rigid cylinder experiments, we conducted experiments using a flexible riser type cylindrical model. The results of these experiments are presented in the last two chapters of this thesis. The difference between the response of the flexible system and its theoretical

estimate based on rigid cylinder results is due to hydroelastic and correlation length effects. The term hydroelastic effects, as used in this thesis, denotes the impact of the motion of the flexible cylinder upon the local hydrodynamic force. The term correlation length denotes the extent of two-dimensionality of the flow in a flexible cylinder. Correlation length effects are coupled with hydroelastic effects because the extent of two-dimensionality of the flow around a flexible cylinder depends also upon its motion.

This chapter continues by providing a brief description of the environmental excitations likely to govern the global dynamic behavior of risers in normal operating conditions. This is followed by a review of the main rigid cylinder experimental results from which a model for the local force acting on risers has been derived for a number of idealized excitation conditions. This review also includes an analysis of the usefulness and the limitations of such experiments. Finally, four idealized excitation conditions are employed to illustrate how to use rigid cylinder experimental results to estimate the static and dynamic response of marine risers. These examples also help us identify areas in which the limitations of rigid cylinder experimental results are likely to be magnified.

IV.2 BRIEF DESCRIPTION OF THE ENVIRONMENT

The exciting forces governing the global dynamic behavior of risers, in normal operating conditions, arise from currents, surface and internal waves and the motion of the upper end.

a) Currents: The current speed, variation with time and vertical distribution is very much site dependent. In general, the current speed changes very slowly in time so it can be treated quasistatically for the purpose of our analysis. Time averaged current speeds can range anywhere from zero to two knots or even higher. The current speed attenuates to practically zero with depth at a rate which is site dependent. Design values for these parameters for the Florida current may be found in Richardson, Schmitz, and Niiler (1969) and Lee, Brooks and Düing (1977). Using typical values for current speed and vertical current profile, preliminary calculations show that a current can exert significant static and dynamic forces on the riser.

b) Surface Waves: They are best described by a mean square spectrum $S(\omega,\theta)$, which is a function of frequency ω and direction of propagation θ. Surface waves have a twofold impact on the riser:

1. They exert forces through the supporting platform, which responds dynamically and gives rise

to a motion of the top end of the riser.

2. They exert steady and unsteady forces on the upper part of the riser directly.

Typical values for the range of ω and estimates for the value of $S(\omega,\theta)$ can be found in Hogben and Lumb (1967) and Hogben (1974). Suggestions for analytic expressions for $S(\omega,\theta)$ can be found in Chryssostomidis and Oakes (1974).

c) Internal Waves: Their generation requires special conditions so their occurrence is not as frequent as that of surface waves. Their generation and propagation characteristics are described, for example, in Phillips (1980). The maximum particle speeds associated with waves of this form are comparable to that of surface currents, see, for example, Boyce (1975) and Osborne et al (1977), while their wavelengths are of the order of a few kilometers. Their frequencies are low compared to the frequencies of surface gravity waves. Horizontal particle velocities due to internal waves decay slowly from the maximum value occurring at the main thermocline and reverse sign across its surface. The property of slow decay of particle velocities below the main thermocline might be of concern for drilling operations both in moderate and deep water. The above discussion shows that internal waves can be treated as currents for the purpose of our analysis.

d) Top End Motion: The motion of the supporting platform includes two components:

1. A fast small amplitude first order component at the frequencies of the incident surface waves.
2. A slow amplitude component due to the wave second order drift forces, the wind and ocean currents. To permit actual operations, the slow component of motion is kept within appropriate bounds by the action of the dynamic positioning and/or the mooring system of the supporting platform. For a discussion of this subject, see Triantafyllou (1979) and (1982).

Order of magnitude calculations show that the spectrum of the exciting forces overlaps with the frequency range of the dynamic response of typical risers. Therefore, dynamic effects must be considered in the design procedure. Because of the virtually unknown non-linear dependence of the local hydrodynamic force upon both the outside excitation and the riser's own motion, excitation from currents, surface waves, and the motion of the top end must be treated simultaneously.

Existing rigid cylinder experiments may be used to provide insight into the dynamic behavior of risers for a limited number of idealized excitation conditions. The basic idealization employed in rigid cylinder experiments is the replacement of a random wave field or oscillatory

motion of a cylinder by a single sinusoid. Experiments using such an idealization have a relatively good resolution with respect to some of the most important non-dimensional parameters. For the case where the sinusoid motion is combined with a current, only the cases where the direction of sinusoid motion is parallel or orthogonal to the current have been investigated in detail.

IV.3 A REVIEW OF RIGID CYLINDER EXPERIMENTS

IV.3.1 INTRODUCTION

As stated at the beginning of this Chapter, information derived from rigid cylinder experiments provides a useful insight into the dynamic behavior of risers because it permits an explicit modelling of the local hydrodynamic force. The review of rigid cylinder experiments developed in this section provides the necessary background needed to develop such a model; in understanding its limitations when used to predict the response of a flexible cylinder; and in identifying areas in which such limitations may be significant.

Rigid circular cylinder experimental results useful for the prediction of the local hydrodynamic force in single tube risers are associated with the following

types of idealized flows:

- Uniform stream orthogonal to the axis of a fixed rigid cylinder.
- Harmonic stream orthogonal to the axis of a fixed rigid cylinder.
- Flow created by harmonic oscillation of a rigid cylinder orthogonal to its axis and at a certain angle with respect to a uniform stream flowing orthogonally to the axis of the cylinder.
- Flow created by the dynamic response of a rigid, flexibly mounted, cylinder in a uniform stream orthogonal to its axis.
- Flow created by the dynamic response of a rigid, flexibly mounted, cylinder in a harmonic stream orthogonal to its axis and to the plane of the response motion.

A brief review of the main experimental works investigating such types of flow are presented in the following five articles.

IV.3.2 UNIFORM STREAM ORTHOGONAL TO A FIXED RIGID CIRCULAR CYLINDER

This type of flow has been studied, for example, by Roshko (1953), (1954), (1961), Bishop and Hassan (1964a), Achenbach (1968), (1971), Jones et al (1969). The non-dimensional hydrodynamic force per unit length for

this type of flow depends upon: the Reynolds number, $Re=V_c D/\nu$; the roughness ratio, k/D; the aspect ratio, $\lambda = L/D$, (together with the end geometry); and the non-dimensional time, $\tau = V_c\, t/D$, where V_c is the stream velocity far from the cylinder, D, L, the cylinder diameter and length respectively, k a typical roughness height, and ν the kinematic viscosity of the fluid. A brief review of the flow changes around a smooth rigid circular cylinder as the Reynolds number increases is given below (see also Bernitsas (1979b).

a) $Re<<1$: The flow is symmetric both in the upstream-downstream and in the left and right directions.
b) $Re\approx 4$: The upstream-downstream symmetry is lost. Two vortices appear behind the cylinder which remain attached up to Re=40 (Tritton, (1977)).
c) $40<Re<150$: The symmetry about the diameter of the cylinder parallel to the incident stream is also lost. Vortices are generated alternatively from the two sides of the cylinder and form an antisymmetric pattern known as the Karman street. The Strouhal number, defined by $St=f_s D/V_c$, where $f_s = 1/T_s$ and T_s is the period of shedding of a pair of vortices varies approximately between 0.12 and 0.17 and is a characteristic property of the flow. Compiled experimental results for the Strouhal number as a function of Reynolds number is shown in Figure 2, borrowed from Chen (1973). The average drag coefficient, c_D,

defined as c_D = average drag/$0.5\rho DV_c^2$, where ρ is the density of the fluid, decreases approximately from 1.67 to 1.28 as the Reynolds number increases. A complete picture of the average drag coefficient c_D as a function of Reynolds number is given in Figure 3, borrowed from Bishop and Hassan (1964a). This picture also includes some experimental data for the inverse of the Strouhal number and the maximum lift coefficient as a function of Re number, defined as c_L=maximum amplitude of the hydrodynamic force orthogonal to the stream/$0.5\rho DV_c^2$. An extensive compilation of experimental results for c_L as a function of Re number is shown in Figure 4, borrowed from Chen (1973).

d) $150<Re<400$: This is the so-called Tritton transition region, in which the flow loses its regularity. The Strouhal number exhibits some scatter and the flow in the vortex turns from laminar to turbulent. The average drag coefficient is a decreasing function of Reynolds number reaching 1.12 around Re=400, see Figure 3.

e) $400<Re<3\times10^5$: The flow becomes regular again and the Strouhal number takes an almost constant value approximately equal to 0.21. The drag coefficient continues to be a decreasing function of Re up to Re=2100, where it reaches the value of 0.9. After that point it increases slowly with Reynolds reaching a value = 1.2 at Re=21000, after which it remains constant until approximately $Re=3\times10^5$, see Figure 3.

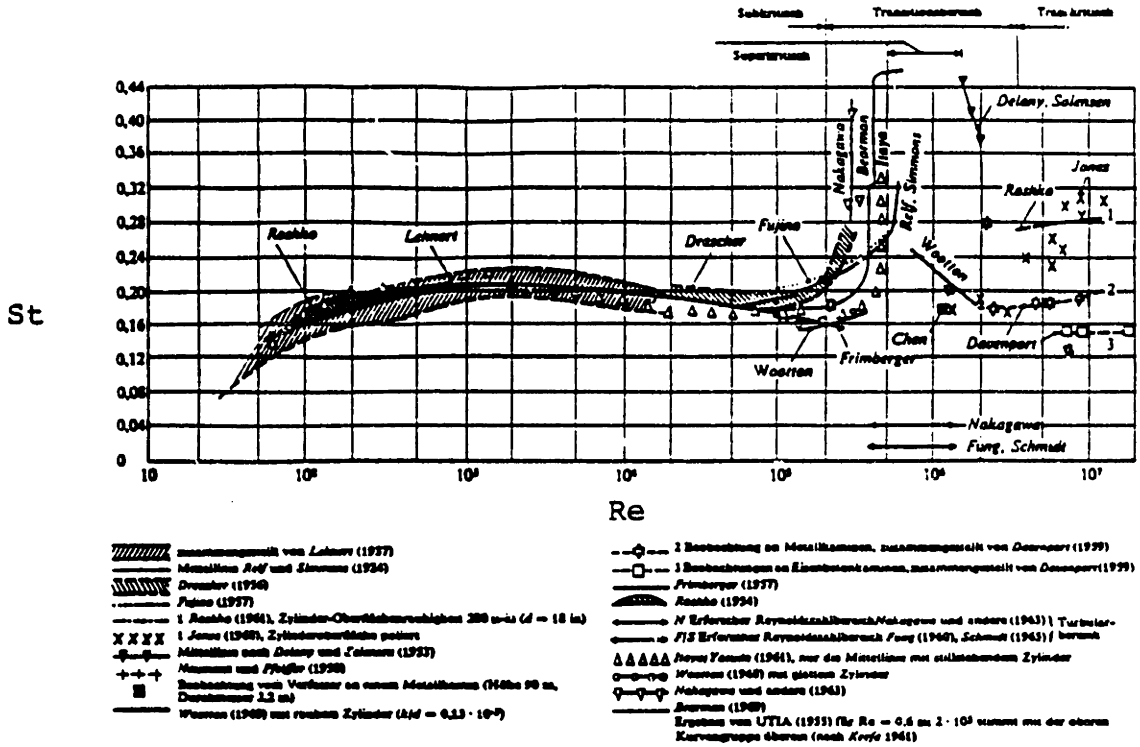

FIGURE 2: Strouhal Number, St, Versus Reynolds Number, Re, for a Uniform Stream Orthogonal to a Fixed Rigid Circular Cylinder, Chen (1973).

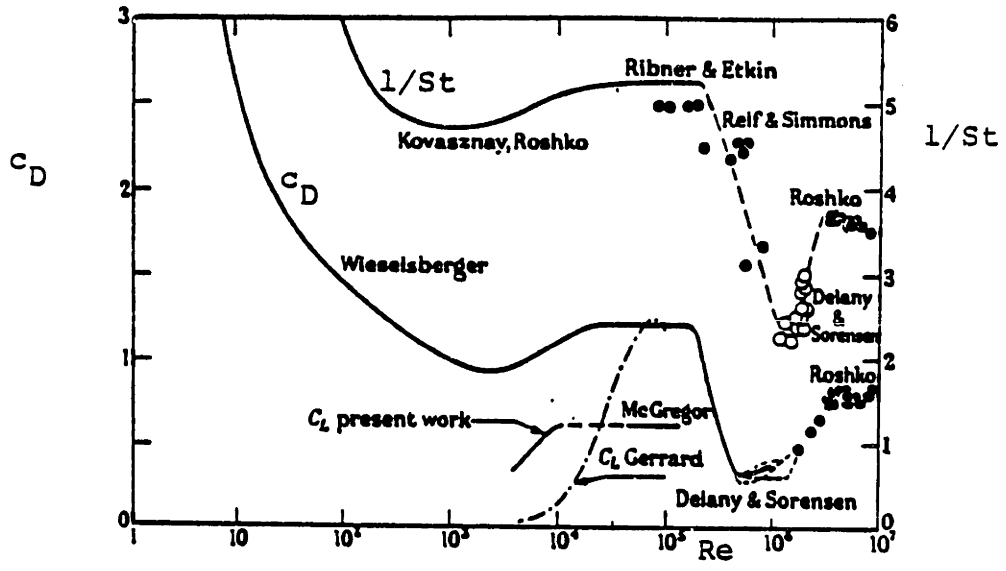

FIGURE 3: Average Drag Coefficient, c_D, Maximum Lift Coefficient, c_L, and Strouhal Number, St, Versus Reynolds Number for a Uniform Stream Orthogonal to a Fixed Rigid Circular Cylinder, Bishop and Hassan (1964a).

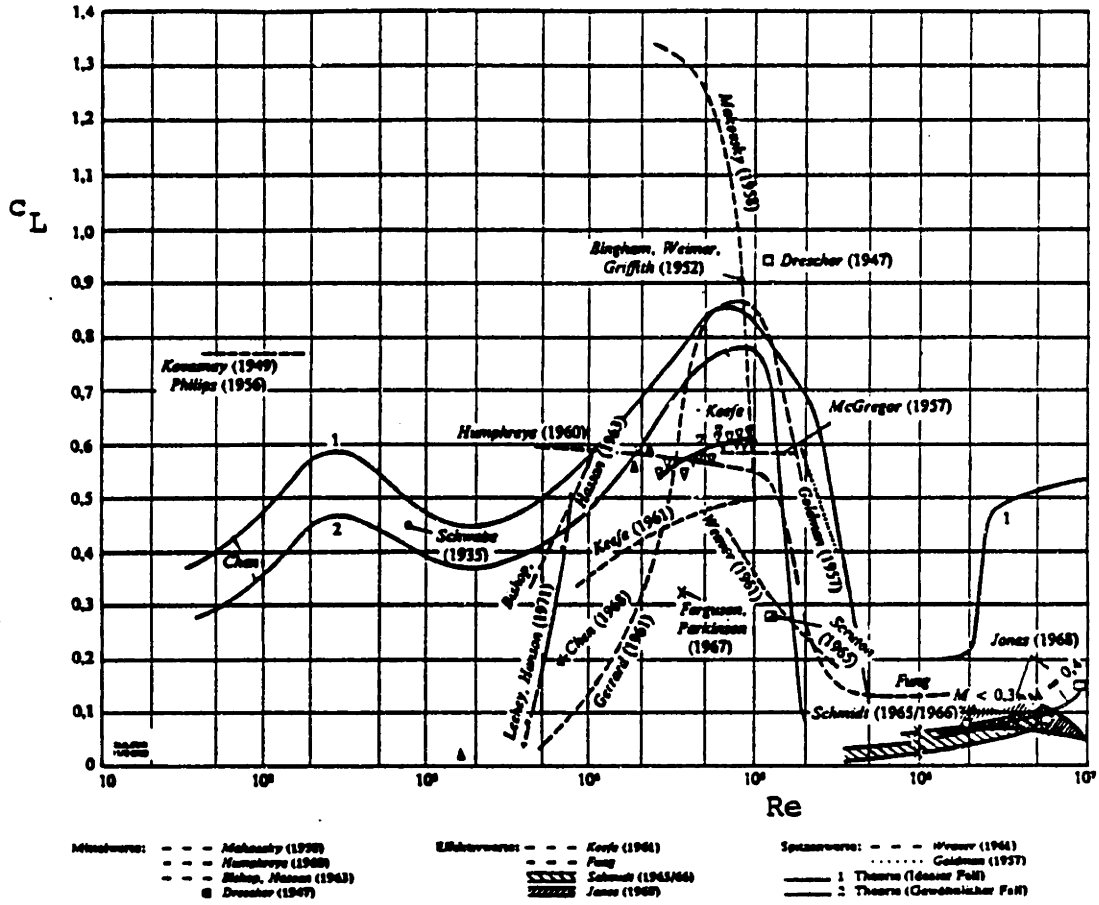

FIGURE 4: Maximum Lift Coefficient, c_L, Versus Reynolds Number for a Uniform Stream Orthogonal to a Fixed Rigid Circular Cylinder, Chen (1973).

f) $3x10^5 < Re < 5x10^5$: This is a critical regime in which the flow loses its regularity and becomes fully turbulent around $5x10^5$. The point of separation moves to the rear face of the cylinder with significant decrease in the average drag coefficient which reaches a minimum value ≈ 0.35 at $Re \approx 5x10^5$.

g) $Re > 5x10^5$: The flow is fully turbulent and the drag coefficient in this region is smaller than the drag coefficient of the subcritical regime, increasing slowly from 0.35 at $Re=5x10^5$ to 0.80 around $Re=3.2x10^6$ after which it remains constant. There is appreciable scatter in the experimental data concerning the lift force and Strouhal number for $Re > 3x10^5$, see Figures 4 and 2. This may be partially explained from three-dimensionality effects.

For subcritical Reynolds numbers, the lift and oscillatory drag forces have an almost periodic character with circular frequencies $\omega_s = 2\pi f_s$ and $2\omega_s$ respectively. For higher Reynolds numbers, a spectral description of the oscillatory lift and drag forces is required. A complete account of experimental and theoretical results for this type of flow is given in Chen (1973).

IV.3.3 HARMONIC STREAM ORTHOGONAL TO A FIXED RIGID CYLINDER

This type of flow has been studied, for example, by Keulegan and Carpenter (1958) and Sarpkaya (1977b). The non-dimensional hydrodynamic force per unit length for this type of flow depends upon: the Reynolds number, $Re = \omega SD/\nu$; the Keulegan-Carpenter number, $KC = 2\pi S/D$; the roughness ratio, k/D; the aspect ratio, $\lambda = L/D$, (together with the end geometry); and the non-dimensional time, $\tau = \omega t$, where ω, S are the circular frequency and amplitude of harmonic motion of a cylinder with diameter D. If the cylinder is stationary, then $S = U_m/\omega$ where U_m is the maximum velocity of the incident harmonic stream U(t) far from the cylinder, with $U(t) = U_m \cos(\omega t)$. The above investigators measured hydrodynamic forces acting on moderate aspect ratio cylinders. The experimental procedure used by all investigators mentioned above provided a measurement of the overall force. Therefore, the hydrodynamic force per unit length reported in the above works corresponds to a spanwise average hydrodynamic force. Further, they provided no information to determine the degree of spanwise correlation of the hydrodynamic force.

Keulegan and Carpenter (1958) performed pioneer

research on this type of flow. They measured and analyzed the hydrodynamic force acting on a cylinder parallel to an incident harmonic stream and have shown that it exhibits a strong dependence upon the ratio of a representative amplitude of fluid motion to the diameter. Sarpkaya (1977b) explained the scatter of the experimental results for the above force by assessing the importance of Reynolds number and roughness ratio. Both investigators have used an equation introduced by Morison et al (1950) to represent the hydrodynamic force F_X parallel to the stream of the form:

$$F_X(t) = c_M \rho A_o U_t + 0.5 c_d \rho D\, U|U|$$

where subscript t denotes derivative with respect to time, $A_o = \pi D^2/4$ and c_M, c_d are inertia and drag coefficients respectively. These are functions of the non-dimensional parameters listed above. Fourier representations of c_M and c_d were introduced and it was found that keeping the time average values of c_M and c_d gave a satisfactory agreement between the force calculated using the above equation and the instantaneous force measured experimentally, except in the range of Keulegan-Carpenter numbers between 6 and 20. In this range of KC, the error between the maximum calculated and measured force can be as large as 12%, Sarpkaya (1975). This is a region of "drastic change", coinciding with shedding of the first few vortices within one cycle, see Bernitsas (1979b). Experimental results for the time average values of c_M and

c_d for smooth cylinders as a function of Re and KC numbers are given in Figures 5 and 6, respectively, borrowed from Sarpkaya (1977b).

Sarpkaya (1977b) also gave estimates of the maximum lift, the force orthogonal to the stream, by presenting the lift coefficient c_L = maximum amplitude of lift force per unit length/$0.5\rho DU_m^2$ as functions of Re, KC numbers. A plot of the maximum lift coefficient for smooth cylinders with respect to the KC number parametrically with respect to Re number is shown in Figure 7, borrowed from Sarpkaya (1977b). This Figure also includes the dependence of c_L upon the frequency parameter defined by $\beta=fD^2/\nu$, where $f = \omega/2\pi$, which could replace Re in the presentation of results. The resulting maximum lift forces are as large as the hydrodynamic forces parallel to the direction of oscillation. Lift forces are particularly large in the range of "drastic change" defined above. Maximum measured lift coefficients reached values as high as 3.7 in the KC range between 6 and 20. In addition, Sarpkaya gave estimates of the ratio f_r of the shedding frequency divided by the oscillation frequency as a function of Re and KC numbers, see Figure 8 (from Sarpkaya (1977b)), and recognized the random character of the lift force.

These results show that, depending on the KC number, the basic spectral character of the lift forces

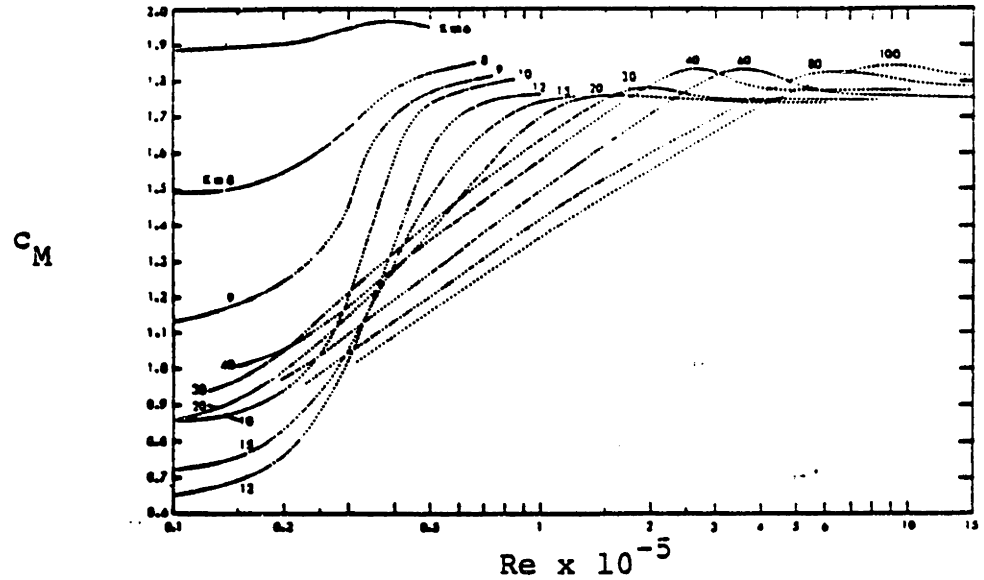

FIGURE 5: Time Averaged Inertia Coefficient, c_M, Versus Reynolds Number Parametrically with Respect to Keulegan-Carpenter Number, K, for a Harmonic Stream Orthogonal to a Fixed Rigid Smooth Circular Cylinder, Sarpkaya (1977b).

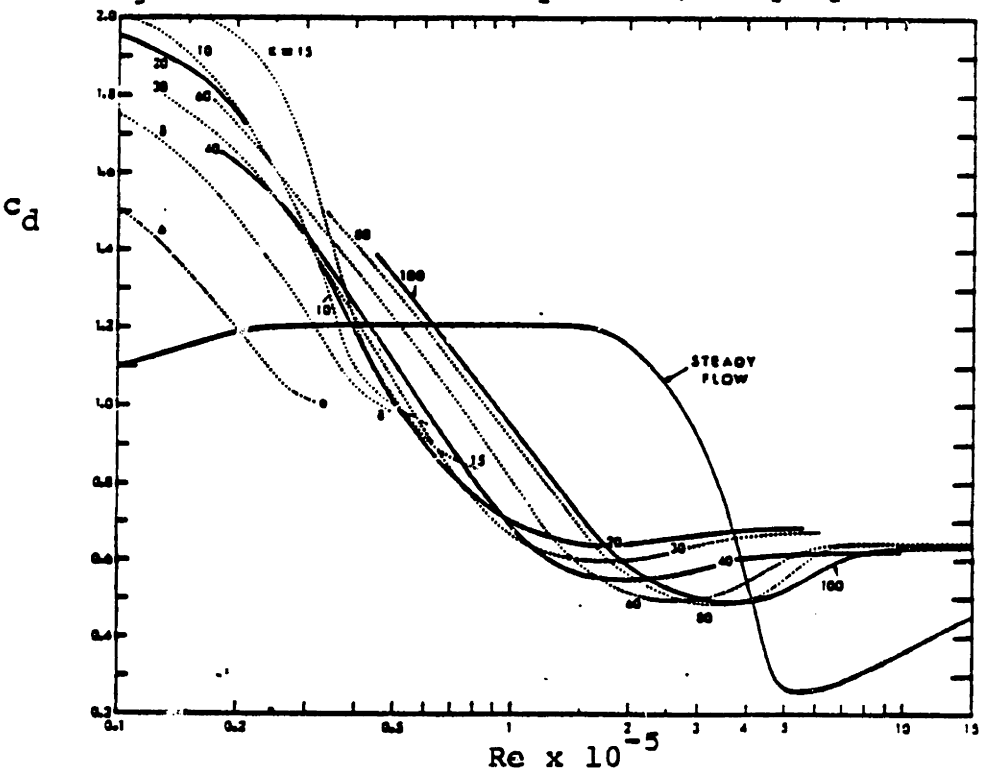

FIGURE 6: Time Averaged Drag Coefficient, c_d, Versus Reynolds Number Parametrically with Respect to Keulegan-Carpenter Number, K, for a Harmonic Stream Orthogonal to a Fixed Rigid Smooth Circular Cylinder, Sarpkaya (1977b).

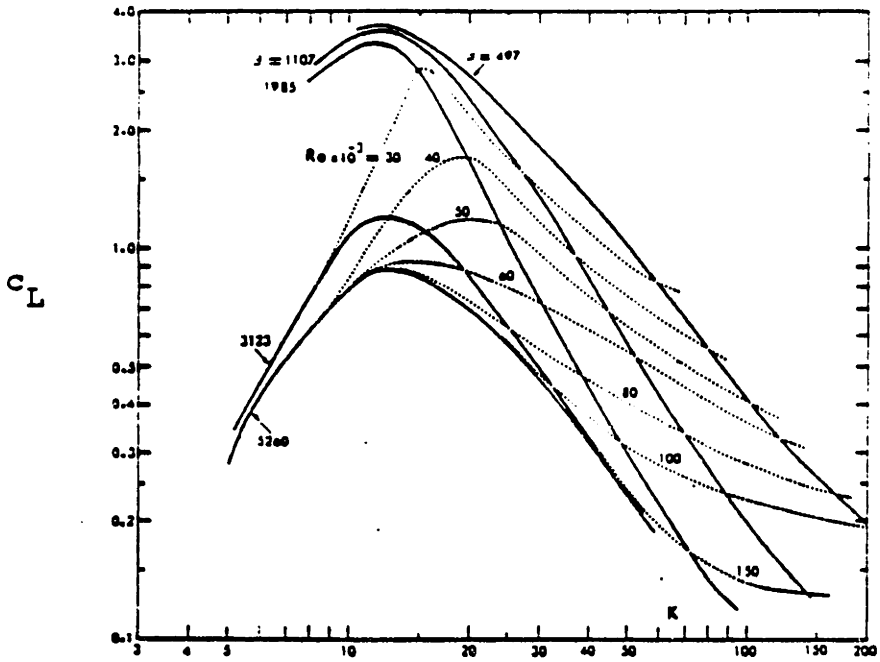

FIGURE 7: Maximum Lift Coefficient, C_L, Versus Keulegan-Carpenter Number, K, Parametrically with Respect to Reynolds Number for a Harmonic Stream Orthogonal to a Fixed Rigid Smooth Circular Cylinder, Sarpkaya (1977b).

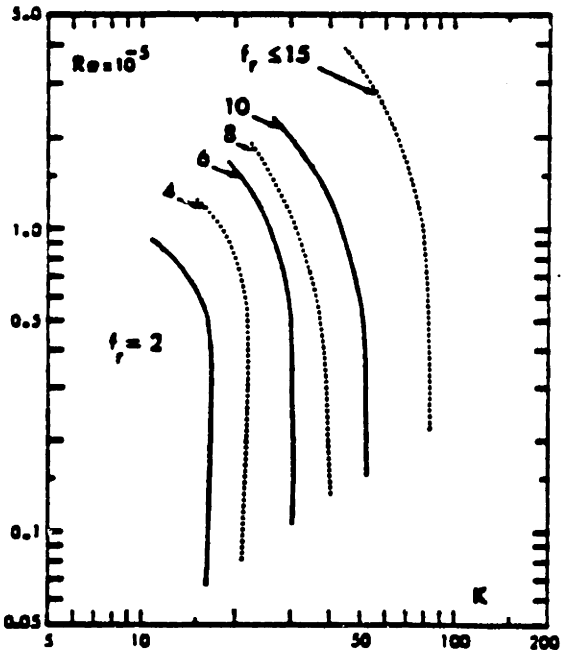

FIGURE 8: Ratio f_r of the Shedding Frequency Divided by the Oscillation Frequency as a Function of the Keulegan-Carpenter Number, K, and the Reynolds Number for a Harmonic Stream Orthogonal to a Fixed Rigid Smooth Circular Cylinder, Sarpkaya (1977b).

remains unchanged for quite disparate Reynolds numbers. For the smaller KC number tested (≈6), this is true for Re between $5x10^3$ and $6x10^4$ and as the KC number increases, this range extends and reaches $Re=3x10^5$ around KC≈80. The maximum lift coefficient is a decreasing function of Reynolds number reaching values≈0.6 for $Re\approx10^5$ for the smaller KC numbers (10-20). This value decreases to 0.2 for $Re\geq2x10^5$ and KC≈100. Finally, the reader is reminded that there is no assurance about the degree of spanwise correlation of the results. This is due to the measurement procedure as explained earlier. Such effects could have an impact on the maximum sectional hydrodynamic force experienced by a rigid cylinder.

IV.3.4 HARMONIC OSCILLATION OF A RIGID CYLINDER AT A CERTAIN ANGLE WITH RESPECT TO AN INCIDENT UNIFORM STREAM, BOTH ORTHOGONAL TO THE AXIS OF THE CYLINDER

This type of flow has been studied, for example, by Bishop and Hassan (1964b), Mercier (1973), Sarpkaya (1977a), Bernitsas (1979a, 1979b), Verley and Moe (1979) and Moeller and Leehey (1982). The non-dimensional hydrodynamic force per unit length depends upon: the Reynolds number, $Re=V_cD/\nu$; the amplitude ratio, $\alpha=S/D$; the reduced velocity (or frequency) of oscillation, $U^*=V_c/fD$, where $f=\omega/2\pi$; the angle of oscillation θ with

respect to the stream; the aspect ratio, $\lambda = L/D$, (together with the end geometry); the non-dimensional roughness ratio, k/D; and the non-dimensional time, $\tau = \omega t$.

Bishop and Hassan (1964b) were the first to conduct experiments of this type with $\theta = 90$ degrees. They demonstrated the possibility of the lock-in phenomenon and the impact of three-dimensionality effects on the character of the forces.

Mercier (1973) studied large amplitude harmonic oscillation of a smooth rigid cylinder at $\theta = 0$ and $\theta = 90$ degrees with respect to a uniform incident stream and gave an analysis of the overall hydrodynamic forces parallel and orthogonal to the stream. Mercier was mainly interested in the dependence of the hydrodynamic forces upon the reduced velocity and amplitude of oscillation. In his experiments, Mercier varied the value of S/D for $\theta = 0$ degrees between 0.3 and 3, while for $\theta = 90$ degrees between 0.3 and 2.5. The value of U* was varied between 0 and 10 and the value of Re between 4000 and 32000, with most experiments performed at Re=8000. The values of λ used in his experiments were 7 and 14. In addition, circular plates were attached to the ends of his model. For the case of $\theta = 90$ degrees, coefficients for the hydrodynamic forces parallel to the oscillation are given for values of S/D between 0.3 and 1.3 only. Systematic

presentation of the results as a function of Reynolds number was not always made. However, he reported that the differences between results at different Re are, for the most part, larger than the scatter of the data for a particular Re. The most important of his results are summarized below.

a) The average drag coefficient, defined as c_D=average drag/$0.5\rho DV_c^2$, is larger than the one measured in an experiment with the same current but no oscillation and is a function of S/D, U* and θ at least.

b) For θ=90 degrees, the oscillatory drag coefficient, c_d, defined as c_d = amplitude of the drag force parallel to the oscillation/$0.5\rho D\omega^2S^2$, is negative around U*=5 and for S/D less than about one, indicating a lock-in situation, see Figure 9 borrowed from Mercier (1973). The inertia coefficient c_M, defined as c_M=amplitude of inertia force/$(\rho A_o\omega^2S)+1$, exhibits substantial fluctuations around U*=5 and S/D less than about one, see Figure 10 borrowed from Mercier (1973). The non-dimensionalization of the force parallel to the oscillation with respect to the amplitudes of the oscillatory velocity and acceleration accentuates the sharpness of the variation of c_M and c_d for small S/D. A picture of the average drag coefficient c_D for θ=90 degrees is given in Figure 11, Mercier (1973). For frequencies of oscillation which are sufficiently below the Strouhal frequency, determined from Figure 2, the roll

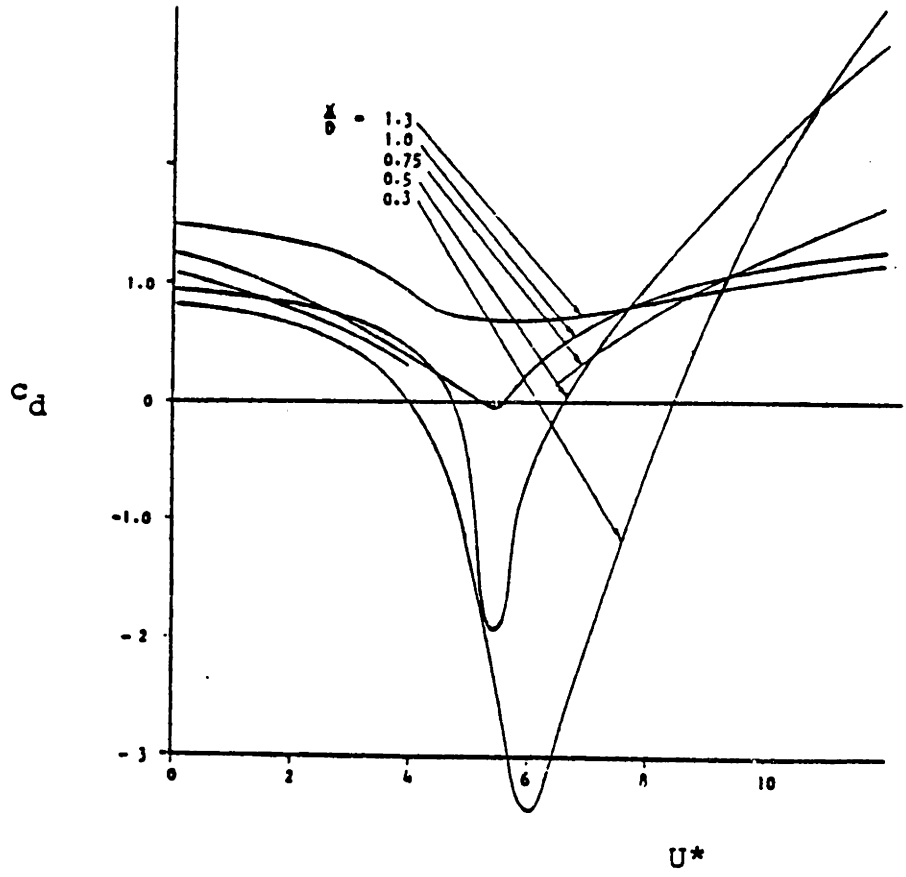

FIGURE 9: Drag Coefficient c_d = Amplitude of Drag Force Parallel to the Oscillation / $0.5\rho D\omega^2 x^2$ as a Function of U* Parametrically with Respect to the Non-Dimensional Amplitude x/D for Harmonic Oscillation at θ=90 Degrees with Respect to a Current, Mercier (1973).

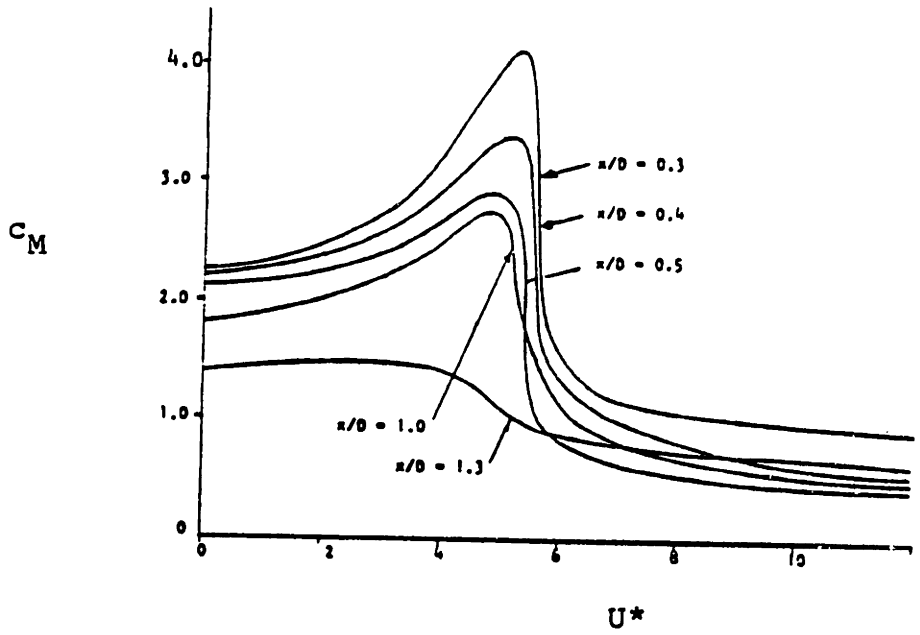

FIGURE 10: Inertia Coefficient c_M = Amplitude of Inertia Force/$\rho A_o \omega^2 x+1$ as a Function of U* Parametrically with Respect to the Non-Dimensional Amplitude x/D for Harmonic Oscillation at θ=90 Degrees with Respect to a Current, Mercier (1973).

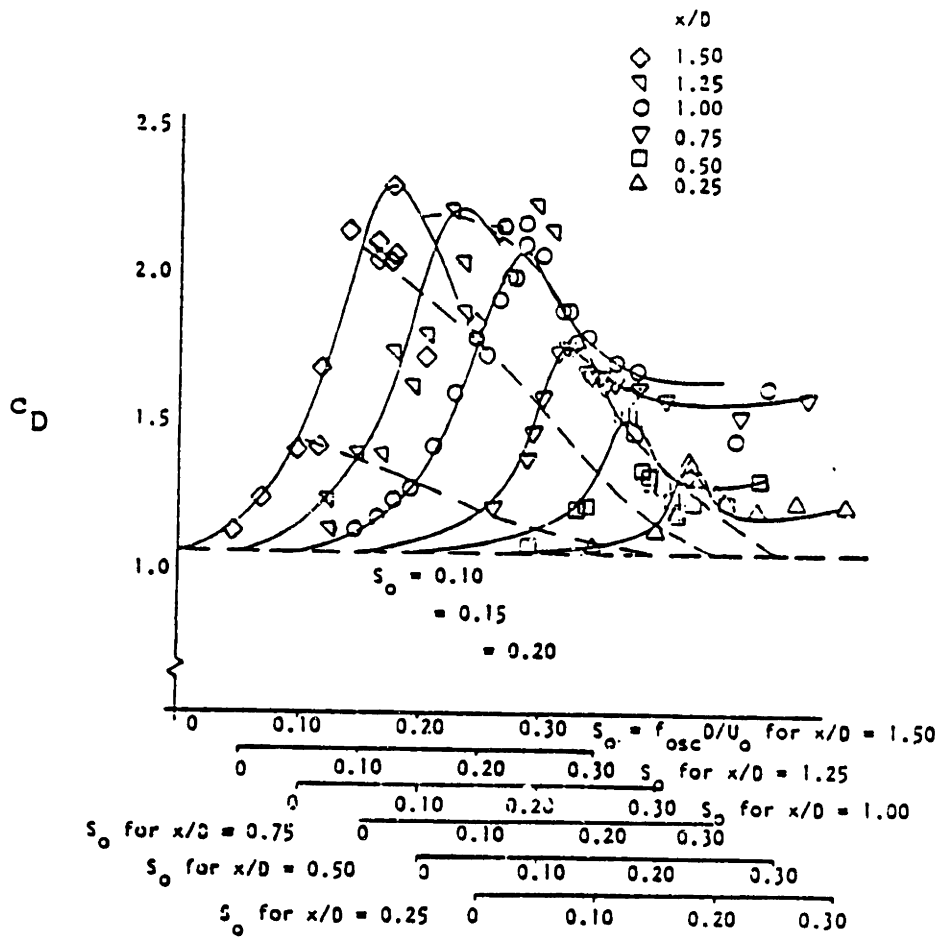

FIGURE 11: Average Drag Coefficient c_D = Average Drag/ $0.5\rho DV_c^2$ as a Function of S_o = 1/U* Parametrically with Respect to the Non-Dimensional Amplitude x/D for Harmonic Oscillations at θ=90 Degrees with Respect to a Current, Mercier (1973).

up of the shear layers occurs quite independently of the cylinder oscillation, leading to a double peaked force transverse to the stream. One peak occurs at the frequency of oscillation and the other at the Strouhal frequency defined above. As the frequency increases, there is a point, which depends upon the amplitude of oscillation, at which the frequency of shedding locks on the frequency of oscillation. This phenomenon persists for a range of frequencies which is also a function of the amplitude of oscillation and is usually referred to as the range of synchronism. When the frequency of oscillation falls above the range of synchronism, the rate of vortex shedding can no longer keep up with the oscillation and the resulting flow is quite irregular. The range of synchronism does not exhibit sharply defined boundaries. In fact, these boundaries are disturbance sensitive, while hysteretic effects for increasing or decreasing frequency may appear. Finally, when vortex shedding is synchronized with the oscillation, the fluctuating drag parallel to the stream occurs at twice the frequency of oscillation and becomes of the same order of magnitude as the drag force transverse to the stream for large S/D and U*. For the largest S/D tested (=2.5) and for U* around 5, an additional component of the fluctuating drag parallel to the stream occurs at four times the oscillation frequency, and reaches the same order of magnitude as the component at twice the oscilating frequency.

c) For θ=0 degrees, no critical range for the hydrodynamic forces parallel to the stream was observed. The lift force character, however, changes at a value of the reduced velocity which is a weak function of the amplitude ratio. For values of the reduced velocity below approximately 3, significant lift components at frequencies 2, 3, and 4 times the oscillation frequency are apparent. The strongest component occurs at twice the oscillation frequency. The magnitude of the lift forces is comparable with the magnitude of the dynamic force parallel to the stream. The second regime occurs for values of U* approximately between 3 and 8. In this regime, significant lift components occur at 1/2, 3/2, 5/2 the oscillation frequency. An important component at 7/2 the oscillation frequency was found for S/D>2. The magnitude of these forces is comparable with the magnitude of the dynamic force parallel to the stream. Flow visualization tests for the second regime revealed that two strong vortices were shed in two successive periods from opposite sides of the cylinder. The shedding of these two strong vortices occurs when the oscillatory velocity adds to the stream velocity. This observation provides a phenomenological explanation of the presence of the harmonics of half the oscillatory frequency in the lift force.

Finally, Mercier observed the existence of forces transverse to the direction of oscillation at the

frequency of oscillation for both θ=0 and 90 degrees. However, he chose not to report them because he felt that they were not sufficiently larger than the effects that arose from the inaccuracies of his experimental set up to allow him to assess their significance.

Sarpkaya (1977a) studied small amplitude harmonic oscillations of a smooth rigid cylinder at θ=90 degrees with respect to a uniform incident stream and gave an analysis of the overall hydrodynamic force parallel to the oscillation and the overall static force parallel to the stream. The dynamic force parallel to the stream he estimated to be less than 7% of the average force and gave no further detail regarding this force. Sarpkaya was mainly interested in the dependence of the hydrodynamic forces upon the reduced velocity and amplitude of oscillation. In his experiments, Sarpkaya varied the value of S/D from 0.13 to 1.03 and the value of U* between 2.5 and 8. Coefficients for the average drag force are given for values of S/D between 0.25 and 0.84. The Reynolds numbers, based on the stream velocity, varied approximately between 3300 and 11000. No systematic presentation of the results as a function of Reynolds number was undertaken. The values of λ used in his experiments from which the average drag force was calculated, were approximately 3.9 and 5.6. In these experiments, he did not use end plates. It is not clear

what values of λ were used in the experiments during which the dynamic force orthogonal to the stream was measured. However, if the same diameter cylinders were used, the resulting values of λ are 10.2 and 14.6. In these experiments, end plates were used but they were not attached to the cylinder.

The average drag coefficients reported by Sarpkaya (1977a) are larger than those reported by Mercier (1973) for S/D between 0.25 and 0.75, but their curves agree in shape. The difference in magnitude is as high as 39%. This difference may be partially due to the difference in the end conditions and the difference in the values of aspect ratios and Reynolds numbers used by the two investigators.

Sarpkaya (1977a), like Mercier (1973), observed a sharp variation of the added mass and drag coefficients, describing the force orthogonal to the stream, around $U^*=5$. Sarpkaya also observed another critical range around $U^*=3.7$ at which the drag coefficients become negative for S/D smaller than approximately 0.6. The lack of experimental resolution in Mercier (1973) led him to fair his experimental data in a misleading way. (Compare Figures 9 and 12.) The difference in the magnitude of c_d and c_M, where both investigators have conducted experiments, may be partially due again to the difference in end conditions and the difference in the values of aspect ratios and Reynolds number as stated earlier.

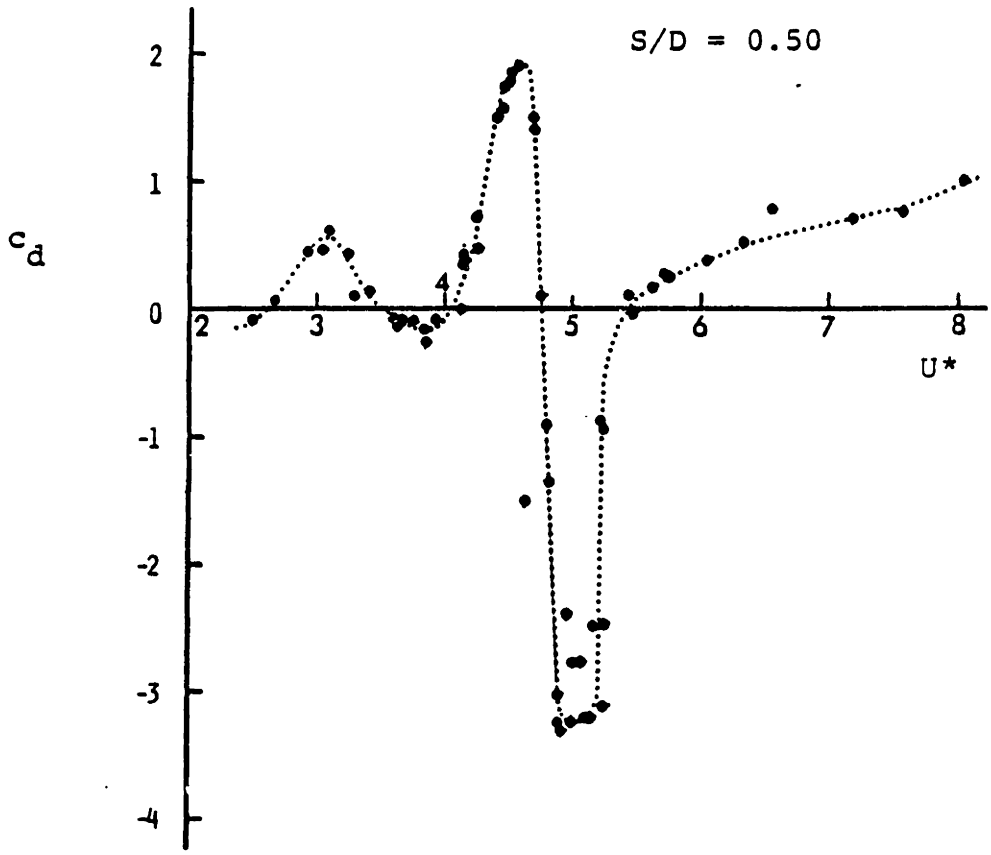

FIGURE 12: Drag Coefficient, c_d = Amplitude of Drag Force Parallel to the Oscillation/$0.5\rho D\omega^2 S^2$ as a Function of U* for a Non-Dimensional Amplitude S/D=0.50 for Harmonic Oscillations at θ=90 Degrees with Respect to a Current, Sarpkaya (1977a).

The only thing absent from Sarpkaya (1977a) is the mass of his model. This does not allow the calculation of the ratio of the mass inertia force divided by the hydrodynamic force orthogonal to the stream, which is essential in determining the accuracy of the calculated values of c_d, when c_d is small.

Bernitsas (1979) studied oblique harmonic oscillations with respect to a uniform incident stream at 15 degree intervals between θ=0 and θ=90 degrees, with S/D=0.375, U*=10.25, Re=7410 and λ=10 with end plates of diameter 4D. His oscillation frequency was 1 Hz and the Strouhal frequency determined from Figure 2 was approximately equal to 2 Hz. As in Mercier (1973), the overall forces were measured. The hydrodynamic force per unit length $\underline{F}$ was analyzed based on a modified Morison type equation of the form:

$$\underline{F}(t)=c_m\rho A_o\underline{a} + 0.5c_d\rho D\underline{A}|\underline{A}| + 0.5c_L\rho D\hat{k}x\underline{A}|\underline{A}|$$

where c_d, c_L, c_m are drag, lift, and inertia coefficients respectively, $\underline{A}$ is a relative velocity defined by:

$$\underline{A} = V_c\hat{i} - \underline{r}_t$$

where $\underline{r}$ is the oscillatory (vector) displacement given by:

$$\underline{r} = S\sin(\omega t)(\hat{i}\cos\theta + \hat{j}\sin\theta)$$

where $\hat{i}$, $\hat{j}$, $\hat{k}$ form a right-handed trial of unit vectors with $\hat{i}$ and $\hat{k}$ parallel to the mean stream and the cylinder axis respectively. The term $\underline{a}$ denotes a relative acceleration of the water with respect to the cylinder

defined by $\underline{a}=-\underline{r}_{tt}$, where subscript t denotes derivative with respect to time. If the analysis is performed in the manner described above, the inertia coefficient does not depend significantly on time and its mean value varies between 1.14 and 1.25, while the time average of the drag coefficient, as defined by Bernitsas (1979), varies between 1.18 and 1.25 as θ varies between 0 degrees and 90 degrees. The most significant oscillatory force components are at f=1Hz and at 2f (approximately the frequency of vortex shedding in a steady stream). Oscillatory force components at 2f are more significant at θ =90 degrees. Higher harmonics exist and are usually more important at intermediate angles rather than at θ=0 degrees and 90 degrees.

Verley and Moe (1979) studied harmonic oscillations of a smooth rigid cylinder at θ=0 degrees with respect to a uniform incident stream and gave an analysis of the overall hydrodynamic force parallel to the stream. In their experiments, Verley and Moe varied S/D between 0.05 and 6.5, U* between 0.6 and 47 and β from 200 to 3000. The values of the aspect ratio used in their experiments were 6.6, 10 and 16. End plates were always employed to increase the two-dimensionality of the flow. No systematic presentation of the results as a function of β or of Reynolds number was undertaken. Verley and Moe used two different forms of the Morison's equation to present

their results for the hydrodynamic force parallel to the stream. The first form used is identical with the form employed by Bernitsas (1979) for $\theta=0$:

$$F_X(t) = c_m\rho A_o a + 0.5c_d\rho D\ A|A|$$

where $A=V_c-r_t$, $a=-r_{tt}$ and $r=S\sin\omega t$.

The second form is the following:

$$F_X(t) = 0.5c_D\rho DV_c^2+c_m\rho A_o a - 0.5c_d'\rho Dr_t|r_t|$$

where c_D is an average drag coefficient and c_d, c_d' are drag coefficients and c_m is an added mass coefficient. The second form was also used by Mercier (1973). Verley and Moe found that the first form leads to smaller variations of the time averaged values of the hydrodynamic coefficients with respect to S/D and U* and therefore concluded that it is a better model for the hydrodynamic force than the second form. The dependence of the time average values of $c_M=c_m+1$ and c_d upon S/D and U* is shown in Figures 13 and 14 respectively. The values of β used to construct the plot for c_d vary between 200 and 500. For U* between 2 and 3 for S/D smaller than approximately 1/8 the drag coefficient becomes negative indicating the occurrence of a lock-in type phenomenon. The results of Mercier (1973) and Verley and Moe (1979) compare well. A random check revealed no difference in magnitude larger than 20%. This difference may be partially due to differences in the values of aspect ratio and Reynolds numbers used by the two investigators. The experimental procedures employed by all investigators mentioned above

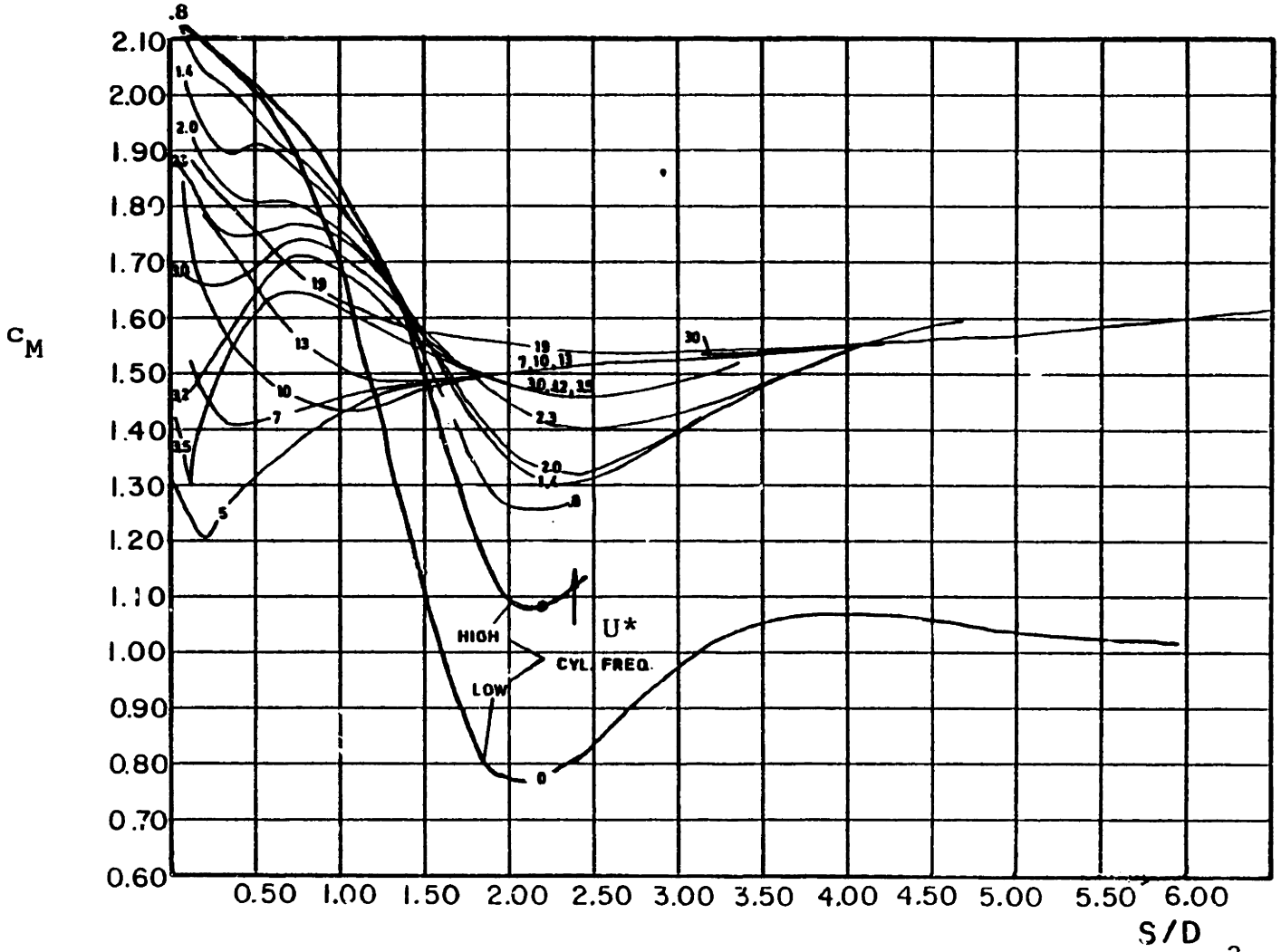

FIGURE 13: Inertia Coefficient c_M = Amplitude of Inertia Force/$\rho A_o \omega^2 S+1$ as a Function of S/D Parametrically with Respect to U* for Harmonic Oscillations at θ=0 Degrees with Respect to a Current, Verley and Moe (1979).

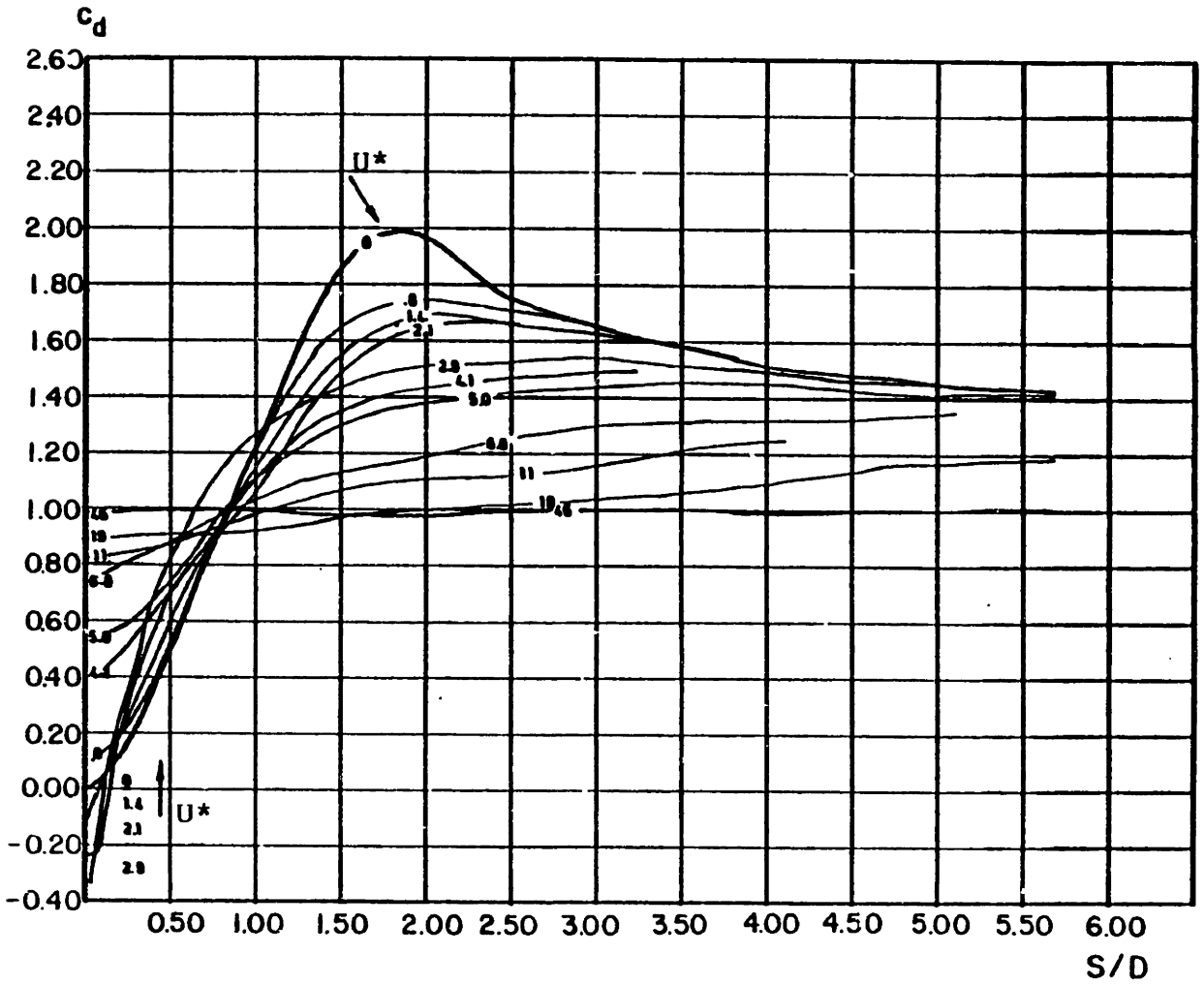

FIGURE 14: Drag Coefficient c_d as a Function of S/D Parametrically with Respect to U* for Harmonic Oscillations at θ=0 Degrees with Respect to a Current, Verley and Moe (1979).

provided a measurement of the overall force, i.e. of the spanwise average hydrodynamic force. Further, they provided no information to determine the spanwise correlation of the hydrodynamic force.

Moeller and Leehey (1982) have recently presented measured spectra of the local hydrodynamic force acting on an instrumented section of a circular cylinder in the direction parallel to its oscillation, which is orthogonal to a uniform stream. The tests were conducted at a Reynolds number equal to 1.93×10^4, at amplitudes of harmonic motion ranging between 0.05 and 0.5 diameters and for reduced velocities between 3.33 and 10. The aspect ratio used was 26 and end plates were used to increase the two-dimensionality of the resulting flow. Lock-in boundaries as a function of the frequency of oscillation non-dimensionalized with respect to the Strouhal frequency, and the amplitude of oscillation non-dimensionalized with respect to the diameter have been determined. The Strouhal frequency used in the non-dimensionalization above is determined from Figure 2.

The above concludes the review of rigid, non-flexibly mounted, cylinder experiments in an a priori defined flow. All investigators reviewed above used the forced oscillation technique except Verley and Moe (1979), who used a free oscillation technique. However, their

experimental set-up was such that it assured that the amplitude of oscillation remained practically constant for the duration of each of their experiments.

IV.3.5 SUMMARY

The review presented above has been kept intentionally brief. General reviews of the main experimental and theoretical results concerning separated flows around circular cylinders have been, for example, compiled by Berger and Wille (1972), Chen (1973), Sarpkaya (1979) and Patrikalakis (1980).

As stated at the beginning of this Chapter, the two major limitations of the hydrodynamic force model used to translate forces measured in rigid cylinder experiments to motion of a flexible cylinder are: a) Force components that would make a flexible cylinder respond in a form other than the one used to conduct the rigid cylinder experiment must be neglected. b) Rigid cylinder experiments cannot provide information on the spanwise correlation of local hydrodynamic forces. The first limitation, for example, implies that we cannot use measurements of the lift, the dynamic force orthogonal to the direction of oscillation, to predict motion in that direction. Similarly, we cannot use measurements of dynamic force components parallel to the direction of

oscillation at frequencies other than the frequency of oscillation to predict motion at those frequencies. Such a situation arises, for example, when the oscillation is orthogonal to the stream and the combination of amplitude and frequency of oscillation is such that synchronization of vortex shedding with the oscillation does not occur.

In an attempt to relate force to a response of different form than the imposed motion, experiments using rigid cylinders, which are mounted on elastic springs and dashpots, have been conducted by a number of investigators. These experiments attempt to represent a continuous system with an idealization which has only a small number of degrees of freedom and allowing the idealized system to respond to the force it experiences. The response in existing experiments of this type is a one degree of freedom translation. This is particularly restrictive when studying the dynamics of moderate and deep water risers as will be explained in detail in Section IV.4.

Existing flexibly mounted cylinder experiments are briefly reviewed in the next two sections, because under specialized conditions they provide some information about the dynamics of risers. The two flow conditions that have been studied are:

1. Flexibly mounted cylinders responding orthogonally or parallel to a uniform stream.

2. Flexibly mounted cylinders responding orthogonally to a harmonic stream.

IV.3.6 FLEXIBLY MOUNTED RIGID CYLINDERS RESPONDING DYNAMICALLY TO VORTEX SHEDDING IN A UNIFORM INCIDENT STREAM

Results of experiments of the above form have, for example, been presented by Vickery and Watkins (1964), Wootton (1968), King (1977a) and Dean et al (1977). Extensive reviews of experiments of this class have been compiled by King (1977b) and Dean and Wootton (1977). A brief review of the flexibly mounted rigid cylinder-fluid interactions are presented below.

The characteristics of vortex shedding for a fixed, rigid cylinder in a uniform stream, briefly described in section IV.3.2, change significantly when the cylinder is permitted to move. Under certain conditions, appreciable oscillations of the cylinder caused by vortex shedding can be excited in the directions parallel or orthogonal to the stream. Oscillations parallel to the flow direction are excited at velocities much lower than the velocities necessary for oscillations orthogonal to the stream.

The non-dimensional hydrodynamic force, $\underline{C}_F = \underline{F}/0.5\rho DLV_c^2$, where $\underline{F}$ is the overall hydrodynamic force

acting on a flexibly mounted rigid cylinder depends upon: the ratio κ of a representative hydrodynamic force to the spring restoring force, $\kappa = 0.5\rho LV_c^2/K$; the ratio m of the rigid body inertial forces to the fluid inertial forces $m=M/(\rho\pi D^2L/4)$; the Reynolds number, $Re=V_cD/\nu$; the ratio $\hat{c}$ of the dashpot damping force to the rigid body inertial force, $\hat{c}=c/(KM)^{1/2}$; the aspect ratio, $\lambda=L/D$, (together with the end geometry); the non-dimensional roughness, k/D; the free stream turbulence and a non-dimensional time $\tau=t(K/M)^{1/2}$, where K is the spring constant, M the mass of the cylinder and c the dashpot damping coefficient. The dashpot damping force is assumed to depend linearly upon the velocity of the cylinder. This is acceptable for the range of amplitudes of practical interest. The instantaneous non-dimensional motion of the cylinder depends upon the same parameters as the non-dimensional hydrodynamic force.

In an attempt to limit the number of experiments required to study all the above parameters, experimentalists have tried to correlate their data on the basis of the following two parameters: a reduced velocity, $U^*_n=V_c/Df_n$ and a stability parameter, $K_s= 2\delta M_e/\rho D^2L$, where f_n is the in-water "natural frequency" of the system, defined by $f_n=(K/M_e)^{1/2}/2\pi$; δ a logarithmic decrement, defined by $\delta=\pi c/(KM_e)^{1/2}$; and M_e an "effective mass", defined as $M_e=M+M_a$, where M_a is an "added mass" of the cylinder in water, defined by

$M_a=c_m\rho\pi D^2L/4$. The parameters U^*_n and K_s are related to the first list of non-dimensional parameters by $U^*_n=\pi^{3/2}(2\kappa(m+c_m))^{1/2}$ and $K_s=\pi^2\hat{c}(m(m+c_m))^{1/2}/2$. Using only U^*_n and K_s to present the data leads to scatter because, as explained above, a much larger set of parameters is needed to describe the phenomenon under consideration. For example, it was reported that changes in parameters such as the aspect ratio, together with end conditions, the non-dimensional roughness and the free stream turbulence have noticeable effects on the results. In addition, because the value of c_m used is not always the same, care must be exercised when comparing results from different investigators.

Vortex excited oscillations of flexibly mounted rigid cylinders orthogonal and parallel to a uniform stream and correlation length changes in such cylinders are briefly discussed in the next three sections.

IV.3.6a VORTEX EXCITED OSCILLATIONS ORTHOGONAL TO A UNIFORM STREAM

A typical behavior of a rigid cylinder supported by elastic springs and dashpots allowed to oscillate orthogonally to a uniform incident stream is shown in Figure 15 derived from the experimental data of Dean et al (1977). The in-water "natural frequency" f_n employed in this Figure is determined using an added mass coefficient c_m equal to one. The values of f_s^{max} and f_s^{min} plotted in Figure 15 correspond to the envelope of experimental data for the vortex shedding frequency for a fixed rigid cylinder in a uniform stream derived from Figure 2 for the corresponding Reynolds number. From Figure 15, it is seen that for the spring mounted cylinder, the vortex shedding frequency, f_s, for values of $U^*_n=V_c/f_nD$ less than 4.5 and bigger than 7.5 approximately is given by the relation $f_s=V_cSt/D$, where St is the Strouhal number as determined from Figure 2. For values of U* between 5 and 6.5 approximately, f_s is approximately equal to f_n. Between U^*_n 6.5 and 7.5 the value of f_s changes smoothly from f_n to V_cSt/D. It should be noted, however, that the value of f_s for $4<U^*_n<8$ is not known accurately because there is considerable experimental scatter. The range where f_s remains approximately equal to f_n is referred to as the lock-in range.

The response frequency, f_r, has only been reported

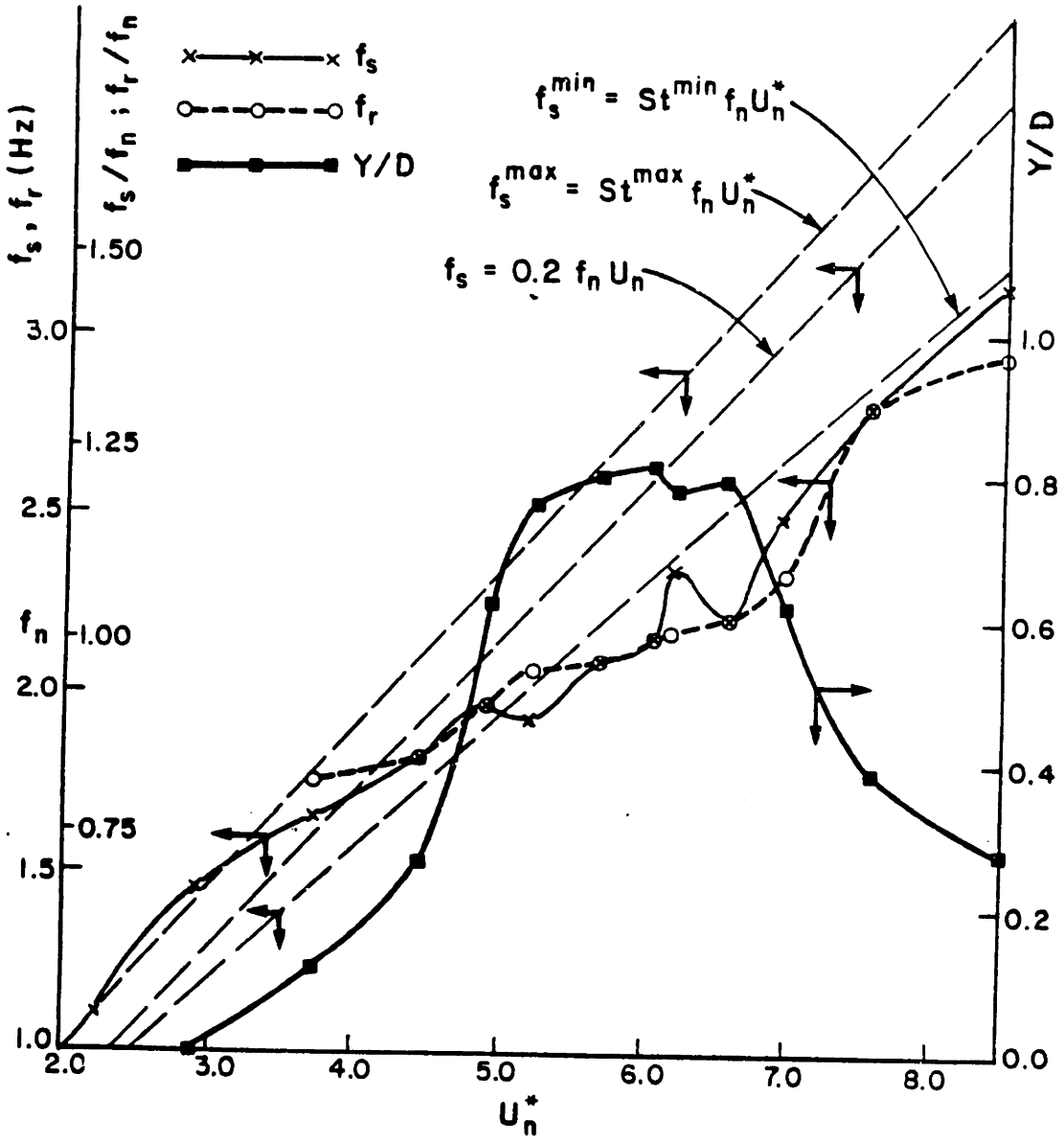

FIGURE 15: Plots of the vortex shedding frequency, f_s, the response frequency, f_r, and the non-dimensional response half amplitude, Y/D, for a smooth spring mounted rigid cylinder oscillating orthogonally to a uniform water stream. Data derived from Dean et al (1977). Model characteristics: f_n=2.15 Hz, D=25.4 mm, m=2.93, $\lambda \simeq 13$, δ= 0.147, K_s= 0.91, Re≈2680 to 10370.

for $3.7 < U^*_n < 8.5$. In this range of U^*_n the response is almost periodic in character (at least for the Reynolds number range studied) with frequency approximately equal to f_s. In this range of U^*_n large amplitudes of oscillation are observed as shown in Figure 15.

King (1977b) defined lock-in as the range of significant response orthogonal to the direction of the current and reports it to occur for $4.5 < U^*_n < 10$. He also indicates that the range of U^*_n where the response is maximum is between 6.5 and 8.

Sarpkaya (1977a) has calculated the maximum response amplitude of a rigid, flexibly mounted, cylinder permitted to respond orthogonally to a uniform stream using his experimental data from forced rigid cylinder experiments. He has also compared his numerical estimates with measurements of the response amplitude of flexibly mounted cylinders at synchronization. The calculated values underpredict the measured maximum amplitudes by no more than 21%.

IV.3.6b VORTEX EXCITED OSCILLATIONS PARALLEL TO A UNIFORM STREAM

When a cylinder is spring mounted so as to allow response in the plane parallel to the stream, vortex excited oscillations appear in that plane for two separate

regions of U^*_n. The first region is defined approximately by $1.25<U^*_n<2.5$, with maximum amplitudes occurring around $U^*_n=2.1$. The second region is defined approximately by $2.7<U^*_n<3.8$ with maximum amplitudes occurring around $U^*_n=3.2$. For very small K_s, the maximum half amplitudes of motion may reach values as high as 0.2 diameters. Maximum amplitudes of motion are a decreasing function of K_s and become nearly zero for K_s around 1.3.

The first of these two regions of vortex excited oscillations parallel to a stream is associated with symmetric shedding while the second with alternate shedding. In the first case the arrangement of symmetric vortices in the wake is unstable. So soon after the vortices are shed they take the familiar staggered arrangement. Up to the beginning of the first "instability" region the cylinder is virtually motionless and the frequency of shedding of a pair of vortices follows the line $f_sD/V_c = St \approx 0.2$. Up to that point shedding is alternate. Within the first "instability" region the cylinder oscillates at its "natural frequency". The value of the shedding frequency in this range seems to only assume values which are rational fractions of the "natural frequency". King reports that in this range of U^*_n the ratio of the "natural frequency" to the shedding frequency decreases from 4 at $U^*_n = 1.25$ to 2 at $U^*_n = 2.5$. Within the second instability region the shedding frequency of a pair of vortices remains constant at

approximately one half the "natural frequency" while in between regions and after the end of the second it follows the line $f_s D/V_c = St \simeq 0.2$ defined earlier. The frequency of cylinder motion within the second "instability" region of oscillation parallel to the stream is equal to the "natural frequency" of the cylinder. The term "natural frequency" is defined the same way as in Section IV.3.6b.

IV.3.6c CORRELATION LENGTH, ASPECT RATIO AND THRESHOLD AMPLITUDES

When a steady stream flows around a smooth large aspect ratio fixed rigid cylinder three-dimensionality effects start appearing for very small Reynolds numbers. For example, for subcritical Reynolds numbers, vortices are shed in distinct cells from fixed cylinders. The flow within each cell is in phase. The length of the cell is called correlation length. For higher Reynolds numbers this heuristic definition of correlation length is no longer plausible. A definition of the correlation length, valid for all Reynolds numbers, may be obtained through measurements of the local lift force L(Z,t), as explained below.

The space-time correlation of the random lift force, which is assumed stationary, is given by:

$$R_L(Z_1, Z_2, \tau) = E(L(Z_1, t)L(Z_2, t+\tau))$$

where E denotes averaging across the ensemble. If, in addition, the process L(Z,t) is assumed ergodic, the space-time correlation can be evaluated by time averaging:

$$R_L(Z_1,Z_2,\tau) = \lim_{T\to+\infty} 1/2T \int_{-T}^{T} L(Z,t)L(Z_2,t+\tau)dt$$

It has been found that for finite length rigid cylinders of large aspect ratio and for locations Z_1, Z_2 away from the ends the space-time correlation depends primarily upon $Z=Z_2-Z_1>0$ and not upon the individual Z_1, Z_2. Such a process is called homogeneous and we can write:

$$R_L(Z,\tau) = R_L(Z_1, Z_2,\tau)$$

The correlation coefficient is defined by:

$$R(Z) = R_L(Z,0)/R_L(0,0)$$

and the correlation length by

$$l_c = \int_0^L R(Z)dZ$$

where L is the length of the cylinder.

A review of correlation length measurements is, for example, given in Graham (1966) and King (1977b). The correlation length on a fixed smooth cylinder in a uniform stream decreases from approximately 20 diameters at Re=40 to 2-3 diameters at Re≈300 and remains approximately constant up to $Re=5x10^4$. Measurements of l_c in the critical region show scatter. For $Re \geq 10^5$, the correlation length is of the order of 1/2 diameter.

When the length of the cylinder is much larger than the correlation length, a reduction of the magnitude of the overall oscillatory force is observed. End and intermediate circular plates orthogonal to the cylinder at

spacings larger than the correlation length increase the overall oscillatory force by increasing the two-dimensionality of the flow. This technique has been used in most rigid cylinder experiments.

King (1977b) reported that when a rigid cylinder in a uniform stream is spring mounted and oscillates at or above a threshold amplitude the correlation length increases. The threshold amplitudes are approximately 10% of the diameter for oscillations orthogonal to the stream and 1% to 2% of the diameter for oscillations parallel to the stream. These observations imply that the reorganization of the vortex shedding process depends upon the particular cylinder motion. Finally, King (1977b) also observed that roughness decreases the spanwise correlation of the hydrodynamic force.

IV.3.7 FLEXIBLY MOUNTED RIGID CYLINDERS RESPONDING DYNAMICALLY TO VORTEX SHEDDING IN A HARMONIC STREAM ORTHOGONAL TO THE PLANE OF THE RESPONSE MOTION

Experiments of the above form have been presented by Sarpkaya (1980), Sarpkaya et al (1981), McConnell and Park (1982) and Verley and Johns (1982). The response motion depends upon the non-dimensional parameters given in Section IV.3.6, where V_c should be replaced by the maximum velocity of the harmonic stream U_m and in addition

upon the Keulegan-Carpenter number $KC = 2\pi S/D = 2\pi U_m/\omega D$.

As for the case of a uniform stream, experimentalists have tried to correlate their results on the basis of a reduced velocity $U^*_n = U_m/f_n D = KC\ f/f_n$ and a response parameter $R_p = M\zeta/\rho D^2 L\ c_L{}^o$, where $f=\omega/2\pi$, $\zeta = 0.5c/(KM)^{1/2}$, and $c_L{}^o$ is the maximum lift coefficient for the same cylinder in the same incident flow but with the cylinder held fixed.

It has been found that R_p can be used to correlate the data for the maximum amplitudes of response orthogonal to the harmonic stream, Sarpkaya (1980). The non-dimensional maximum response half amplitude is a decreasing function of R_p and for the smallest value of R_p studied, $R_p=0.1$, it reaches a value approximately equal to six tenths of a diameter. Maximum response amplitudes and lift coefficients have been encountered for reduced velocities around 5.3 at which synchronization of the response frequency with the "natural frequency" occurs, Sarpkaya (1980). A plot of the non-dimensional response amplitude (half height), Y_M/D, at synchronization as a function of R_p is given in Figure 16 taken from Sarpkaya (1980).

It has been reported, Sarpkaya et al(1981), that the response orthogonal to the stream is not monoharmonic in general, however, no detailed spectral results are available. Plots of the main frequency of response orthogonal to a harmonic stream, defined as the frequency

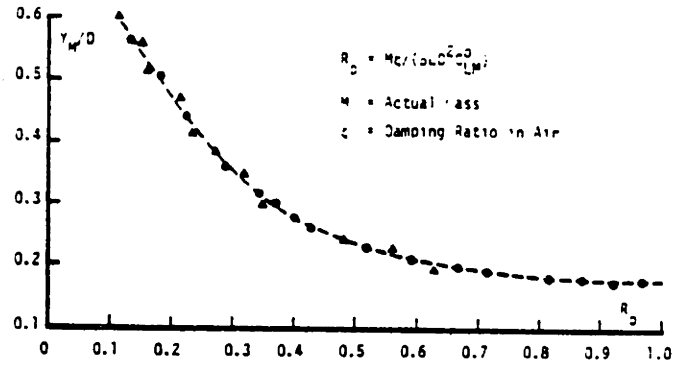

FIGURE 16: Plot of the Non-Dimensional Response Amplitude (Half Height) Orthogonal to a Harmonic Stream, Y_M/D, at Synchronization, as a Function of the Response Parameter, R_p, for Spring Mounted Smooth and Rough Cylinders, Sarpkaya (1980).

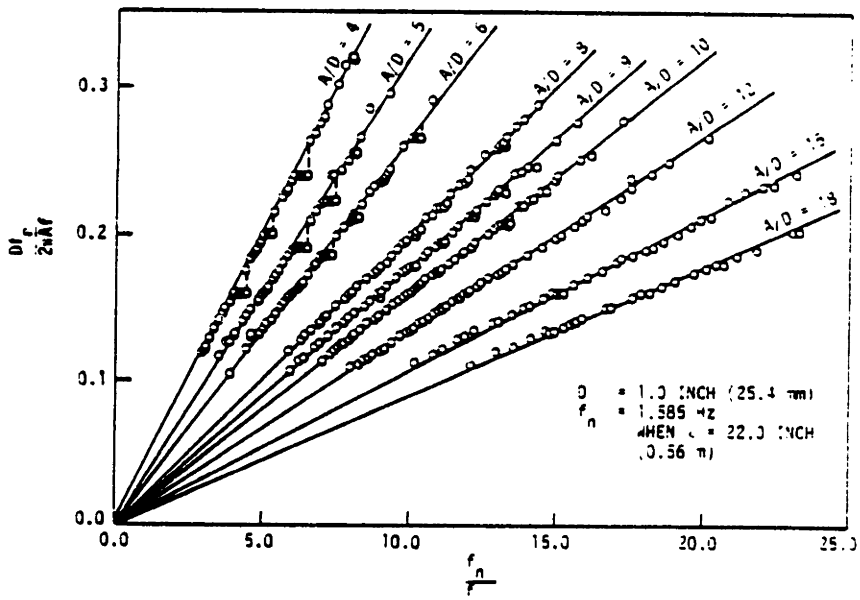

FIGURE 17: Plot of the Ratio $f_r/(f \cdot KC)$ Versus the Ratio f_n/f Parametrically with Respect to the Non-Dimensional Amplitude, A/D, of the Forced Oscillation, where $KC=2\pi A/D$, McConnell and Park (1982).

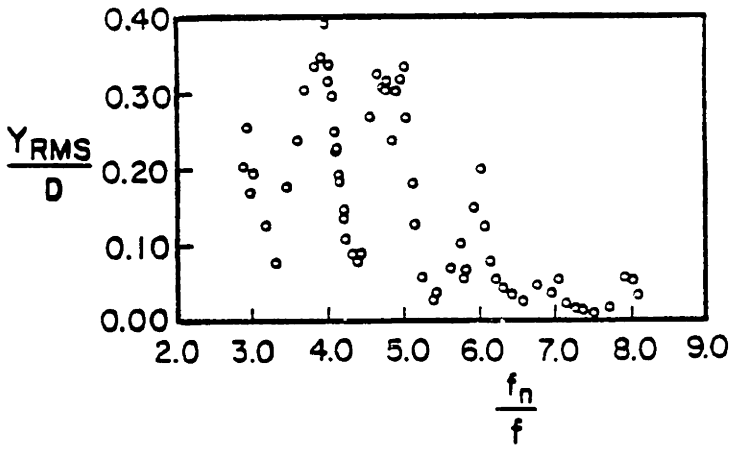

FIGURE 18: Plot of the RMS Response Amplitude Orthogonal to a Harmonic Stream Divided by the Diameter as a Function of f_n/f for KC ≃ 25 for a Smooth Spring Mounted Rigid Cylinder, McConnell and Park (1982).

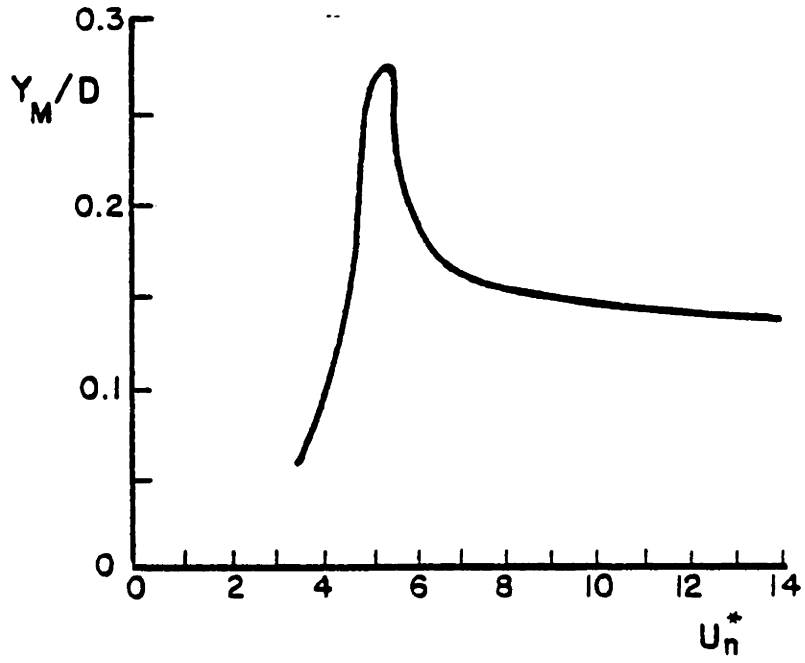

FIGURE 19: Typical Plot of the Maximum Response Amplitude Orthogonal to a Harmonic Stream Divided by the Diameter as a Function of U_n^* for a Sand-Roughened Cylinder with k/D = 0.01, Sarpkaya (1980).

of the highest peak of the lift spectrum, have been recently presented by McConnell and Park (1982). The ratio f/f_n employed in their experiments was not larger than 1/3. The KC numbers studied in their experiments were larger than 25. Their conclusion is that the main response frequency, f_r, as defined above, equals the "natural frequency" of the system in water, except near lock-in regions where the ratio of the main response frequency divided by the driving frequency, f, has a strong tendency to be an integer number especially for KC numbers less than 63 and when the ratio of the in-water "natural frequency" to the driving frequency is an integer. What value this ratio takes depends on the value of KC and the ratio f_n/f, see Figure 17 taken from McConnell and Park (1982). This type of consistent behavior was not obtained for KC larger than approximately 63. The term "natural frequency" as used by McConnell and Park (1982) was obtained from a decay test of their system oscillating in still water, when the rms amplitude of oscillation was approximately equal to one tenth of the cylinder diameter. A plot of rms response amplitude orthogonal to the harmonic stream divided by the diameter as a function of f_n/f for KC=25 is shown in Figure 18 taken from McConnell and Park (1982). A typical plot of the maximum response amplitude divided by the diameter as a function of U^*_n is shown in Figure 19 taken from Sarpkaya (1980).

IV.4 APPLICATION OF RIGID CYLINDER RESULTS FOR THE PREDICTION OF THE RESPONSE OF A MARINE RISER UNDER IDEALIZED EXCITATION CONDITIONS

Existing rigid cylinder experiments can be employed to obtain some information about the dynamic behavior of risers for the following four idealized conditions:

a) Riser excitation by a uniform incident stream.

b) Harmonic oscillation of the top end of a riser in an otherwise quiescent fluid.

c) Harmonic oscillation of the top end of a riser in a direction orthogonal to an incident stream.

d) Harmonic oscillation of the top end of a riser in a direction parallel to an incident stream.

The following four sections illustrate how to use rigid cylinder results to acquire some information about the dynamic behavior of risers. The limitations and difficulties of their use in predicting the response of risers is also discussed in more specific terms. Finally, a brief review of previously existing experimental results of flexible, large aspect ratio, cylindrical models in current or waves is also included.

IV.4.1 RISER EXCITATION BY A UNIFORM INCIDENT STREAM

In Section IV.3.6, using flexibly mounted rigid cylinder experiments, the importance of motion was established in determining the frequency of vortex shedding from a rigid cylinder in a uniform stream. Existing flexibly mounted rigid cylinder experiments, however, can only provide reliable information when the response of the riser is in the first mode primarily. Typical risers are expected to respond in more than one mode and usually not the first. Therefore, if we use existing spring mounted rigid cylinder experimental results to predict the response amplitude at these higher modes we should not expect the same accuracy in our predictions, as in the case where the response is primarily in the first mode. In addition, available spring mounted cylinder experiments cannot model the interactions between dynamic motions of a flexible cylinder in more than one plane. For example, as it is apparent from the discussion of Sections IV.3.4 and IV.3.6b, a typical moderate to deep water riser may be excited primarily at its fourth flexural mode in the plane orthogonal to the stream and at its sixth or seventh mode or both in the plane parallel to the stream for likely values of the current speed. Therefore, using available results to predict the amplitude of the response in such cases can at best be approximate.

The following two examples illustrate in what way we can use rigid and spring mounted rigid cylinder results to acquire information about the dynamic response of risers.

Example 1

Suppose the current speed is such that $U^*_1 = V_c/f_1D$, where f_1 is the first "natural frequency" in water of a riser, is in the range 1.25 to 2.5. Given that for a typical riser $f_2 > 2f_1$, where f_2 is the second "natural frequency" in water, the first mode parallel to the stream will be excited primarily, as the discussion of Section IV.3.6b suggests, and the resulting response parallel to the stream will be at a frequency very close to f_1, when U^*_1 varies within 1.25 and 2.5 (King, 1977a). If the response frequency is known, we may use the results of Verley and Moe (1979) to calculate the static and dynamic response amplitudes parallel to the stream. An alternative method of direct evaluation of both the frequency and the amplitude of response based on rigid cylinder results alone is now under investigation. An inspection of Figure 14 reveals that the drag coefficients become negative in the above range of reduced velocities and for amplitudes of oscillation smaller than approximately 1/8 diameters and sharply increase for larger amplitudes of motion. Given that the energy generated or dissipated per unit length is roughly proportional to the cube of the local dynamic

amplitude and the drag coefficient, a maximum calculated amplitude (half height) only slightly above 1/8 of the diameter is expected for negligible structural damping. This, for example, has been observed in experiments using a cantilever flexible pile (King, 1977a).

If the reduced velocity U^*_1 is between 2.7 and 3.8 then for typical moderate and deep sea risers the reduced velocity U^*_2, defined using f_2, is likely to be between 1.35 and 1.9, which means that possibly both the first and the second mode will be excited in the plane parallel to the stream. Such a situation cannot be modelled by available flexibly mounted rigid cylinder experiments, unless we are willing to make an additional assumption. Similar difficulties are encountered when the stream speed is such as to excite response parallel to the stream at higher modes.

Example 2

More interesting is the case in which U^*_1 is between approximately 4 and 10. Larger vortex-excited oscillations orthogonal to the stream at frequencies close to f_1 and primarily in the first flexural mode are expected. In order to use spring mounted cylinder experiments (with direction of permitted motion orthogonal to a stream) we must again neglect the measured dynamic force components parallel to the stream as we did for rigid cylinder experiments with forced motion. If we do this, we may say that for a certain V_c, we estimate that

the ratio f/f_1, where f is the response frequency of the flexible cylinder from a spring mounted cylinder experiment with the same U^*_1 (see for example Figure 15). Specifically, we assume $f/f_1 = f_m/f_{n,m}$, where f_m is the response frequency and $f_{n,m}$ the in-water "natural frequency" of a spring mounted cylinder. At this point, we must remind the reader of the limitation of performing such an estimate if the remaining non-dimensional parameters described in Section IV.3.6 are not scaled properly between spring mounted model and flexible cylinder. For example, the "natural frequency" of the flexible cylinder and of the flexibly mounted rigid cylinder must be determined using the same method. Estimates of $f_m/f_{n,m}$ for various values of m and various levels of structural damping for a range of Re between 2800 and 10000 approximately may be found, for example, in Dean et al (1977). Once we know f, we may use the results, for example, of Mercier (1973) for θ=90 degrees, Sarpkaya (1977a) or Dean et al (1977) to determine the hydrodynamic force orthogonal to the stream as a function of $U^* = V_c/fD$ and S(Z)/D at least and calculate the steady state amplitudes S(Z)/D orthogonal to the stream. An alternative method of direct evaluation of both the frequency and amplitude of response based on the rigid results alone is now under investigation. In addition, we may use the results of Mercier (1973) for θ=90 degrees, or Sarpkaya (1977a) for the static force parallel to the

stream as a function of the previously calculated dynamic amplitudes orthogonal to the stream for each elevation Z.

Similar calculations can be performed for reduced velocities based on higher "natural frequencies", leading to flexural response orthogonal to the stream primarily in a single higher flexural mode. Energy arguments based on the variation of c_d for a certain U* as a function of S/D show that a maximum calculated amplitude (half height) somewhat above one diameter is expected for cases of negligible structural damping. Such an argument is corroborated from measurements of maximum amplitudes of various flexible cylindrical models orthogonal to a stream as in Figure 20, taken from Dean et al (1977).

Comparisons of the fundamental mode response orthogonal to a stream of a horizontal flexible and tensioned cylinder of aspect ratio equal to 240 with theoretical predictions based on their data from spring mounted cylinder experiments have been presented by Dean et al (1977). The theoretical calculation overpredicts the amplitude of response of the flexible cylinder by an amount as large as 130%. Smaller overprediction (14%) occurs at the peak of the curve of response amplitude versus reduced velocity (based on the "natural frequency"), occurring around $U^*_1=6$. It is difficult to draw conclusions from this comparison because, it appears, that a number of parameters have not been scaled. For example, Reynolds number, Re, and mass to displaced

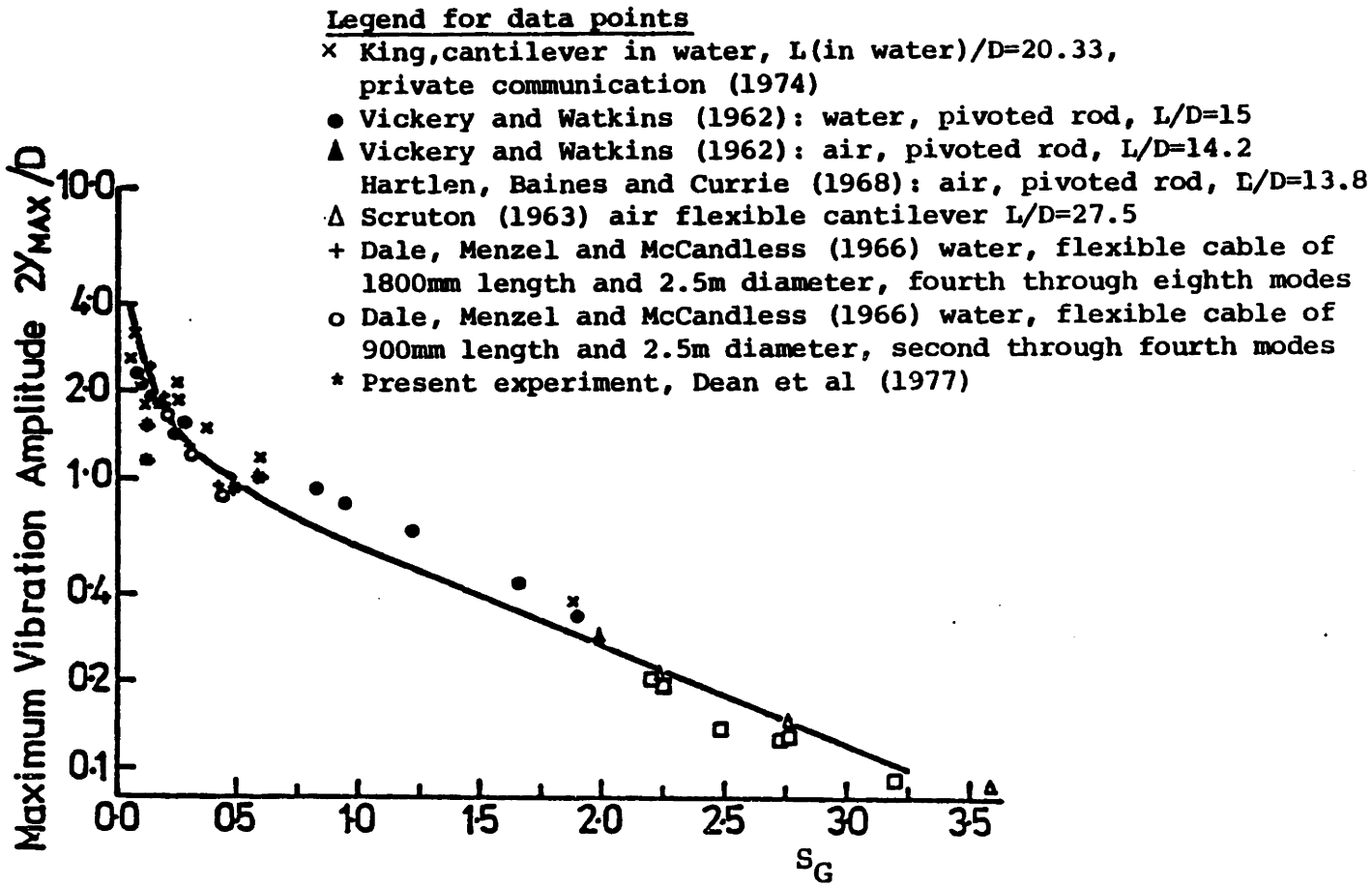

FIGURE 20: Maximum Peak to Peak Amplitude of Vibration, $2Y_M$, of Various Flexible Cylindrical Models in a Uniform Stream Divided By the Diameter as a Function of $S_G = 2\pi St^2 K_s$, Dean et al (1977).

volume, m, have not been scaled, see also Griffin (1981). In addition, it is unclear whether the response frequency for the flexible cylinder was assumed to be its "natural frequency" regardless of the valued U^*_n or the frequency implied by the spring mounted rigid model. The term "natural frequency" as employed in the above statement is measured from a decay test in water with original amplitude of oscillation of the order of one diameter. We feel that the variation of response frequency for changes of the reduced velocity between 4 and 8 should not be neglected. To do this, reliable estimates of the response frequencies for the spring mounted cylinder are required. The effective bandwidth for estimation of the response frequency must be kept very small in comparison to the bandwidth of the spring mounted system when this undergoes vortex excited oscillations. The term bandwidth denotes the difference of response frequencies of the spring mounted system corresponding to amplitudes equal to the peak value divided by $2^{1/2}$. The bandwidth for Figure 15 is 0.4Hz. The reader must also be reminded that the value of the "natural frequency" employed must correspond to similar experimental conditions for both the spring mounted rigid and the flexible cylinder. If this is not done consistently ambiguities prohibit an independent interpretation of the results. Finally, it should be mentioned that for horizontal flexible cylinder experiments the effects of sag, coupling of extensional

and flexural oscillations, depending on the boundary conditions, must be taken into account, so as to allow independent interpretation of the experimental results.

McGlothlin (1982) has also presented experimental results from a flexible, tensioned, horizontal cylindrical model excited by a uniform stream. His results for the response orthogonal to the stream are in agreement with previous investigators. In addition, McGlothlin (1982) has reported estimates for the dynamic response motion parallel to the stream. The frequency of this response is in agreement with the results of Mercier (1973). He also observed that the resulting amplitude of the dynamic response parallel to the current was of comparable magnitude to the response orthogonal to the stream.

The difference between measured response of a flexible cylinder and theoretical predictions using rigid cylinder experimental results, assuming no experimental errors, is due to the combined hydroelastic and correlation length effects. This is the fundamental limitation of existing predictive codes reviewed, for example, in Griffin (1981). There is, however, a practical limitation when using these codes to study the dynamic behavior of deep sea risers, because the "natural frequencies" near which response is likely to be excited for typical values of the current speed, are very close to each other. This leads to ambiguity in selecting the "natural frequency" of the riser on the basis of which the

response frequency is calculated using results from flexibly mounted rigid cylinder experiments.

Existing codes can also be adapted to deal with the case where there is a uniform current extending only over a fraction of the length of the riser without any additional assumption. However, it is not apparent how existing codes can be extended to deal with the case of a sheared current without top end motion. A review of some experimental results from sheared flows and correlation measurements in the wake of flexible cylinders is given in Griffin (1981).

IV.4.2 HARMONIC OSCILLATION OF THE TOP END OF A RISER IN AN OTHERWISE QUIESCENT FLUID

Forced harmonic oscillation of the top end of a moderate to deep water riser at typical wave frequencies leads to flexural dynamic response parallel and orthogonal to the direction of imposed motion. The response parallel to the direction of the top end oscillation is concentrated primarily at the frequency of the imposed oscillation. For amplitudes of oscillation of the top end of the order of one to two riser diameters (which is representative of typical first-order platform motions), the corresponding local Keulegan-Carpenter numbers over a large fraction of the length of the riser are larger than

five. Rigid cylinder results with rectilinear harmonic motion suggest that, for such Keulegan-Carpenter numbers, substantial lift force components at frequencies twice or higher integer multiples of the frequency of excitation might be present, see Figures 7 and 8, Sarpkaya (1977). The maximum lift coefficient reported from rigid cylinder experiments of the above form is a decreasing function of Reynolds number. However, for the range of KC numbers of interest (KC<25 approximately) the resulting lift force maintains a value comparable to the force parallel to the direction of oscillation even for Re as high as 1.5×10^5. This value of Re is representative of prototype conditions. The frequency at which the lift force measured in rigid cylinder experiments is maximum, also suggests that the lift response of a riser excited with a harmonic oscillation at its top end is primarily concentrated at higher flexural modes than the response in the direction parallel to the imposed oscillation. For example, if a deep sea riser responds primarily at its third mode parallel to the direction of oscillation of the top end, then lift response at its fifth to eighth modes might be present.

In order to use rigid cylinder results with forced harmonic motion, we must again neglect the lift force measured in such experiments. If we do this, we may use the following expression for the sectional hydrodynamic force parallel to the direction of oscillation of the top

end to estimate the dynamic motion u(Z,t) in the same direction:

$$F_X(Z,t) = -c_m \rho A_o u_{tt} - 0.5 \rho D c_d u_t |u_t|$$

where $c_m = c_M - 1$ and c_d are determined from rigid cylinder experiments. For smooth cylinders, the values of c_M and c_d are primarily functions of the local KC and Re numbers, see Figures 5 and 6. As already stated in Section IV.3.3, the instantaneous force calculated from the above expression is only approximately equal to the force measured in a rigid cylinder experiment when KC is between 6 and 20. It should be mentioned also that such a model for the estimation of the hydrodynamic force $F_X(Z,t)$ does not take into account hydroelastic and correlation length effects. For example, it does not take into account the effect of motion of the flexible cylinder in the lift direction upon the force F_X.

In Section IV.3.7, using flexibly mounted rigid cylinder experiments, the importance of the ratio f_n/f was established in determining the characteristics of response orthogonal to the harmonic stream. As stated earlier, only small values of KC are of interest for the type of riser excitation considered in this section. For the smallest KC number for which data is available, KC≈25, McConnell and Park (1982) report that there exists appreciable response orthogonal to the direction of oscillation when the ratio f_n/f is an integer less than 6, see Figure 18. We remind the reader that in the McConnell

and Park experiments the ratio f_n/f was not smaller than 3. It is, however, reasonable to expect another peak at $f_n/f=2$ as the small KC results of Sarpkaya (1977) might suggest. For KC≈25, the highest peak occurs for $f_n/f=4$ which corresponds to $U^*_n=6.28$. There is some disagreement with the results of Sarpkaya (1980), who reports that the highest peak occurred at $U^*_n\approx5.4$. Differences in the value of KC, Re and roughness between the two experiments might explain the above disagreement. Figure 18 also indicates that smaller peaks occur at $f_n/f=3$ and 5 ($U^*_n=8.38$ and 5.03 respectively).

McConnell and Park (1982) also found that the response amplitude orthogonal to the stream tends to increase as the KC number decreases at least within the range of Re studied. It should also be noted that for large KC number the multiple peaks of the response disappear. However, we wish to remind the reader at this point that the KC numbers, which are encountered in risers excited by first order platform motions, are smaller than 25 approximately. The above results can also be used to analyze the case where surface waves are also present. The only additional assumption needed is that the effect of the vertical wave velocity must be neglected.

The above discussion and the distributions of the in-water "natural frequencies" of typical moderate and deep water risers imply that appreciable response orthogonal to the direction of the top end oscillation at

more than one frequencies and modes might be present. This response is expected at more than one integer multiple of the frequency of excitation, see Sarpkaya (1977). An extrapolation of the results of McConnell and Park (1982) suggests that when these frequencies are close to the "natural frequencies" of the system in water an increase in the lift response should be expected. Such a situation cannot be adequately described by one-degree of freedom idealizations of the flexible cylinder, as we also saw in Section IV.4.1. Therefore, spring mounted rigid cylinder experimental results cannot be expected, in general, to provide accurate quantitative information about the behavior of the flexible system. The above comments also imply that the relative position of the "natural frequencies" of the system in water is an important factor in determining the response in the lift direction. The relative position of the "natural frequencies" plays an important role in scaling prototypes to small scale flexible models. This subject is discussed in some detail in Chapter V. Finally, we should also mention as in Section IV.4.1, that available spring mounted rigid cylinder experiments do not model the interactions between the dynamic motions of a flexible system in more than one plane.

In order to acquire an estimate of the highest peak of the spectrum of the lift response of a riser excited by a harmonic oscillation of its top end, we must

identify which of the first few harmonics of the frequency of excitation is closest to one of the in-water "natural frequencies" of the riser. Having estimated this "natural frequency", we will assume that the lift response is concentrated in the corresponding flexural mode. On the basis of the structural damping ratio of the riser in air corresponding to this mode and an average lift coefficient, $\overline{c_{LM}^{o}}$, derived on the basis of the calculated response parallel to the excitation of the top end, we may estimate an average value of the response parameter $\overline{R_p} = M\zeta_n/\rho D^2\overline{c_{LM}^{o}}$. The value of $\overline{c_{LM}^{o}}$ is obtained as the spanwise average of the maximum sectional lift coefficients derived on the basis of the local calculated KC and Re numbers, from Figure 7, as suggested in Sarpkaya et al (1981). We may also define an average reduced velocity, $\overline{U^*_n}=\overline{U_m}/f_nD$, where f_n is the "natural frequency" near which the peak of the lift response is assumed to exist and $\overline{U_m}$ the spanwise average of the calculated velocity of the riser parallel to the excitation. From the values of $\overline{R_p}$ and $\overline{U^*_n}$ and Figures such as 16 and 19, we may estimate the response amplitude of the corresponding mode. We must remind the reader at this point that Figures 16 and 19 do not correspond to fixed KC and Re numbers. In addition, Figure 19 corresponds to results from a rough rigid spring mounted cylinder experiment with roughness ratio equal to 0.01, while Figure 16 incorporates results from various smooth and rough

cylinders, Sarpkaya (1980). A procedure such as the one shown above, based on spring mounted rigid cylinder experiments cannot take into account local effects, nor can it give estimates of non-resonant response. The feasibility of a procedure based on rigid cylinder results with forced motion for the prediction of the frequency and amplitude of the lift response of a flexible cylinder in harmonic flows, with proper treatment of local effects and phase, is now under investigation.

Research, related to the type of excitation studied in this section, using flexible cantilevered cylindrical piles excited by surface regular waves have been presented, for example, by Verley and Every (1977), Sawaragi et al (1977), Zedan and Rajabi (1981) and Sarpkaya et al (1981). The first two works have been briefly reviewed in Sarpkaya (1980). The work of Sarpkaya et al (1981) includes references to previous associated research. The experimental results presented in Sarpkaya et al (1981) imply that the first flexural mode of the cantilevered pile was excited for both the drag and lift directions, while the wave frequency was kept smaller than the first in-water "natural frequency" of the pile. This is in agreement with the geometry of typical offshore piles and typical wave spectra. Lift force components at the first three integer multiples of the wave frequency were found. The dominant lift contribution was at twice the wave frequency for the KC numbers studied. Secondary

lift contributions at f_w and $3f_w$ were more pronounced when these frequencies were closer to the "natural frequency" of the pile in water, where f_w denotes the wave frequency. Lift response at $2f_w$ and $3f_w$ encountered in these experiments were expected from rigid cylinder experiments, Sarpkaya (1977).

Finally, Patel and Sarohia (1982) recently presented a preliminary analysis of experimental results obtained using a flexible riser type model of length 6.93m excited by harmonic motion of its top end and surface waves propagating in the direction of the top end motion. Their results are in the form of half-envelopes of response motion and stresses parallel to the direction of wave propagation. They also presented preliminary comparisons of these results with theoretical predictions based on constant values of the drag and inertia coefficients, independent of the values of KC and Re numbers encountered in their experiments. Lift response at twice the wave frequency was reported, however, spectral analyses of the results were not presented.

IV.4.3 HARMONIC OSCILLATION OF THE TOP END OF A RISER ORTHOGONAL TO AN INCIDENT STREAM

Harmonic oscillation of the top end of a moderate to deep water riser at typical wave frequencies

orthogonally to the direction of an incident stream leads to flexural dynamic response parallel and orthogonal to the stream. The response orthogonal to a uniform incident stream, as Sections IV.3.4 and IV.3.6 suggest depends upon the amplitude of oscillation and the relative position of the frequency of excitation with respect to the "natural frequencies" of the flexible system and with respect to the vortex shedding frequency. Depending on the value of these parameters, the response transverse to the stream may contain:

1. One component at the frequency of oscillation of the top end and another at the vortex shedding frequency, or
2. One component at the frequency of oscillation of the top end.

In the last case, vortex shedding is synchronized with the oscillation. When there is no synchronization, the vortex shedding frequency may be estimated from spring mounted rigid cylinder experiments as explained in Section IV.4.1. Such a prediction is expected to be reliable only when some very specialized conditions are true. For example, when the frequency of oscillation is much lower than the first "natural frequency" of the riser in water, the vortex shedding frequency can be estimated from Figure 15, as long as it is much larger than the frequency of the imposed oscillation. In addition, as the discussion of Section IV.3.4 suggests, there is evidence that

appreciable oscillatory drag force parallel to the stream exists at twice the frequency of imposed oscillation. This happens when vortex shedding is synchronized with the oscillation orthogonal to the stream and for reduced velocities, U*, larger than about two, Mercier (1973). The oscillatory drag parallel to the stream, measured in rigid cylinder experiments, reaches amplitudes comparable to the force orthogonal to the stream for large amplitudes S/D of the oscillation orthogonal to the stream and large U*, Mercier (1973). For the largest S/D reported by Mercier (1973), S/D=2.5, an additional component of the oscillatory drag parallel to the stream at a frequency equal to four times the frequency of imposed oscillation exists and is comparable to the component of the oscillatory drag at twice the frequency of oscillation. For amplitudes of oscillation of the top end of a riser of the order of one to two diameters, which is representative of first order platform motions and for typical wave frequencies, the resulting average amplitude of oscillation orthogonal to the stream is expected to be appreciable of the order of one or two diameters. This means that significant dynamic response parallel to the stream may also be present for typical values of the current speed.

In order to use rigid cylinder results with direction of oscillation orthogonal to a stream, we must again neglect the dynamic forces parallel to the stream

and responses in any frequency other than the frequency of imposed oscillation. If we do this we may use the following expression for the sectional force orthogonal to the stream to predict the motion v(Z,t) in the same direction:

$$F_y(Z,t) = -c_m \rho A_o v_{tt} - 0.5\, c_d \rho D v_t |v_t|$$

where $c_m = c_M - 1$ and c_M, c_d are estimated, for example, from Figures 10 and 9 as functions of the local response amplitude orthogonal to the stream divided by the diameter, S(Z)/D, and the reduced velocity $U^*(Z) = 2\pi V_c(Z)/\omega D$, where ω is the circular frequency of the oscillation of the top end. For the special case where $V_c(Z)$=constant, the frequency of imposed oscillation is much lower than the first "natural frequency" of the riser in water, and the vortex shedding frequeny is much larger than the frequency of imposed oscillation, then a better estimate of the dynamic response orthogonal to the current can be made as follows. First, the response at the frequency of imposed oscillation is determined with the above equation. Next, the same equation with homogeneous boundary conditions is used to determine the response at the frequency of vortex shedding. Of course, such a procedure does not yield any phase information between the response at the vortex shedding frequency and the response at the frequency of imposed oscillation.

The static component of the response can be estimated using a sectional static force:

$$F_{X,static}(Z) = 0.5 c_D \rho D V_c^2$$

where c_D is again a function of $U^*(Z)$ and $S(Z)/D$. For example see Figure 11. However it is impossible to use rigid cylinder results to determine the dynamic force components in the X direction at ω and 2ω for the reasons given in the previous section.

The above procedure can be extended to handle the case where a surface wave propagating orthogonally to the current is also present.

IV.4.4 HARMONIC OSCILLATION OF THE TOP END OF A RISER PARALLEL TO AN INCIDENT STREAM

As in the previous two excitation conditions, harmonic oscillation of the top end of a moderate to deep water riser at typical wave frequencies parallel to the direction of an incident stream leads to flexural dynamic response parallel and orthogonal to the stream. The dynamic response parallel to the stream is concentrated primarily at the frequency of the imposed oscillation. Lack of spectral analyses of the force parallel to the stream, measured in rigid cylinder experiments, with oscilation parallel to the stream, does not permit us to evaluate other frequency components of this force. For V_c = constant, depending on the reduced velocity and the amplitude of oscillation, the lift force measured in a

rigid cylinder experiment may contain:

1) One strong component at twice the frequency of imposed oscillation, or

2) Strong components at the first few integer multiples of one half the frequency of the imposed oscillation.

The lift force measured in a rigid cylinder experiment is also comparable to the dynamic force parallel to the direction of oscillation. In addition, the spectral character of the lift force measured in a rigid cylinder experiment suggests that the lift response of a riser will be at higher or at both lower and higher modes than the dynamic response parallel to the stream depending on the reduced velocity and amplitude of oscillation.

It should be mentioned at this point, that the statements concerning the magnitude and character of the hydrodynamic forces for the excitation conditions studied in the previous and present sections, are based on rigid cylinder experiments performed at Reynolds numbers smaller than typical prototype values. For example, Mercier (1973) performed his experiments in the range of 4×10^3 to 3.2×10^4. However, most of his experiments were conducted at Re equal to 8×10^3. It is perhaps worth noting that, the few figures of Mercier's work that exhibit Reynolds dependence, show that, for a smooth cylinder and Re in the above range, there is no appreciable change of the character of the hydrodynamic forces with Reynolds number.

In addition, some of the changes of the magnitude of the hydrodynamic coefficients observed in his experiments for different Re might be partially due to changes of the aspect ratio employed.

In order to use rigid cylinder results to estimate the static and dynamic response of a riser, u(Z,t), parallel to the stream, we must again neglect the lift forces measured in these experiments. If we do this, we can employ the following expression for the sectional hydrodynamic force parallel to the stream:

$$F_X(Z,t) = -c_m \rho A_o u_{tt} + 0.5\, c_d \rho D (V_c(Z)-u_t)\,|V_c(Z)-u_t|$$

where $c_m=c_M-1$ and c_M, c_d may be estimated from Figures 13 and 14 as functions of the local reduced velocity $U^*(Z)=V_c(Z)/fD$ and the non-dimensional local dynamic amplitude of motion in the X direction, S(Z)/D.

The above procedure can be extended to handle the case where a surface wave propagating parallel to the stream is also present.

Chapter V

EXPERIMENTAL ESTIMATION OF HYDROELASTIC EFFECTS ON THE DYNAMIC RESPONSE OF MARINE RISERS

V.1 INTRODUCTION

In an attempt to provide a quantitative estimate of hydroelastic and correlation length effects on the global dynamic behavior of marine risers we performed experiments using a flexible and tensioned cylindrical model. The non-dimensional parameters of our model were carefully selected to allow us to answer the question whether hydroelastic coupling in riser type systems is strong enough to alter the character of the surrounding flow and give rise to a dynamic behavior which is significantly different from the one estimated using rigid cylinder results in a stripwise manner as explained in Chapter IV.

The present Chapter includes the following:

a. The scaling procedure.

b. A description of the model.

c. Presentation of experimental results, and quantitative comparisons of experimental and theoretical predictions.

V.2 SCALING PROCEDURE

In addition to the assumptions leading to equations III.87 and III.88 and boundary conditions III.89 and III.90, the following assumption is made concerning the geometry of the surface of the riser model. The outer surface of the riser is modelled as a smooth cylindrical surface. No variations of the outside geometry due to buoyancy modules, flanges, kill and choke lines are taken into account. This is partially justified given that the kill and choke lines are embedded in the buoyancy and modules for most of the length of a typical deep sea riser. The effect of the modules is taken into account as a uniform buoyancy distribution, but their contribution to the bending rigidity is neglected. This is justified because the Young's modulus of the buoyancy material is several orders of magnitude less than that of steel.

For the purpose of our experiments, the following additional assumptions are made regarding the environment idealization and platform motion:

1. The environment is idealized by a current V_c constant along the length of the riser, which can be easily constructed in a towing tank where our experiment was performed. The constant current is an over-idealization of the environment but it still allows

the study of the hydroelastic interactions. Since this is our principal objective, this limitation was accepted. The case of zero current speed is also studied in this work.

2. The platform motion is simulated by a sinusoid motion of amplitude A, circular frequency ω and direction θ with respect to the current. This idealization was accepted for the same reason given above. It should also be noted that under such idealized excitation conditions, comparisons between experimental results from the flexible model and theoretical calculations based on existing rigid cylinder results is possible. The design of the mechanism providing the motion of the top end of the model is such that it will permit the creation of other top end motion. For example, if a model of a 500 m or longer riser were to be tested, slow drift platform oscillations would have to be included because they might cause dynamic response. The design of a top end mechanism allows this type of motion to be simulated. In theory, our top end mechanism should be able to simulate any prescribed motion we desire.

The presence of surface waves is not taken into account in this study in order to keep the number of experiments manageable. Even if only regular waves were to be studied, it would have been necessary to add three new independent parameters: amplitude, phase with respect

to the top end motion and direction of propagation with respect to the current. The absence of surface waves still permits us to fulfill cur principal objective.

The presence of ambient turbulence is also neglected in our experiments. In addition, the effect of surface roughness is another factor that is not studied in these experiments.

If the above assumptions are made, the local horizontal sectional hydrodynamic force $\underline{F}(Z,t)$ depends primarily upon:

a) The bending stiffness EI, where E is the Young's modulus of the material and I the cross-sectional moment of inertia about the neutral axis.

b) The average effective weight per unit length $\overline{We}$. The use of the spanwise average value of the effective weight is permitted, because we are only interested in the global dynamic behavior of the riser.

c) The effective overpull at the lower ball joint Pe(0).

d) The length L between ball joints.

e) The outer effective diameter D_e. For the prototype D_e is defined as:

$$D_e = (L_b/L)D_b + (1-L_b/L)D_o$$

f) The average mass per unit length M, which includes the mass of the riser tubes, flanges, kill and choke lines, mud, buoyancy modules and drill string.

g) The current velocity V_c.

h) The amplitude A, circular frequency ω and direction θ

with respect to the current direction of the applied top end motion.

i) The physical constants, density ρ, and kinematic viscosity, ν, of the water and the acceleration of gravity, g.

j) The elevation Z of a section from the lower ball joint and the distance Z_1, Z_2 of the upper and lower ball joints from the surface and bottom respectively.

k) The structural damping coefficients c_n, n=1,2,... for the nth flexural mode defined by equation (III.91). These may be estimated experimentally by decay oscillation tests in air for the first few modes.

l) The time t.

The above nineteen dimensional parameters may be arranged in sixteen non-dimensional parameters:

$$\underline{C}_f = \frac{\underline{F}\ (Z,t)}{\frac{1}{2}\rho D_e V_c^2} \qquad (V.1)$$

$$\varepsilon = \frac{EI}{Pe(0)L^2} \qquad (V.2)$$

$$\mu = \frac{\overline{W}eL}{Pe(0)} \qquad (V.3)$$

$$\kappa = \frac{\frac{1}{2}\rho D_e L V_c^2}{Pe(0)} \qquad (V.4)$$

$$\lambda = \frac{L}{D_e} \tag{V.5}$$

$$m = \frac{M}{\frac{\pi}{4}\rho D_e^2} \tag{V.6}$$

In the prototype m is determined as:

$$m = \frac{M}{\frac{\pi}{4}\rho \cdot \left[\frac{L_b}{L} D_b^2 + (1 - \frac{L_b}{L}) D_o^2\right]} \tag{V.6a}$$

$$U^* = \frac{2\pi V_c}{\omega D_e} \tag{V.7}$$

$$\alpha = \frac{A}{D_e} \tag{V.8}$$

$$Re = \frac{V_c D_e}{\nu} \tag{V.9}$$

$$F = \omega (D_e/g)^{1/2} \tag{V.10}$$

$$\hat{Z} = Z/L \tag{V.11}$$

$$\hat{Z}_1 = Z_1/L \tag{V.12}$$

$$\hat{Z}_2 = Z_2/L \tag{V.13}$$

$$\theta \tag{V.14}$$

$$\tau = \omega t \tag{V.15}$$

$$\hat{c}_n = c_n L \, [MPe(0)]^{-1/2} \tag{V.16}$$

In the case of no current Equations (V.1), (V.4), and (V.9) take the form:

$$\underline{C}_f = \frac{\underline{F}(Z,t)}{\frac{1}{2}\rho D_e A^2 \omega^2} \qquad \text{(V.1a)}$$

$$\kappa = \frac{\frac{1}{2}\rho D_e L A^2 \omega^2}{Pe(0)} \qquad \text{(V.4a)}$$

$$Re = \frac{A\,\omega D_e}{\nu} \qquad \text{(V.9a)}$$

The remaining non-dimensional parameters are the same except for (V.7) and (V.14) which are of course absent. Equation (V.1) gives a measure of the ratio of the total local hydrodynamic force per unit length to the static drag per unit length. Equation (V.1a) gives the same measure but this time with respect to a representative dynamic drag force per unit length.

Equation (V.2) gives a measure of the ratio of bending to effective tension forces.

Equation (V.3) gives:

a. The rate of change of the effective tension "stiffness" with respect to depth, and

b. The ratio of the total effective riser weight to the effective tension at the lower ball joint.

Equation (V.4), the Cauchy number, gives the ratio of the static drag forces to the effective tension. Equation (V.4a) gives the ratio of a representative hydrodynamic force to the effective tension.

Equation (V.5), the aspect ratio, gives proper scaling of the three-dimensionality of the flow.

Equation (V.6) ensures proper scaling of the structural inertia to the fluid inertia forces.

Equation (V.7), the reduced frequency or velocity, ensures kinematic flow similarity.

Equations (V.8), (V.11), (V.12), (V.13) and (V.14) ensure geometric similarity.

Equation (V.9) or (V.9a), the Reynolds number, give a ratio of inertial to viscous fluid forces.

Equation (V.10), the Froude number, gives the ratio of the inertial to the gravitational fluid forces.

Equation (V.15) gives the time as a fraction of the period of the imposed top end oscillation.

Equation (V.16) may be seen to be proportional to $c_n/M\omega$ if (V.4), (V.5), (V.6), (V.7) are kept constant and therefore ensures proper scaling of the ratio of the structural damping forces to the structural inertial forces.

All non-dimensional parameters (V.2) to (V.16) must be kept constant between model and prototype to ensure kinematic and dynamic similarity of the physical phenomena between them. If equations (V.2) to (V.16) are kept constant, then equation (V.1), the non-dimensional total local hydrodynamic force is automatically kept constant between model and prototype. They also imply that the non-dimensional horizontal displacement in each

direction x, y as a function of the non-dimensional elevation Z will be equal point by point between model and prototype for the same non-dimensional time, because the non-dimensionalized partial differential equations of motion (III.87) and (III.88) and boundary conditions (III.89) and (III.90) will be identical between model and prototype.

In riser model experiments, it is very difficult to achieve Reynolds number similarity between model and prototype. This is also the case with the present experiments. However, the present experiments permit us to evaluate our thecretical capabilities to estimate the static and dynamic response of a riser type structure at the model scale at the Reynolds numbers tested, using rigid cylinder experimental results. It is perhaps worth noting that rigid cylinder results suggest that the spectral character of the lift forces remains virtually unchanged for quite disparate Reynolds numbers. For example, for a rigid cylinder in a steady stream, the Strouhal number, $St=f_s D_e/V_c$, where f_s is the vortex shedding frequency, is approximately equal to 0.2 for Re between 400 and 3×10^5, see Figure 2, Chapter IV. In pure harmonic flow and for constant moderate KC numbers ($\simeq$15), the Strouhal number, $St=(f_s/f)/KC$, is not a function of Re for $5\times10^3<Re<6\times10^4$, see Figure 8, Chapter IV. However, prototypes excited by surface waves and first order platform motions usually have at least part of their

length operate at Reynolds above 6×10^4 and therefore rigid cylinder results suggest that scaling of model results to prototype behavior might not be very successful in this case.

The Froude number does not have to be kept constant between model and prototype, because free surface effects are unimportant in our problem.

The model selected for the proposed experiments does not correspond to a specific prototype. However, all its non-dimensional parameters are carefully selected to allow us to achieve our main objective, which as stated earlier, is the evaluation of our theoretical capabilities to predict the static and dynamic response of a riser type structure based on rigid cylinder experimental results.

V.3 A DESCRIPTION OF THE MODEL

Our model is made up of an aluminum tube covered externally with a sealing material. The overall model

Length between ball joints - (L) =	3.000 m
Aluminum tube I.D. - (D_i) =	10.92 mm
Aluminum tube O.D. - (D_o) =	12.61 mm
External sealing diameter - (D_e) =	15.3 mm
Average mass per unit length - (M) =	0.327 kg/m
Average effective weight per unit length - ($\overline{We}$) =	1.378 N/m

Effective overpull at the lower ball joint - (Pe(0)) = 1.72 N

Bending stiffness of a cross section - (EI) = 37.6 Nm^2

The inside of the aluminum tube is filled with a glycerin solution in water of density approximately equal to 900 Kg/m^3. At the ends of the model there are ball joints which minimize the end bending moments, while above the upper ball joint there is a slip joint, which is designed to minimize tension variations due to flexural motions. The riser model also was designed so it could be tensioned to the desired tension. The first two "natural frequencies" of the model in water are approximately equal to 1.57 and 6.06 Hz, respectively. These have been determined theoretically using c_m=1 and have been verified from a decay test in quiescent water with original amplitude of the order of 1/10 of the effective diameter.

The model is instrumented at ten equidistant locations, 1-10, each with two strain gage full bridges installed on the outer surface of the aluminum tube, designed to isolate bending from tension and to measure bending strains on two orthogonal directions A and B. In the vertical static equilibrium condition, planes A and B are parallel and orthogonal to the centerline of the towing tank, respectively. The actual location of each branch of the bending bridges is at approximately 9.80

degrees from planes A and B. The numbering of the bridges begins at the upper end, while their elevation is measured from the axis of the lower ball joint. The first and last bending bridges are L/11 from the axes of the top and bottom ball joints respectively, and the separation between the bending bridges is L/11. For example, bridge A6 measures bending strains created by deflections in plane A at an elevation Z=5L/11 from the axis of the lower ball joint. In addition, the model is instrumented at two extra positions T1 and T2, 101 mm from the axes of each ball joint, by specially designed full bridges isolating tension from bending. Tension bridge T2 is at the lower end of the model. Finally, the model is instrumented at an additional location, Q1, 1773 mm from the upper ball joint, by a full torsion bridge. The mass per unit length of a single wire is 0.198 grams/m, while the total mass of all wires for all 23 full bridges is 2.73% of the total model mass. Their total volume is approximately equal to 5.32 cm^3. The four wires of each bridge are braided to avoid interference and are sent internally to the lower end of the model.

The oscillation of the top end of the model was created by a DC motor driven by a signal generator and controlled by a tachometer measuring angular velocities and a linear variable differential transducer, LVDT, measuring displacements. The rotational motion of the motor was converted to linear motion via a specially

designed rack and anti-backlash pinion system.

During the experiments, measurements from a number of strain bridges and the LVDT were made simultaneously and were recorded digitally. Using the torque bridge, it was observed that the structural torsion was negligible, which was expected from the analysis of Chapter III. It was estimated analytically and also confirmed by the tension bridge measurements that the tension variation during the experiments was small (5%) in comparison to the effective tension. In addition, even for the lowest excited mode, the ratio of the change of restoring force due to tension variation to the overall restoring force is very small (0.3%). This means that the assumption of constant effective tension with time is an acceptable approximation for theoretical estimates of the response. From calibration experiments in air, it was estimated that the structural damping ratio ζ was approximately equal to 0.016 and 0.010 for the first and second flexural modes, respectively. This implies that typical fluid drag forces are much larger than our estimates of the structural damping forces. Our experiments in air also revealed that when the upper end of the model is oscillated in air in a certain plane, some flexural response orthogonal to this plane exists. This happens because our model was not rotationally uniform. It was estimated that the flexural response orthogonal to the direction of excitation was not larger than approximately 12% of the response in the plane

of applied oscillation. It was felt that such an imperfection would not substantially affect the experimental results in water and therefore the model was accepted.

V.4 PRESENTATION OF EXPERIMENTAL RESULTS

The experiments presented in this study involve harmonic excitation of the top end of the riser model at an amplitude approximately equal to two effective diameters for the conditions shown in Table V.1. They are subdivided in three broad categories. The first does not involve current, while the second and the third involve harmonic oscillations of the top end parallel and orthogonal to a uniform current respectively.

The experimental results reported here include: 1) The root mean square dynamic bending response strains as a function of the response frequency. The root mean square response is the square root of the product of the power spectral density of the response times the effective bandwidth B_e employed in the Fourier analysis of the results. The root mean square rather than the magnitude of the power spectral density was selected for presentation because in most cases the experimental response was practically periodic. The logarithmic representation of the power spectral density was not selected because it tends to exaggerate visually the

TABLE V.1

Direction of Excitation θ of Top End w.r.t. Centerline of the Tank in Degrees	Current Speed V_c in mm/s	Frequency of Excitation f_e of Top End in Hz
0	0	0.75, 1, 1.5, 2.92
0	120	1, 1.5, 2.3, 3
0	240	1, 1.5, 2.3, 3
90	120	0.5, 0.775, 1.5, 1.95, 2.925
90	240	0.5, 0.775, 1.5, 1.95, 2.925

significance of smaller components which are not important in this problem. For each peak, the overall root mean square of the response is shown numerically. This is computed as the square root of the sum of the squares of the rms response strains at discrete frequencies B_e Hz apart in the neighborhood of each peak. In addition, the total dynamic root mean square of the response is shown numerically.

2) The static bending strain parallel to the current direction when this is not zero.

3) Maximum bending strains parallel and orthogonal to the oscillation.

4) Maximum bending strains independent of direction.

The elevations of the points at which the above results are presented can be found in each of the following three sections. The nomenclature used in the figures is defined below:

The experiment number corresponds to the numbering system employed during the performance of the experiments. BE is the effective bandwidth B_e employed in the Fourier analysis in Hz. THETA is the angle of oscillation of top end with respect to the longer side of the towing tank in degrees. VC is the current speed V_c in mm/s. FE is the

nominal frequency of excitation f_e of the top end in Hz. A/DE is the ratio of the measured amplitude A of excitation of the top end divided by the effective diameter D_e.

V.4.1 HARMONIC OSCILLATION OF THE TOP END OF THE MODEL IN AN OTHERWISE QUIESCENT FLUID

In all experiments described in this section, the direction of oscillation of the top end was parallel to the longer side of the towing tank (plane A). The amplitude of oscillation was approximately equal to two effective diameters. The water temperature was 13 degrees C. Bending strains in plane A at Z=3L/11, 5L/11 and 8L/11 and in plane B at Z=3L/11, 6L/11 and 8L/11 were recorded simultaneously together with the motion of the upper end. For reasons of brevity, root mean square response strain as a function of the response frequency at elevations Z=3L/11, 5L/11 for plane A and Z=3L/11 and 6L/11 for plane B are only included. The Figures of root mean square response strain are referred to by the experiment identification number and the bridge name. The Figures showing maxima and theoretical predictions are referred to by the experiment identification number and the plane name. Figures showing the measured response strain in plane A as a function of the measured response strain in plane B are referred to by the experiment identification

number and the letter S (strain). Figures showing the measured displacement in plane A as a function of the displacement in plane B follow the same rules as the S Figures except that the letter D (displacement) is used instead of S. In all Figures of type S and D, TIME denotes the time span of the plot in seconds. A collective description of the experiments analyzed in this section is shown in Table V.2.

Table V.2 also includes information about the theoretical prediction of the response at $f=f_e$ in plane A performed as described in Section IV.4.2. The way in which $\hat{c}_m$ and $\hat{c}_d$ shown in Table V.2 have been derived from the local c_m and c_d is explained in Appendix B. The estimates of the local c_m and c_d employed in the iteration procedure are based on extrapolation of rigid cylinder results shown in Figures 5 and 6 of Chapter IV. Note that the smaller Re for which rigid cylinder data is available is equal to 10^4.

Table V.3 provides information about the theoretical prediction of the lift response following the method described in Section IV.4.2. The spanwise average values of $\overline{c_{LM}^{o}}$ are based on the theoretically calculated response in plane A and Figure 7 of Chapter IV. For most of the KC numbers encountered in this study, the smallest value of β reported in Figure 7 is 1107 and therefore extrapolation for smaller β's was necessary. Linear extrapolation was used. For the values of $\overline{R_p}$ encountered

TABLE V.2

EXPERIMENT NUMBER	14	17	20	23
Frequency of Excitation f_e in Hz	0.75	1	1.5	2.92
Measured A/D_e	2.04	1.98	2.05	2.01
Added Mass Coefficient $\hat{c}_m$ Used in Theoretical Prediction	0.07	0.07	0.08	0.48
Drag Coefficient $\hat{c}_d$ Used in Theoretical Prediction	2.37	2.35	2.31	2.11
Maximum Calculated Re	1870	2420	3750	7150
Maximum Calculated KC	12.82	12.44	12.88	12.63
Mean Calculated Re	1110	1568	2550	2870
Mean Calculated KC	7.59	8.06	8.77	5.06

TABLE V.3

EXPERIMENT NUMBER		14	20	23
β		146	291	566
$\overline{c^{\circ}_{LM}}$		3.02	3.48	2.17
First Flexural Mode	$\overline{R_{p,1}}$	0.007	0.006	-
	a_1^{max}/D_e	0.97	0.97	-
	$\overline{U^*}_1=\overline{KC}\cdot f_e/f_1$	3.63	8.38	-
	a_1/D_e	0.23	0.55	-
Second Flexural Mode	$\overline{R_{p,2}}$	-	0.004	0.006
	a_2^{max}/D_e	-	0.97	0.97
	$\overline{U^*}_2=\overline{KC}\cdot f_e/f_2$	-	2.17	2.44
	a_2/D_e	-	0.10	0.11

in our experiments, extrapolation of Figure 16 of Chapter IV for $R_p<0.1$ must be performed to calculate the maximum amplitude of motion, Y_M, of the corresponding rigid, flexibly mounted cylinder at synchronization. For $R_p<0.2$, the following approximation of the curve of Figure 16 of Chapter IV is used: $Y_M/D\simeq 0.124(0.033+R_p^2)^{-1/2}$. The assumption used in Park (1981) to relate lift force with motion in the same direction is also used in our work. The above assumption for sinusoidal modes leads to $a_i^{max}=\sqrt{2}Y_M$, where a_i^{max}, i=1,2,..., is the maximum amplitude of the ith flexural mode at synchronization. For the model used in this work, the use of purely sinusoidal flexural modes is adequate. Figure 19 of Chapter IV scaled up to a maximum a_i^{max} for the ith mode, provides an estimate of the amplitude of motion a_i in the ith mode for values of $\overline{U^*_i}$ different from the critical value. Extrapolation of Figure 19 of Chapter IV for small values of $\overline{U^*_i}$ was necessary to perform some of the estimates of Table V.3. At this point, we must again remind the reader of the limitations of using Figures 16 and 19 of Chapter IV to perform estimates of the lift response as explained in Section IV.4.2. Please also note that experiment 17 is absent from Table V.3, because the lift response happens to be at frequencies which are not close to the "natural frequencies" of the model in water. This does not permit use of Figures 16 and 19 of Chapter IV, which were constructed on the basis of the assumption that the

response was at the "natural frequency".

From all experiments of this class, it can be seen that when the frequency of imposed oscillation is not very close to one of the "natural frequencies" of the flexible system (see experiments 14, 17, and 23) the strain response in the A plane is primarily concentrated at $f=f_e$. However, some strain response exists at $f=2f_e$, $3f_e$ and $4f_e$ which, in general, is not insignificant in determining the maxima of the measured response in plane A. When the frequency of the imposed oscillation is close to a "natural frequency" of the flexible system, (see experiment 20), the strain response in the A plane is almost exclusively at $f=f_e$. These results are summarized in Figures 14A, 17A, 20A, and 23A, where the theoretical and experimental dynamic response strain at $f=f_e$ and maximum dynamic response strain in plane A are shown. The theoretical maximum dynamic strain response and the theoretical dynamic strain response at $f=f_e$ in plane A are the same. From these figures we can see that the theoretical prediction of the maximum dynamic response strain is good when there is no significant response at frequencies other than f_e in plane A and no significant response in plane B. Please observe that the maximum dynamic response strain in plane A is larger in experiment 23 than in experiment 20 because the second mode was excited in experiment 23.

In the lift direction, when the frequency of

imposed oscillation is not close to a "natural frequency" of the flexible system the dynamic strain response is primarily at $f=2f_e$, (see experiments 14, 17, and 23). However, some strain response exists at $f=f_e$ which, in general, is not insignificant in determining the maxima of the measured response in plane B. When the frequency of imposed oscillation is close to a "natural frequency" of the flexible system, (see experiment 20), the dynamic strain response in the B plane is at $f=nf_e$ where n is a small integer (up to 6) and is so determined so that f is close to a "natural frequency" of the flexible system. The same conclusion was reached in run 903 reported in Chryssostomidis and Patrikalakis (1982b) where the model described in this thesis extended to 10.091 m was used. The extended model was supported by a tension leg platform subjected to surface wave excitation. In this run the frequency of excitation, f_e, was close to f_2 and $2f_e$ was close to f_3. Lift response at both f_e and $2f_e$ was observed. The lift response for experiments 14, 17, and 23 at $f=2f_e$ is comparable to the drag response at $f=f_e$. These results are summarized in Figures 14B, 17B, 20B, and 23B. In Figures 14B and 23B the following information is shown:

1) The experimental dynamic response strain at $f=2f_e$ in plane B.

2) The theoretical dynamic response strain in plane

B at $f=f_1$ for experiment 14 and $f=f_2$ for experiment 23, where f_1, f_2 are the first two "natural frequencies" of our model, respectively. For experiment 14, f_1 is the "natural frequency" closer to $2f_e$ and for experiment 23, f_2 is the "natural frequency" closer to $2f_e$.

3) The maximum measured dynamic response strain in plane B.

4) The maximum measured dynamic response strain independent of plane.

5) A theoretical estimate of the maximum dynamic response strain independent of plane. This estimate is obtained as the square root of the sum of the squares of the response in planes A and B.

In Figure 17B no theoretical estimate of the dynamic response strain in plane B is provided for the reason given above. Therefore, the theoretical maximum dynamic response strain independent of plane in Figure 17B is the same as the theoretical prediction in plane A. Item 1 shown in Figure 17B is the same as in Figures 14B and 23B. For experiment 20, the experimental dynamic response strain in plane B at $f=f_e$ is shown in Figures 20Ba and 20Bc and the response at $f=4f_e$ is shown in 20Bb. The

theoretical dynamic response strain in plane B at $f=f_1$ is shown in Figure 20Ba, while the theoretical dynamic response strain in plane B at $f=f_2$ is shown in Figure 20Bb. In addition, the theoretical estimate of the maximum dynamic response strain in plane B obtained by summing the responses at $f=f_1$ and $f=f_2$ is shown in Figure 20Bc. Items 3 and 4 in Figures 14B, 17B, 20B and 23B are the same. A theoretical estimate of the maximum dynamic response strain independent of plane is shown in Figures 20Ba, 20Bb, and 20Bc. This estimate is obtained as the square root of the sum of the squares of the response in plane A from Figure 20A, and of the response in plane B from Figure 20Bc.

For the responses in plane B, unfortunately no general conclusions can be drawn because of the need to extrapolate Figures 16 and 19 of Chapter IV. Therefore, Figure 20Bc, which indicates that the theoretical predictions at $f=f_1$ and $f=f_2$ can be added together to give an estimate of the maximum response in plane B, should be interpreted accordingly. For the theoretical estimate of the maximum response independent of plane there is the additional complication that the phase between the response in the A and B planes is unknown. Therefore, even when the prediction in the A and B planes are good, the theoretical estimate of the maximum response independent of plane is by necessity conservative (see experiment 20). The "S" Figures of each experiment help

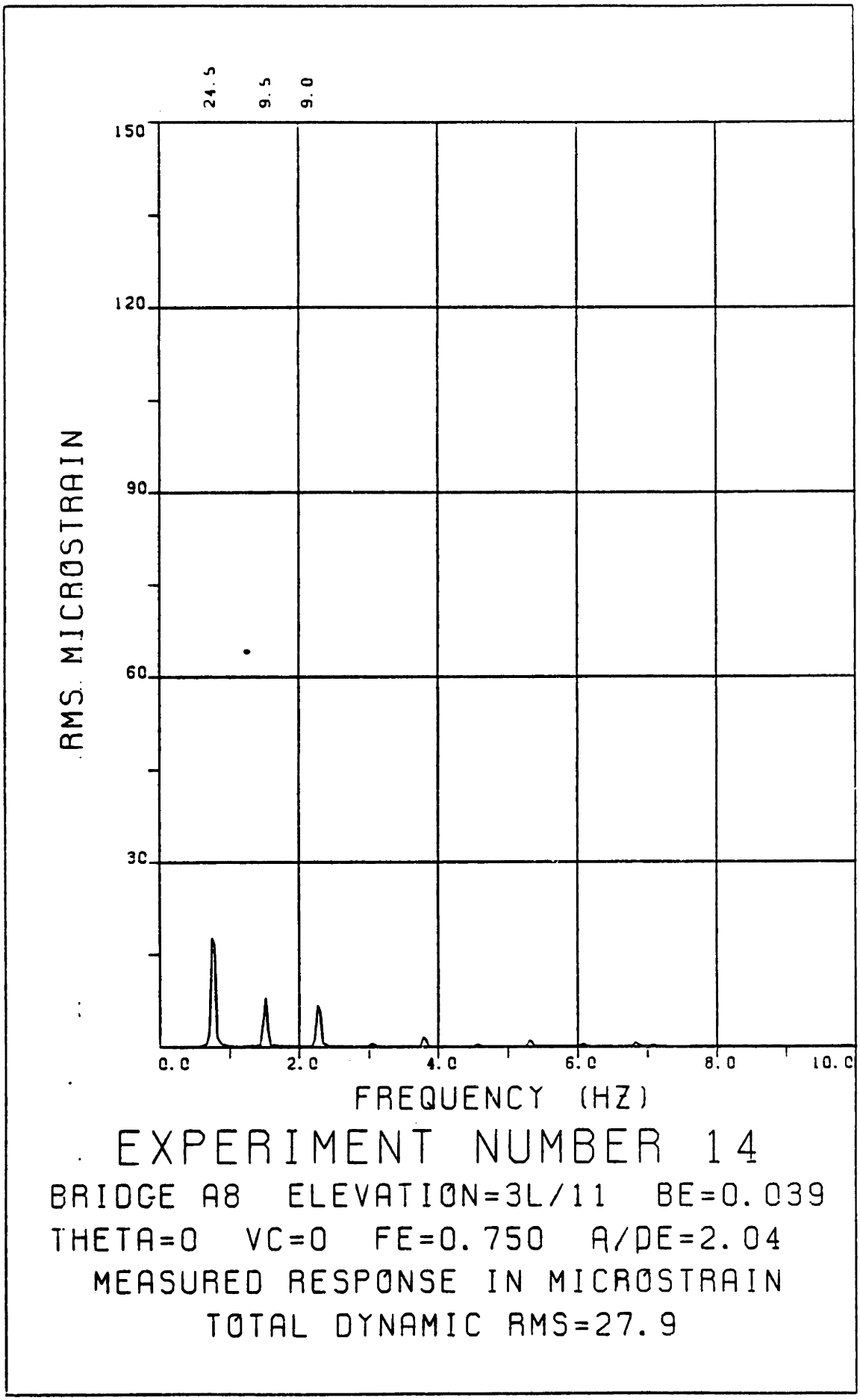

EXPERIMENT NUMBER 14

BRIDGE A8 ELEVATION=3L/11 BE=0.039

THETA=0 VC=0 FE=0.750 A/DE=2.04

MEASURED RESPONSE IN MICROSTRAIN

TOTAL DYNAMIC RMS=27.9

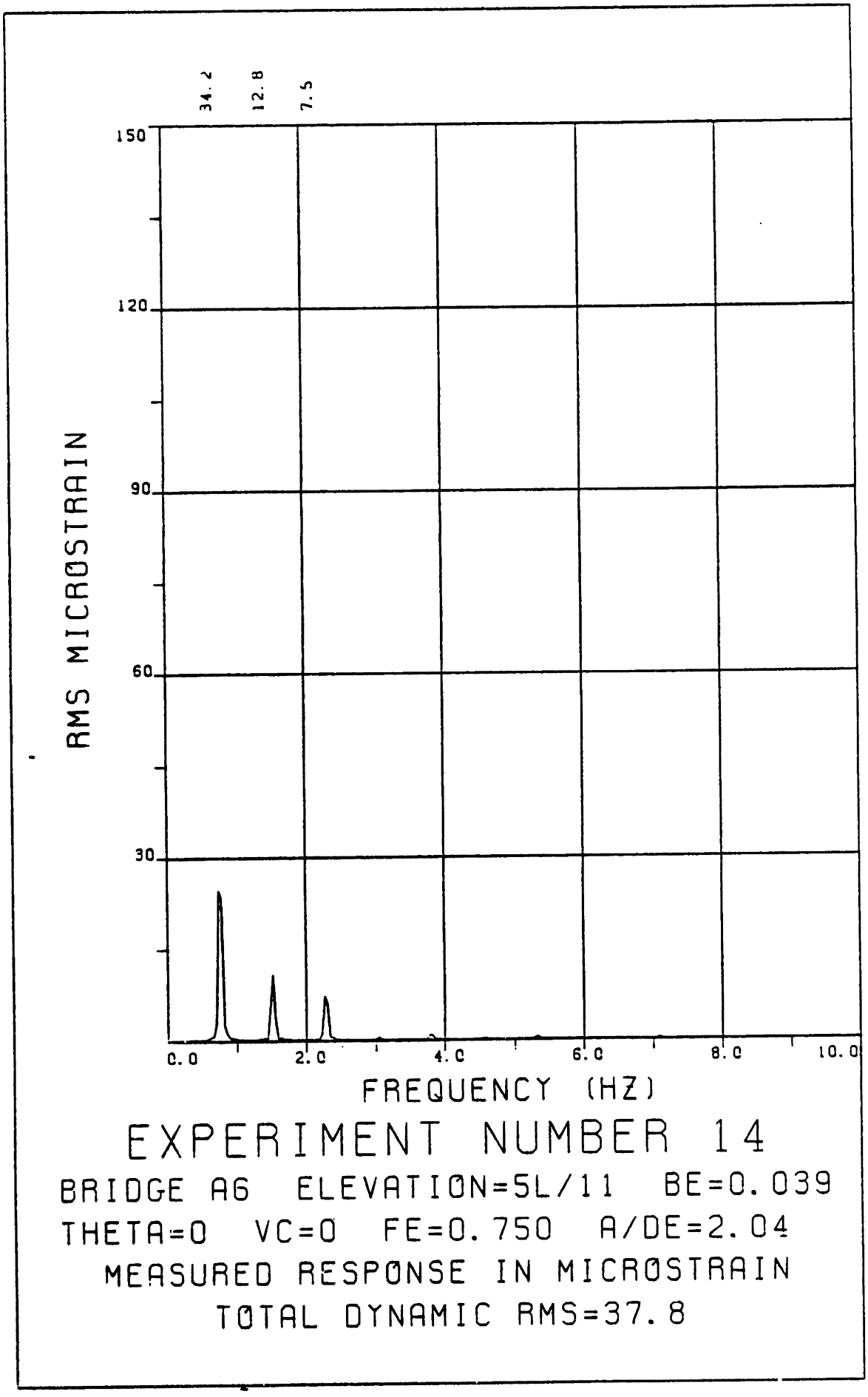

EXPERIMENT NUMBER 14

BRIDGE A6 ELEVATION=5L/11 BE=0.039

THETA=0 VC=0 FE=0.750 A/DE=2.04

MEASURED RESPONSE IN MICROSTRAIN

TOTAL DYNAMIC RMS=37.8

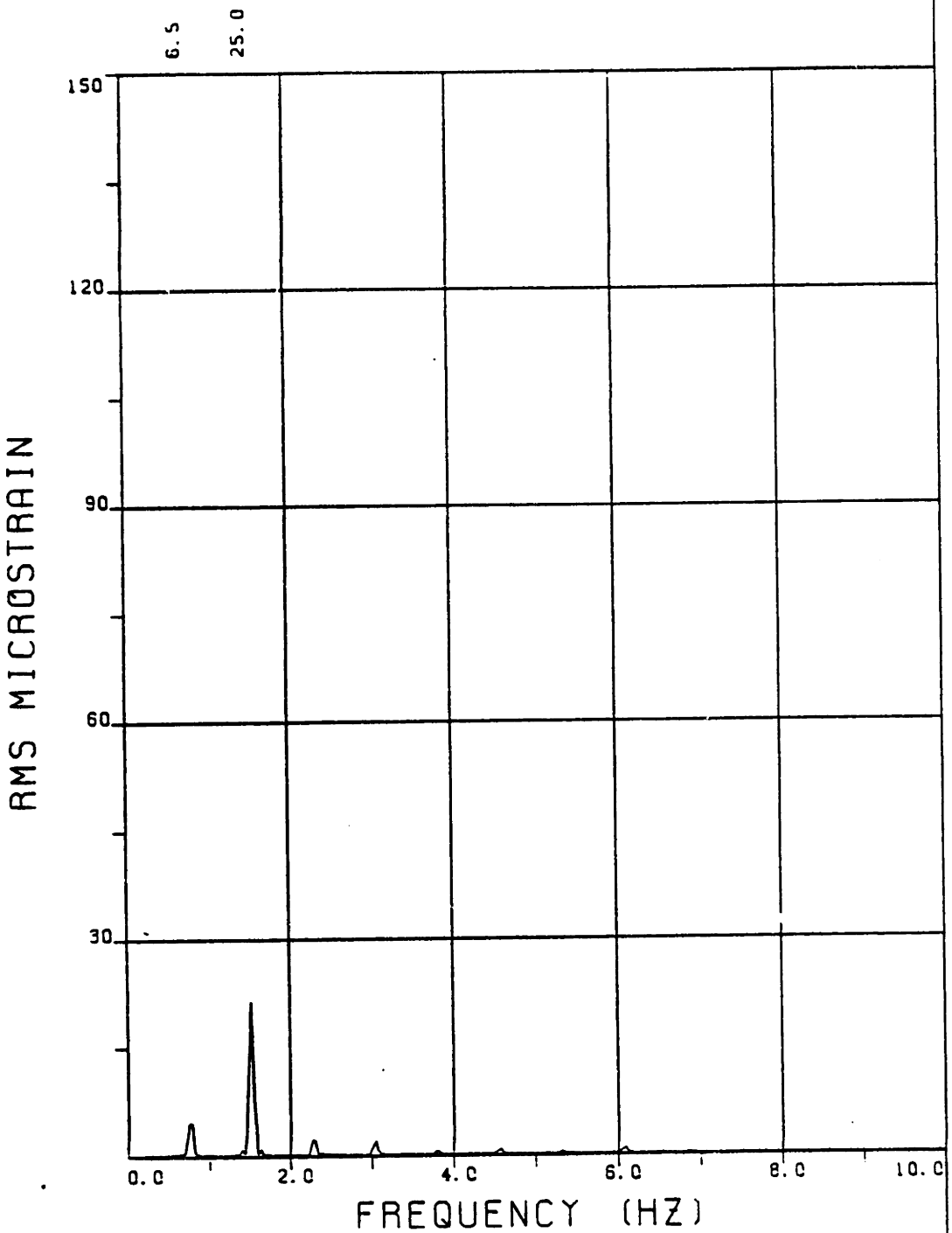

EXPERIMENT NUMBER 14

BRIDGE B8 ELEVATION=3L/11 BE=0.039

THETA=0 VC=0 FE=0.750 A/DE=2.04

MEASURED RESPONSE IN MICROSTRAIN

TOTAL DYNAMIC RMS=26.2

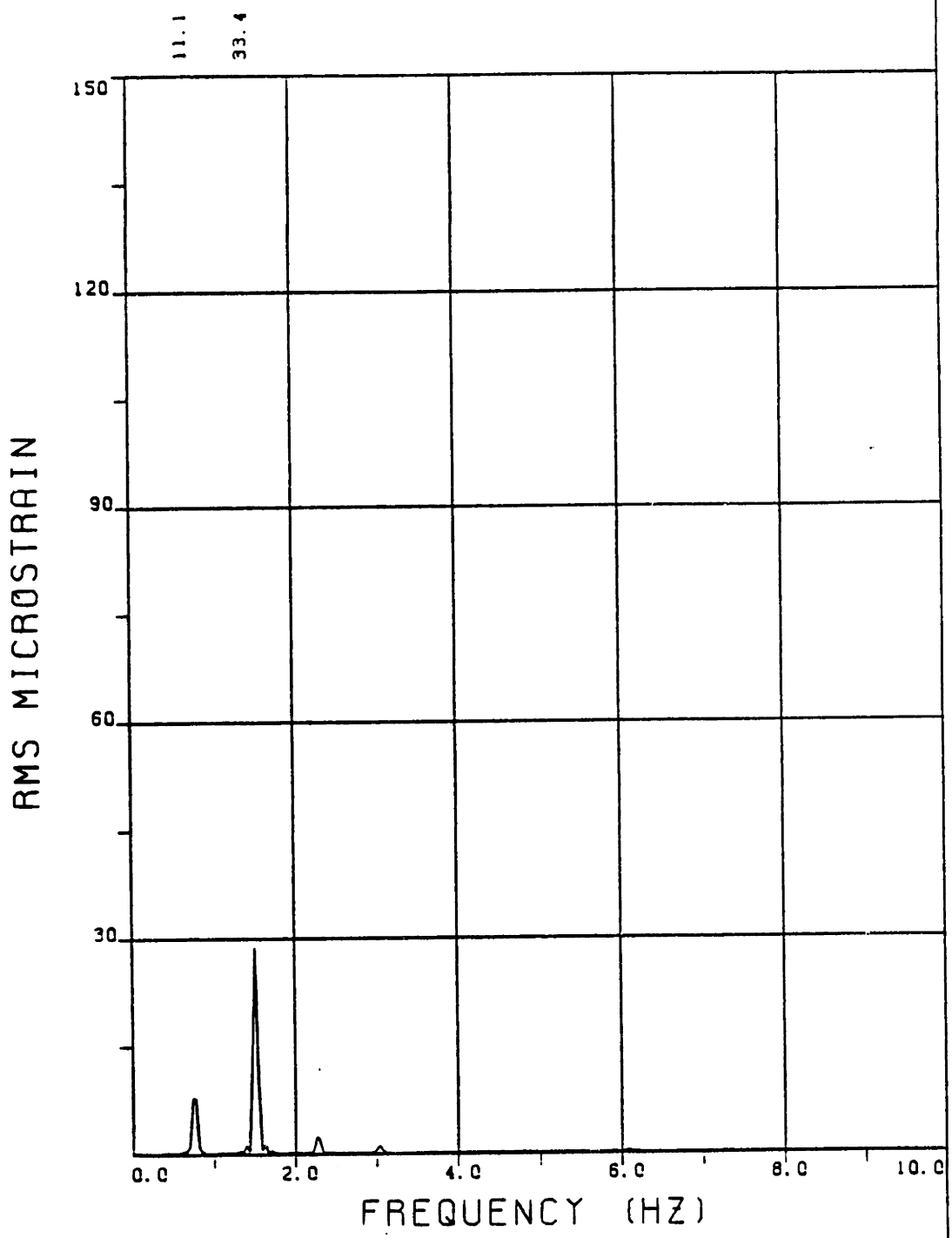

EXPERIMENT NUMBER 14

BRIDGE B5 ELEVATION=6L/11 BE=0.039

THETA=0 VC=0 FE=0.750 A/DE=2.04

MEASURED RESPONSE IN MICROSTRAIN

TOTAL DYNAMIC RMS=35.4

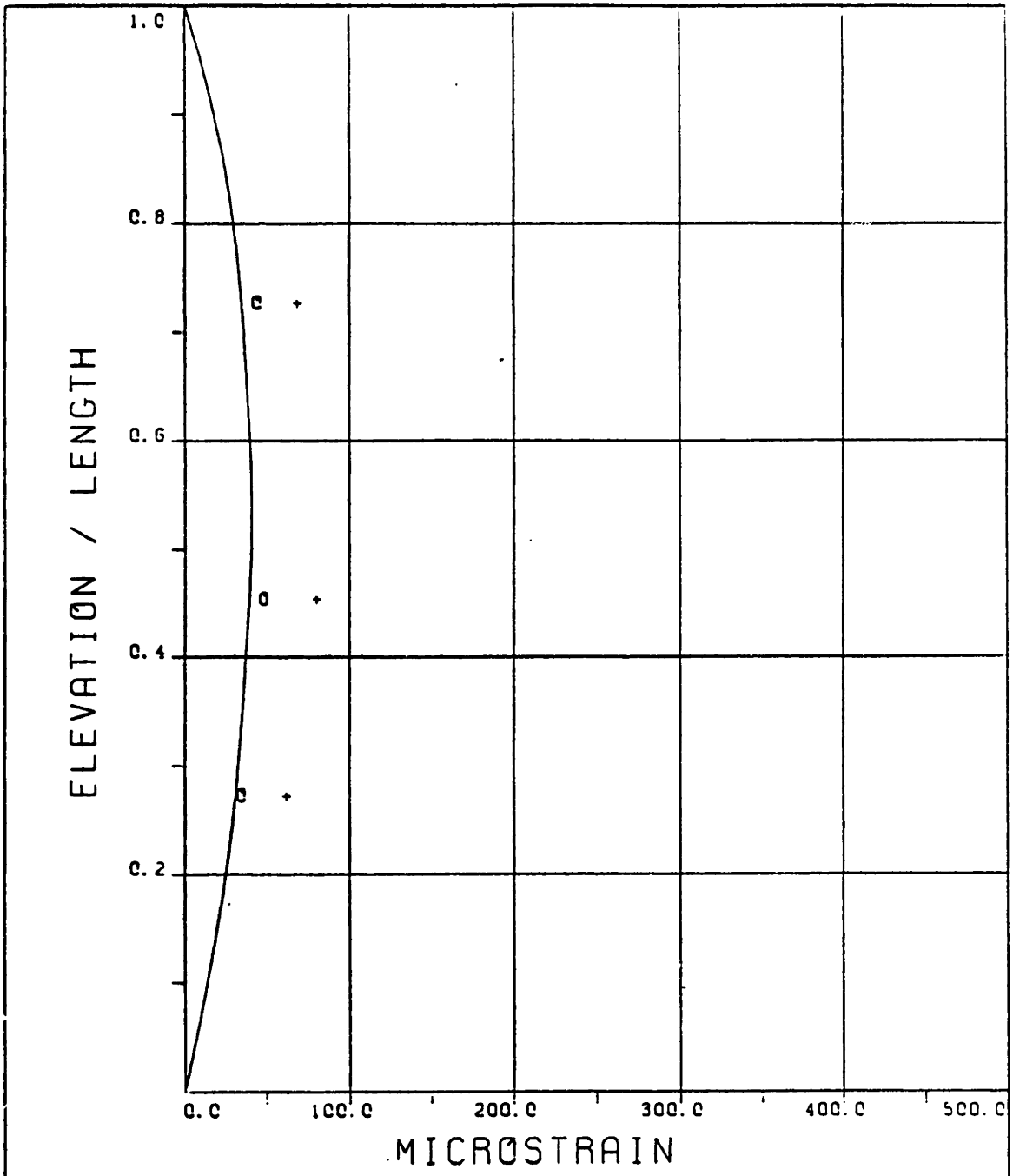

EXPERIMENT NUMBER 14

THETA=0 VC=0 FE=0.750 A/DE=2.04

DYNAMIC RESPONSE AT F=FE IN PLANE A

——— THEORY o o o EXPERIMENT

MAXIMUM DYNAMIC RESPONSE IN PLANE A

——— THEORY + + + EXPERIMENT

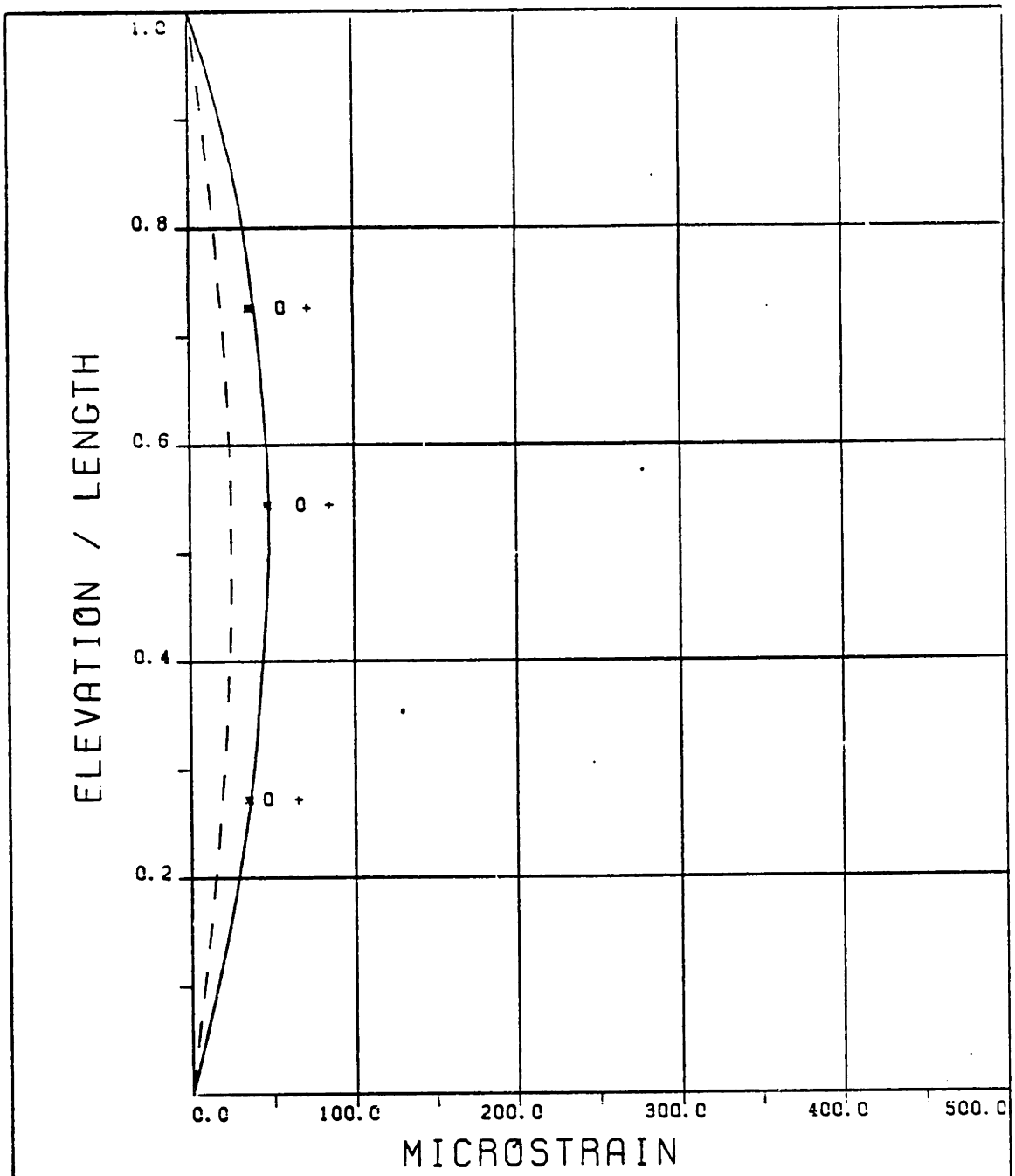

EXPERIMENT NUMBER 14

THETA=0 VC=0 FE=0.750 A/DE=2.04

DYNAMIC RESPONSE IN PLANE B AT F=2FE

----- THEORY * * * EXPERIMENT

MAXIMUM RESPONSE IN PLANE B

o o o EXPERIMENT

MAXIMUM RESPONSE

_____ THEORY + + + EXPERIMENT

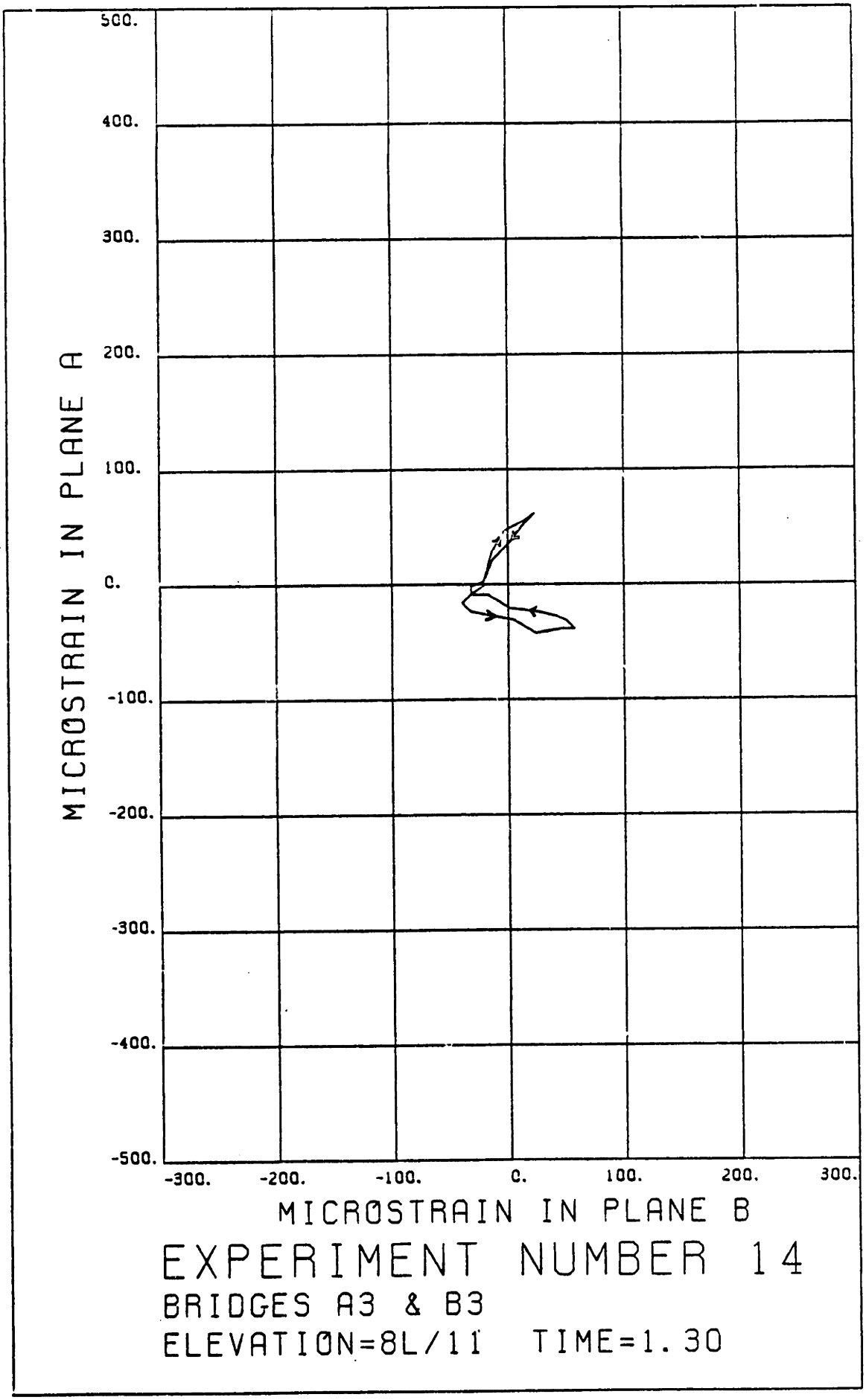
500.
400.
300.
200.
100.
0.
-100.
-200.
-300.
-400.
-500.
MICROSTRAIN IN PLANE A
-300.
-200.
-100.
0.
100.
200.
300.
MICROSTRAIN IN PLANE B
EXPERIMENT NUMBER 14
BRIDGES A3 & B3
ELEVATION=8L/11 TIME=1.30

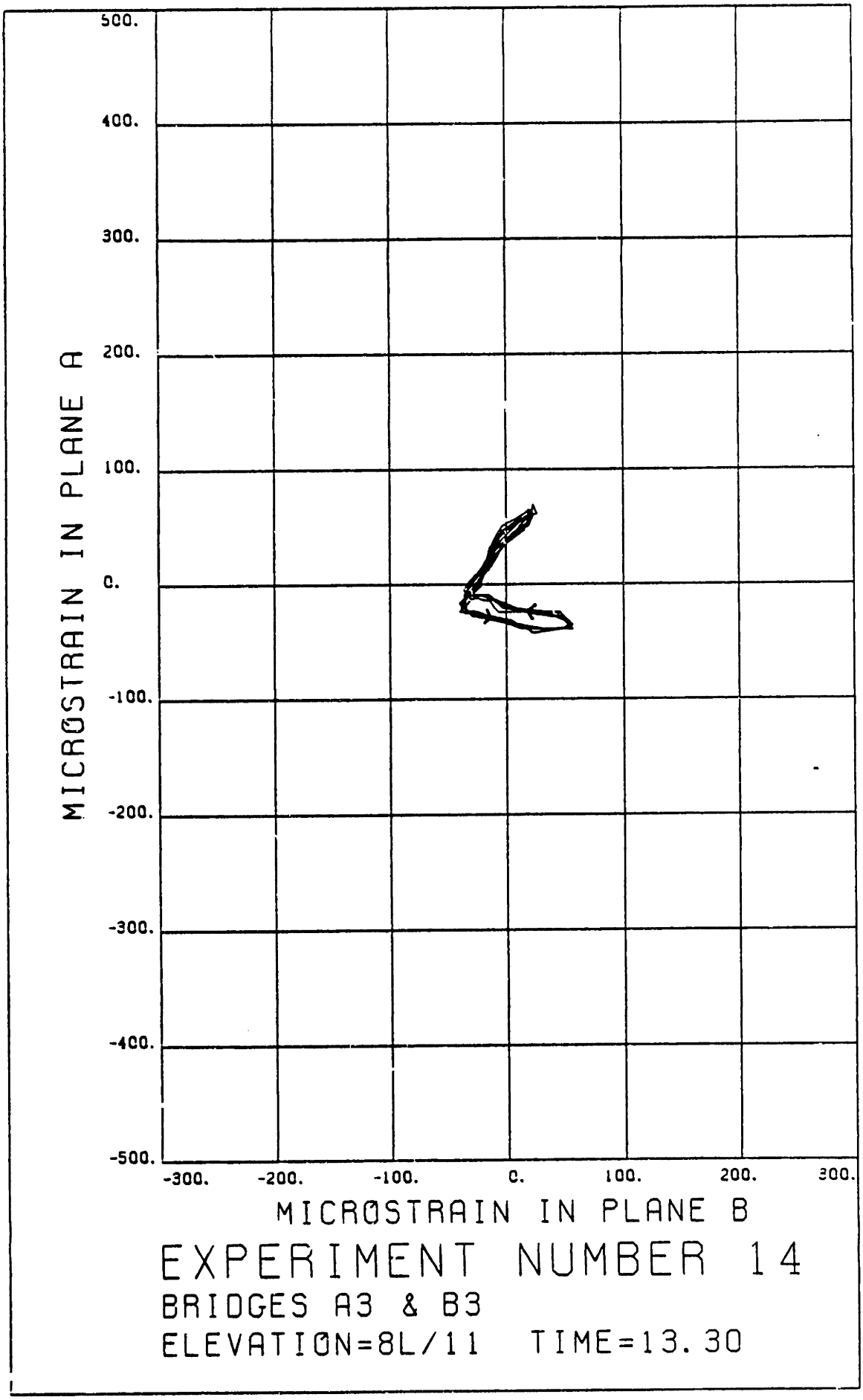
500.
400.
300.
200.
100.
0.
-100.
-200.
-300.
-400.
-500.
MICROSTRAIN IN PLANE A
-300.
-200.
-100.
0.
100.
200.
300.
MICROSTRAIN IN PLANE B
EXPERIMENT NUMBER 14
BRIDGES A3 & B3
ELEVATION=8L/11 TIME=13.30

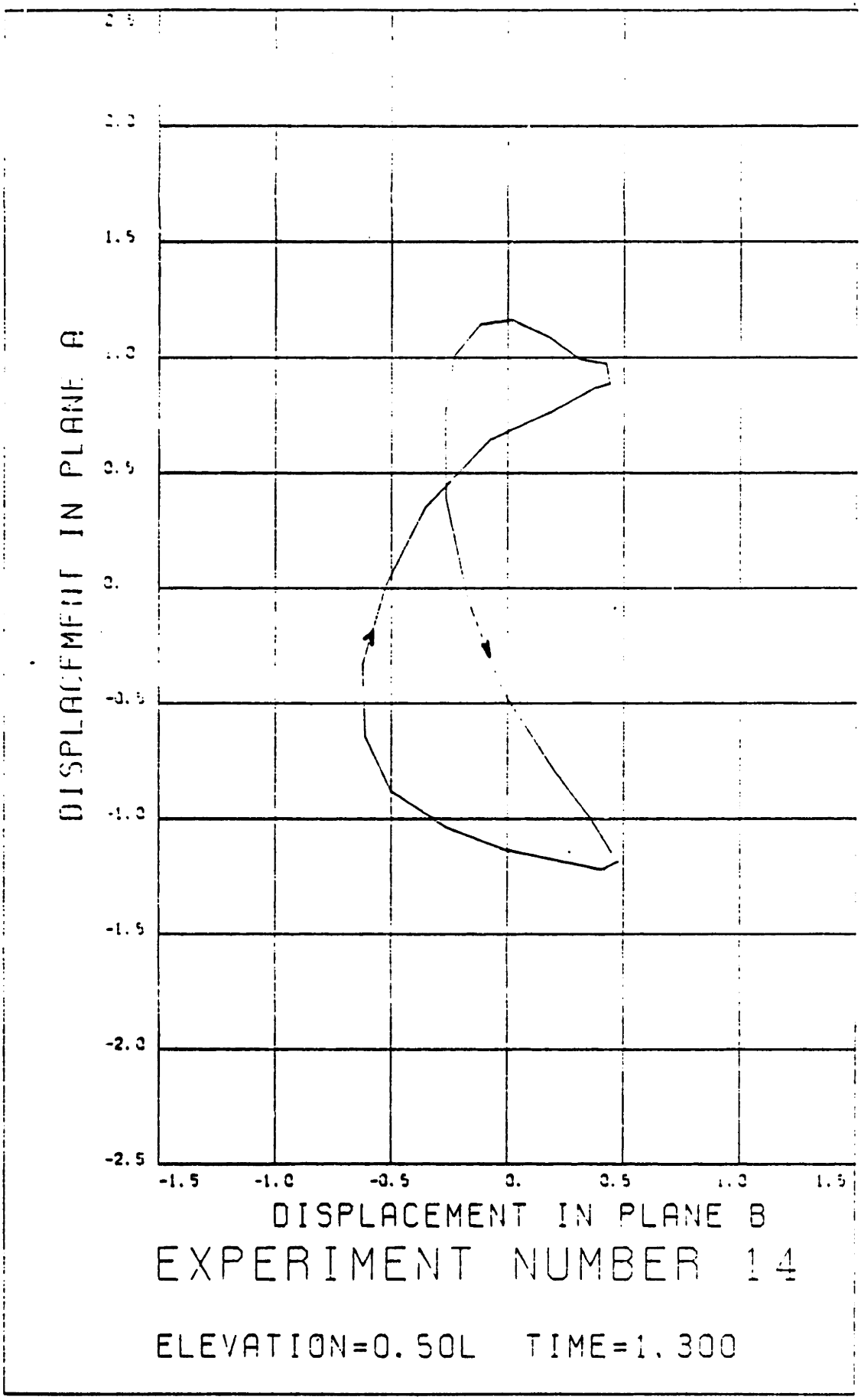
DISPLACEMENT IN PLANE A
2.5
2.0
1.5
1.0
0.5
0.
-0.5
-1.0
-1.5
-2.0
-2.5
-1.5
-1.0
-0.5
0.
0.5
1.0
1.5
DISPLACEMENT IN PLANE B
EXPERIMENT NUMBER 14
ELEVATION=0.50L TIME=1.300

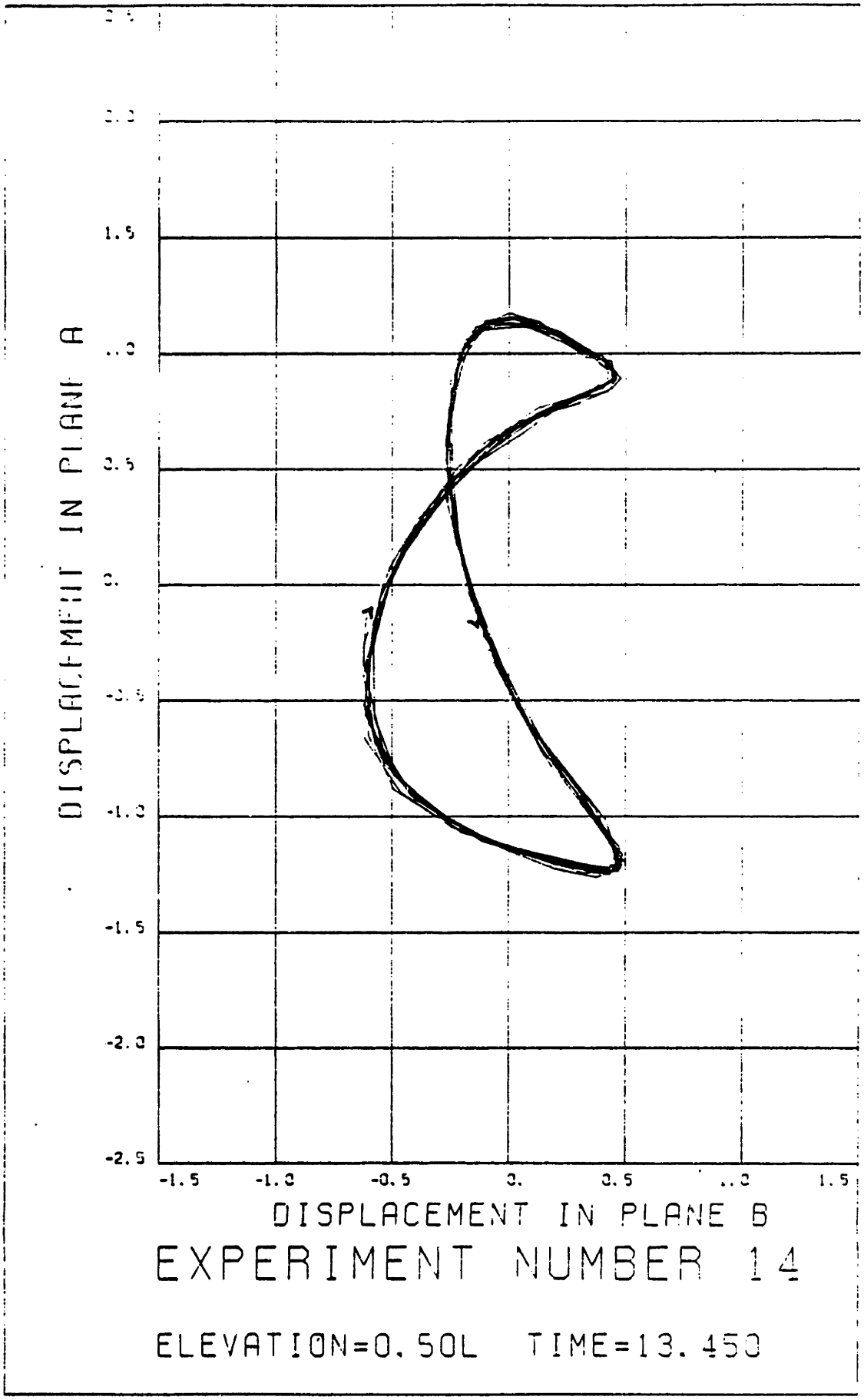
DISPLACEMENT IN PLANE A
1.5
0.5
-1.5
-2.0
-2.5
-1.5
-1.0
-0.5
0.
0.5
1.5
DISPLACEMENT IN PLANE B
EXPERIMENT NUMBER 14
ELEVATION=0.50L TIME=13.450

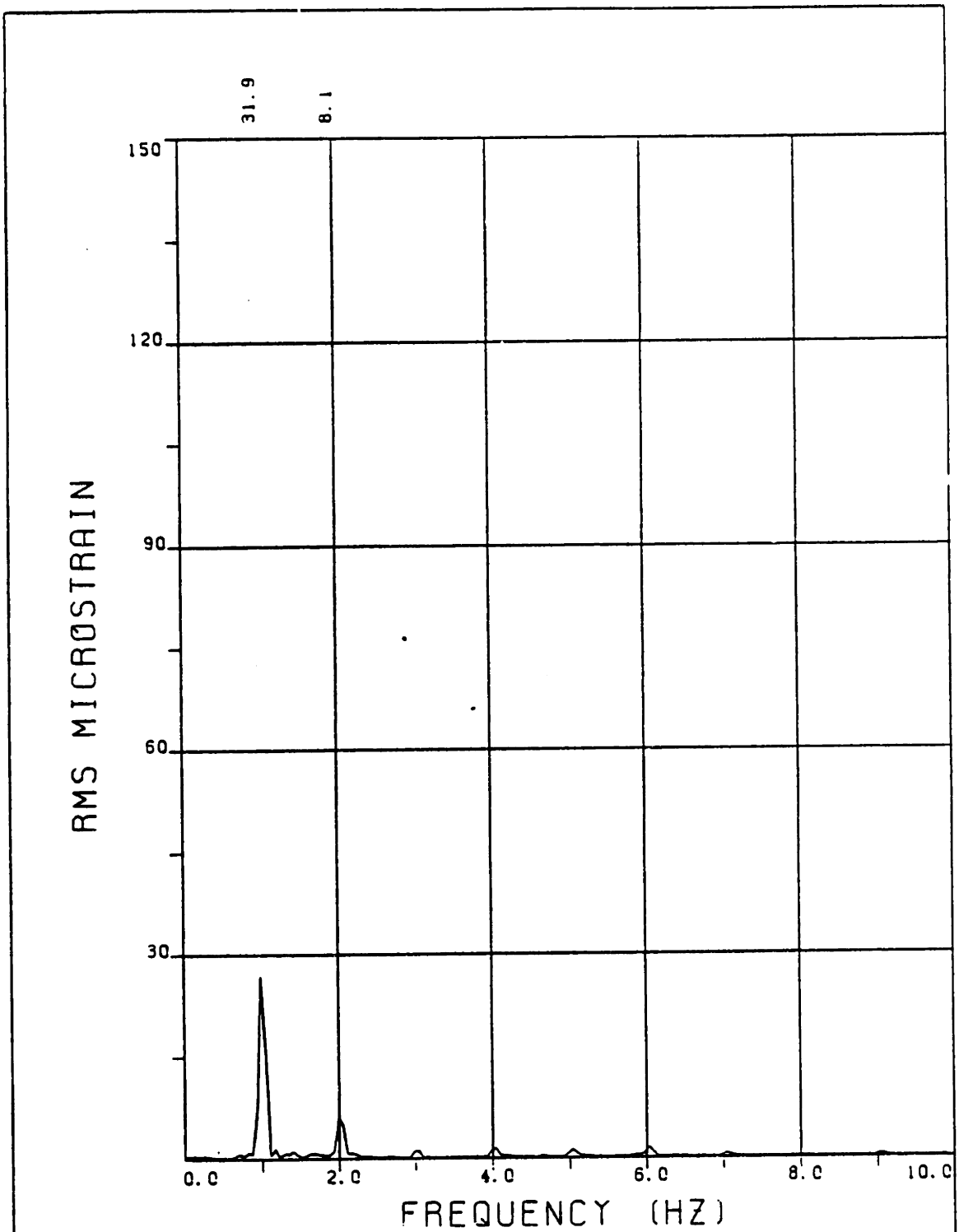

EXPERIMENT NUMBER 17

BRIDGE A8 ELEVATION=3L/11 BE=0.059

THETA=0 VC=0 FE=1.000 A/DE=1.98

MEASURED RESPONSE IN MICROSTRAIN

TOTAL DYNAMIC RMS=33.2

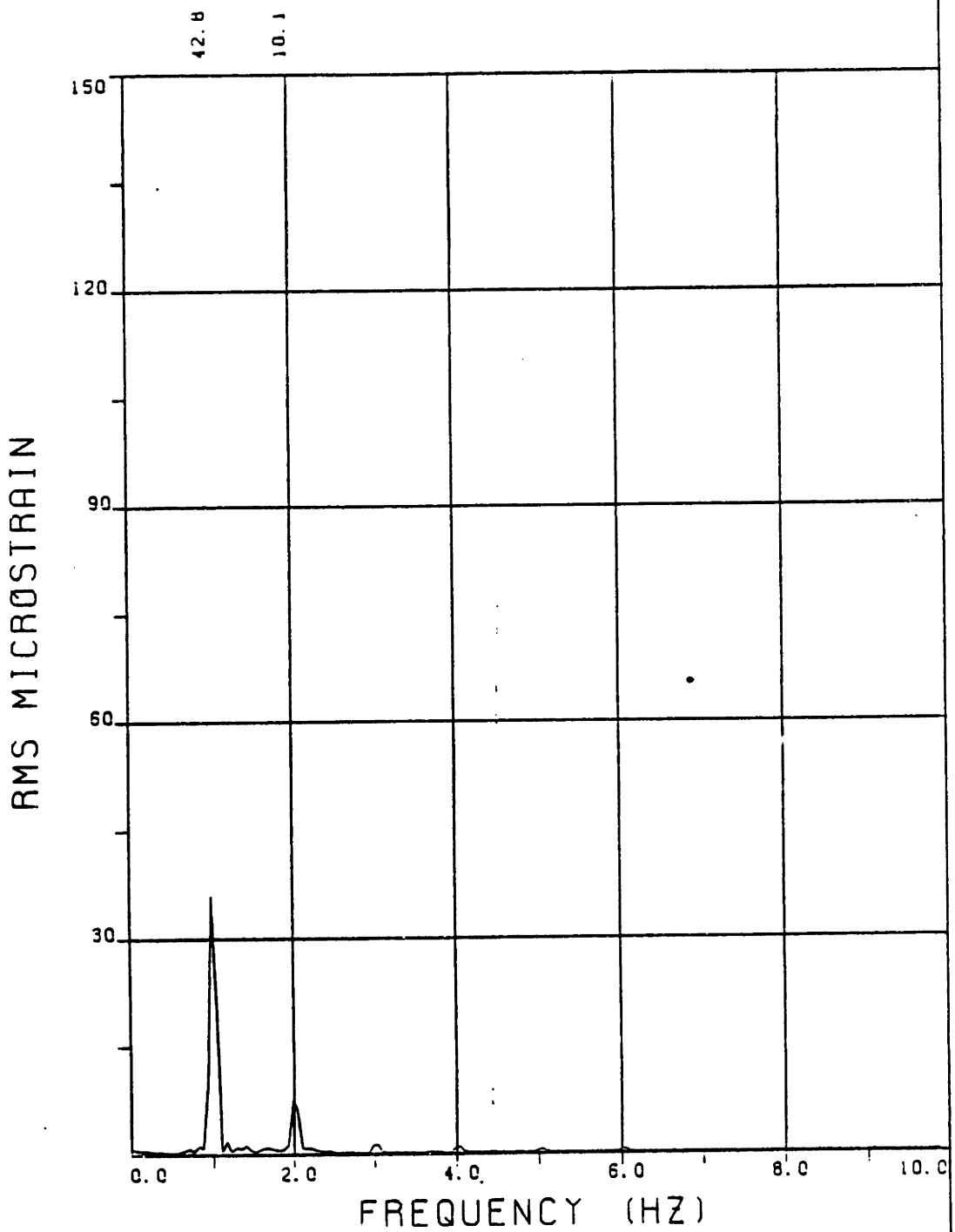

EXPERIMENT NUMBER 17

BRIDGE A6 ELEVATION=5L/11 BE=0.059

THETA=0 VC=0 FE=1.000 A/DE=1.98

MEASURED RESPONSE IN MICROSTRAIN

TOTAL DYNAMIC RMS=44.1

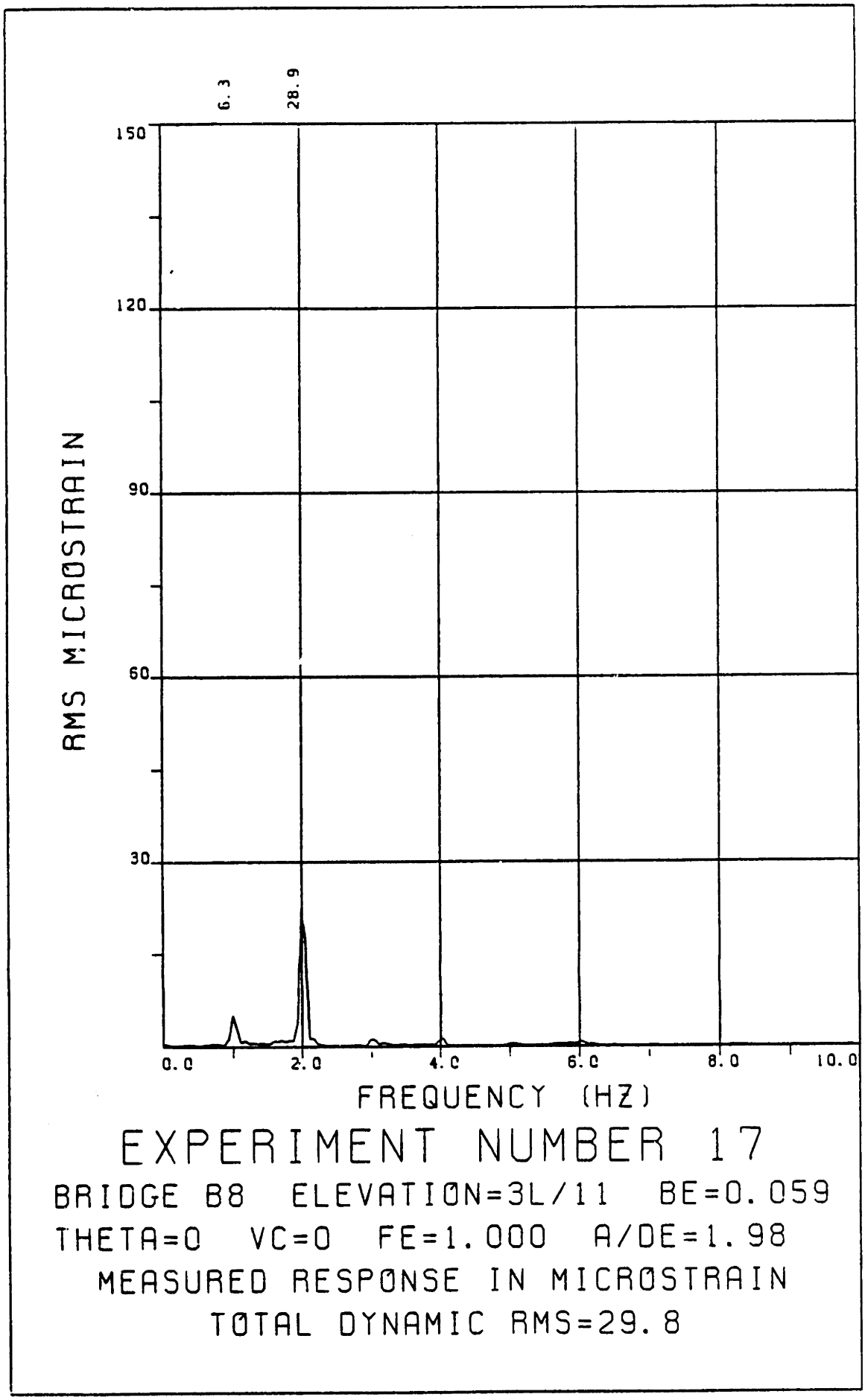
6.3
28.9
150
120
90
60
30
RMS MICROSTRAIN
0.0
2.0
4.0
6.0
8.0
10.0
FREQUENCY (HZ)
EXPERIMENT NUMBER 17
BRIDGE B8 ELEVATION=3L/11 BE=0.059
THETA=0 VC=0 FE=1.000 A/DE=1.98
MEASURED RESPONSE IN MICROSTRAIN
TOTAL DYNAMIC RMS=29.8

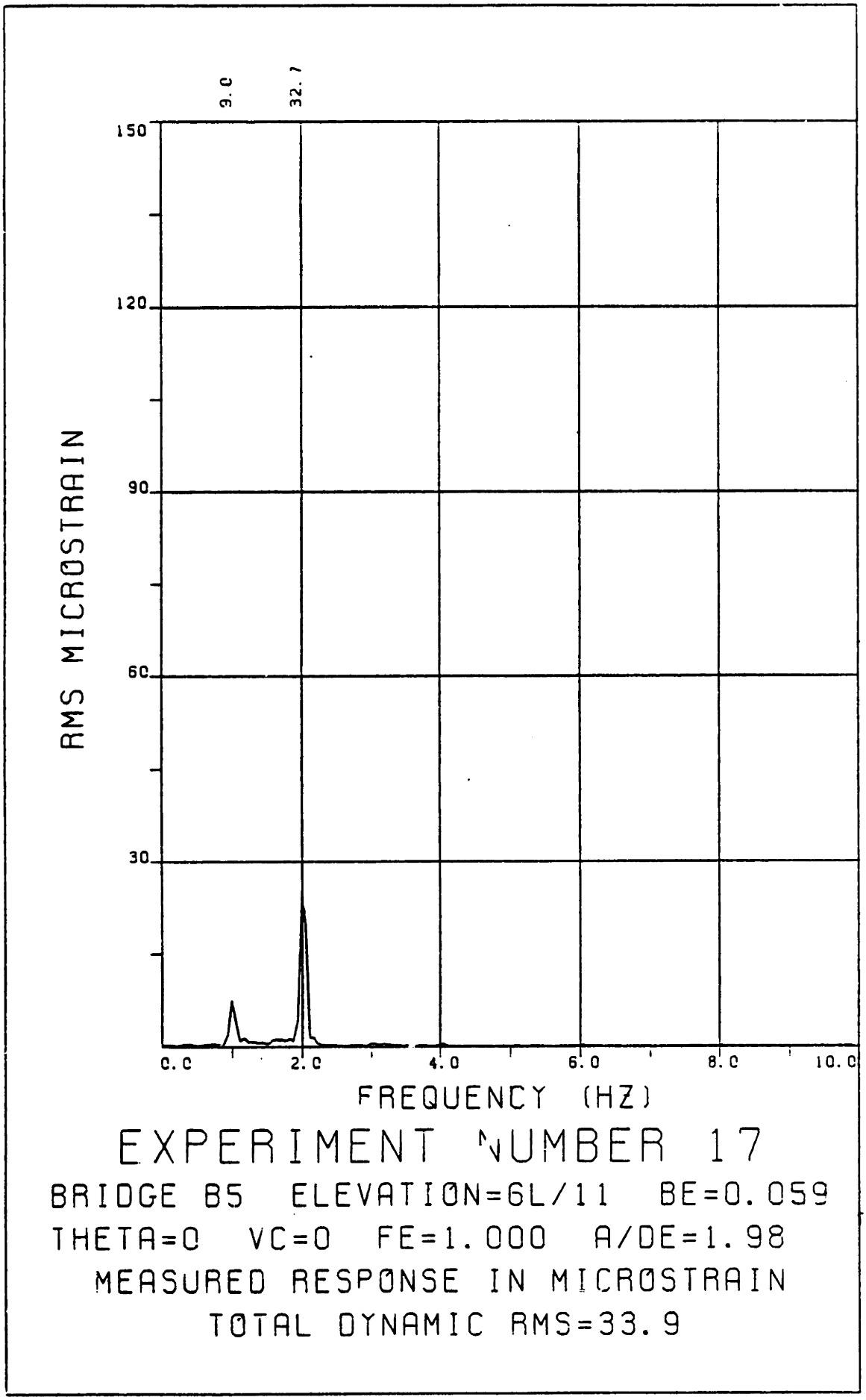
9.0
32.7
150
120
90
60
30
RMS MICROSTRAIN
0.0
2.0
4.0
6.0
8.0
10.0
FREQUENCY (HZ)
EXPERIMENT NUMBER 17
BRIDGE B5 ELEVATION=6L/11 BE=0.059
THETA=0 VC=0 FE=1.000 A/DE=1.98
MEASURED RESPONSE IN MICROSTRAIN
TOTAL DYNAMIC RMS=33.9

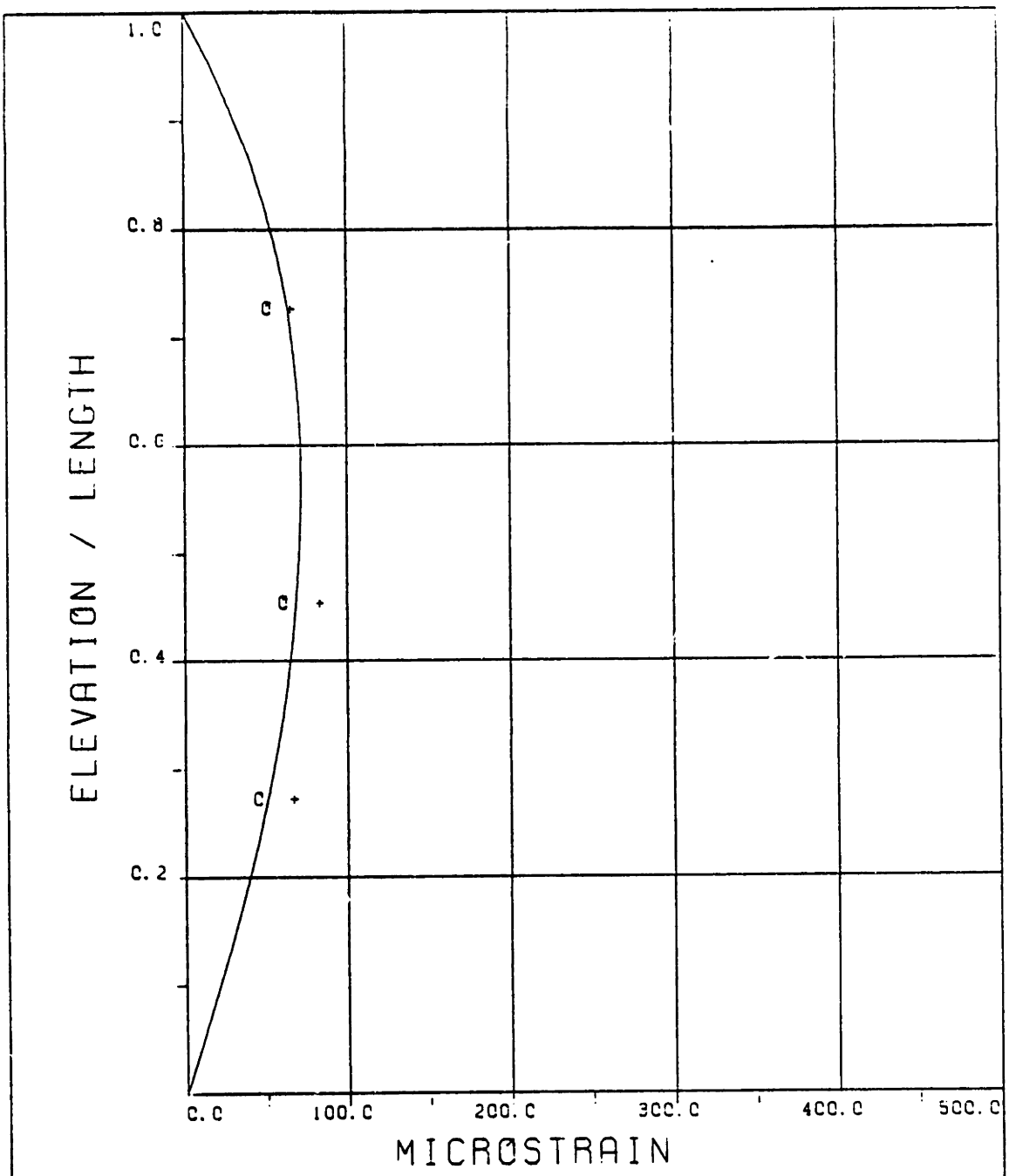

EXPERIMENT NUMBER 17

THETA=0 VC=0 FE=1.000 A/DE=1.98

DYNAMIC RESPONSE AT F=FE IN PLANE A

——— THEORY o o o EXPERIMENT

MAXIMUM DYNAMIC RESPONSE IN PLANE A

——— THEORY + + + EXPERIMENT

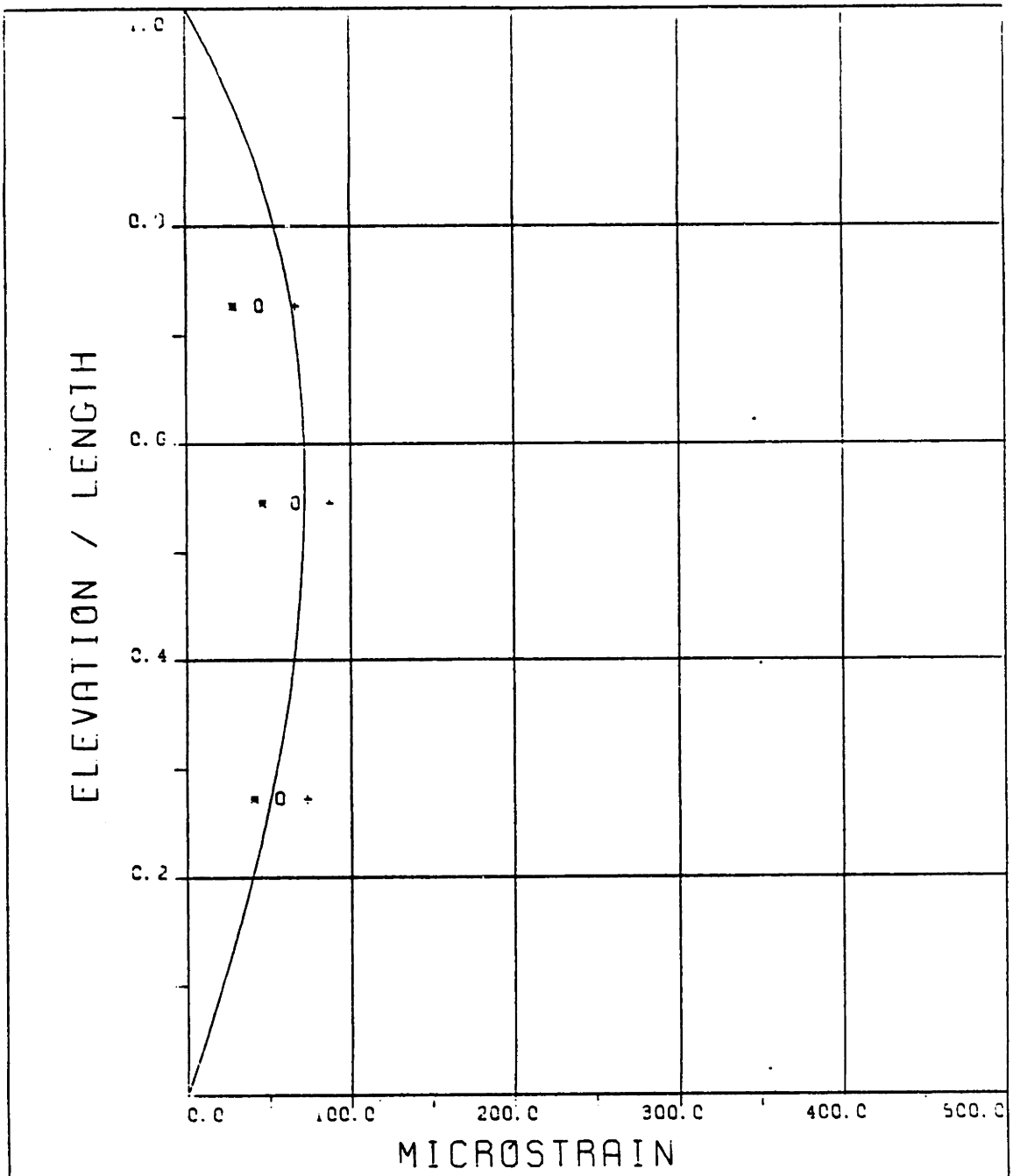

EXPERIMENT NUMBER 17

THETA=0 VC=0 FE=1.000 A/DE=1.98

DYNAMIC RESPONSE IN PLANE B AT F=2FE

* * * EXPERIMENT

MAXIMUM RESPONSE IN PLANE B

o o o EXPERIMENT

MAXIMUM RESPONSE

_____ THEORY + + + EXPERIMENT

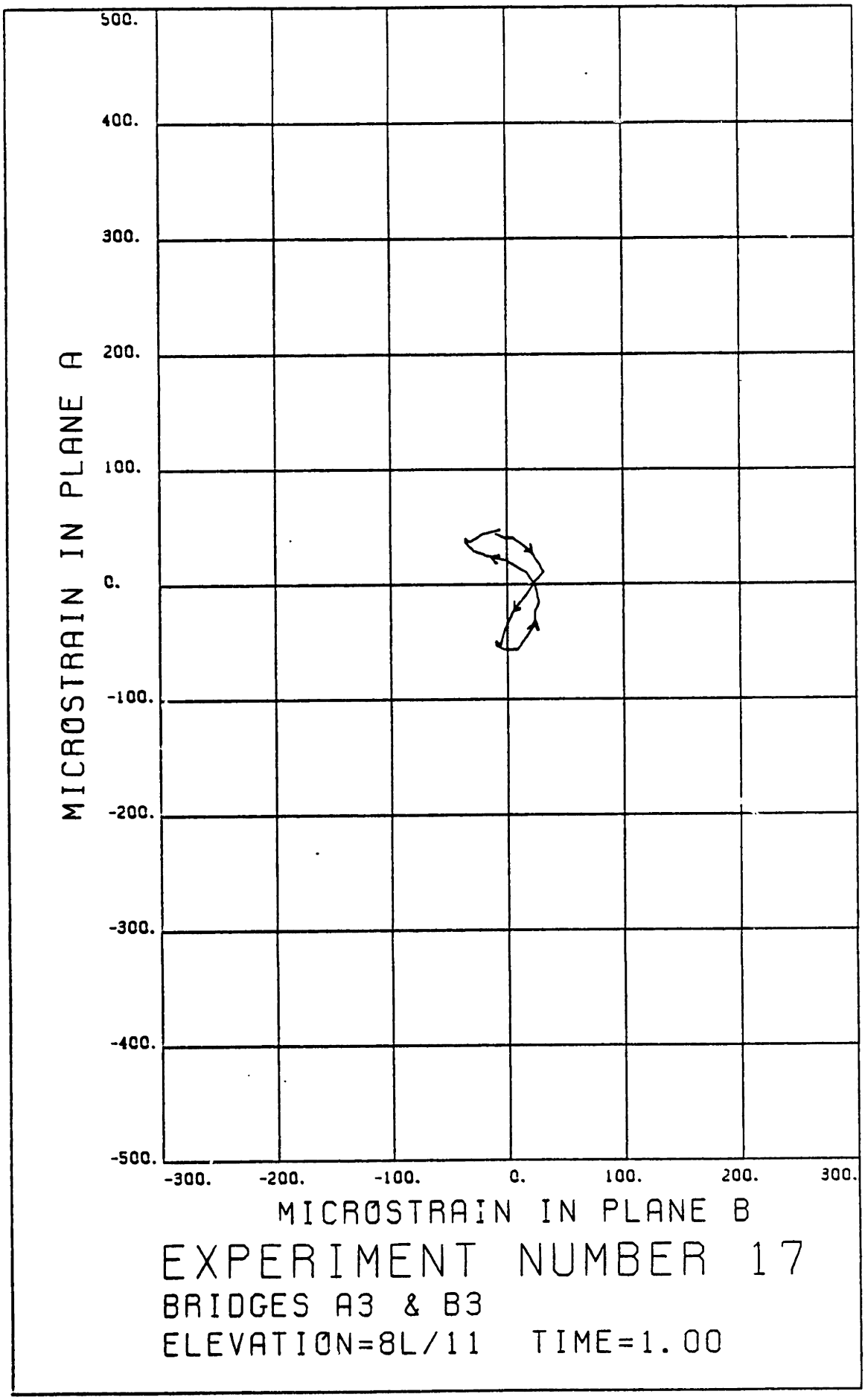
500.
400.
300.
200.
100.
0.
-100.
-200.
-300.
-400.
-500.
MICROSTRAIN IN PLANE A
-300.
-200.
-100.
0.
100.
200.
300.
MICROSTRAIN IN PLANE B
EXPERIMENT NUMBER 17
BRIDGES A3 & B3
ELEVATION=8L/11 TIME=1.00

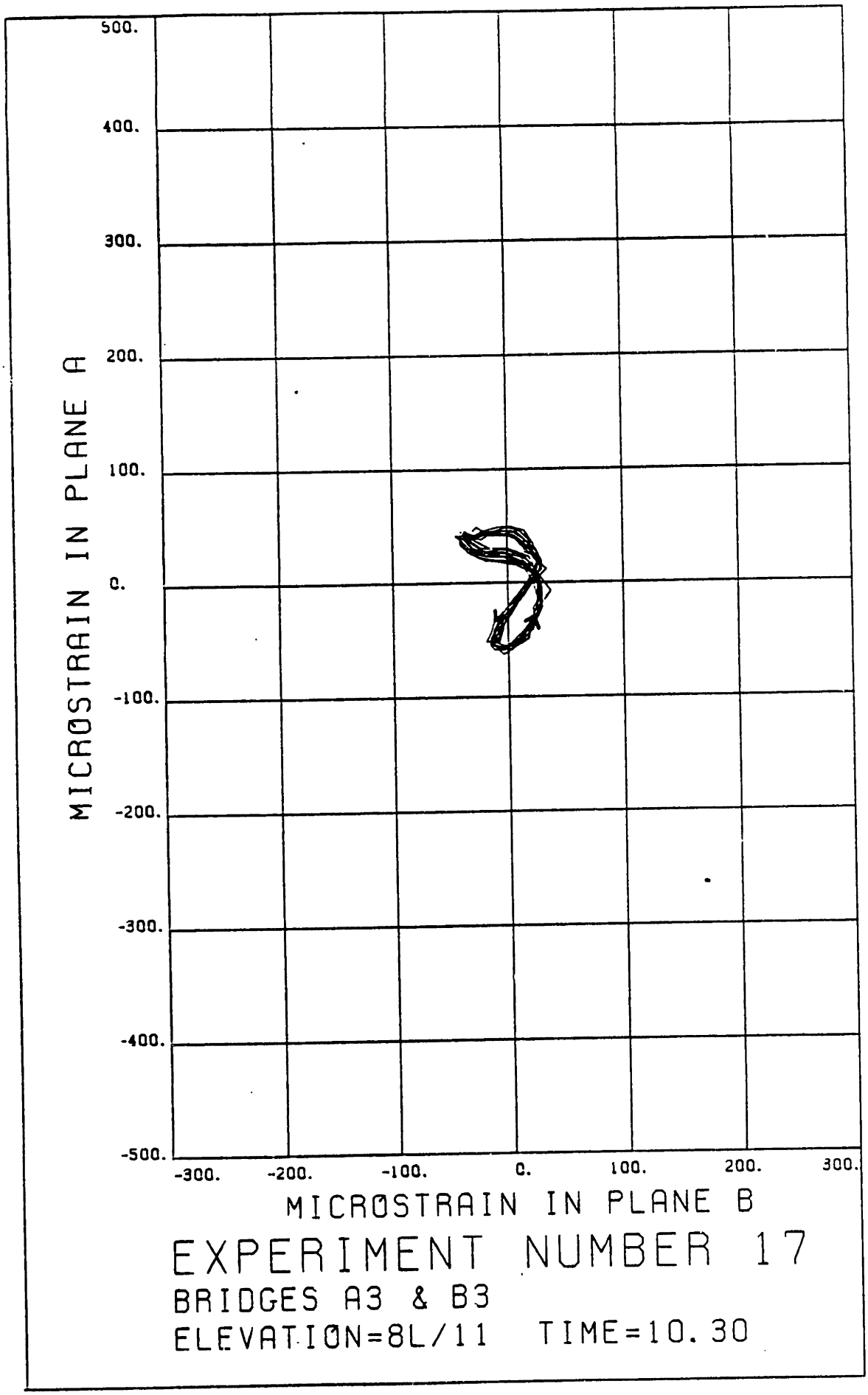
500.
400.
300.
200.
100.
0.
-100.
-200.
-300.
-400.
-500.
MICROSTRAIN IN PLANE A
-300.
-200.
-100.
0.
100.
200.
300.
MICROSTRAIN IN PLANE B
EXPERIMENT NUMBER 17
BRIDGES A3 & B3
ELEVATION=8L/11 TIME=10.30

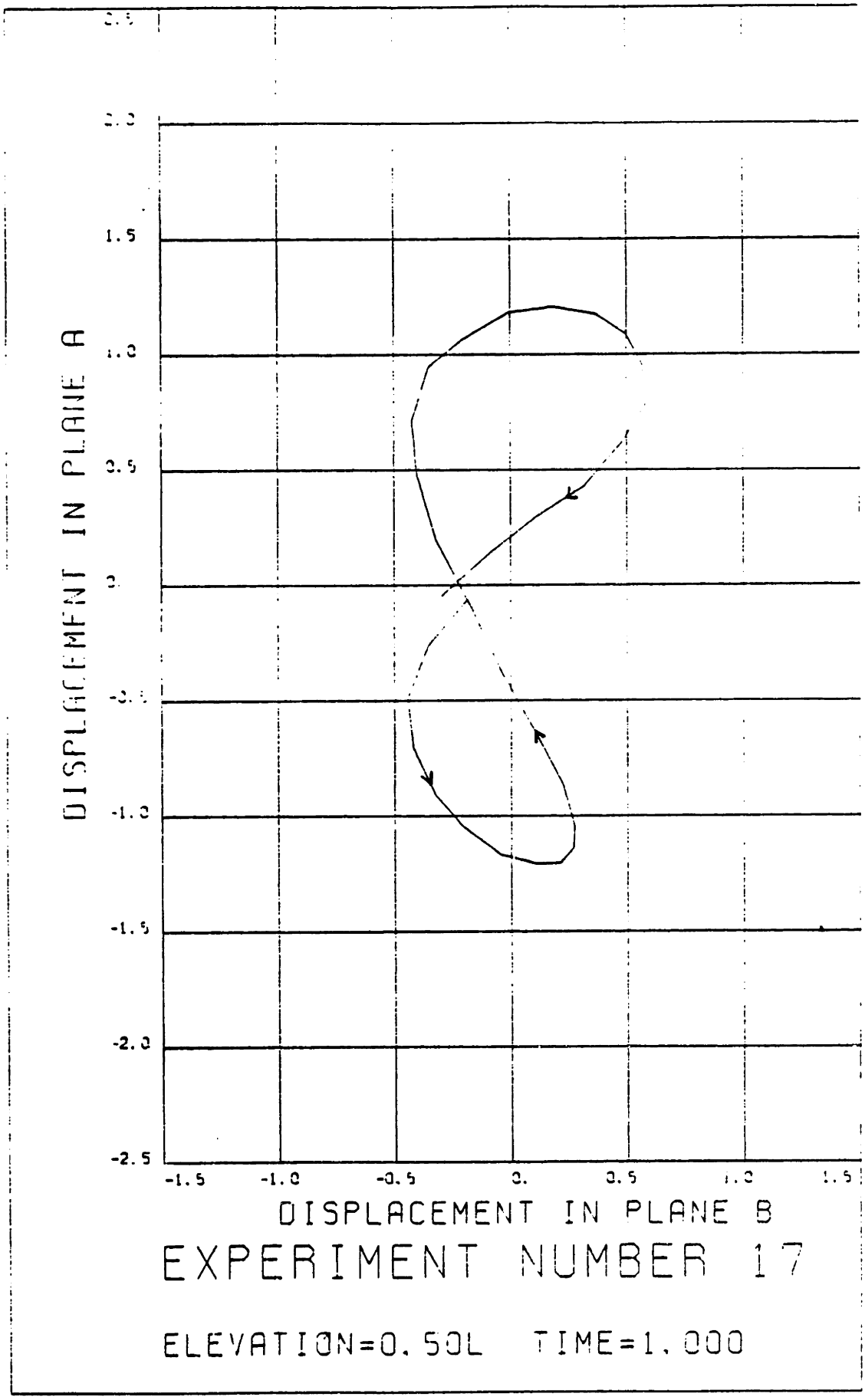
DISPLACEMENT IN PLANE A
2.5
2.0
1.5
1.0
0.5
0.
-0.5
-1.0
-1.5
-2.0
-2.5
-1.5
-1.0
-0.5
0.
0.5
1.0
1.5
DISPLACEMENT IN PLANE B
EXPERIMENT NUMBER 17
ELEVATION=0.50L TIME=1.000

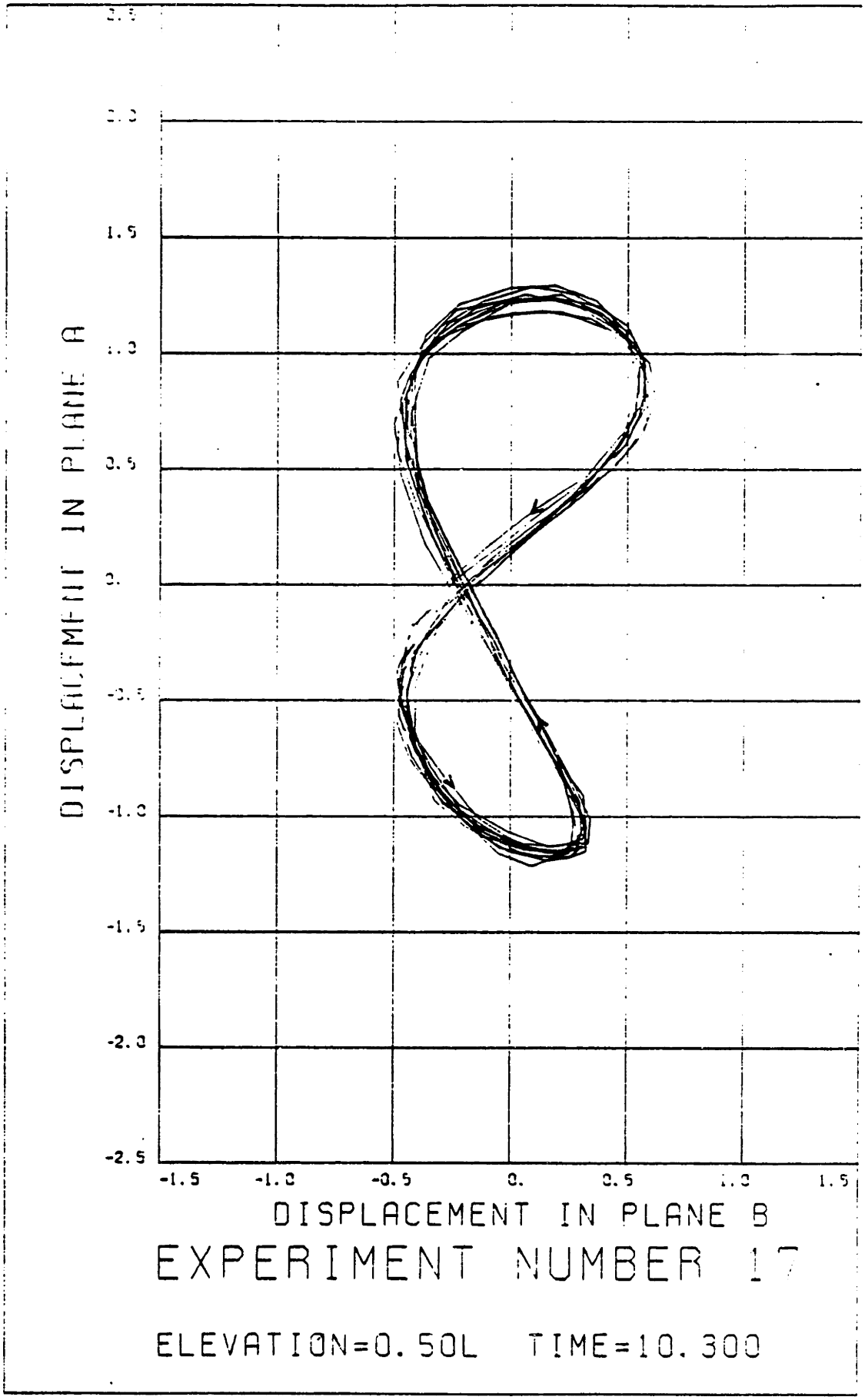
DISPLACEMENT IN PLANE A
1.5
1.0
0.5
0.
-1.0
-1.5
-2.0
-2.5
-1.5
-1.0
-0.5
0.
0.5
1.0
1.5
DISPLACEMENT IN PLANE B
EXPERIMENT NUMBER 17
ELEVATION=0.50L TIME=10.300

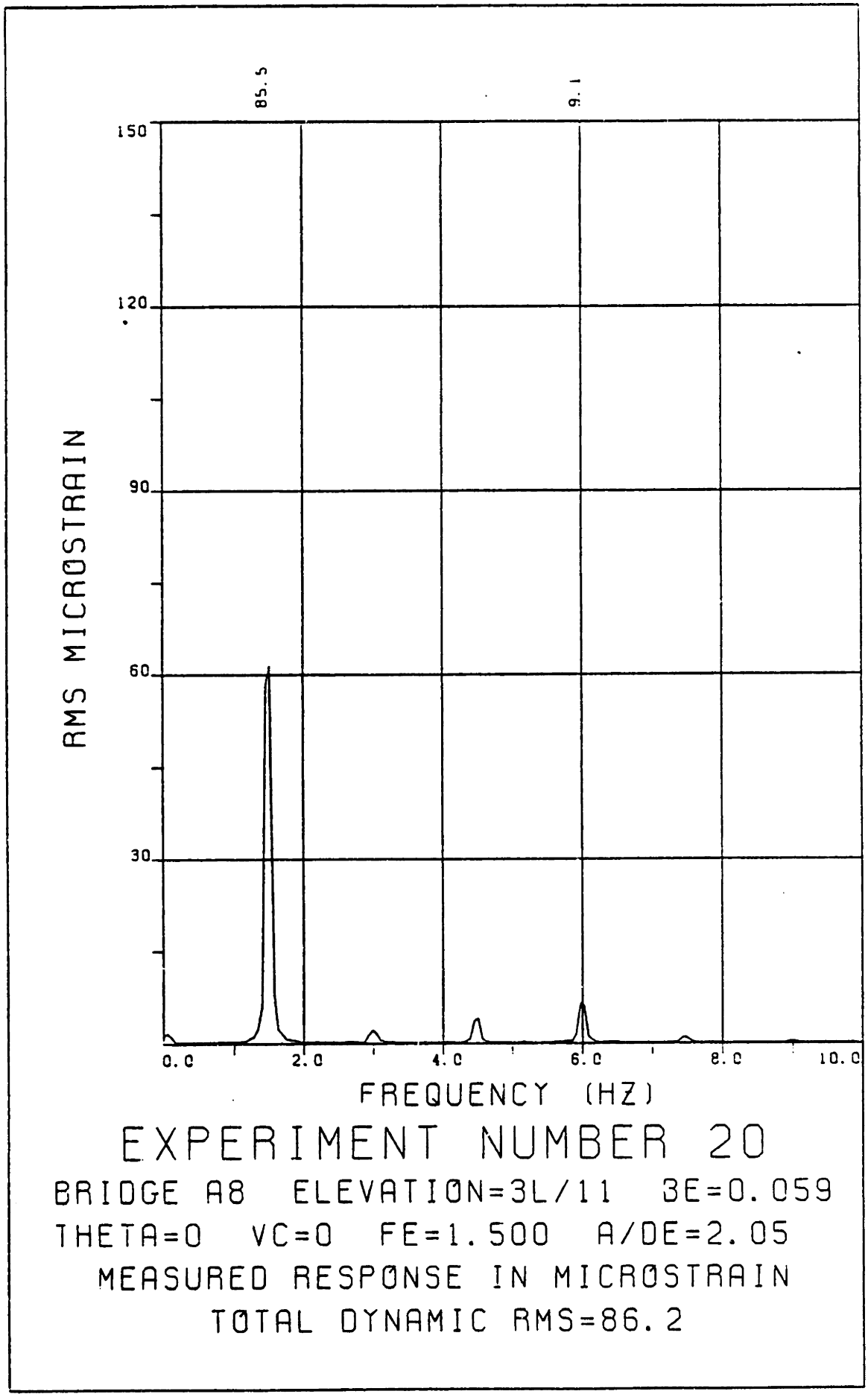
85.5
9.1
150
120
90
60
30
RMS MICROSTRAIN
0.0
2.0
4.0
6.0
8.0
10.0
FREQUENCY (HZ)
EXPERIMENT NUMBER 20
BRIDGE A8 ELEVATION=3L/11 3E=0.059
THETA=0 VC=0 FE=1.500 A/DE=2.05
MEASURED RESPONSE IN MICROSTRAIN
TOTAL DYNAMIC RMS=86.2

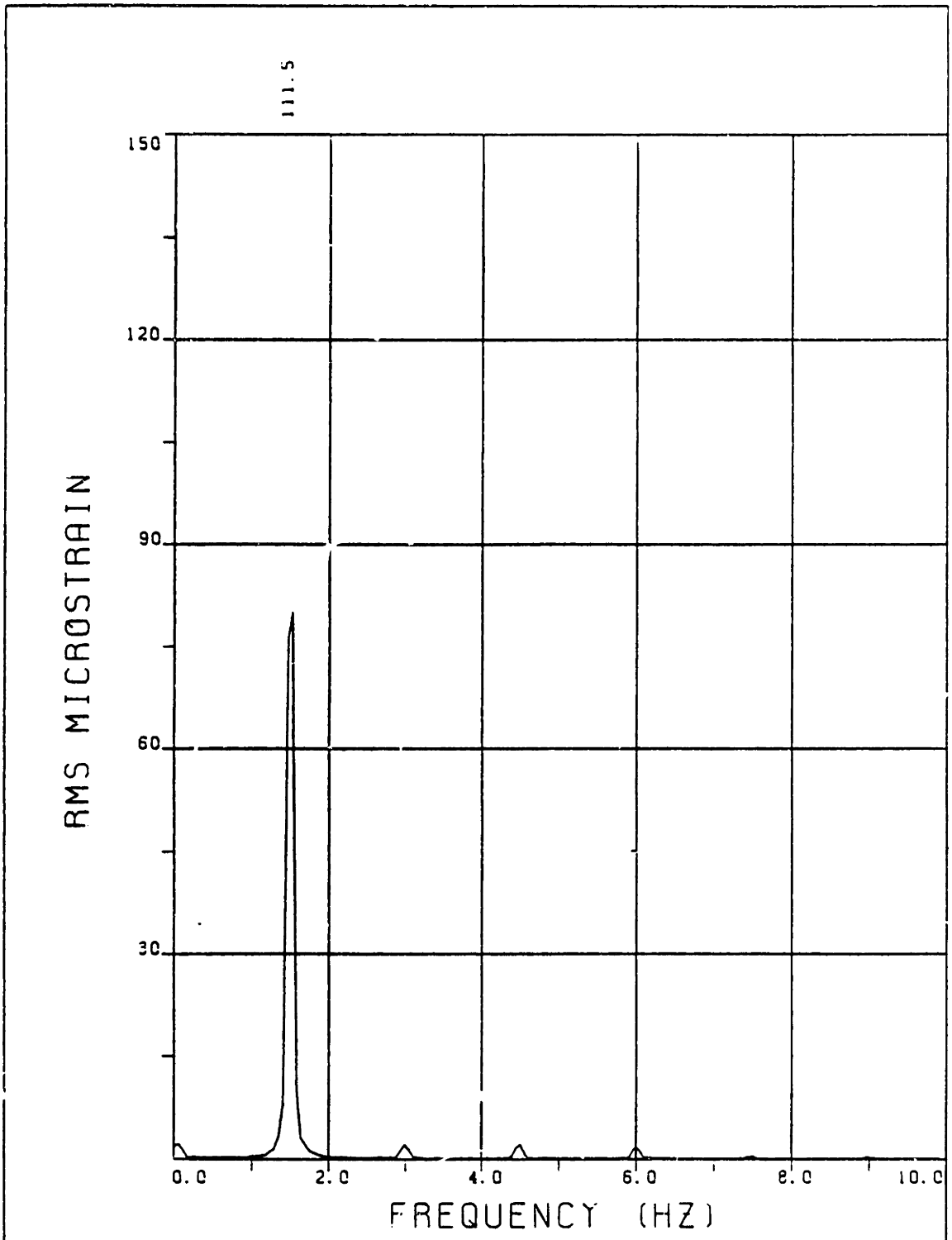

EXPERIMENT NUMBER 20

BRIDGE A6 ELEVATION=5L/11 BE=0.059

THETA=0 VC=0 FE=1.500 A/DE=2.05

MEASURED RESPONSE IN MICROSTRAIN

TOTAL DYNAMIC RMS=111.7

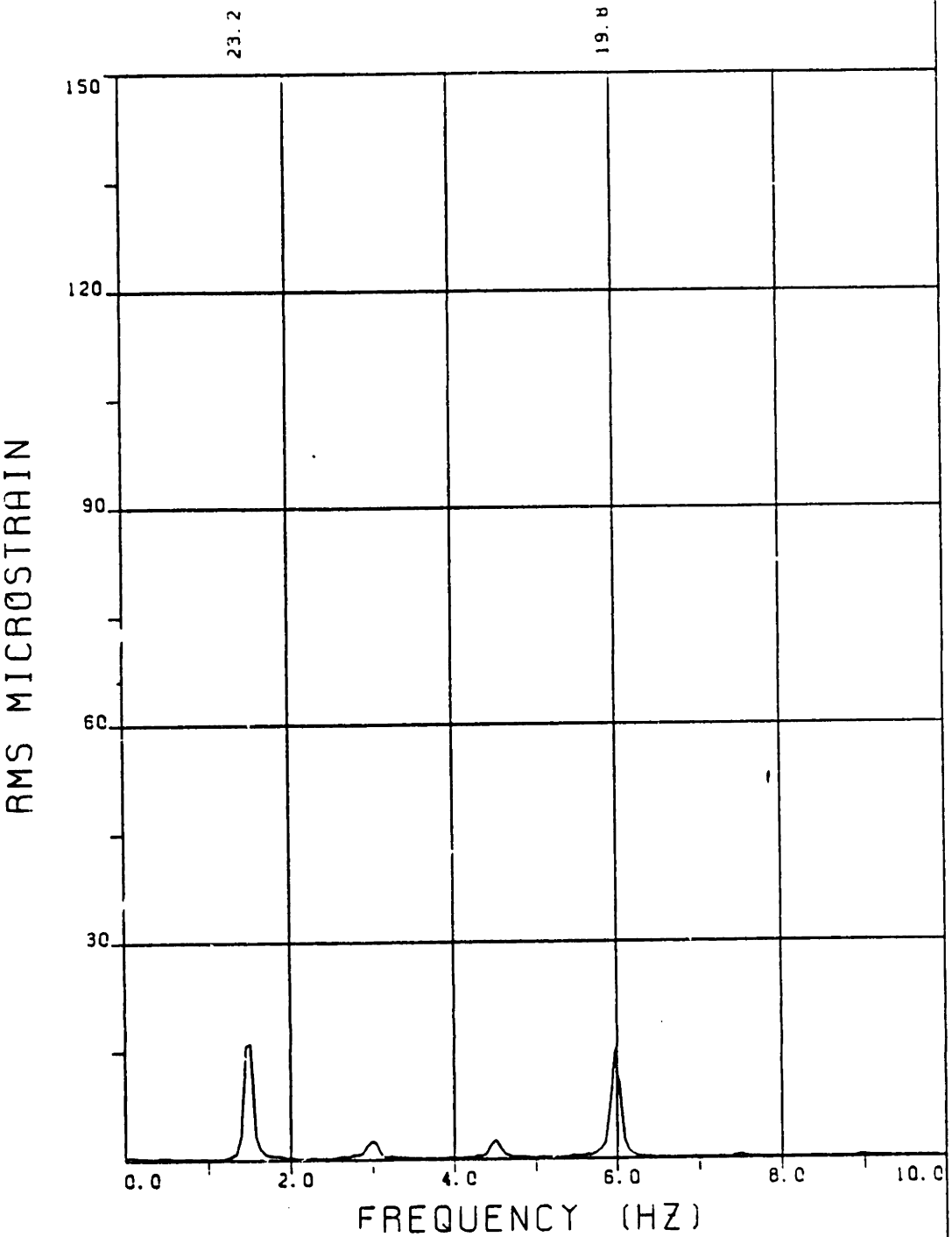

EXPERIMENT NUMBER 20

BRIDGE B8 ELEVATION=3L/11 BE=0.059

THETA=0 VC=0 FE=1.500 A/DE=2.05

MEASURED RESPONSE IN MICROSTRAIN

TOTAL DYNAMIC RMS=31.1

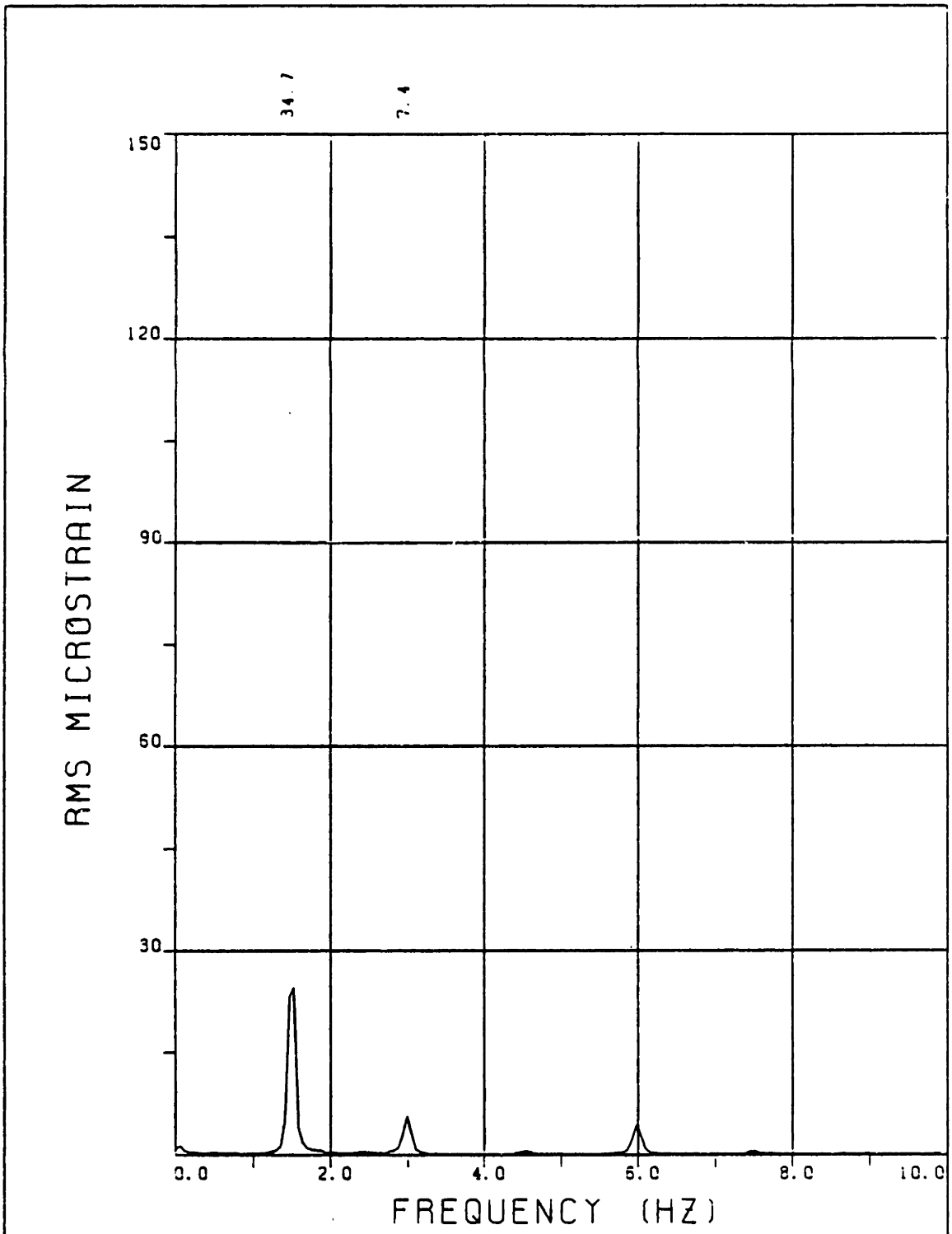

EXPERIMENT NUMBER 20

BRIDGE B5 ELEVATION=6L/11 BE=0.059

THETA=0 VC=0 FE=1.500 A/DE=2.05

MEASURED RESPONSE IN MICROSTRAIN

TOTAL DYNAMIC RMS=36.0

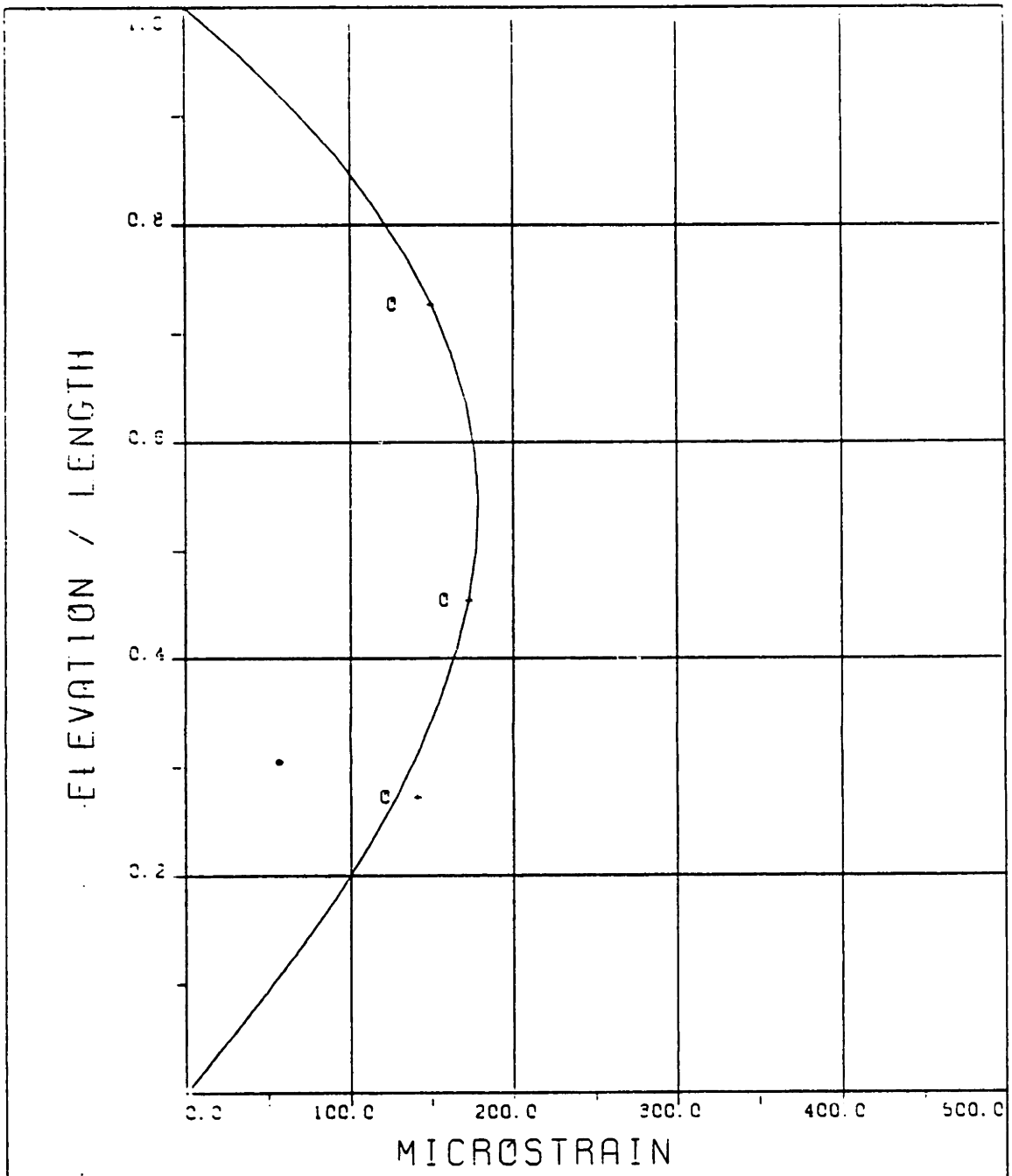

EXPERIMENT NUMBER 20

THETS=0 VC=0 FE=1.500 A/DE=2.05

DYNAMIC RESPONSE AT F=FE IN PLANE A

——— THEORY o o o EXPERIMENT

MAXIMUM DYNAMIC RESPONSE IN PLANE A

——— THEORY + + + EXPERIMENT

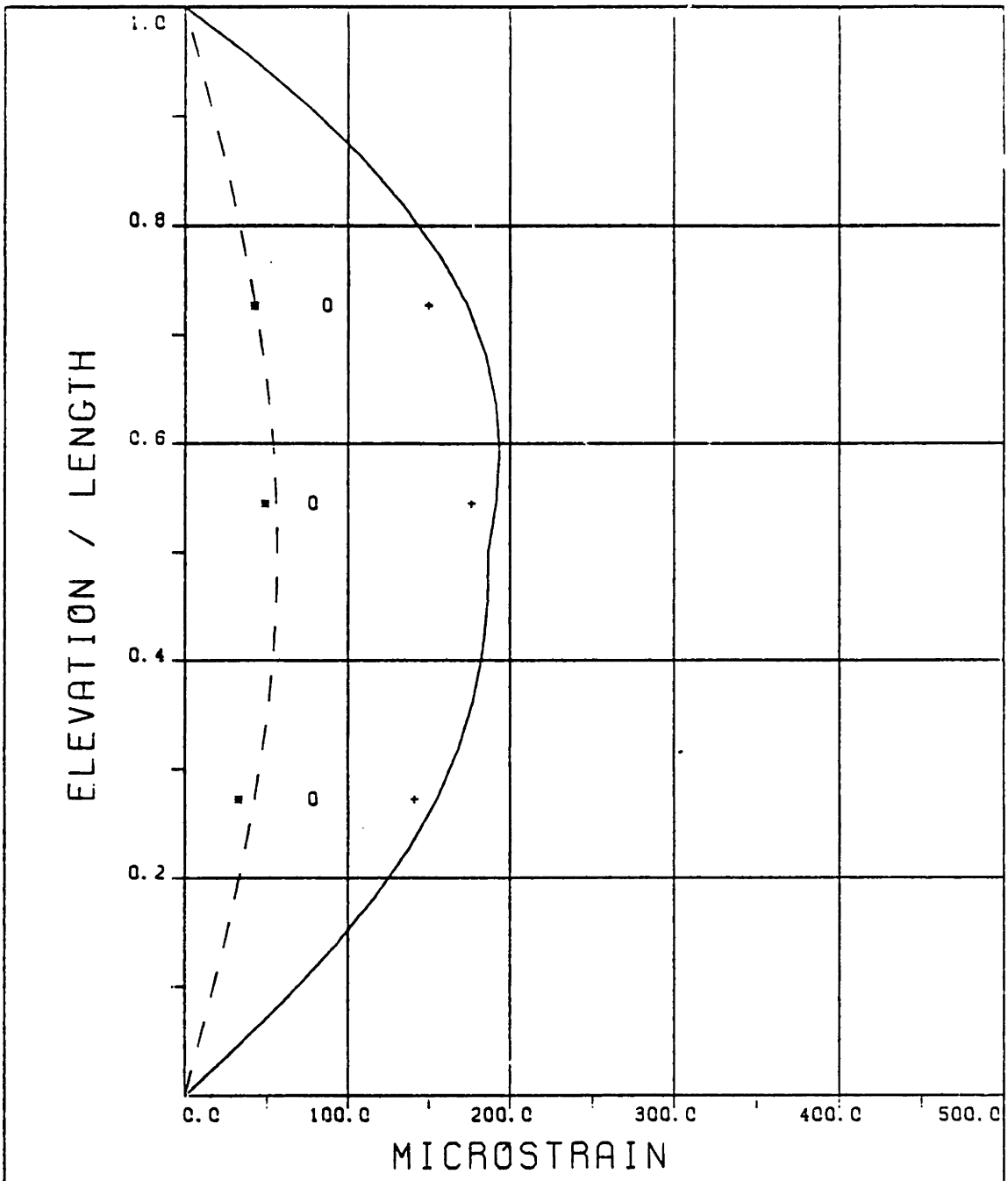

EXPERIMENT NUMBER 20a

THETA=0 VC=0 FE=1.500 A/DE=2.05

DYNAMIC RESPONSE IN PLANE B AT F=FE

----- THEORY * * * EXPERIMENT

MAXIMUM RESPONSE IN PLANE B

o o o EXPERIMENT

MAXIMUM RESPONSE

_____ THEORY + + + EXPERIMENT

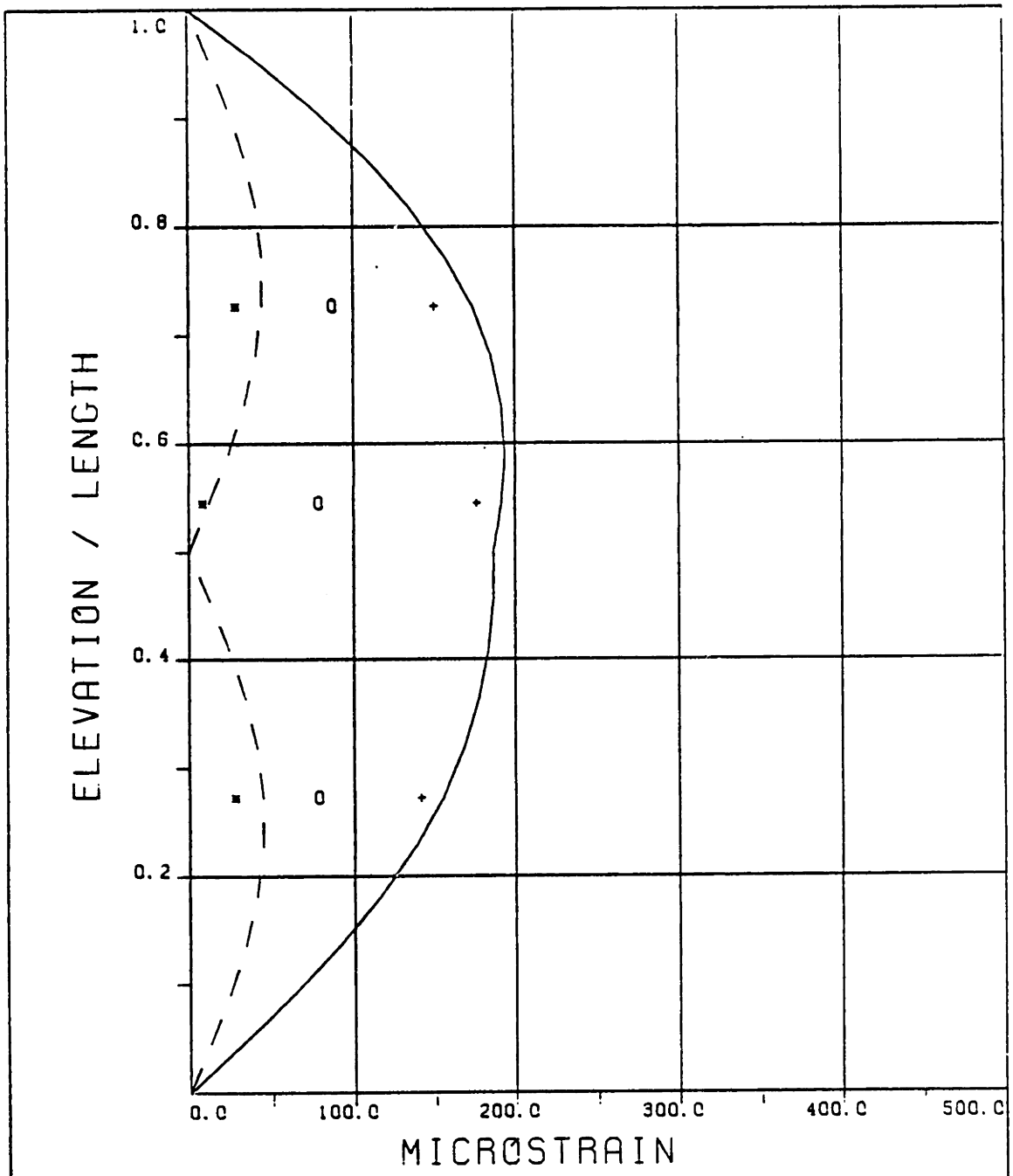

EXPERIMENT NUMBER 20b

THETA=0 VC=0 FE=1.500 A/DE=2.05

DYNAMIC RESPONSE IN PLANE B AT F=4FE

----- THEORY * * * EXPERIMENT

MAXIMUM RESPONSE IN PLANE B

o o o EXPERIMENT

MAXIMUM RESPONSE

_____ THEORY + + + EXPERIMENT

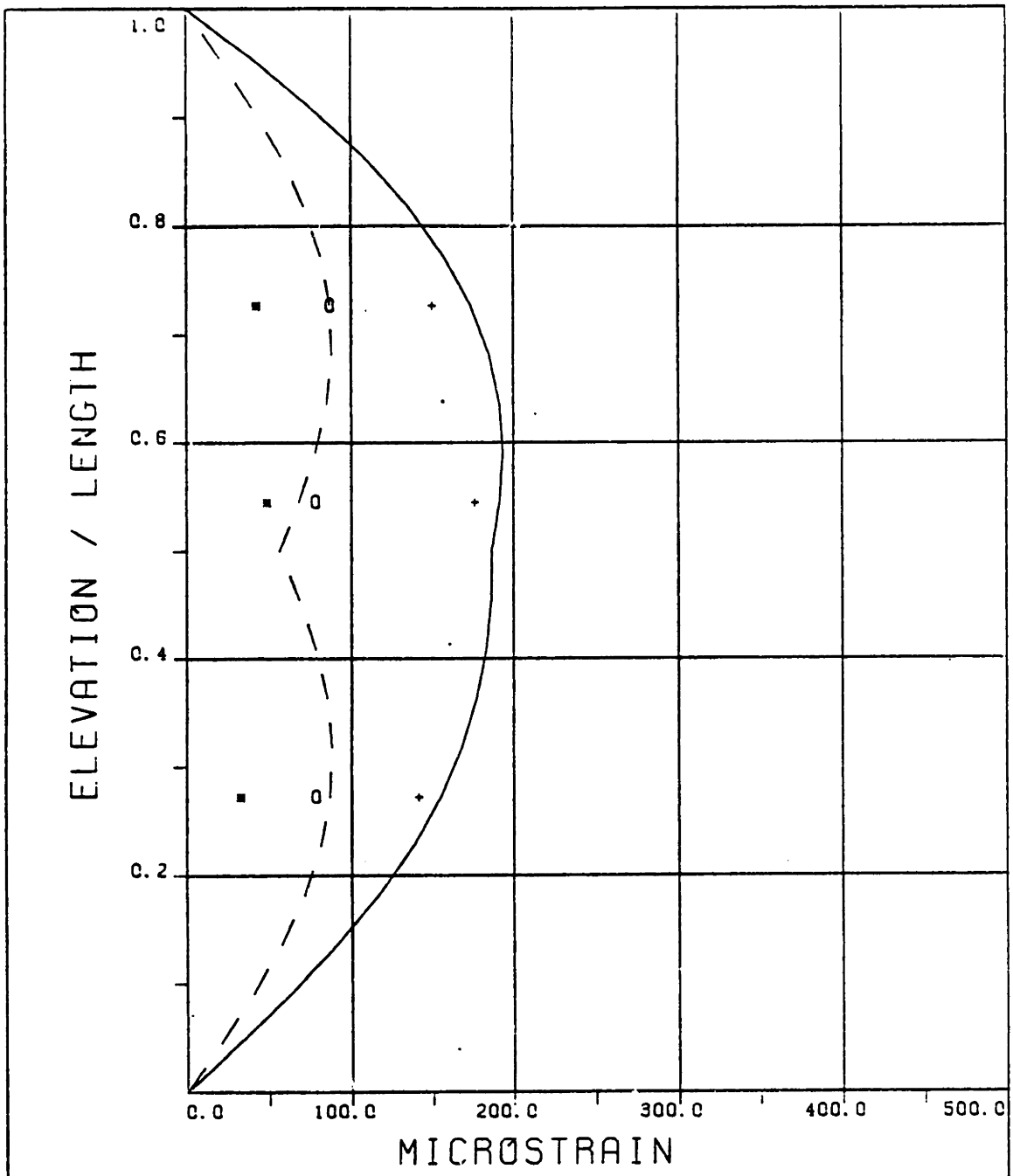

EXPERIMENT NUMBER 20c

THETA=0 VC=0 FE=1.500 A/DE=2.05

DYNAMIC RESPONSE IN PLANE B AT F=FE

* * * EXPERIMENT

MAXIMUM RESPONSE IN PLANE B

----- THEORY o o o EXPERIMENT

MAXIMUM RESPONSE

_____ THEORY + + + EXPERIMENT

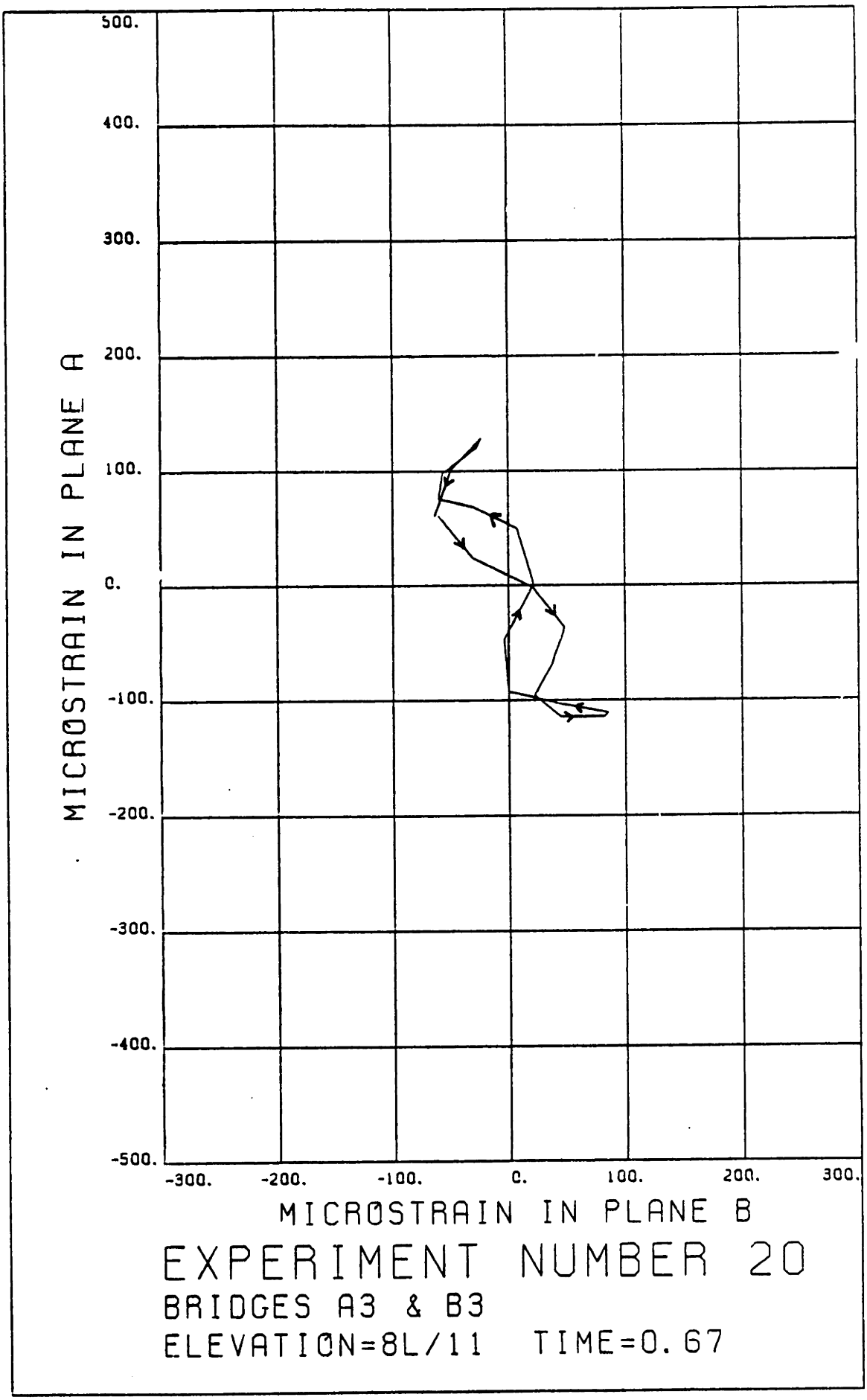
500.
400.
300.
200.
100.
0.
-100.
-200.
-300.
-400.
-500.
MICROSTRAIN IN PLANE A
-300.
-200.
-100.
0.
100.
200.
300.
MICROSTRAIN IN PLANE B
EXPERIMENT NUMBER 20
BRIDGES A3 & B3
ELEVATION=8L/11 TIME=0.67

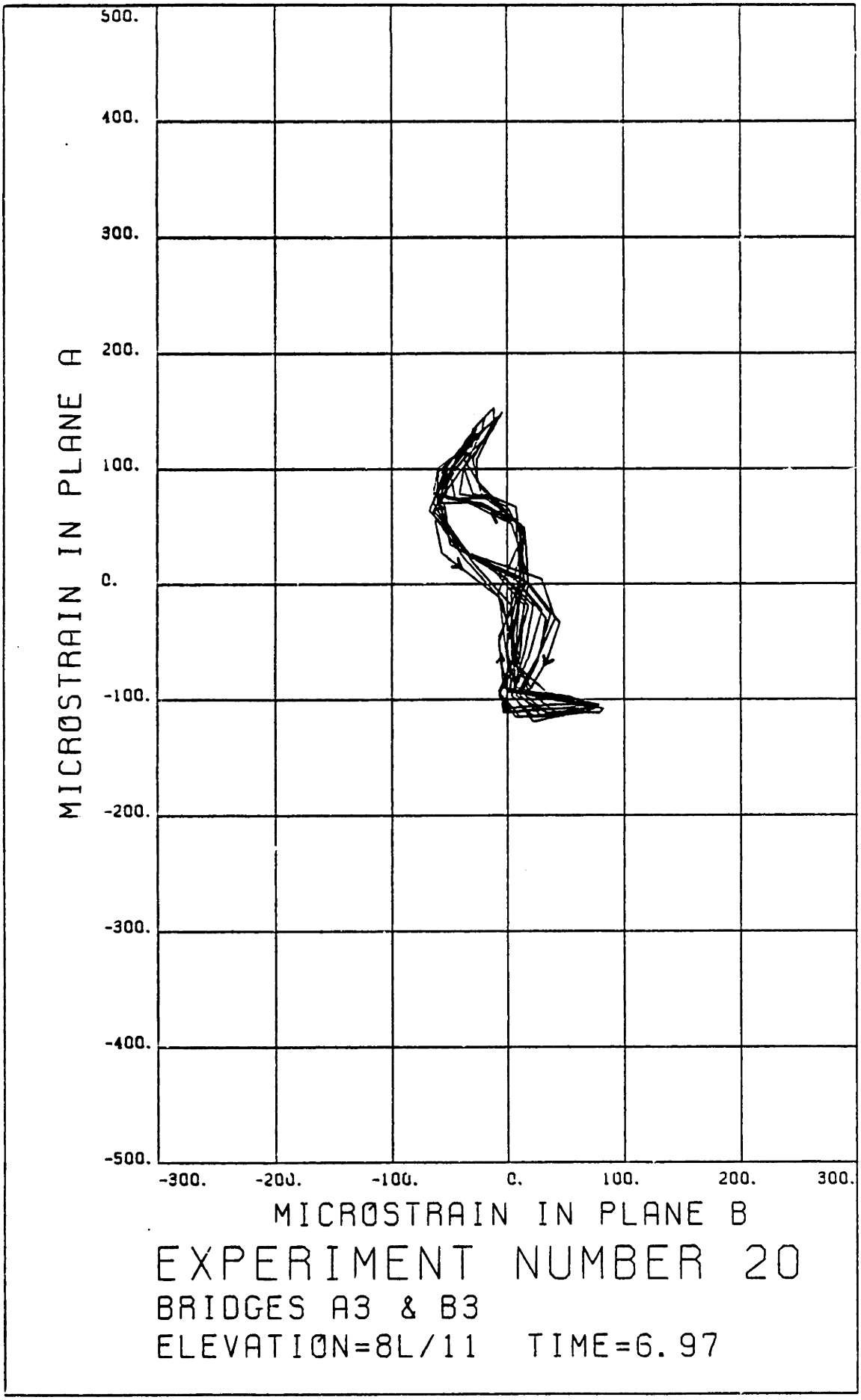
500.
400.
300.
200.
100.
0.
-100.
-200.
-300.
-400.
-500.
MICROSTRAIN IN PLANE A
-300.
-200.
-100.
0.
100.
200.
300.
MICROSTRAIN IN PLANE B
EXPERIMENT NUMBER 20
BRIDGES A3 & B3
ELEVATION=8L/11 TIME=6.97

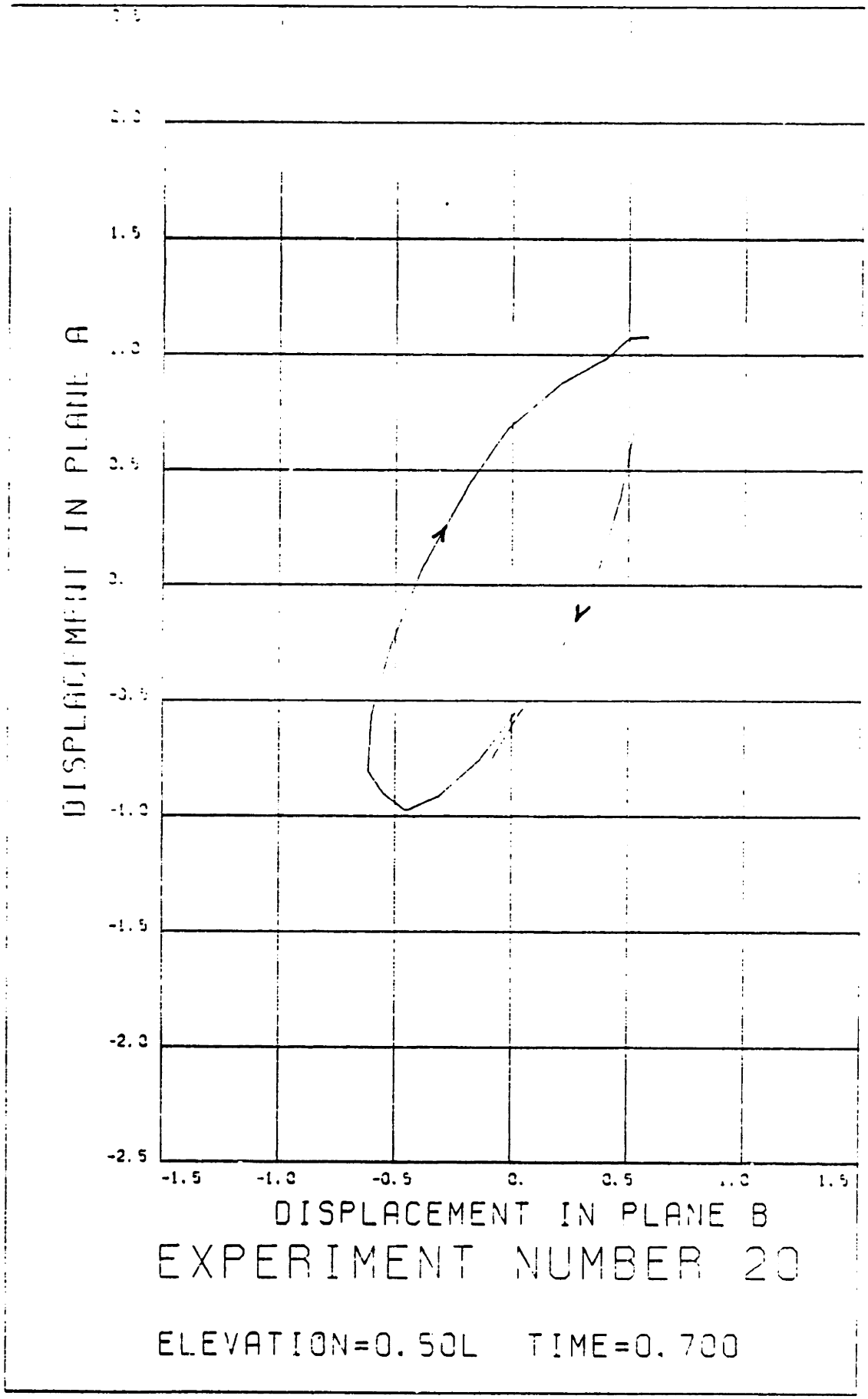
DISPLACEMENT IN PLANE A
1.5
-1.5
-2.0
-2.5
-1.5
-1.0
-0.5
0.
0.5
1.0
1.5
DISPLACEMENT IN PLANE B
EXPERIMENT NUMBER 20
ELEVATION=0.50L TIME=0.700

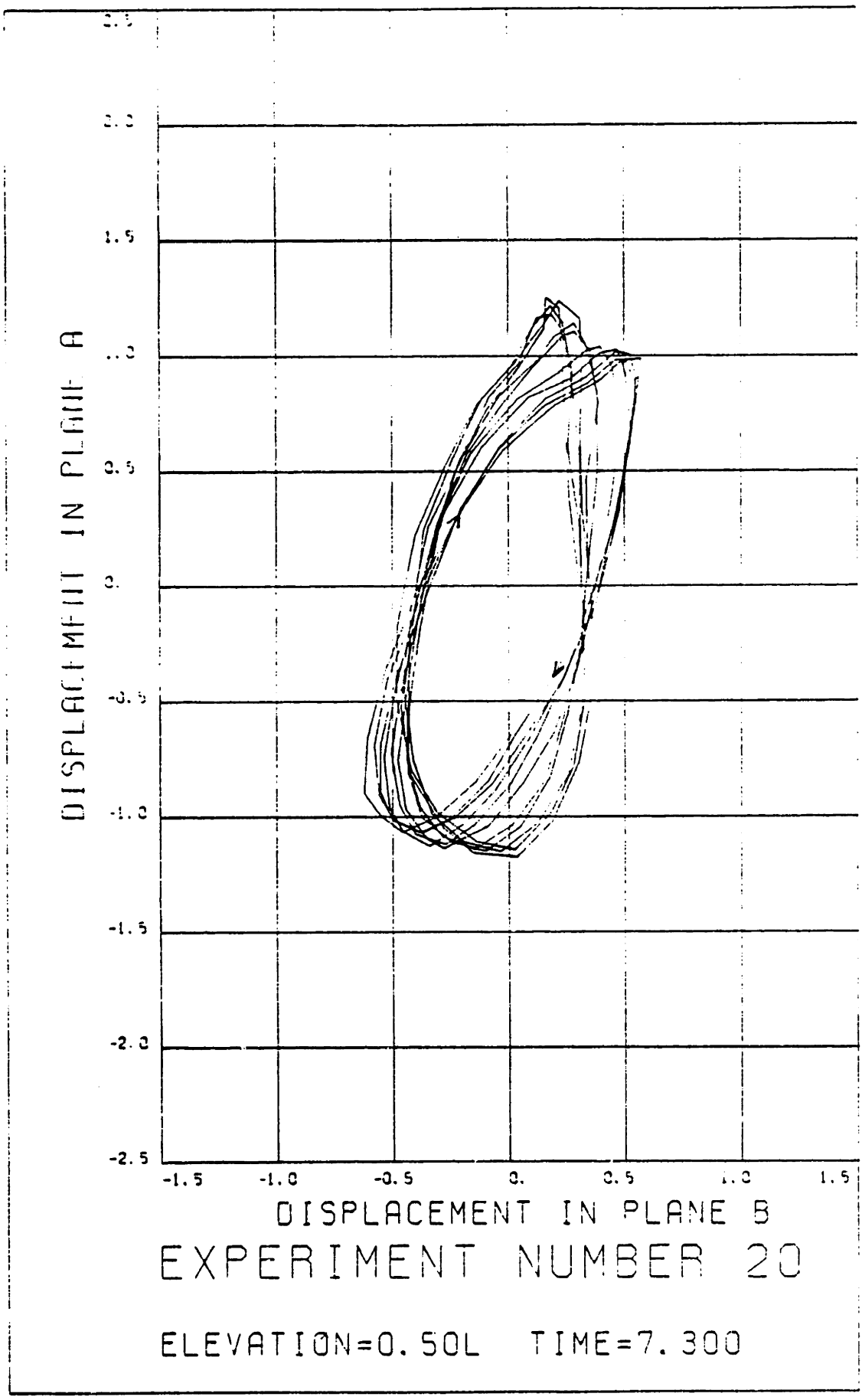
DISPLACEMENT IN PLANE A
DISPLACEMENT IN PLANE B
EXPERIMENT NUMBER 20
ELEVATION=0.50L TIME=7.300

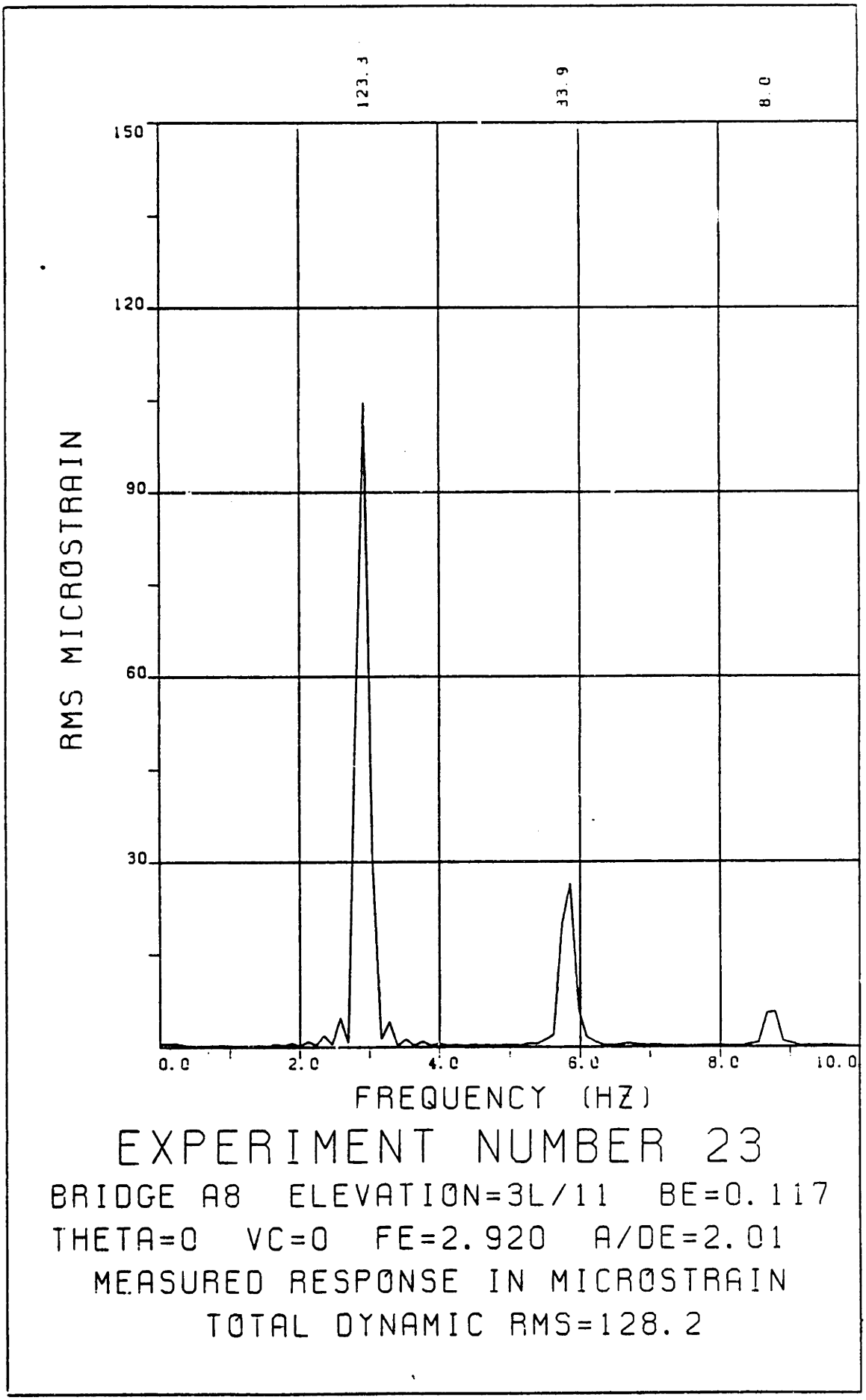

EXPERIMENT NUMBER 23

BRIDGE A8 ELEVATION=3L/11 BE=0.117

THETA=0 VC=0 FE=2.920 A/DE=2.01

MEASURED RESPONSE IN MICROSTRAIN

TOTAL DYNAMIC RMS=128.2

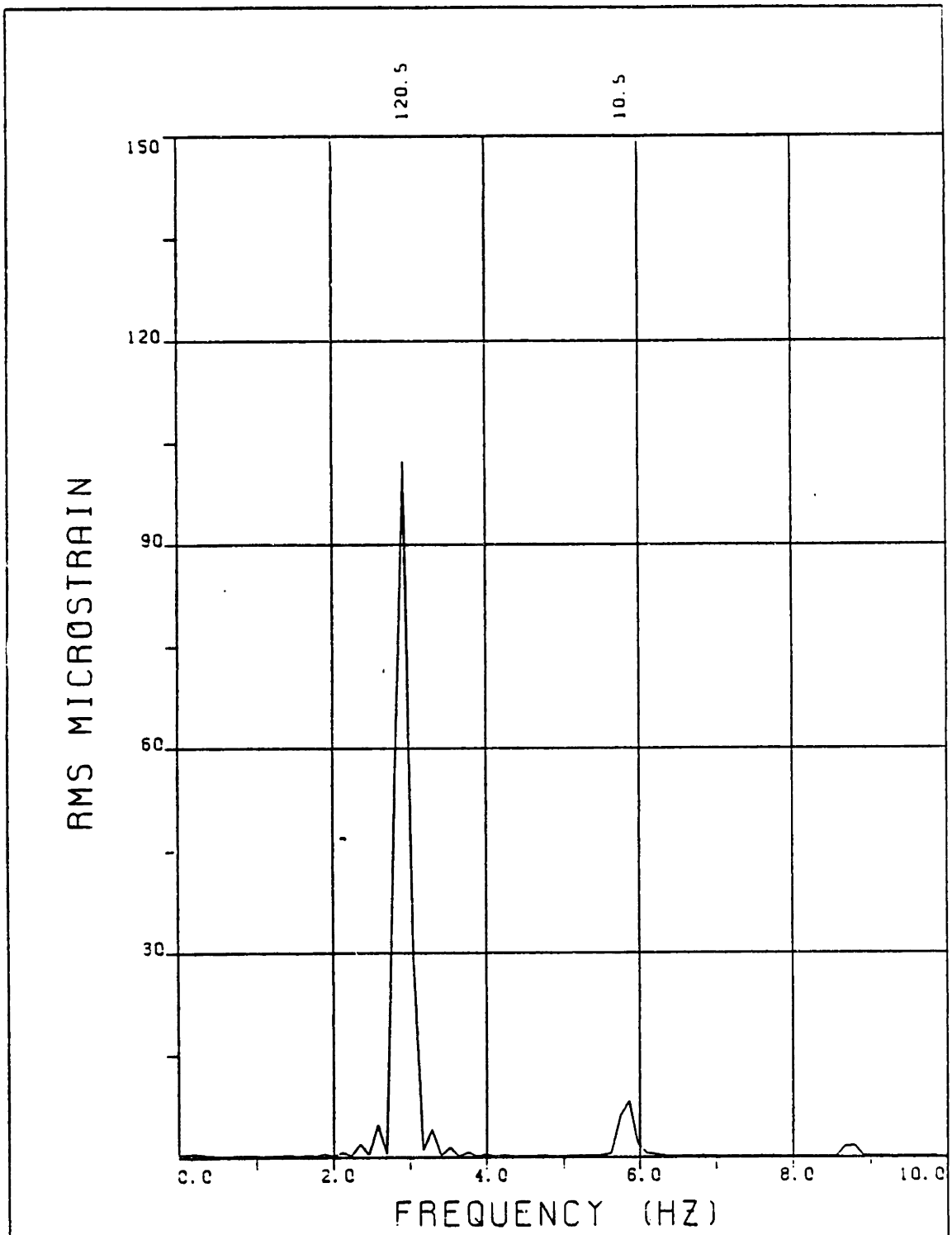

EXPERIMENT NUMBER 23

BRIDGE A6 ELEVATION=5L/11 BE=0.117

THETA=0 VC=0 FE=2.920 A/DE=2.01

MEASURED RESPONSE IN MICROSTRAIN

TOTAL DYNAMIC RMS=121.0

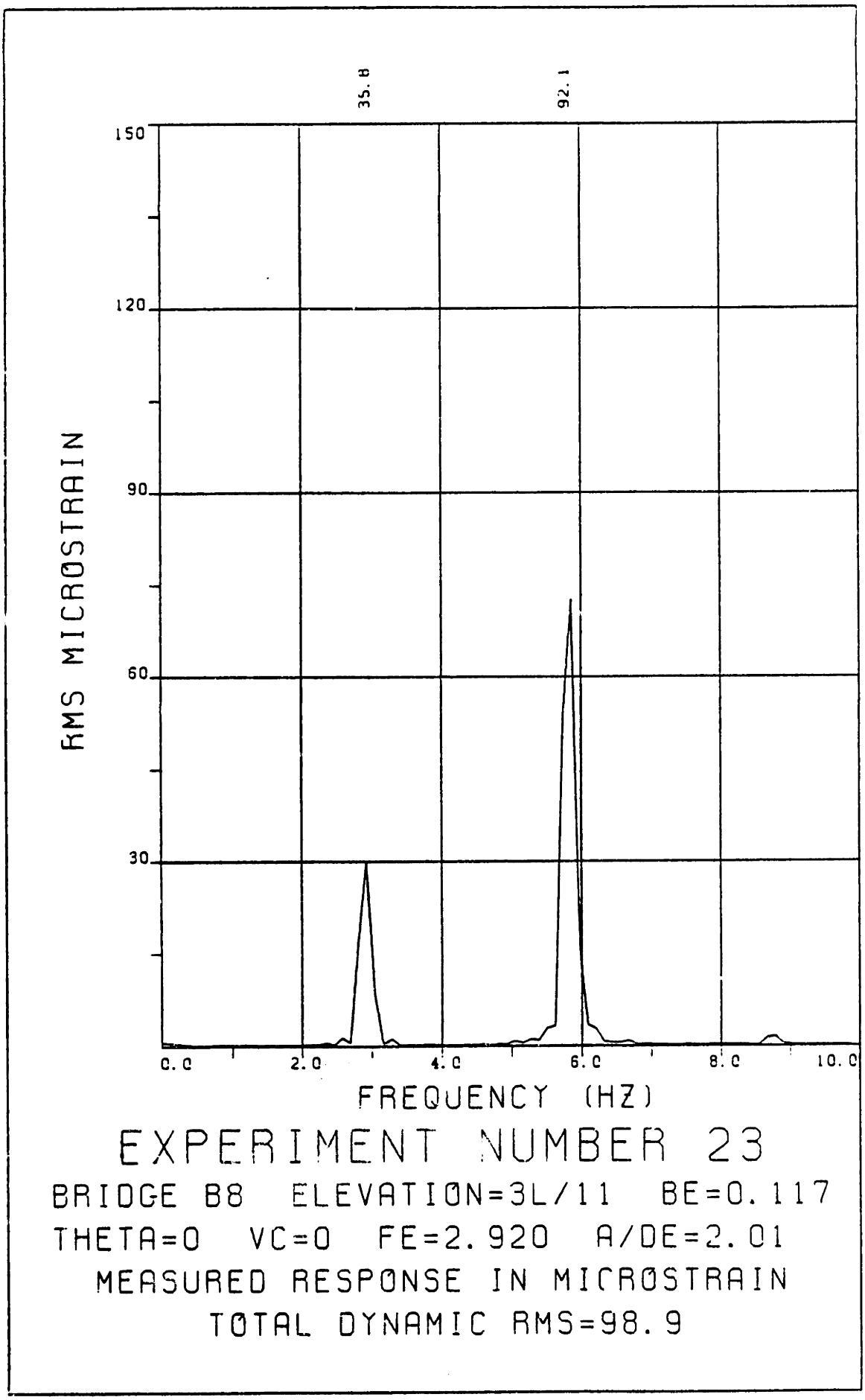

EXPERIMENT NUMBER 23

BRIDGE B8 ELEVATION=3L/11 BE=0.117

THETA=0 VC=0 FE=2.920 A/DE=2.01

MEASURED RESPONSE IN MICROSTRAIN

TOTAL DYNAMIC RMS=98.9

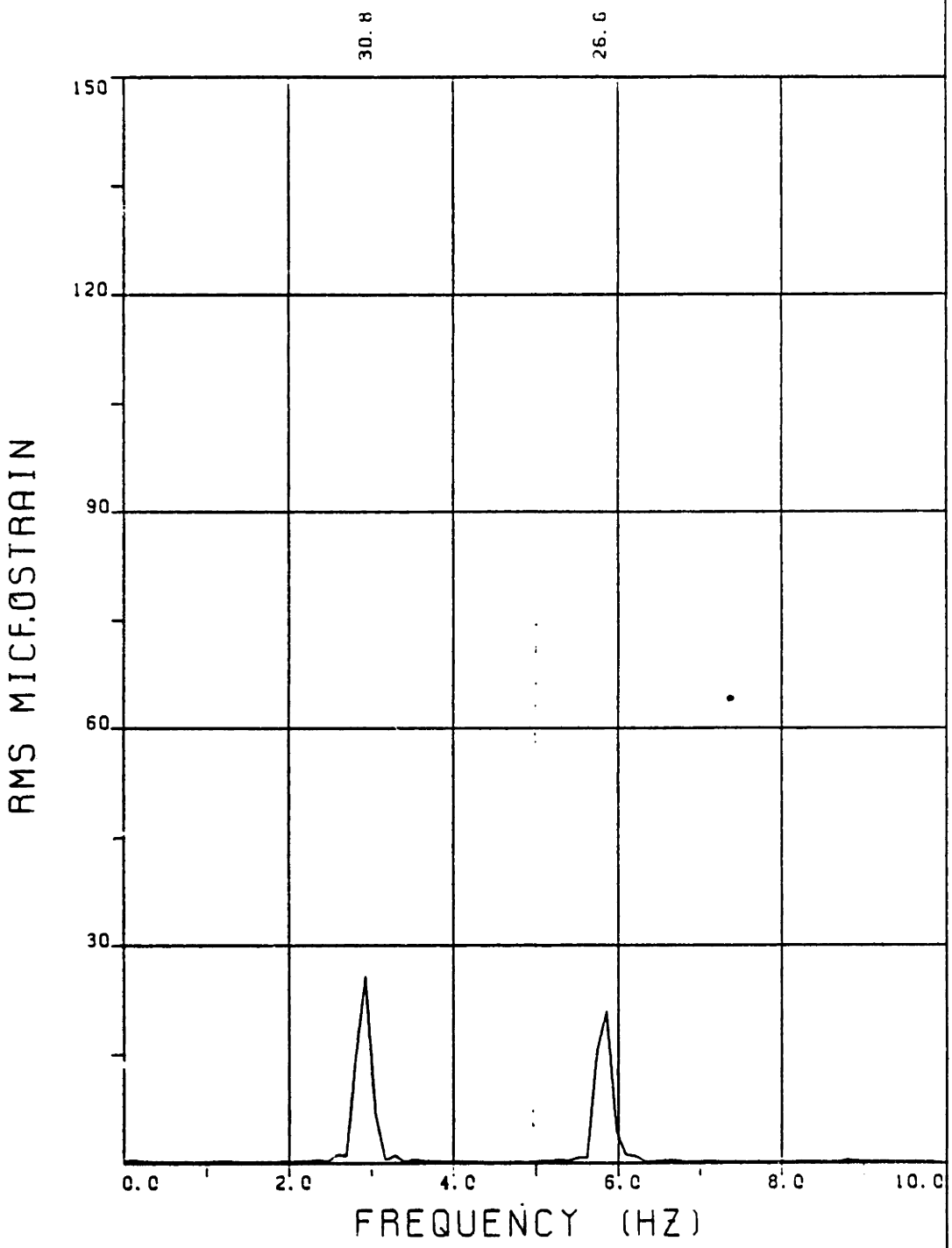

EXPERIMENT NUMBER 23

BRIDGE B5 ELEVATION=6L/11 BE=0.117

THETA=0 VC=0 FE=2.920 A/DE=2.01

MEASURED RESPONSE IN MICROSTRAIN

TOTAL DYNAMIC RMS=40.8

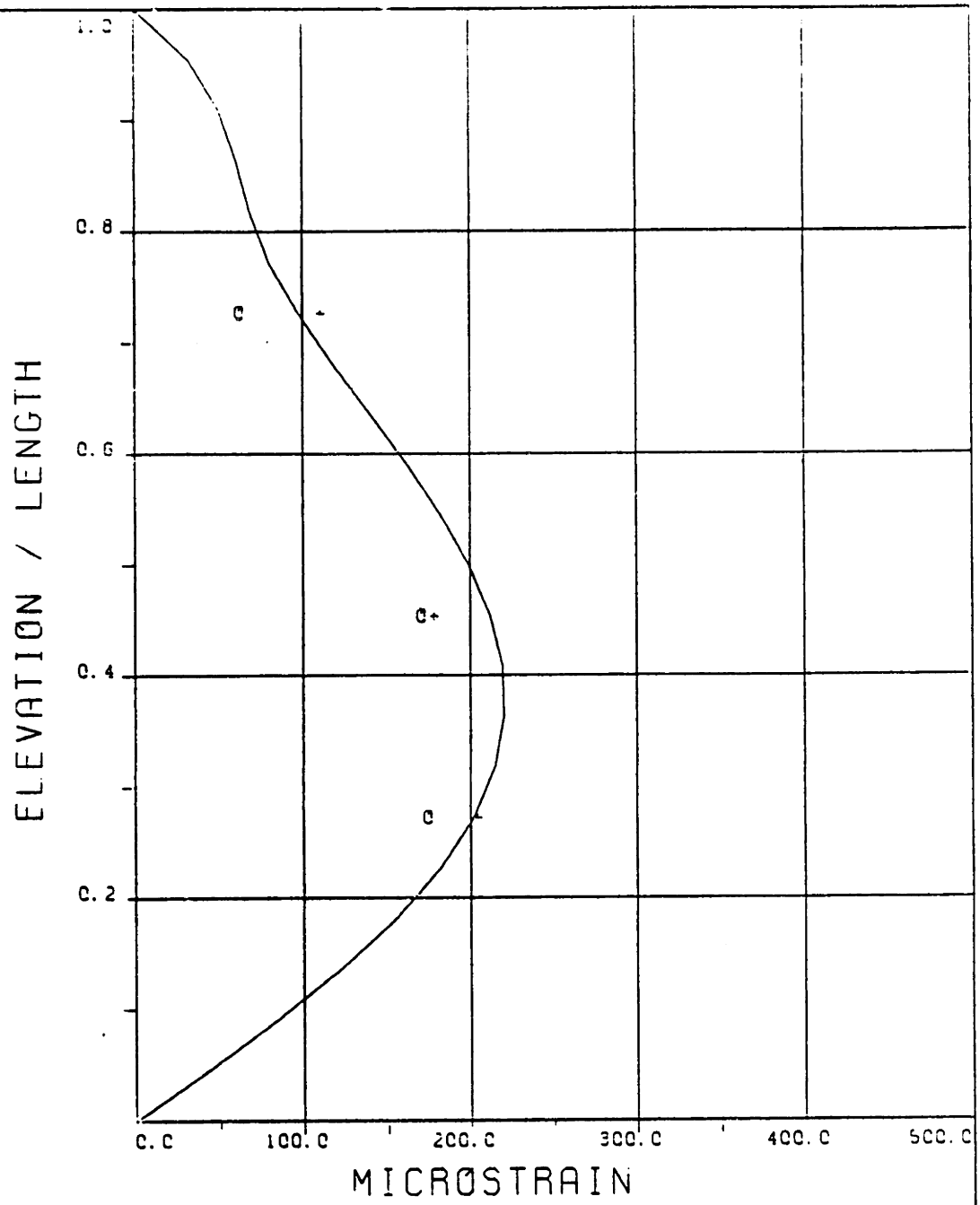

EXPERIMENT NUMBER 23

THETA=0 VC=0 FE=2.920 A/DE=2.01

DYNAMIC RESPONSE AT F=FE IN PLANE A

——— THEORY o o o EXPERIMENT

MAXIMUM DYNAMIC RESPONSE IN PLANE A

——— THEORY + + + EXPERIMENT

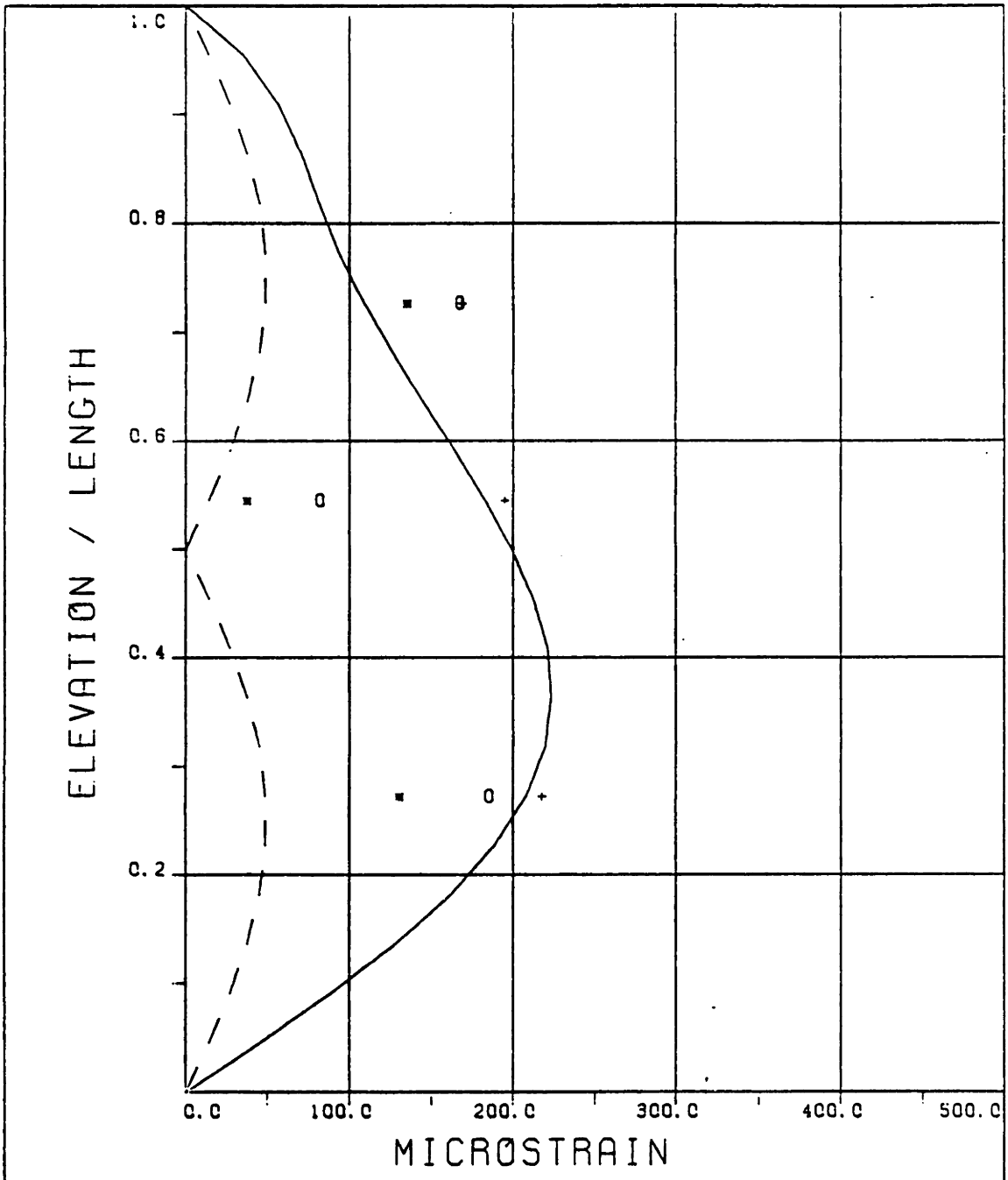

EXPERIMENT NUMBER 23

THETA=0 VC=0 FE=2.920 A/DE=2.01

DYNAMIC RESPONSE IN PLANE B AT F=2FE

----- THEORY * * * EXPERIMENT

MAXIMUM RESPONSE IN PLANE B

o o o EXPERIMENT

MAXIMUM RESPONSE

_____ THEORY + + + EXPERIMENT

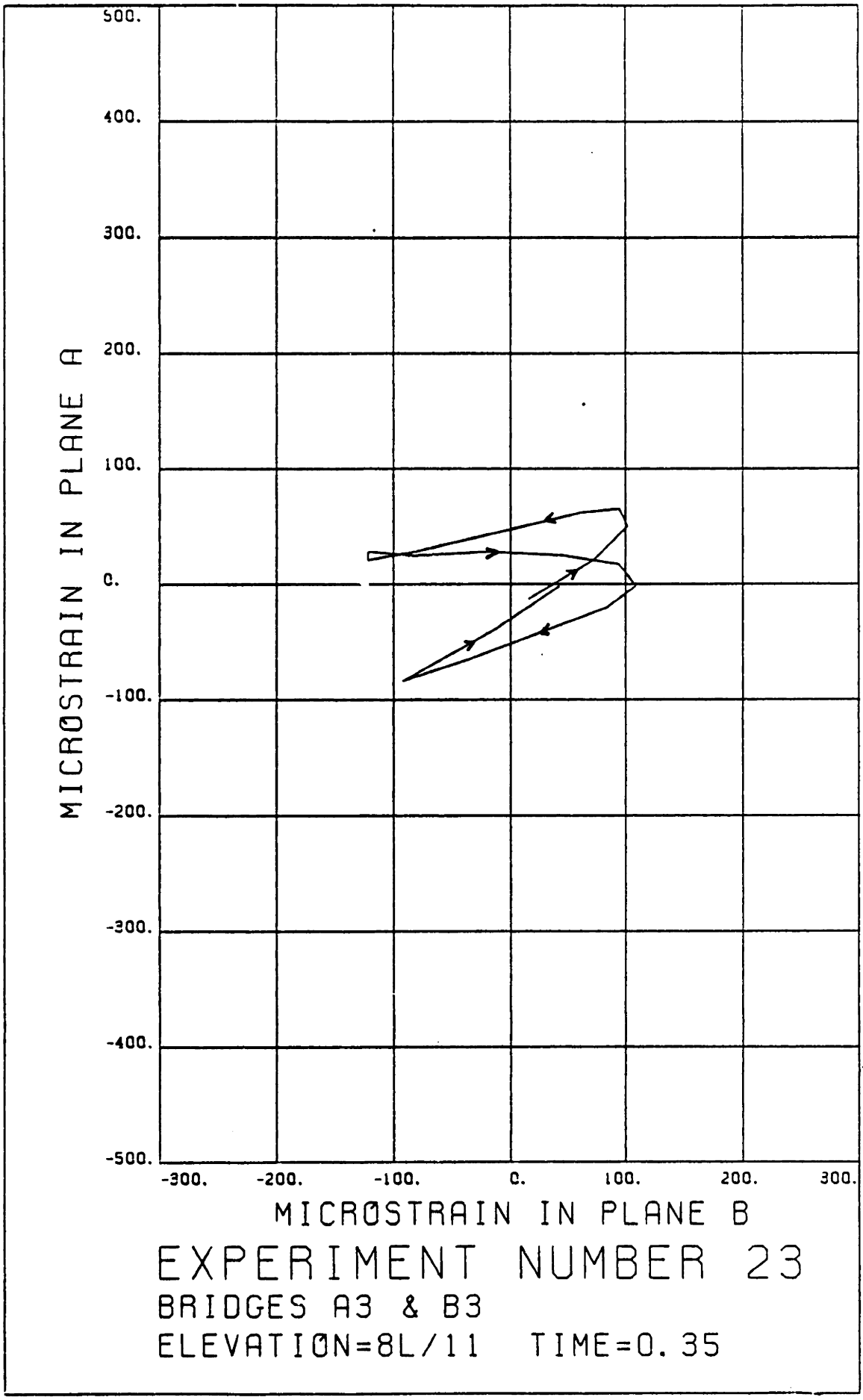
500.
400.
300.
200.
100.
0.
-100.
-200.
-300.
-400.
-500.
MICROSTRAIN IN PLANE A
-300.
-200.
-100.
0.
100.
200.
300.
MICROSTRAIN IN PLANE B
EXPERIMENT NUMBER 23
BRIDGES A3 & B3
ELEVATION=8L/11 TIME=0.35

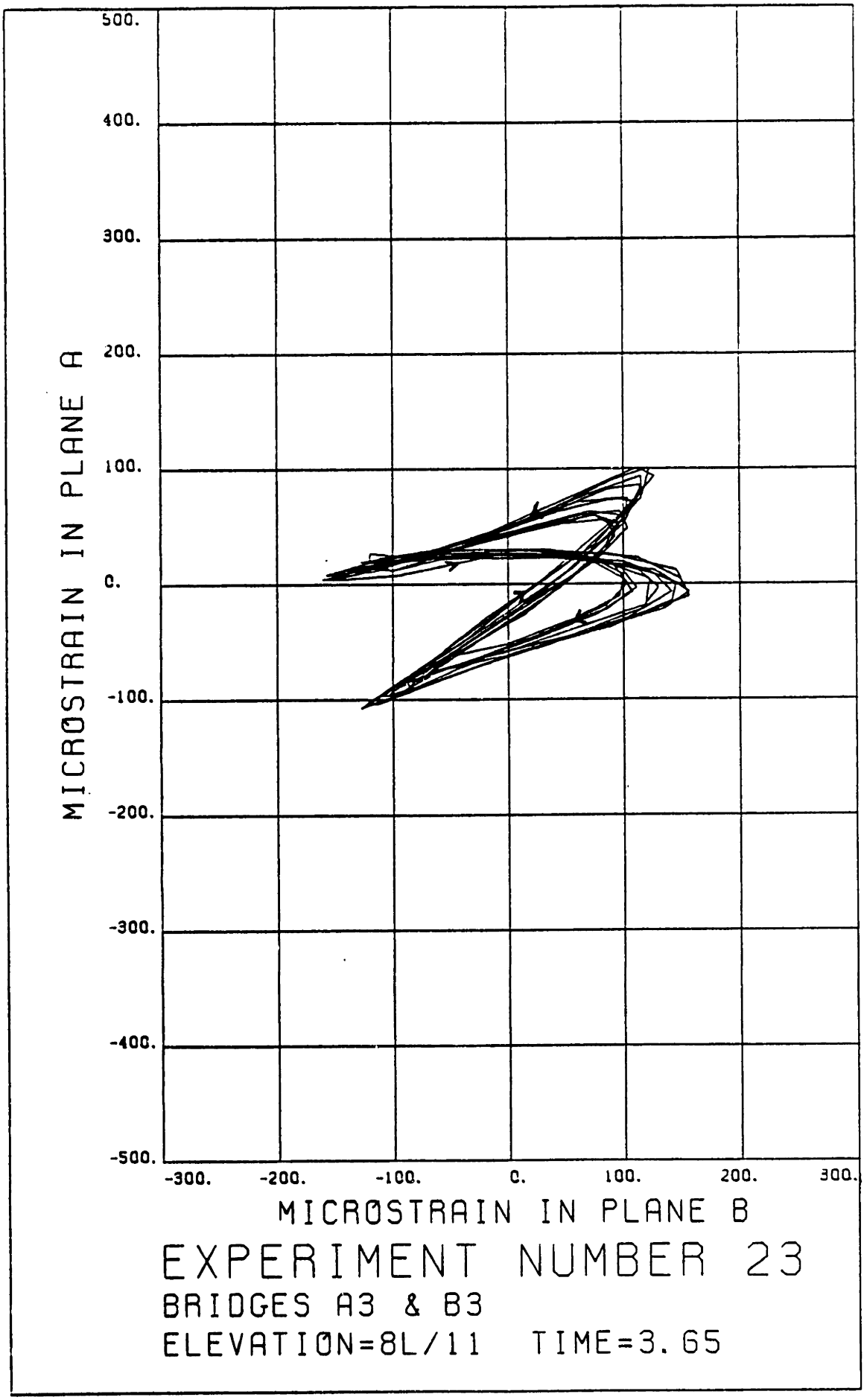
500.
400.
300.
200.
100.
0.
-100.
-200.
-300.
-400.
-500.
MICROSTRAIN IN PLANE A
-300.
-200.
-100.
0.
100.
200.
300.
MICROSTRAIN IN PLANE B
EXPERIMENT NUMBER 23
BRIDGES A3 & B3
ELEVATION=8L/11 TIME=3.65

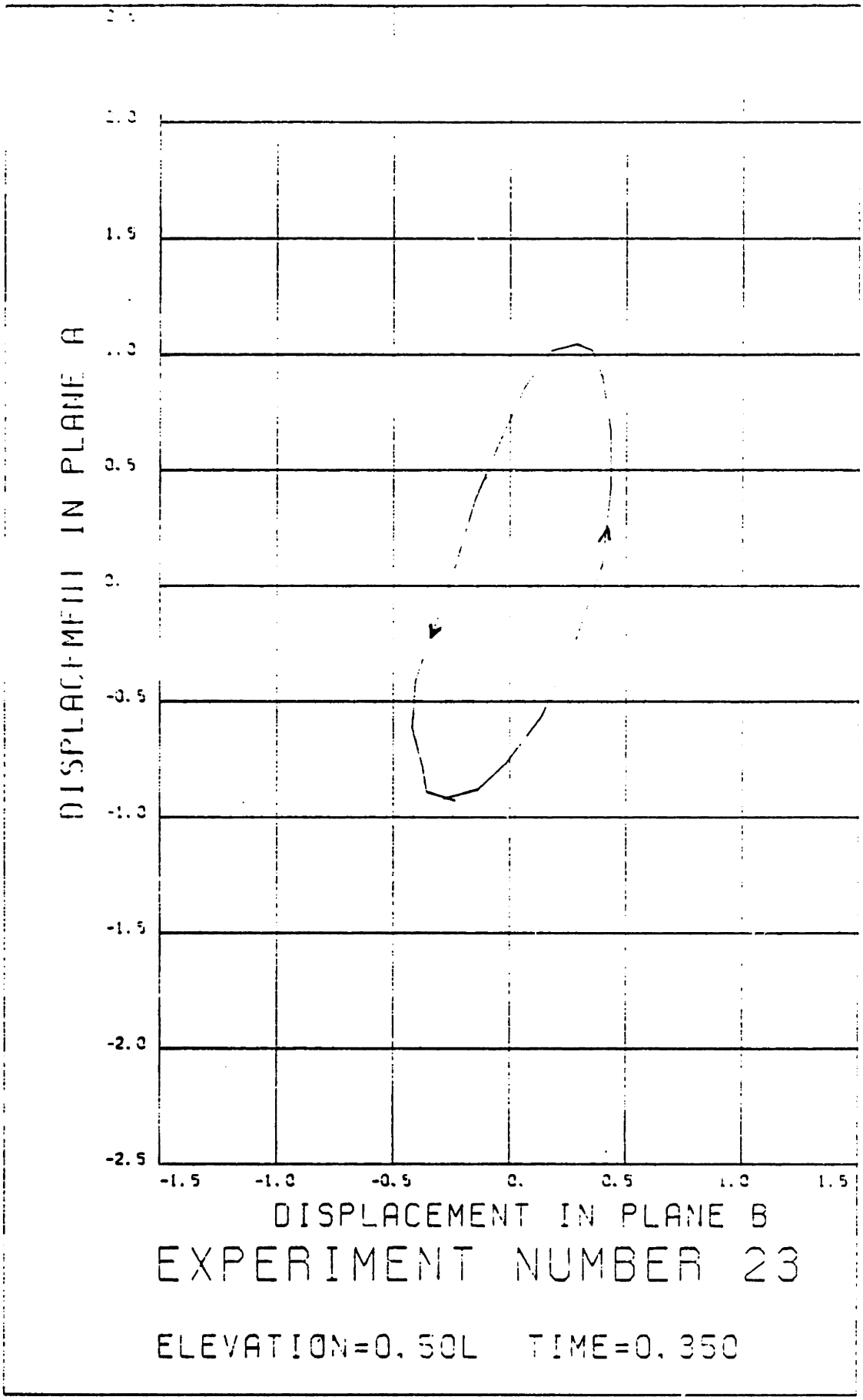
DISPLACEMENT IN PLANE A
1.5
0.5
0.
-0.5
-1.0
-1.5
-2.0
-2.5
-1.5
-1.0
-0.5
0.
0.5
1.0
1.5
DISPLACEMENT IN PLANE B
EXPERIMENT NUMBER 23
ELEVATION=0.50L TIME=0.350

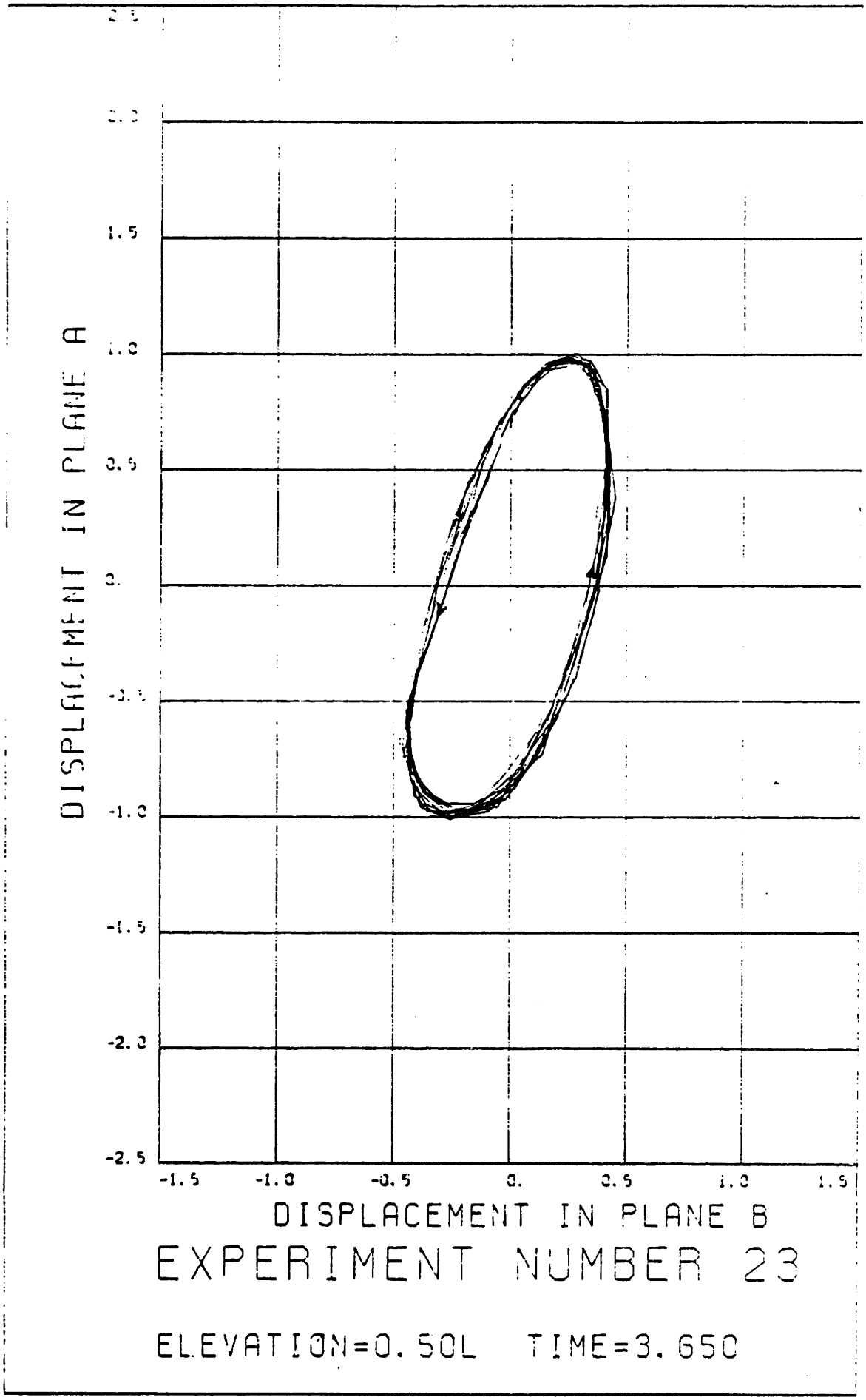
DISPLACEMENT IN PLANE A
2.5
2.0
1.5
1.0
0.5
0.
-0.5
-1.0
-1.5
-2.0
-2.5
-1.5
-1.0
-0.5
0.
0.5
1.0
1.5
DISPLACEMENT IN PLANE B
EXPERIMENT NUMBER 23
ELEVATION=0.50L TIME=3.650

the reader to visualize the importance of this additional assumption. The "D" Figures of each experiment allows the reader to visualize the difference between the assumed and actual motion. The motion shown in the "D" Figures has been computed by expanding the response in each plane in the first three modes, calculating the amplitude of each mode and by summation of the contribution of each mode and the top end motion.

V.4.2 HARMONIC OSCILLATION OF THE TOP END OF THE MODEL PARALLEL TO A UNIFORM STREAM

In all experiments described in this section the direction of oscillation of the top end was parallel to the long side of the towing tank and the current (plane A). The amplitude of oscillation was approximately equal to two effective diameters. The water temperature was 13 degrees C. Bending strains in plane A at Z = 3L/11, 5L/11 and 8L/11 and in plane B at Z = 3L/11, 6L/11 and 8L/11 were recorded simultaneously together with the motion of the upper end. The root mean square response strain as a function of the response frequency at elevations Z = 3L/11 and 5L/11 for plane A and Z = 3L/11 and 6L/11 for plane B recently have been presented in Chryssostomidis and Patrikalakis (1982a) and are not repeated here. A collective description of the experiments analyzed in this section is shown in Table V.4.

TABLE V.4

Experiment Number	V_c ($\frac{mm}{s}$) / Re	Frequency of Excitation f_e in Hz / Frequency Parameter β	Measured A/D_e / U*	$\hat{c}_m$	$\hat{c}_d$	Maximum Calculated Dynamic x/D_e	Mean Calculated Dynamic x/D_e
2	120	1	2.01	0.50	1.15	2.01	1.46
	1520	194	7.84				
1	120	1.5	2.01	0.49	1.34	2.07	1.59
	1520	291	5.15				
3	120	2.3	2.02	0.60	1.30	2.02	0.99
	1520	446	3.41				
4	120	3	2.04	0.64	1.31	2.04	0.80
	1520	582	2.61				
9	240	1	2.03	0.53	1.02	2.03	1.20
	3040	194	15.68				
10	240	1.5	2.01	0.47	1.07	2.01	1.31
	3040	291	10.03				
8	240	2.3	2.04	0.47	1.10	2.04	0.92
	3040	446	6.82				
7	240	3	2.04	0.45	1.20	2.04	0.79
	3040	582	5.22				

Table V.4 also includes information about the theoretical prediction of the static and dynamic response at f_e in plane A, performed as described in Section IV.4.4. The way in which $\hat{c}_m$ and $\hat{c}_d$ shown in Table V.4 have been derived from the local c_m and c_d is explained in Appendix B. The estimates of the local c_m and c_d employed in the iteration procedure are based on rigid cylinder results shown in Figures 13 and 14 of Chapter IV. In our experiments, the frequency parameter β varied betweeen 194 and 582, which for the most part overlaps with the range of β employed by Verley and Moe (1979).

From all experiments of this class, it can be seen that the strain response in plane A is primarily concentrated at $f=f_e$, see Chryssostomidis and Patrikalakis (1982a). However, some strain response in plane A at frequencies other than f_e exists and is not, in general, insignificant in determining the maxima of the measured response in plane A. Our inability to model components of dynamic response in plane A at frequencies other than f_e is somewhat reflected in our theoretical prediction of the maximum response in plane A. These conclusions are summarized in Figures 2A, 1A, 3A, 4A, 9A, 10A, 8A, and 7A where the following theoretical and experimental results are included: the static response strain, the static plus the dynamic response strain at $f=f_e$ in plane A; the maximum response strain in plane A. The theoretical static plus dynamic response strain at $f=f_e$ in plane A is

also our theoretical estimate for the maximum response strain in this plane.

In general, the responses in plane B are as significant as the dynamic responses in plane A. This can be seen from Figures 1 through 4 and 7 through 10 and from the figures showing the rms response strain in the A and B planes presented in Chryssostomidis and Patrikalakis (1982a). The frequencies at which there is significant lift response depend upon the value of the reduced velocity U*. When the value of the reduced velocity U* is less than approximately 3, the lift is concentrated at $f=2f_e$ with some response also at $f=f_e$, see experiment 4, where U*=2.61, and Chryssostomidis and Patrikalakis (1982a). This is consistent with rigid cylinder results for values of U* less than approximately 3, Mercier (1973). When the value of the reduced velocity U* is larger than approximately 3, significant lift response is present at multiples of $f_e/4$ for the smaller of the Reynolds numbers tested. For the larger of the two Reynolds numbers tested and for values of the reduced velocity U* larger than 3, significant lift response occurs at multiples of $f_e/2$. Lift response at multiples of $f_e/2$ is consistent with rigid cylinder results, Mercier (1973), for values of U* larger than approximately 3. The Reynolds number corresponding to the larger of the two speeds tested is closer to the range of Reynolds numbers

studied in Mercier (1973). The Strouhal frequency, as determined from Figure 2 of Chapter IV, may vary between 1.49 and 1.79 Hz for the smaller current speed and between 2.98 and 3.58 Hz for the larger current speed studied in this work. The frequencies of lift response of our flexible model, when no oscillation of the top end is applied, are equal to f_{r_1}=1.32 Hz and f_{r_2}=2.14 Hz for the smaller and the larger current speed, respectively. Except for experiment 10, for which $f_{r_2} \simeq 3f_e/2$, no appreciable response at f_{r_1} or f_{r_2} is found. This observation implies that currents and harmonic oscillations parallel to currents are coupled in a manner in general leading to a different dynamic behavior of a flexible cylinder than the current or the oscillation alone. The forces acting on rigid cylinders in a current and harmonic oscillations at θ=0 degrees provide an explanation of such a behavior.

Figures 2B, 1B, 3B, 4B, 9B, 10B, 8B and 7B summarize the following results: the maximum experimental dynamic response strain in plane B; the maximum experimental static and dynamic response strain independent of plane; our present theoretical estimate of the maximum static and dynamic response strain independent of plane. The latter is the same as our theoretical estimate of the static plus dynamic response strain at f_e in plane A, because no information is available to us to make an estimate of the magnitude of the lift response.

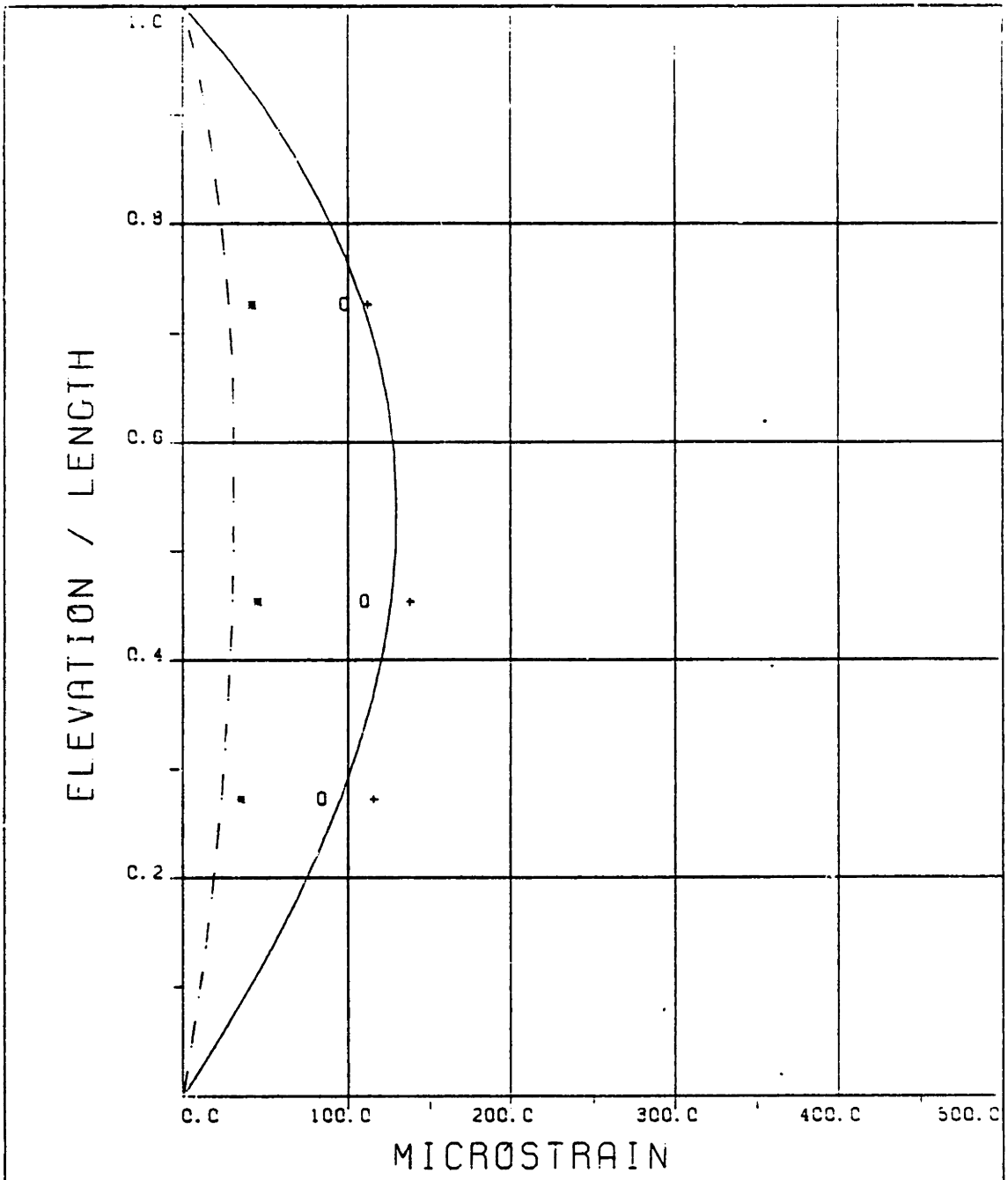

EXPERIMENT NUMBER 2

THETA=0 VC=120 FE=1.000 A/DE=2.01

STATIC RESPONSE IN PLANE A

----- THEORY * * * EXPERIMENT

STATIC RESPONSE PLUS DYNAMIC RESPONSE AT F = FE IN PLANE A

_____ THEORY o o o EXPERIMENT

MAXIMUM RESPONSE IN PLANE A

_____ THEORY + + + EXPERIMENT

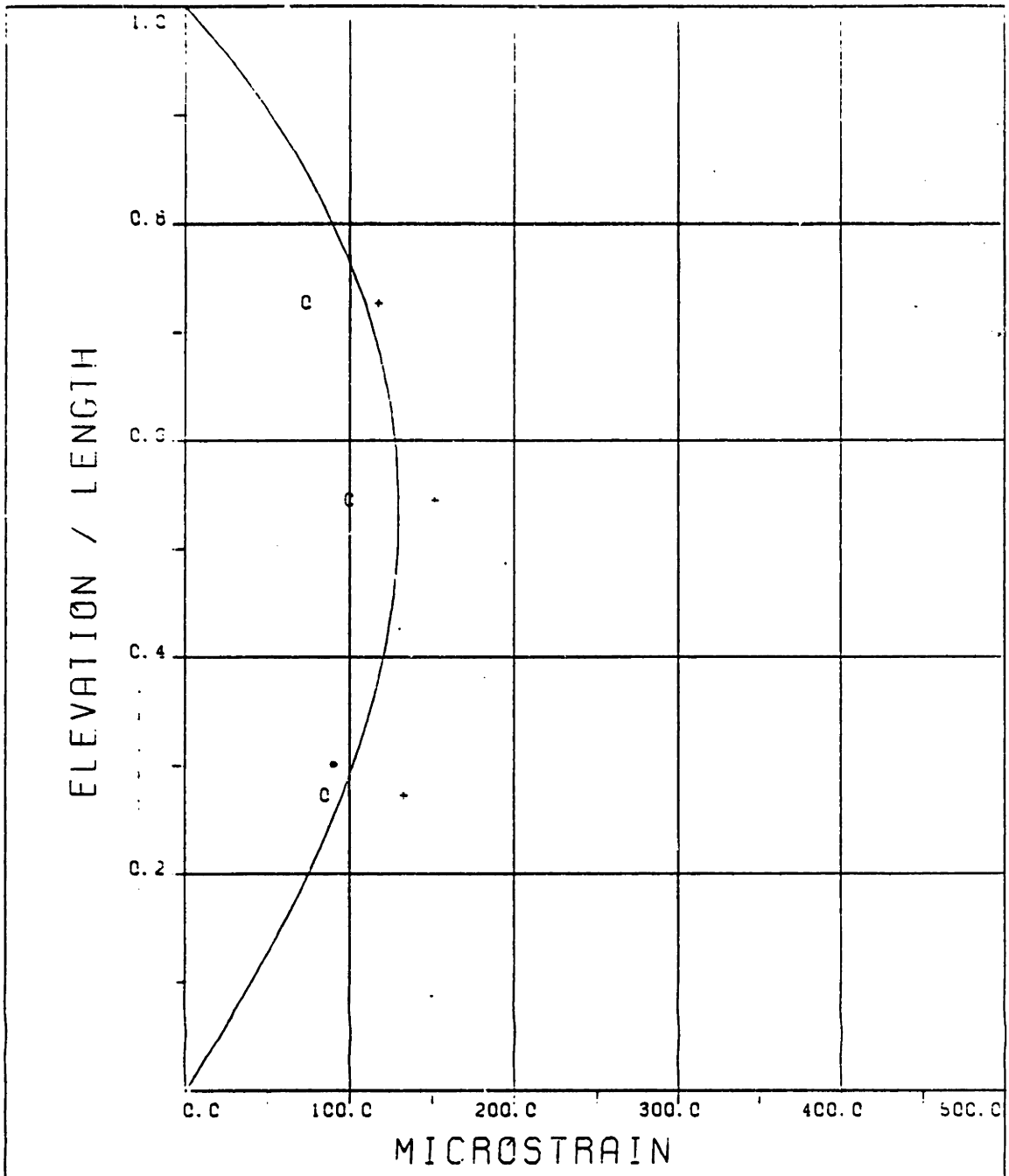

EXPERIMENT NUMBER 2

THETA=0 VC=120 FE=1.000 A/DE=2.01

MAXIMUM DYNAMIC RESPONSE IN PLANE B

c c c EXPERIMENT

MAXIMUM RESPONSE

_____ THEORY + + + EXPERIMENT

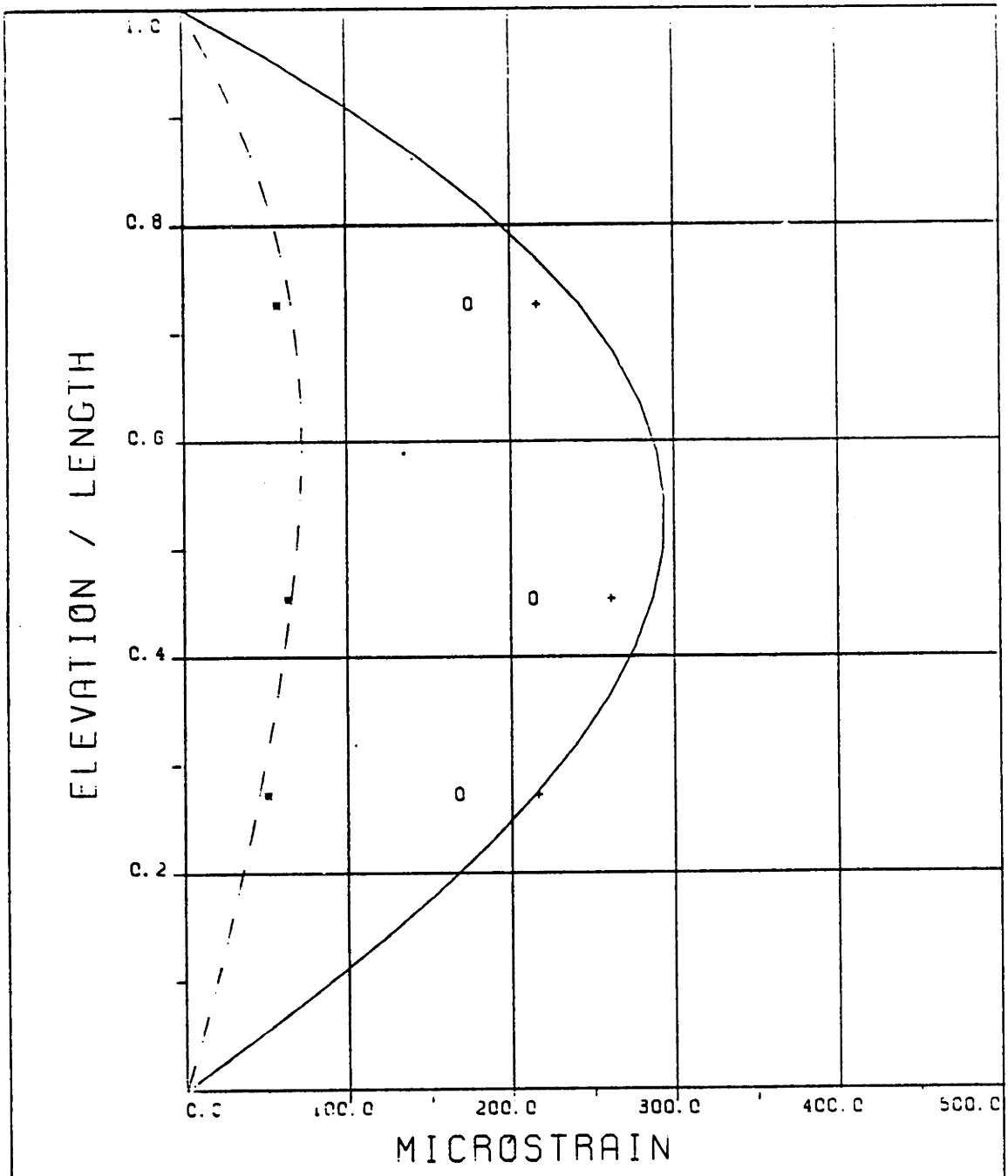

EXPERIMENT NUMBER 1

THETA=0 VC=120 FE=1.500 A/DE=2.01

STATIC RESPONSE IN PLANE A

----- THEORY * * * EXPERIMENT

STATIC RESPONSE PLUS DYNAMIC RESPONSE AT F = FE IN PLANE A

_____ THEORY o o o EXPERIMENT

MAXIMUM RESPONSE IN PLANE A

_____ THEORY + + + EXPERIMENT

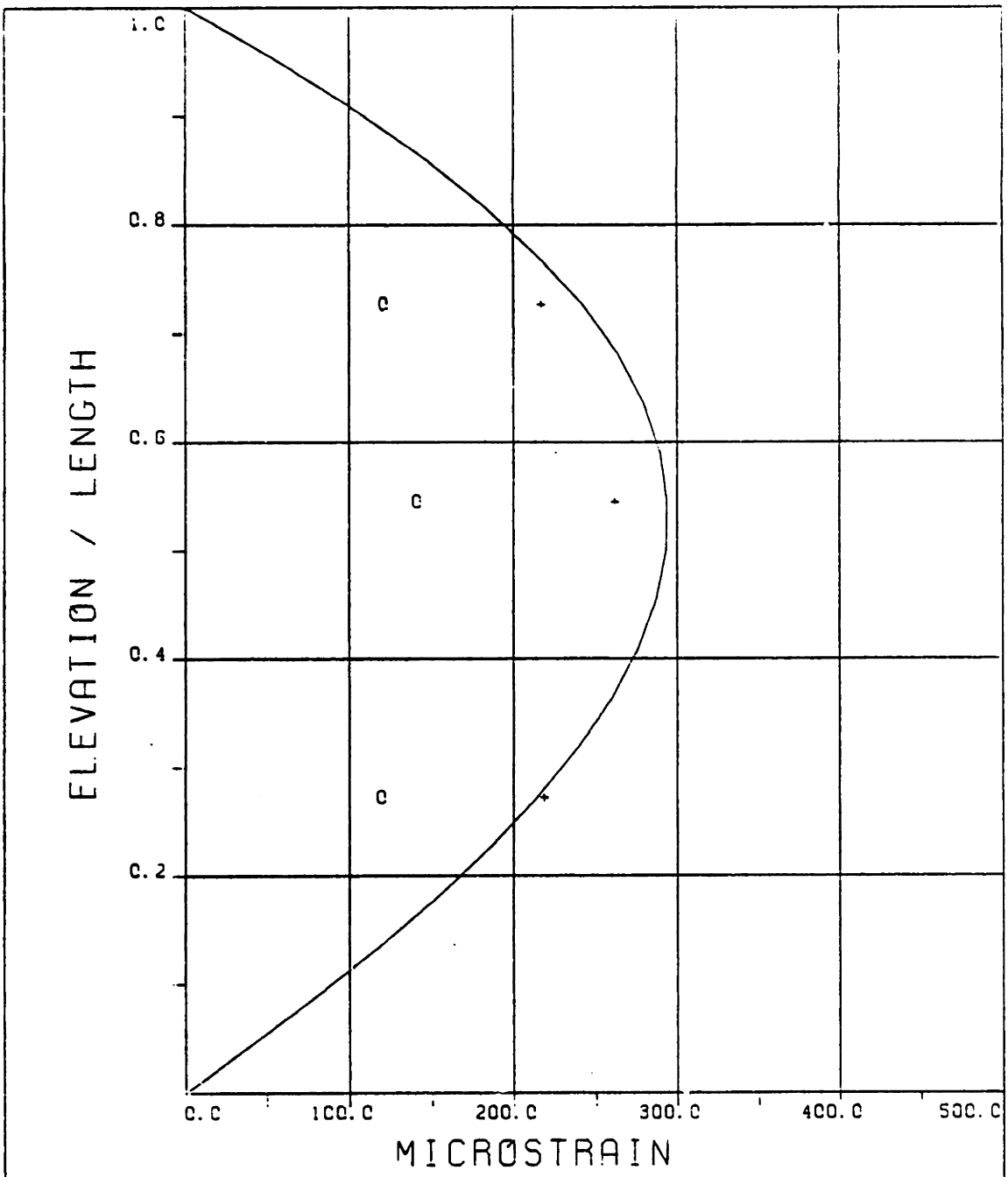

EXPERIMENT NUMBER 1

THETA=0 VC=120 FE=1.500 A/DE=2.01

MAXIMUM DYNAMIC RESPONSE IN PLANE B

c o c EXPERIMENT

MAXIMUM RESPONSE

_____ THEORY + + + EXPERIMENT

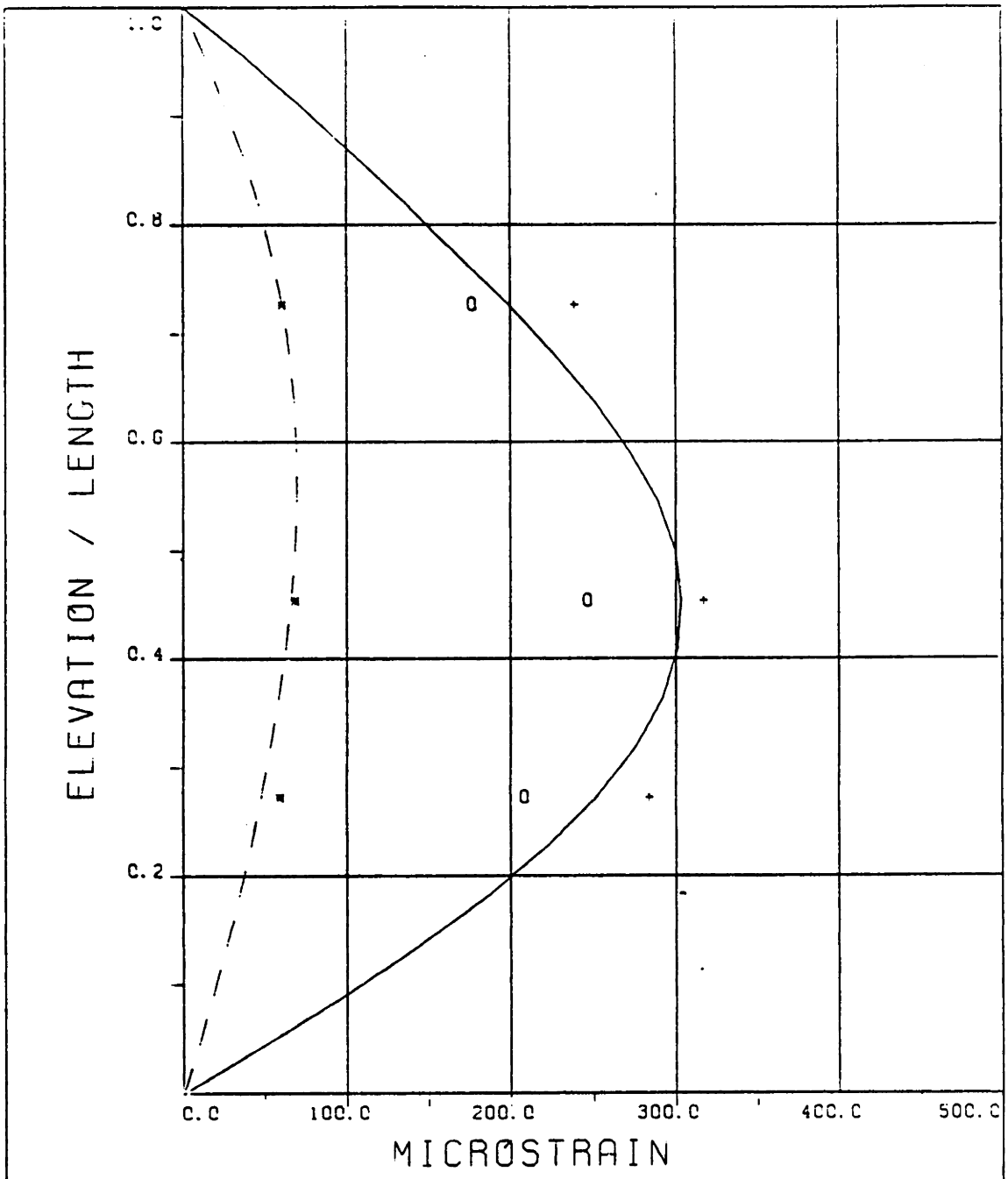

EXPERIMENT NUMBER 3

THETA=0 VC=120 FE=2.300 A/DE=2.02

STATIC RESPONSE IN PLANE A

----- THEORY * * * EXPERIMENT

STATIC RESPONSE PLUS DYNAMIC RESPONSE AT F = FE IN PLANE A

_____ THEORY o o o EXPERIMENT

MAXIMUM RESPONSE IN PLANE A

_____ THEORY + + + EXPERIMENT

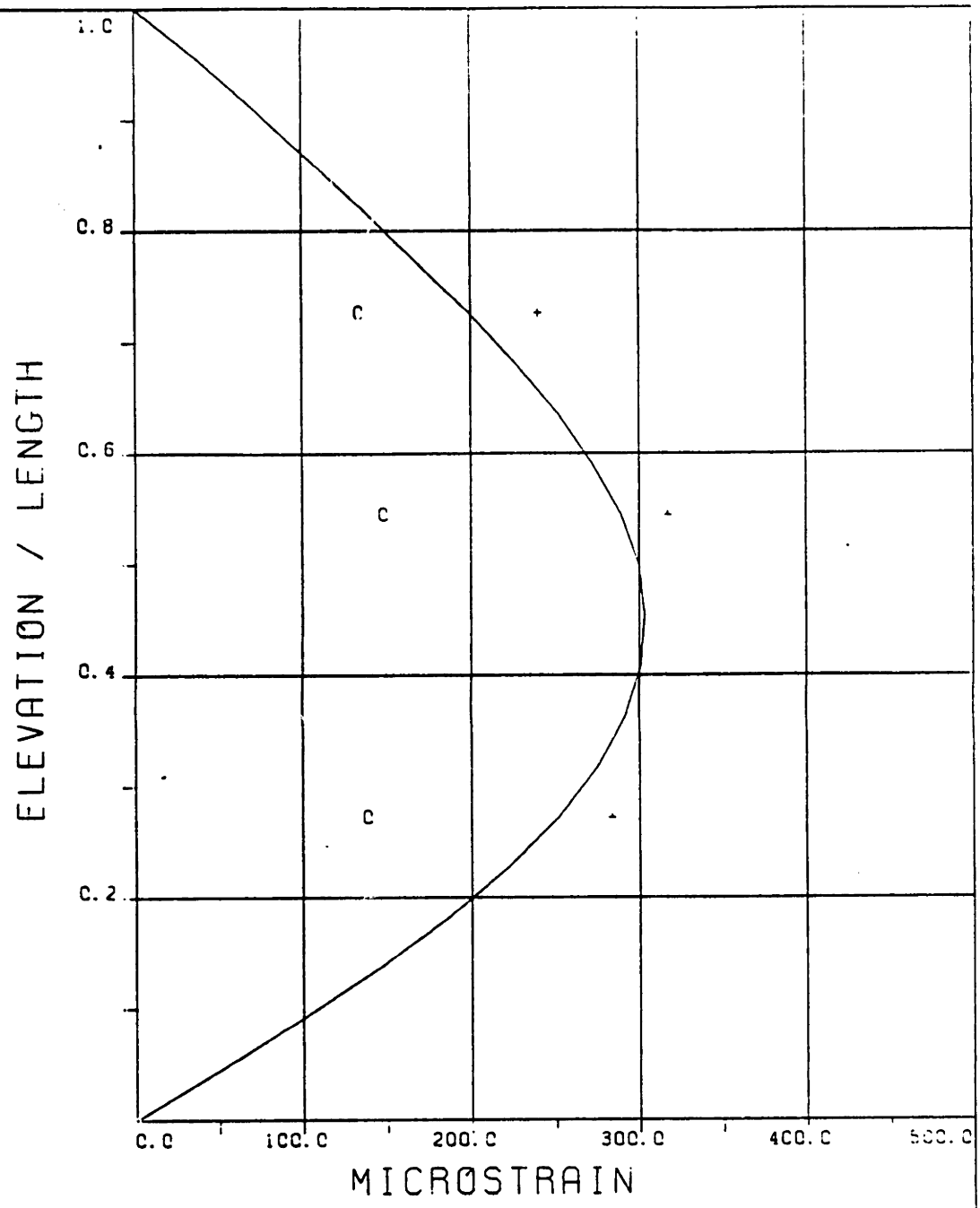

EXPERIMENT NUMBER 3

THETA=0 VC=120 FE=2.300 A/DE=2.02

MAXIMUM DYNAMIC RESPONSE IN PLANE B

c c o EXPERIMENT

MAXIMUM RESPONSE

——— THEORY + + + EXPERIMENT

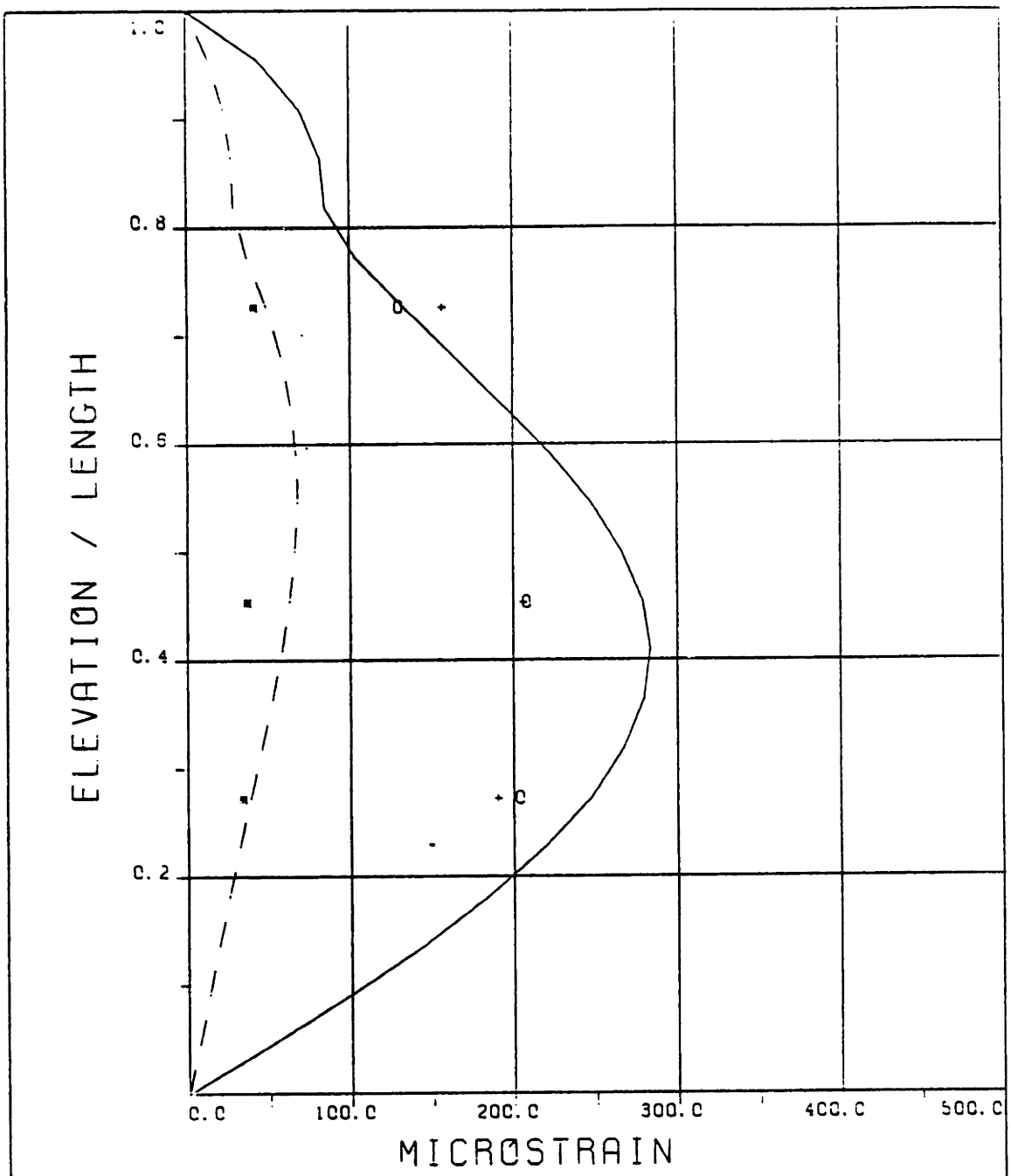

EXPERIMENT NUMBER 4

THETA=0 VC=120 FE=3.000 A/DE=2.04

STATIC RESPONSE IN PLANE A

----- THEORY * * * EXPERIMENT

STATIC RESPONSE PLUS DYNAMIC RESPONSE AT F = FE IN PLANE A

_____ THEORY o o o EXPERIMENT

MAXIMUM RESPONSE IN PLANE A

_____ THEORY + + + EXPERIMENT

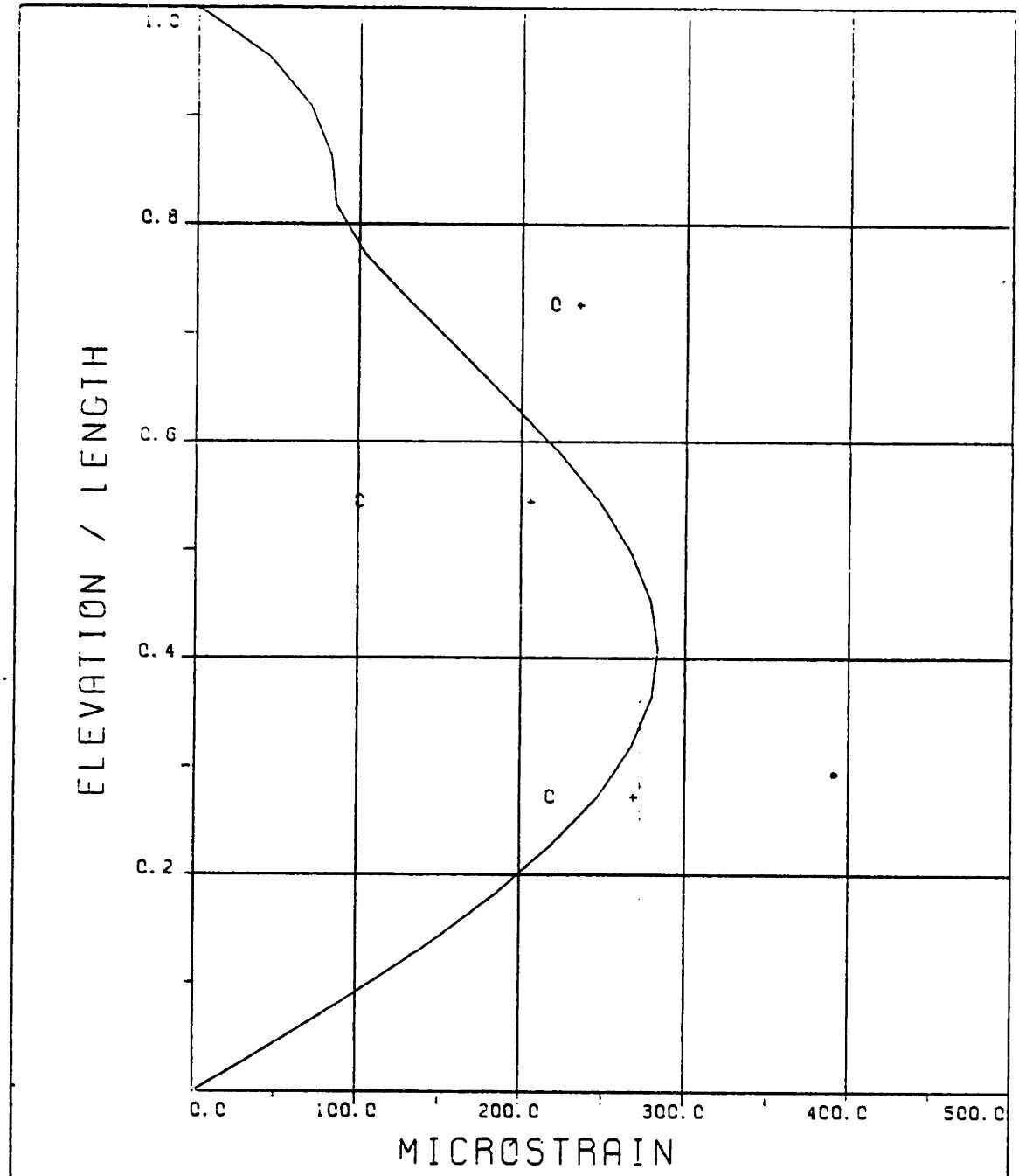

EXPERIMENT NUMBER 4

THETA=0 VC=120 FE=3.000 A/DE=2.04

MAXIMUM DYNAMIC RESPONSE IN PLANE B

c c c EXPERIMENT

MAXIMUM RESPONSE

——— THEORY + + + EXPERIMENT

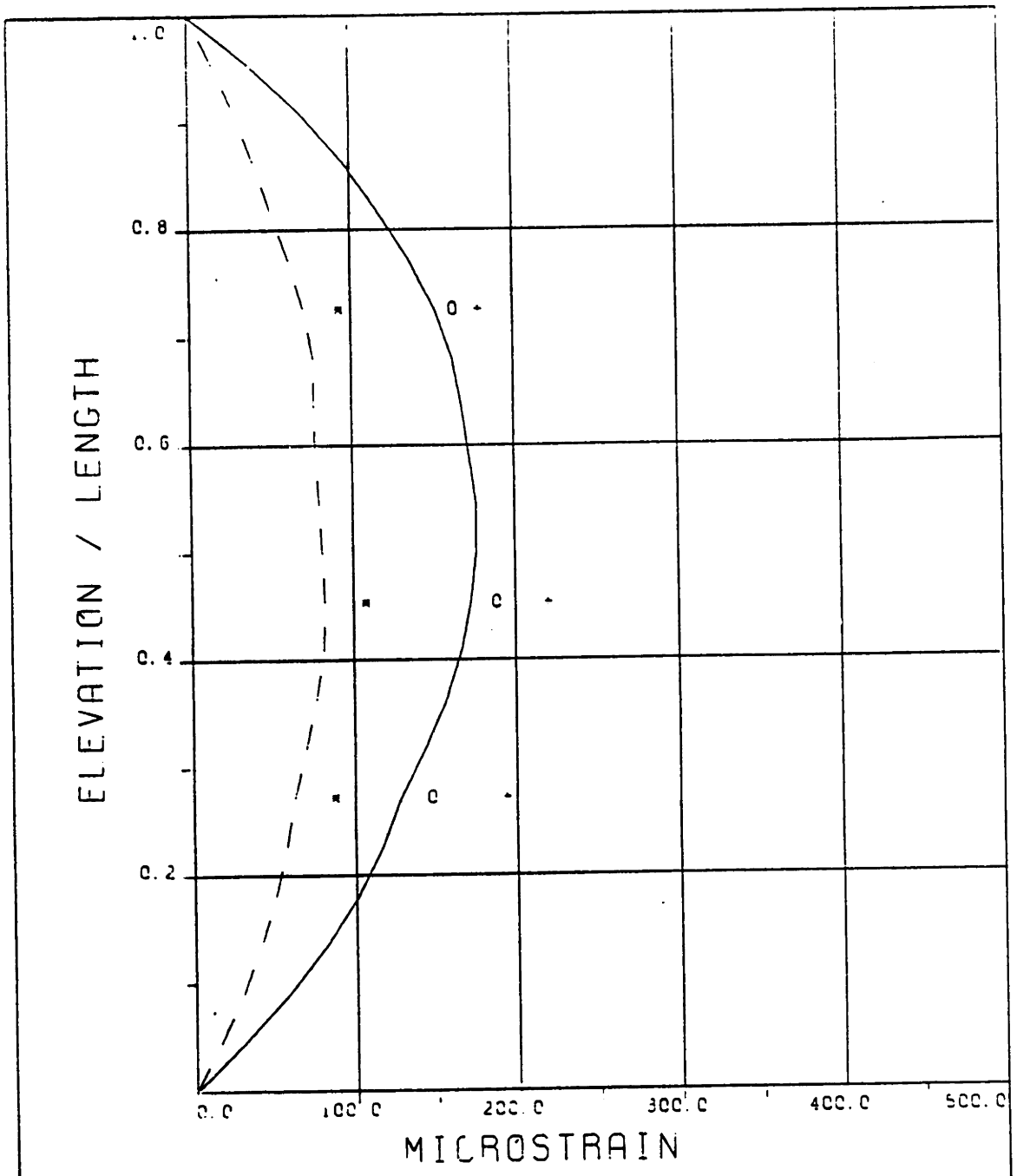

EXPERIMENT NUMBER 9

THETA=0 VC=240 FE=1.000 A/DE=2.03

STATIC RESPONSE IN PLANE A

----- THEORY * * * EXPERIMENT

STATIC RESPONSE PLUS DYNAMIC RESPONSE AT F = FE IN PLANE A

_____ THEORY o o o EXPERIMENT

MAXIMUM RESPONSE IN PLANE A

_____ THEORY + + + EXPERIMENT

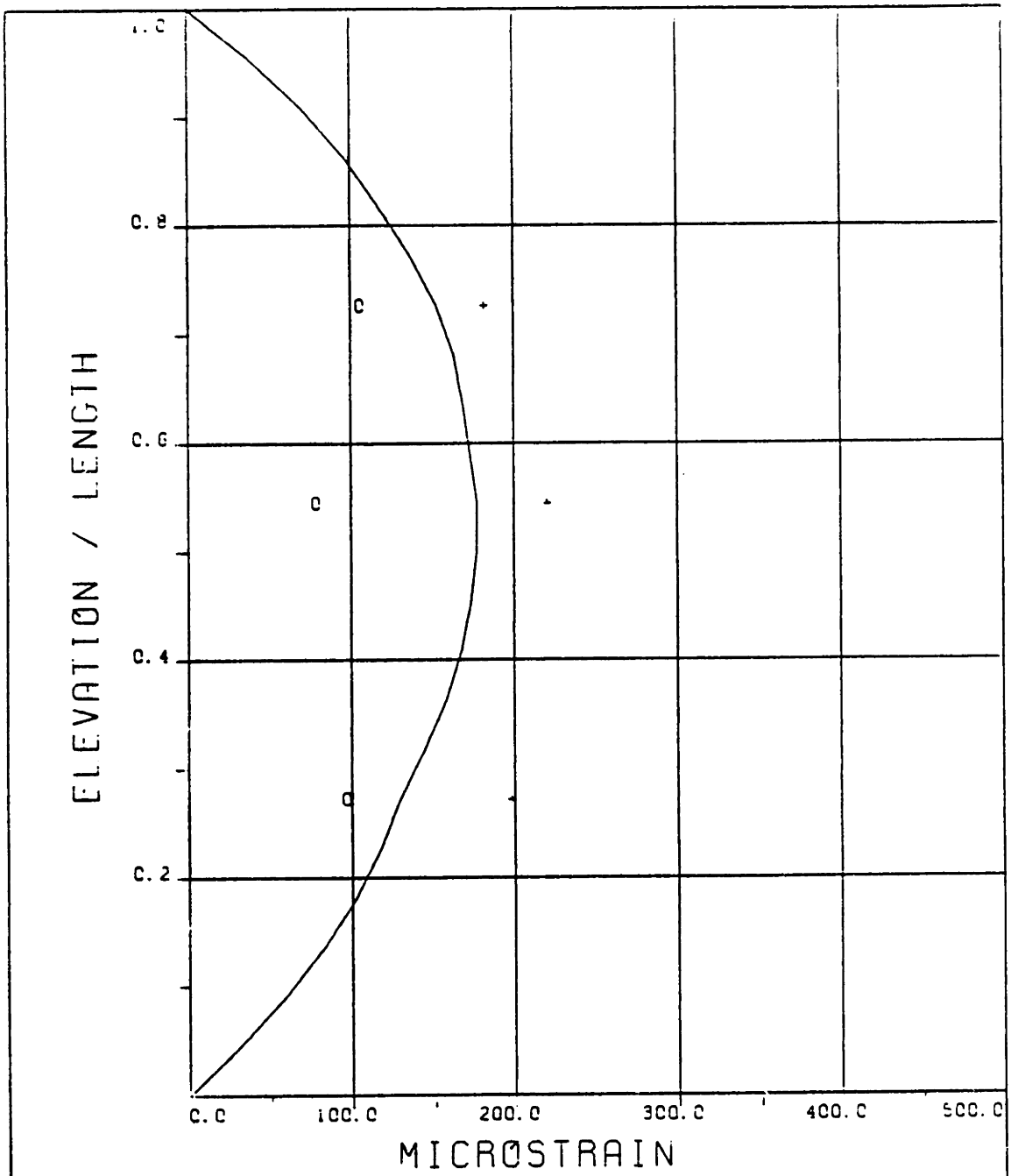

EXPERIMENT NUMBER 9

THETA=0 VC=240 FE=1.000 A/DE=2.03

MAXIMUM DYNAMIC RESPONSE IN PLANE B

c c c EXPERIMENT

MAXIMUM RESPONSE

_____ THEORY + + + EXPERIMENT

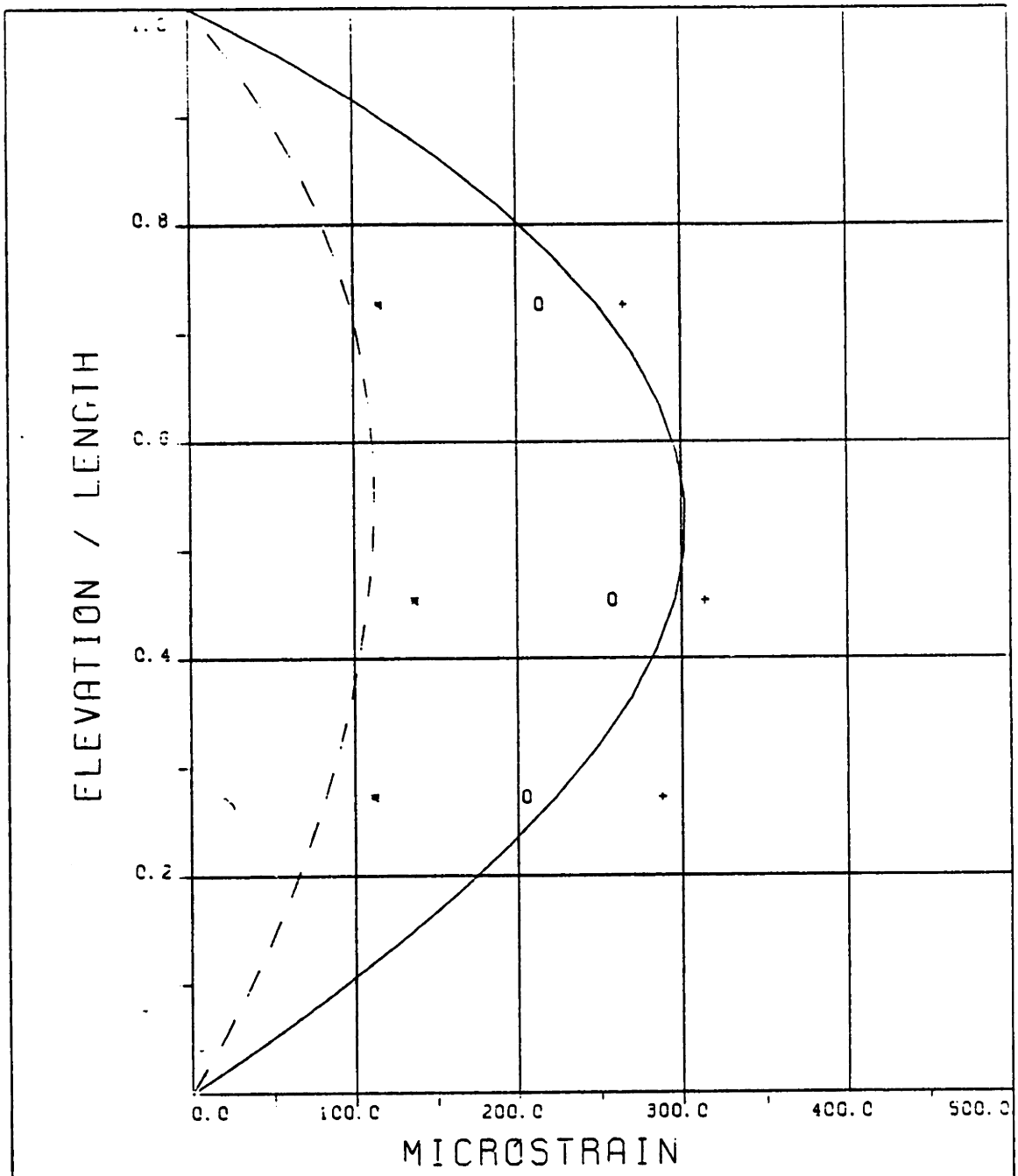

EXPERIMENT NUMBER 10

THETA=0 VC=240 FE=1.500 A/DE=2.01

STATIC RESPONSE IN PLANE A

----- THEORY * * * EXPERIMENT

STATIC RESPONSE PLUS DYNAMIC RESPONSE AT F = FE IN PLANE A

_____ THEORY o o o EXPERIMENT

MAXIMUM RESPONSE IN PLANE A

_____ THEORY + + + EXPERIMENT

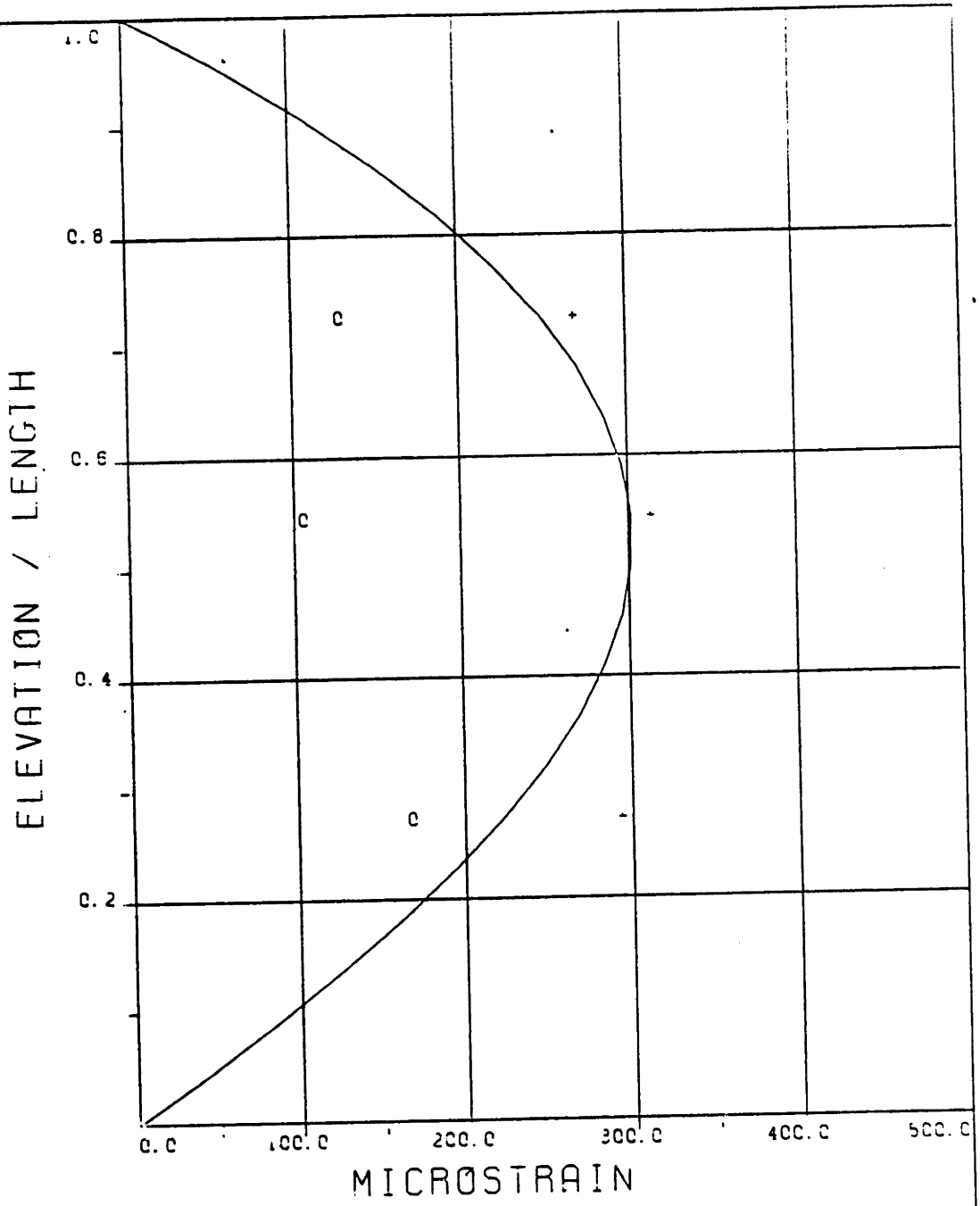

EXPERIMENT NUMBER 10

THETA=0 VC=240 FE=1.500 A/DE=2.01

MAXIMUM DYNAMIC RESPONSE IN PLANE B

c c c EXPERIMENT

MAXIMUM RESPONSE

_____ THEORY + + + EXPERIMENT

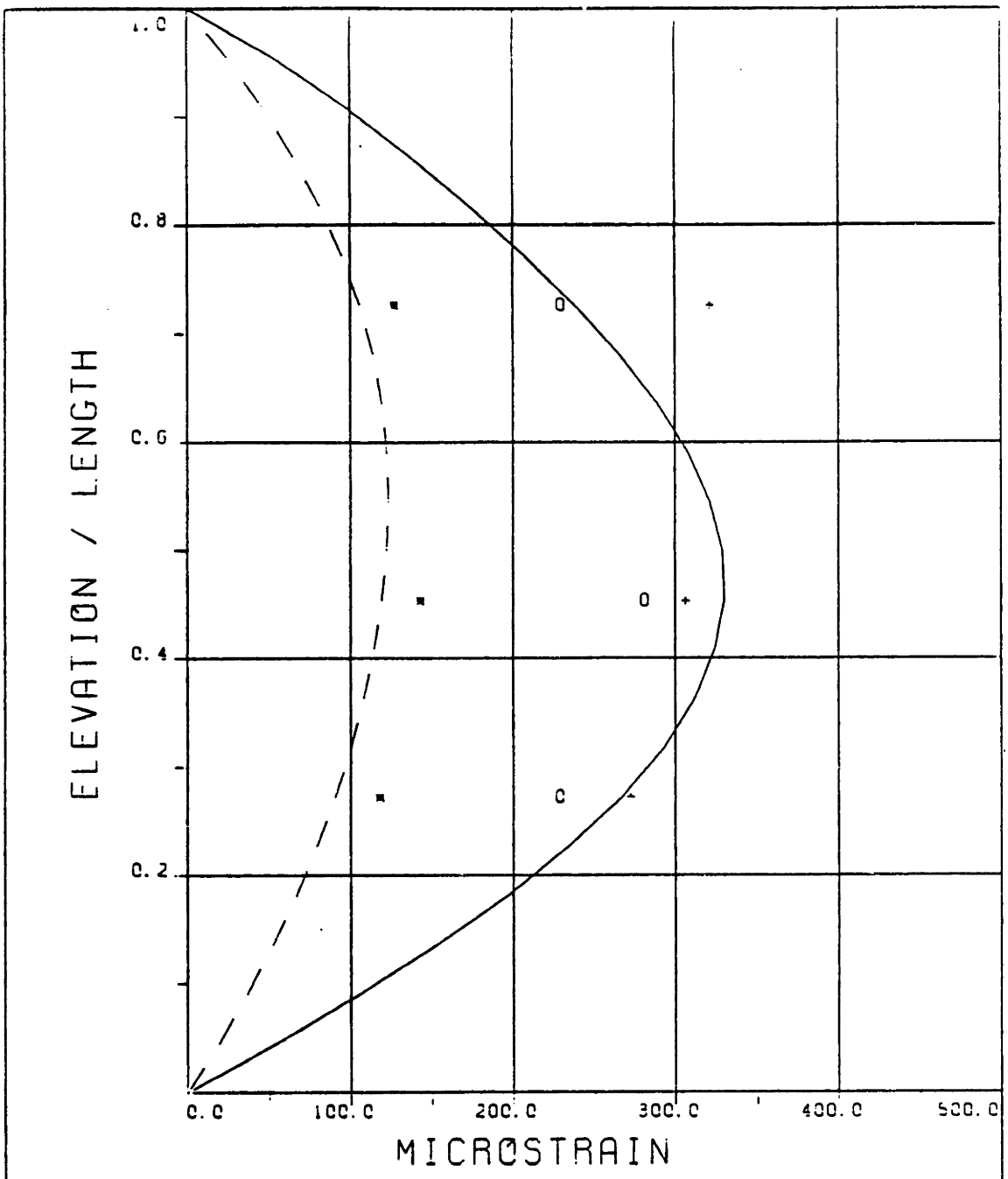

EXPERIMENT NUMBER 8

THETA=0 VC=240 FE=2.300 A/DE=2.04

STATIC RESPONSE IN PLANE A

----- THEORY * * * EXPERIMENT

STATIC RESPONSE PLUS DYNAMIC RESPONSE AT F = FE IN PLANE A

_____ THEORY o o o EXPERIMENT

MAXIMUM RESPONSE IN PLANE A

_____ THEORY + + + EXPERIMENT

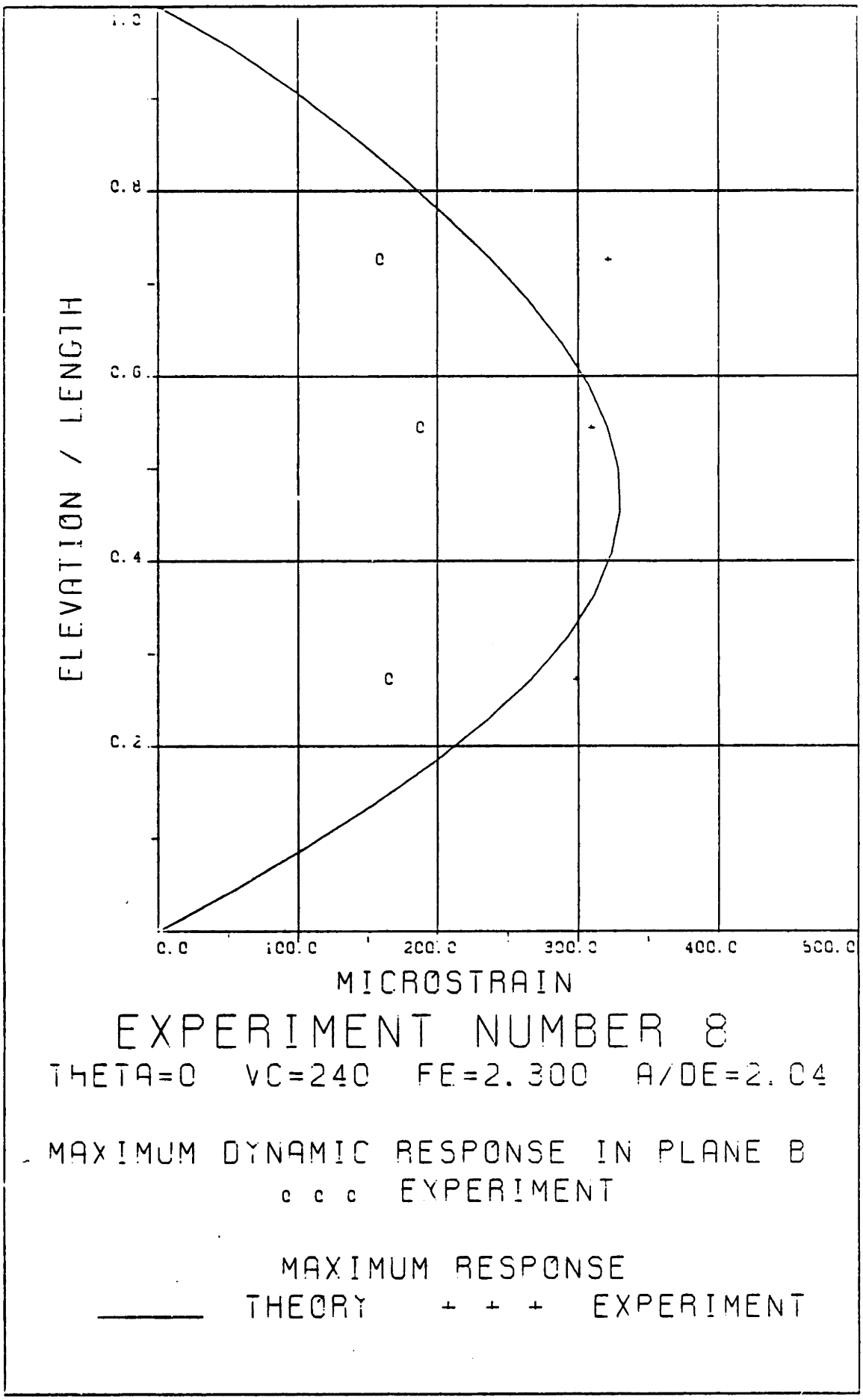
1.0
0.8
0.6
0.4
0.2
ELEVATION / LENGTH
0.0
100.0
200.0
300.0
400.0
500.0
MICROSTRAIN
EXPERIMENT NUMBER 8
THETA=0 VC=240 FE=2.300 A/DE=2.04
MAXIMUM DYNAMIC RESPONSE IN PLANE B
c c c EXPERIMENT
MAXIMUM RESPONSE
THEORY
+ + + EXPERIMENT

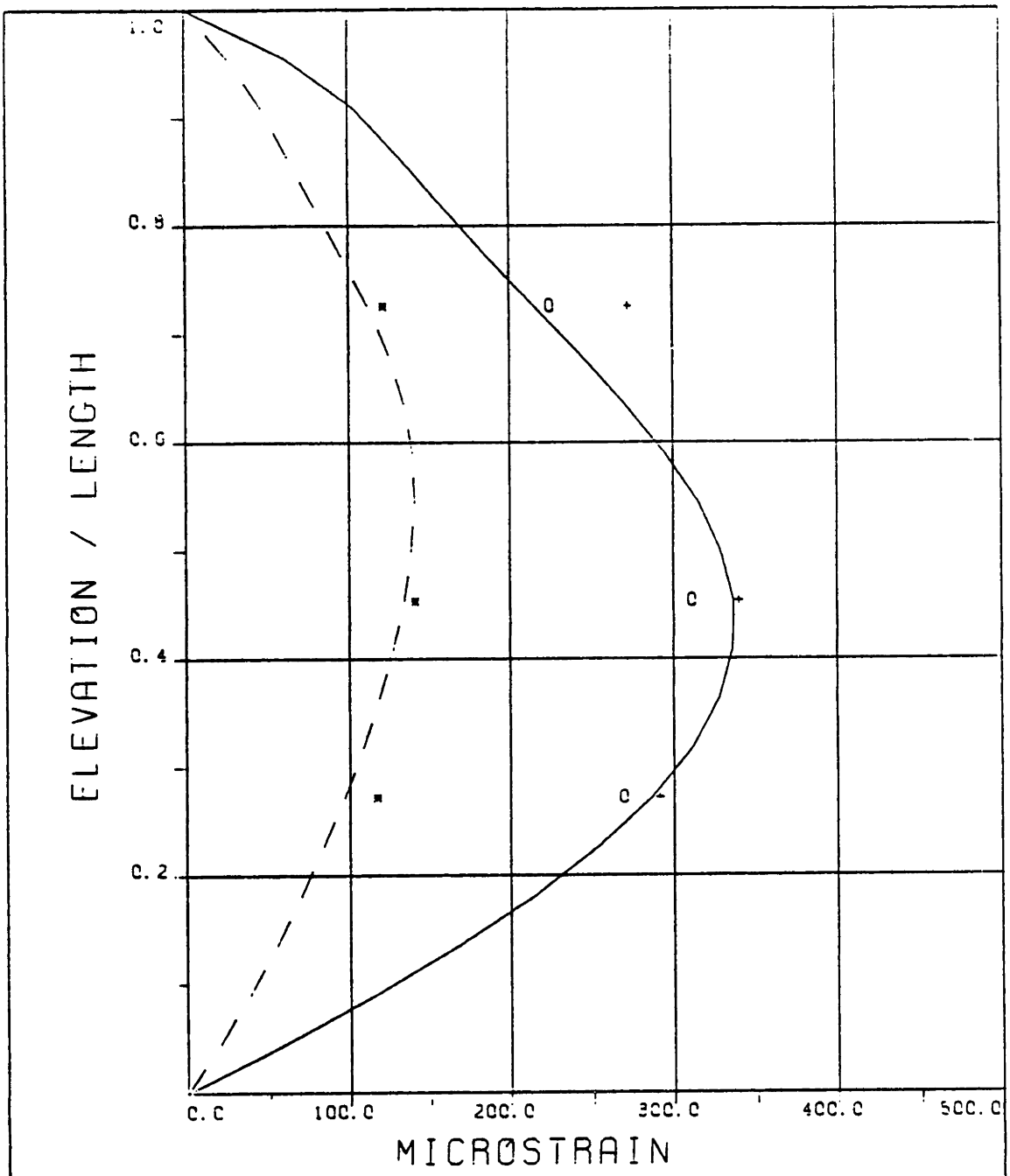

EXPERIMENT NUMBER 7

THETA=0 VC=240 FE=3.000 A/DE=2.04

STATIC RESPONSE IN PLANE A

----- THEORY * * * EXPERIMENT

STATIC RESPONSE PLUS DYNAMIC RESPONSE AT F = FE IN PLANE A

_____ THEORY o o o EXPERIMENT

MAXIMUM RESPONSE IN PLANE A

_____ THEORY + + + EXPERIMENT

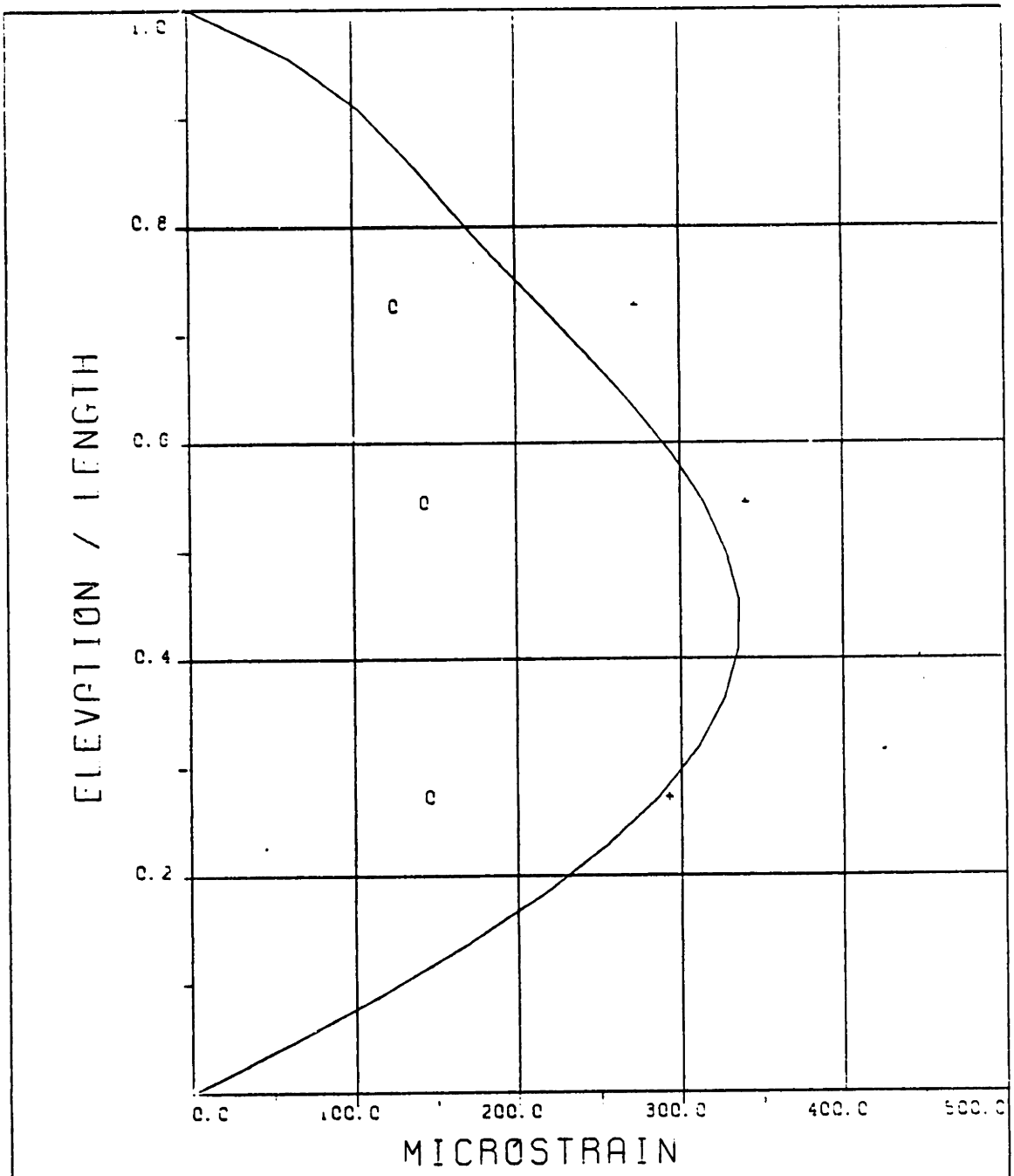

EXPERIMENT NUMBER 7

THETA=0 VC=240 FE=3.000 A/DE=2.04

MAXIMUM DYNAMIC RESPONSE IN PLANE B

c c c EXPERIMENT

MAXIMUM RESPONSE

_____ THEORY + + + EXPERIMENT

Suitable flexibly mounted rigid cylinder results will be able to provide us with such an estimate.

From the A and B type Figures of this class of experiments, and for reduced velocities of the order of ten, the results of Bernitsas (1979) provide a partial phenomenological explanation of why our predictions of the static and dynamic response at f_e in plane A are good even though the motion in the B plane is substantial. Namely, for angles of oscillation between 0 and 45 degrees with respect to a current, the static force and the component of the dynamic force parallel to the current at f_e do not depend much upon θ, at least for the amplitude studied by Bernitsas (1979).

V.4.3 HARMONIC OSCILLATION OF THE TOP END OF THE MODEL ORTHOGONAL TO A UNIFORM STREAM

In all experiments described in this section, the direction of oscillation of the top end was orthogonal to the long side of the towing tank and the current. The amplitude of oscillation was again approximately equal to two effective diameters. The water temperature was 14.1 degrees C. Bending strains in plane A at Z=3L/11, 5L/11 and 8L/11, and in plane B at Z=3L/11, 5L/11, 6L/11 and 8L/11 were recorded simultaneously together with the motion of the top end. The root mean square response strain as a

function of the response frequency at elevations Z=3L/11 and 5L/11 for plane A and B have been recently presented in Chryssostomidis and Patrikalakis (1982a) and are not repeated here. A collective description of the experiments analyzed in this Section is shown in Table V.5.

Table V.5 also includes information about the theoretical prediction of the dynamic response at f_e in plane B and of the static response in plane A, performed as described in Section IV.4.3. The way in which $\hat{c}_m$ and $\hat{c}_d$ shown in Table V.5 have been derived from the local c_m and c_d is explained in Appendix B. The estimates of the local c_m and c_d employed in the iteration procedure are based on rigid cylinder results shown in Figures 10 and 9 of Chapter IV, respectively. These results are, for the most part, based on experiments performed at Reynolds number 8000. The trend of available data for $U^* \to 0$ is that substantial increases of the drag coefficients are expected for decreasing Reynolds number. No corrections for Reynolds number have been included for the predictions described in Table V.5. This implies that at least for small U^* and if the correct data are used, a better agreement between theory and our experiment is expected. As it can be also observed from Table V.5 and Figures 9 and 10, extrapolation for amplitudes larger than 1.3 diameters was necessary for the calculation of c_m and c_d. The analysis of Appendix B implies that the larger

TABLE V.5

Experiment Number	V_c ($\frac{mm}{s}$) / Re	Frequency of Excitation f_e in Hz	Measured A/D_e / U*	$\hat{c}_m$	$\hat{c}_d$	Maximum Calculated y/D_e	Mean Calculated y/D_e	$\hat{c}_D$
52	120 / 1568	0.5	1.89 / 15.69	-0.28	1.03	1.89	1.02	1.18
59	120 / 1568	0.775	1.90 / 10.12	-0.27	1.02	1.90	1.11	1.29
71	120 / 1568	1.5	1.91 / 5.23	0.10	0.72	2.61	1.94	2.35
80	120 / 1568	1.95	1.93 / 4.02	0.42	0.95	2.15	1.49	1.66
89	120 / 1568	2.925	1.94 / 2.68	1.03	1.02	1.94	0.77	1.62
51	240 / 3136	0.5	1.90 / 31.37	-0.28	1.03	1.90	1.02	1.13
60	240 / 3136	0.775	1.90 / 20.24	-0.27	1.02	1.90	1.11	1.18
70	240 / 3136	1.5	1.91 / 10.46	-0.26	1.01	2.10	1.60	1.52
81	240 / 3136	1.95	1.92 / 8.04	-0.25	1.00	2.10	1.57	1.78
88	240 / 3136	2.925	1.94 / 5.36	0.50	0.38	1.94	0.84	1.85

amplitudes weigh heavily in determining appropriate hydrodynamic coefficients. Linear extrapolation was employed. Therefore, the theoretical predictions of this section should be judged accordingly. To simplify the calculations, the average drag coefficient employed was estimated on the basis of the average calculated amplitude in the B plane and Figure 11 of Chapter IV. Again, some extrapolation was occasionally necessary. Until the controversy of existing data is resolved, more complicated calculation schemes are not warranted. All trends of existing data show that when the complete set of revised rigid cylinder experiments become available the correlation between theory and our experiment will improve.

From all experiments of the present class, it can be seen that the response in the B direction shows two distinct regimes. First, when the frequency of oscillation of the top end is sufficiently smaller than the Strouhal frequency then the response in the B plane includes two components at f_e and f_r. The frequency f_r is not the same as in Figure 2 of Chapter IV. Due to the motion in the lift direction, there is a change of the response frequency f_r from the Strouhal relationship of Figure 2 of Chapter IV to a relationship similar to the one described by Figure 15 of Chapter IV. In the second regime, the vortex shedding frequency locks on the frequency of oscillation and the response in the B plane

is nearly monochromatic. This occurs when the frequency of oscillation is sufficiently close to the Strouhal frequency. Finally, some very low frequency response orthogonal to the current is also encountered. This is associated with slow variation of the spanwise correlation of the lift force, see Mercier (1973).

A summary of our results for the response in plane B is shown in Figures 52B, 59B, 71B, 803, 89B, 51B, 60B, 70B, 81B, and 88B. These include the theoretical and experimental dynamic response strain at f_e and the maximum dynamic response strain in plane B. Our present theoretical estimate of the maximum response in plane B is the same as our estimate of the dynamic response at f_e in plane B. This is expected to give realistic results for the maximum in plane B when the response orthogonal to the current is practically monochromatic. When the frequency of imposed oscillation is much lower than the first "natural frequency" of the cylinder and the Strouhal frequency, the procedure suggested in Section IV.4.3 may be employed to estimate the magnitude of the response at the Strouhal frequency. This procedure does not supply any phase information between the response at f_e and the Strouhal frequency. In addition, it assumes that there are no appreciable interactions between force components at f_e and the Strouhal frequency.

The dynamic response in plane A is significant when compared to the dynamic response in plane B. When

the Strouhal frequency, f_r, is not synchronized with the frequency of oscillation, dynamic response in plane A occurs at f_e, f_r and $f_r \pm f_e$. When the Strouhal frequency, f_r, is synchronized with the frequency of oscillation, dynamic response in plane A occurs at nf_e, where n is an integer up to three, and is magnified when nf_e is close to a "natural frequency" of the model. Some low frequency response in plane A is also encountered. This is associated with slow variation of the spanwise correlation of the dynamic force parallel to the current, see Mercier (1973).

A summary of our results for the response in plane A is shown in Figures 52A, 59A, 71A, 80A, 89A, 51A, 60A, 70A, 81A, and 88A. These include: the theoretical and experimental static response strain; the maximum experimental dynamic response strain; the maximum experimental response strain independent of plane; and our present theoretical estimate of the maximum response strain independent of plane. The latter is computed as the square root of the sum of the squares of the static strain and of the maximum dynamic response strain in plane B. No estimate of the magnitude of the dynamic response in plane A is possible with the data currently available. We expect to be able to estimate this response, when appropriate flexibly mounted rigid cylinder experiments become available.

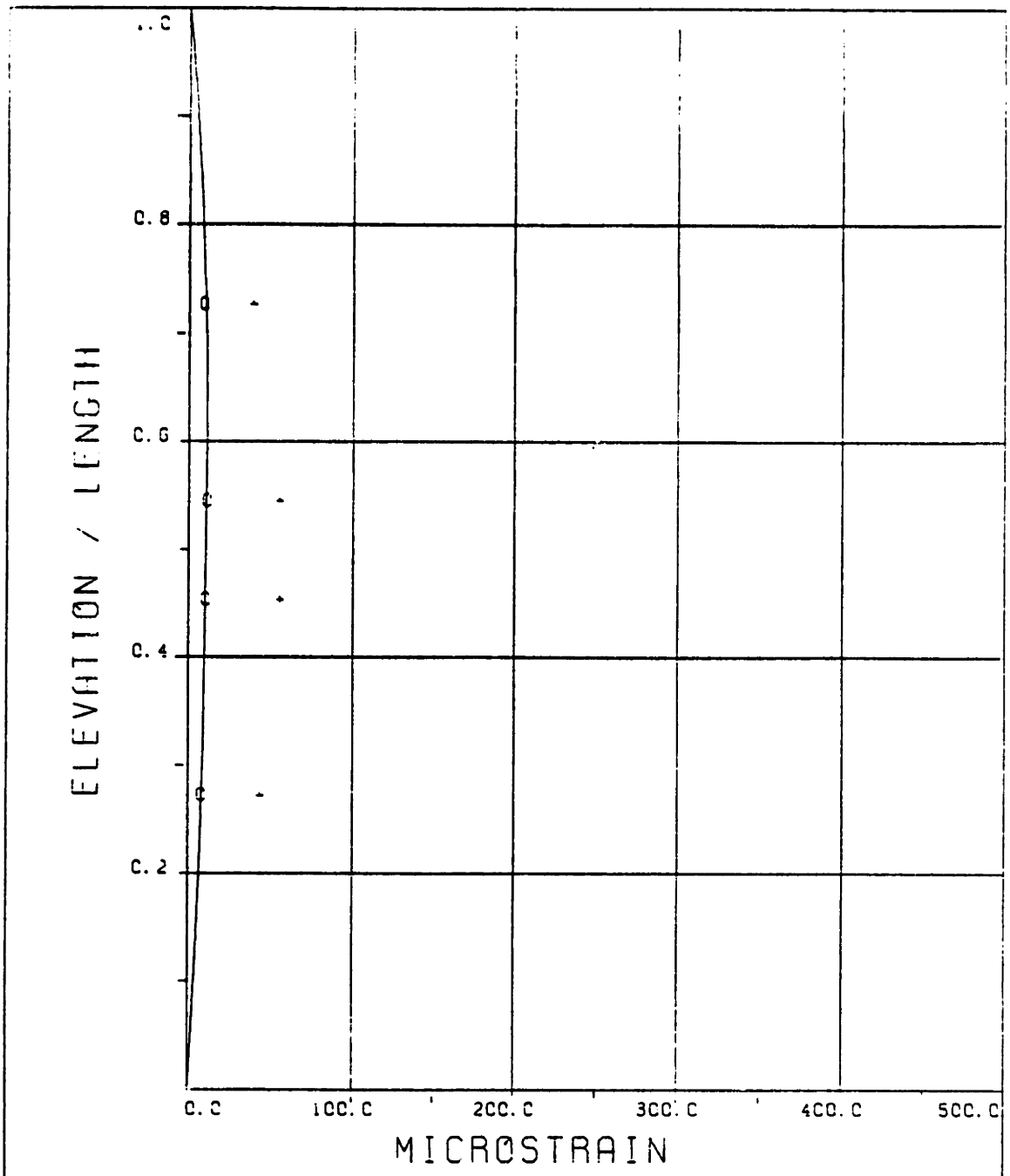

EXPERIMENT NUMBER 52

THETA=90 VC=120 FE=0.500 Ω/DE=1.89

DYNAMIC RESPONSE AT F=FE IN PLANE B

——— THEORY c c c EXPERIMENT

MAXIMUM DYNAMIC RESPONSE IN PLANE B

——— THEORY + + + EXPERIMENT

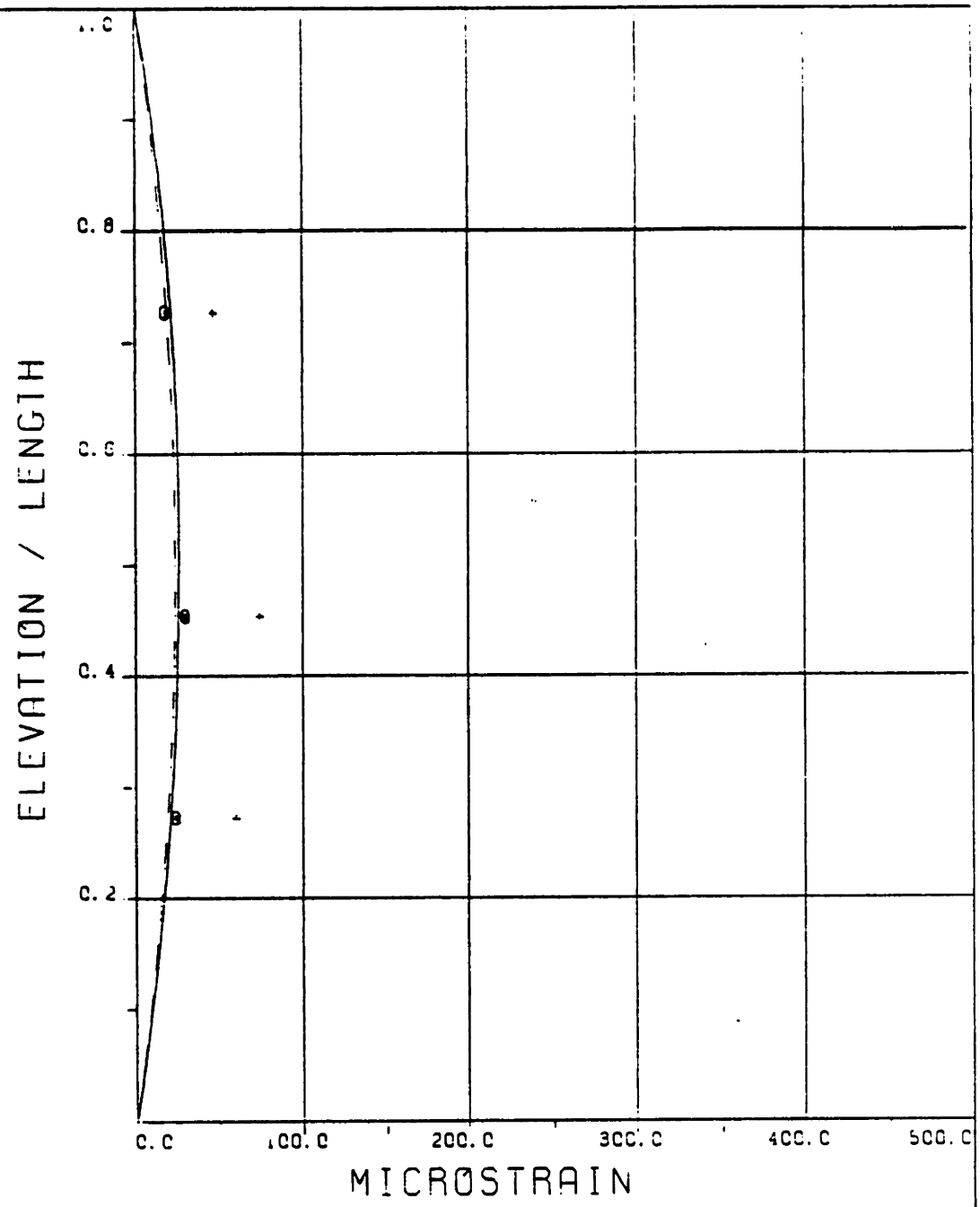

EXPERIMENT NUMBER 52

THETA=90 VC=120 FE=0.500 Ω/DE=1.89

STATIC RESPONSE IN PLANE 9

----- THEORY * * * EXPERIMENT

MAXIMUM DYNAMIC RESPONSE IN PLANE 9

c c c EXPERIMENT

MAXIMUM RESPONSE

_____ THEORY + + + EXPERIMENT

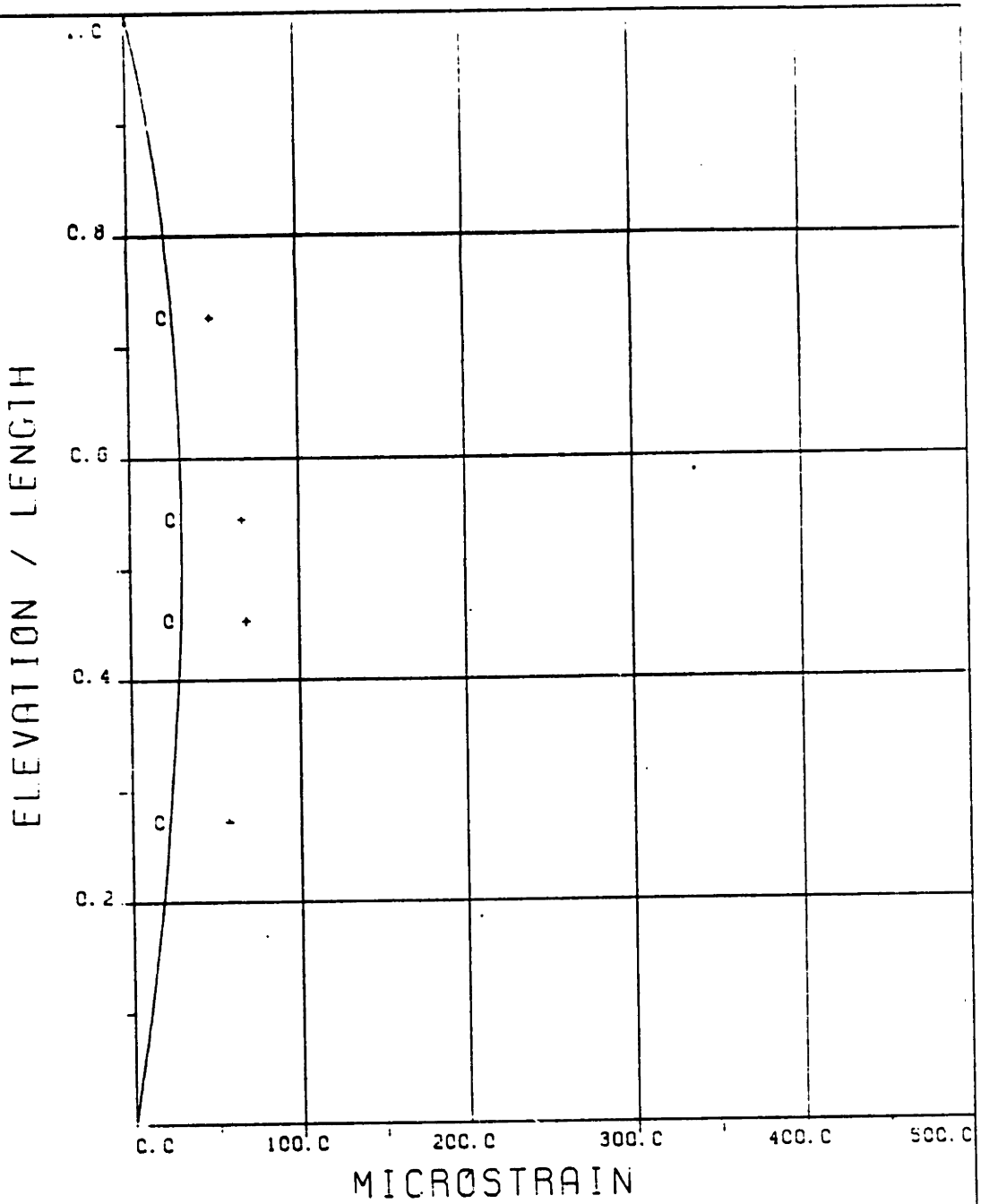

EXPERIMENT NUMBER 59

THETA=30 VC=120 FE=0.775 A/BE=1.90

DYNAMIC RESPONSE AT F=FE IN PLANE B

——— THEORY o o o EXPERIMENT

MAXIMUM DYNAMIC RESPONSE IN PLANE B

——— THEORY + + + EXPERIMENT

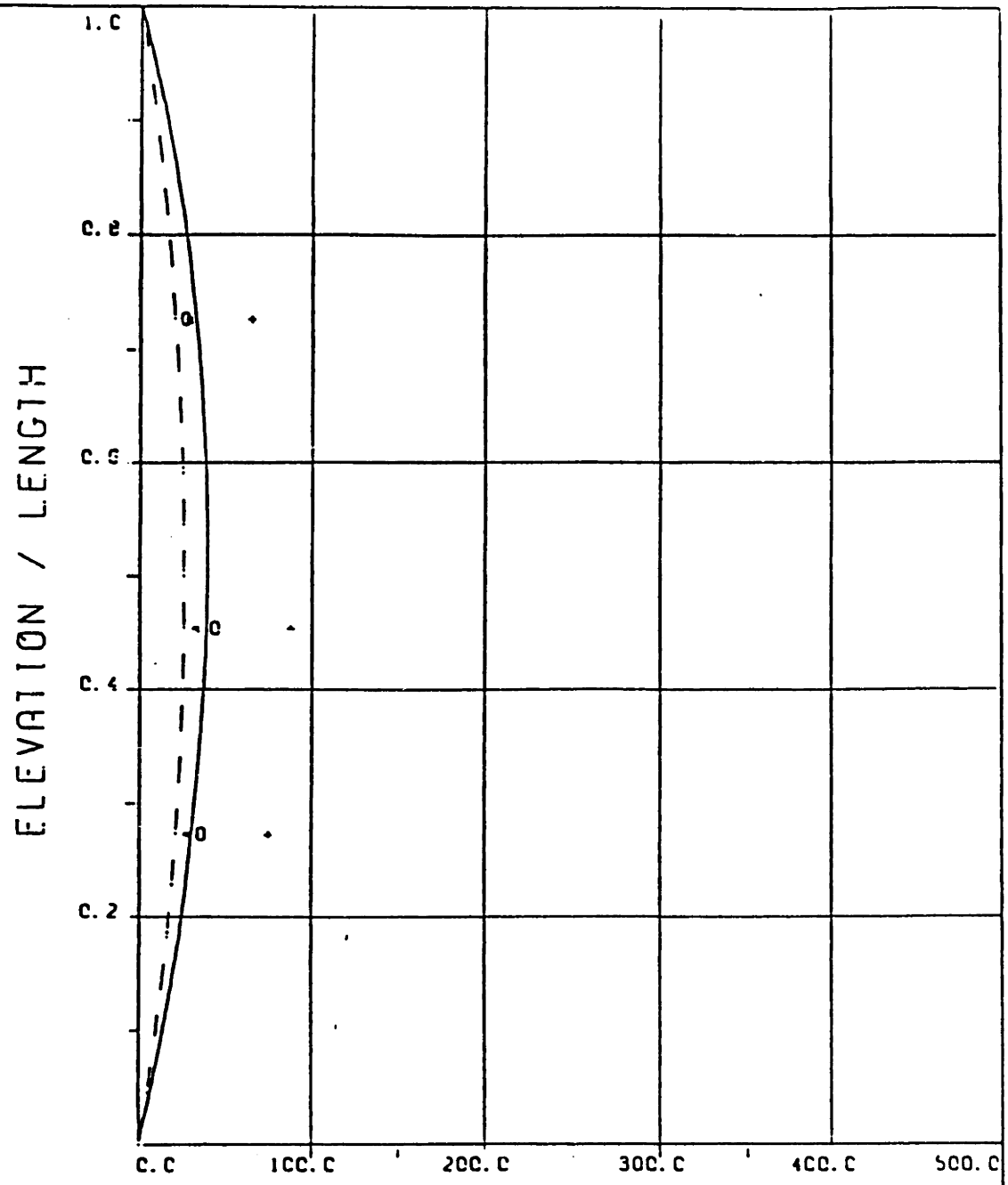

EXPERIMENT NUMBER 59

THETA=90 VC=120 FE=0.775 A/DE=1.90

STATIC RESPONSE IN PLANE A

----- THEORY * * * EXPERIMENT

MAXIMUM DYNAMIC RESPONSE IN PLANE A

c c c EXPERIMENT

MAXIMUM RESPONSE

_____ THEORY + + + EXPERIMENT

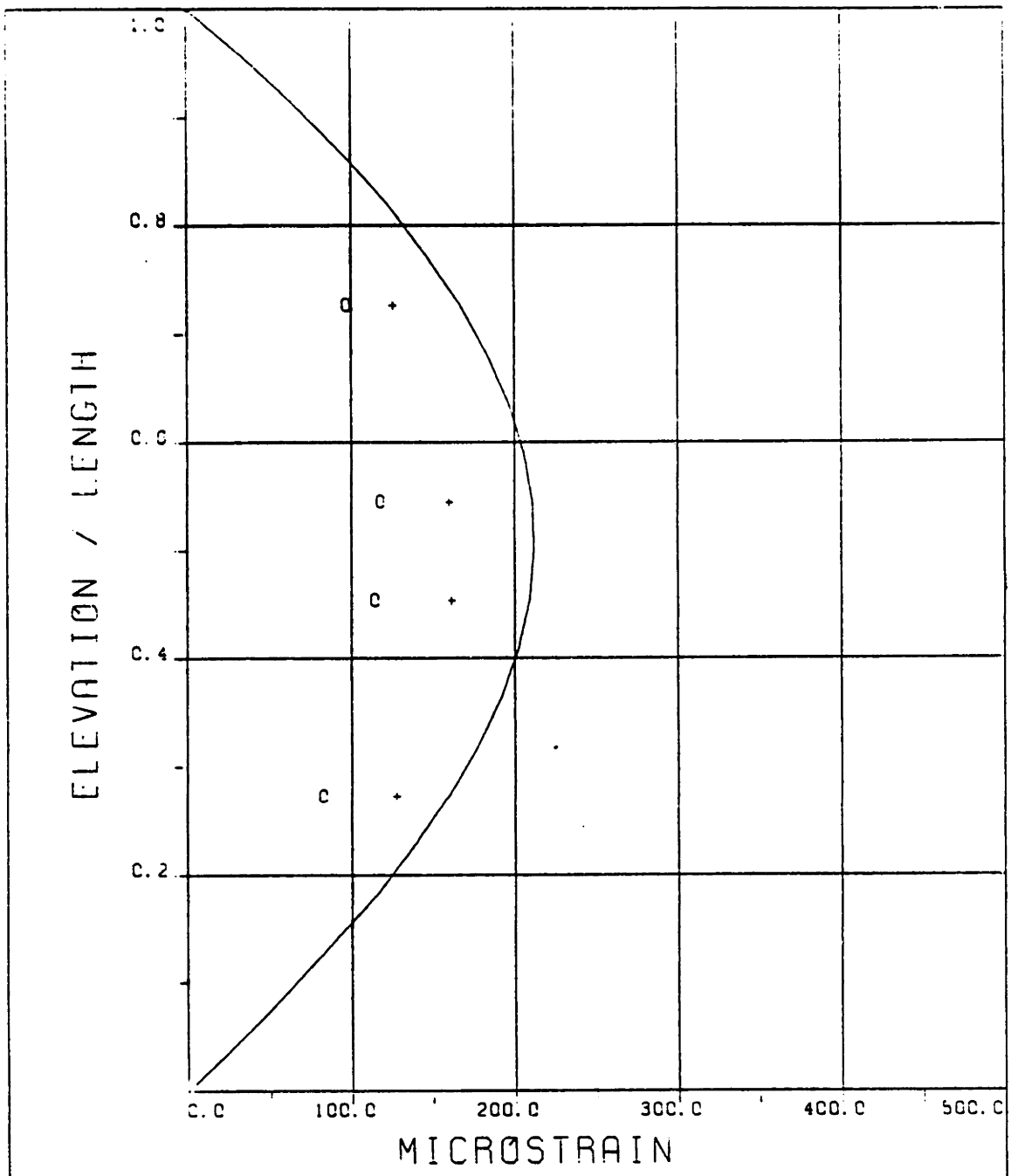

EXPERIMENT NUMBER 71

THETA=90 VC=120 FE=1.500 A/DE=1.91

DYNAMIC RESPONSE AT F=FE IN PLANE B

——— THEORY c c c EXPERIMENT

MAXIMUM DYNAMIC RESPONSE IN PLANE B

——— THEORY + + + EXPERIMENT

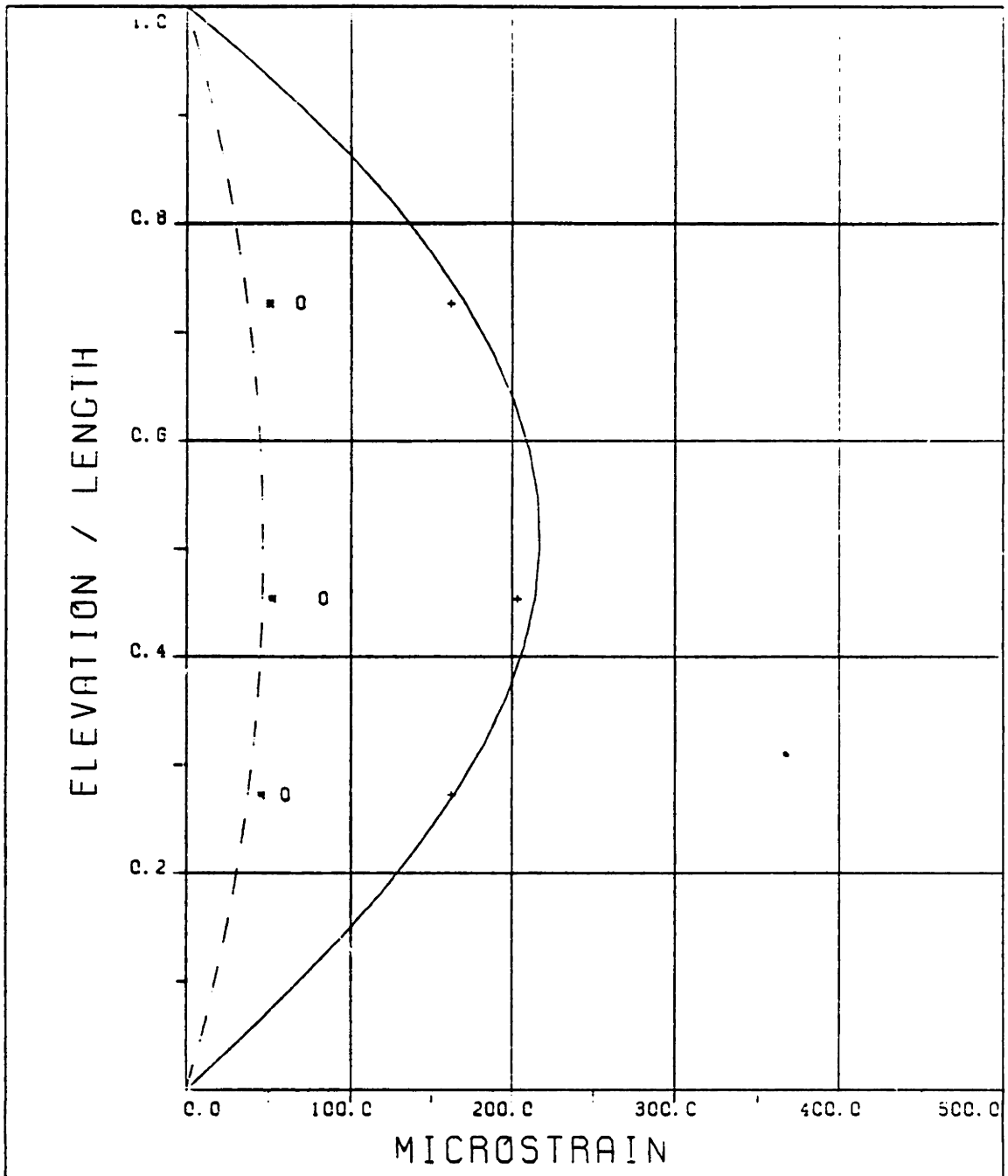

EXPERIMENT NUMBER 71

THETA=90 VC=120 FE=1.500 A/DE=1.91

STATIC RESPONSE IN PLANE A

----- THEORY * * * EXPERIMENT

MAXIMUM DYNAMIC RESPONSE IN PLANE A

c c c EXPERIMENT

MAXIMUM RESPONSE

_____ THEORY + + + EXPERIMENT

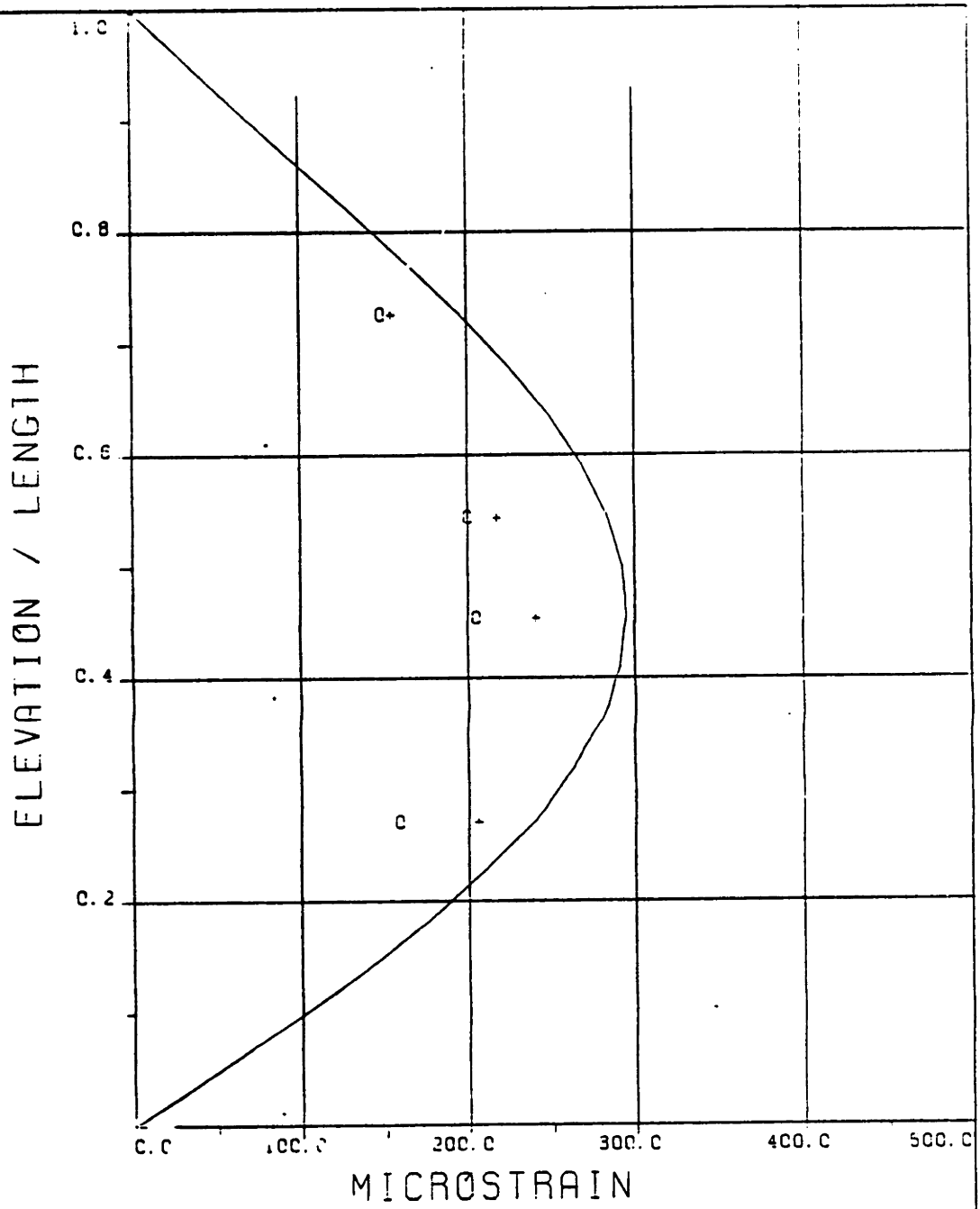

EXPERIMENT NUMBER 80

THETA=90 VC=120 FE=1.950 A/DE=1.93

DYNAMIC RESPONSE AT F=FE IN PLANE B

——— THEORY o o o EXPERIMENT

MAXIMUM DYNAMIC RESPONSE IN PLANE B

——— THEORY + + + EXPERIMENT

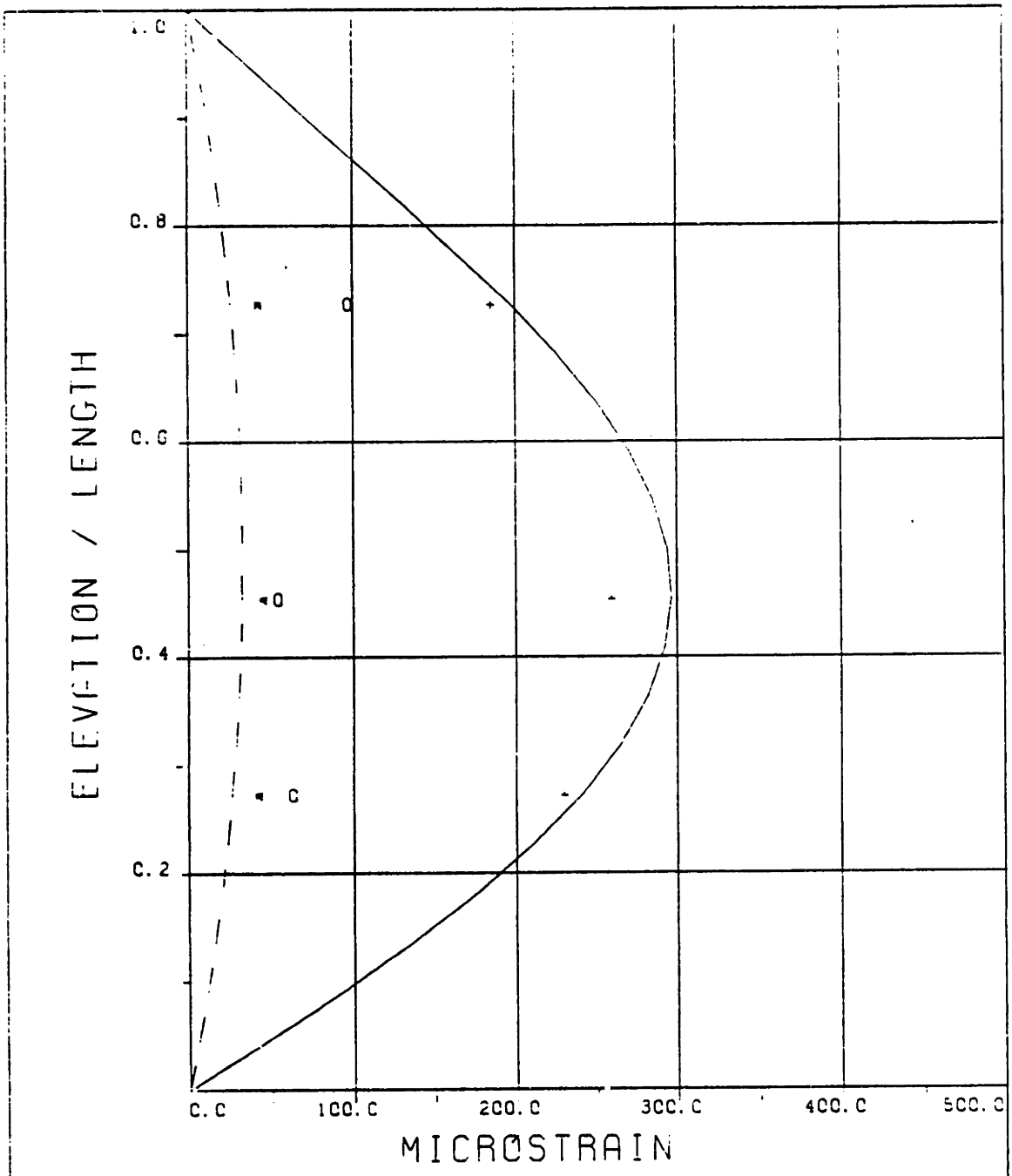

EXPERIMENT NUMBER 80

THETA=90 VC=120 FE=1.950 A/DE=1.93

STATIC RESPONSE IN PLANE A

----- THEORY * * * EXPERIMENT

MAXIMUM DYNAMIC RESPONSE IN PLANE A

c c c EXPERIMENT

MAXIMUM RESPONSE

_____ THEORY + + + EXPERIMENT

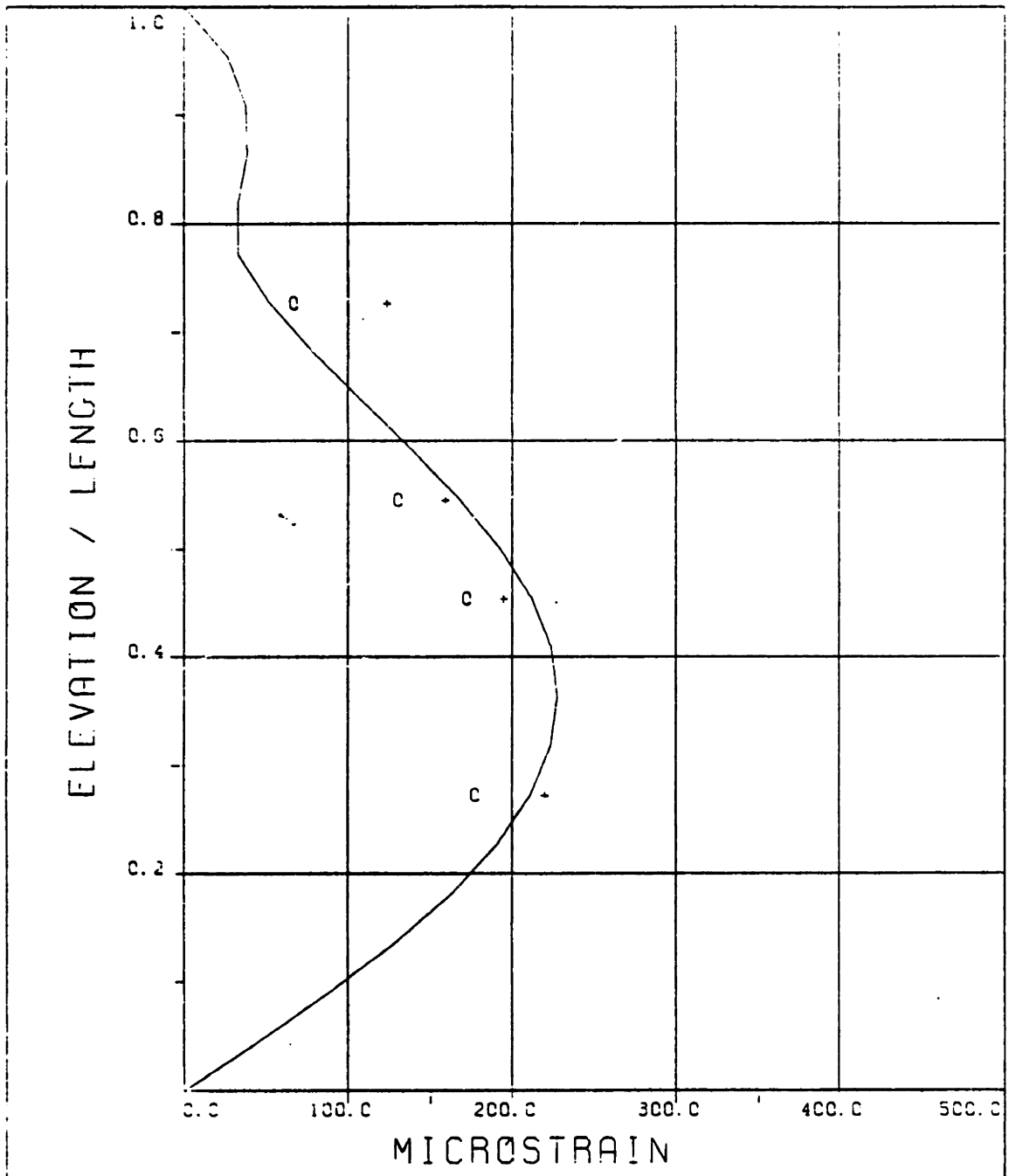

EXPERIMENT NUMBER 89

THETA=90 VC=120 FE=2.925 A/DE=1.94

DYNAMIC RESPONSE AT F=FE IN PLANE B

——— THEORY o o o EXPERIMENT

MAXIMUM DYNAMIC RESPONSE IN PLANE B

——— THEORY + + + EXPERIMENT

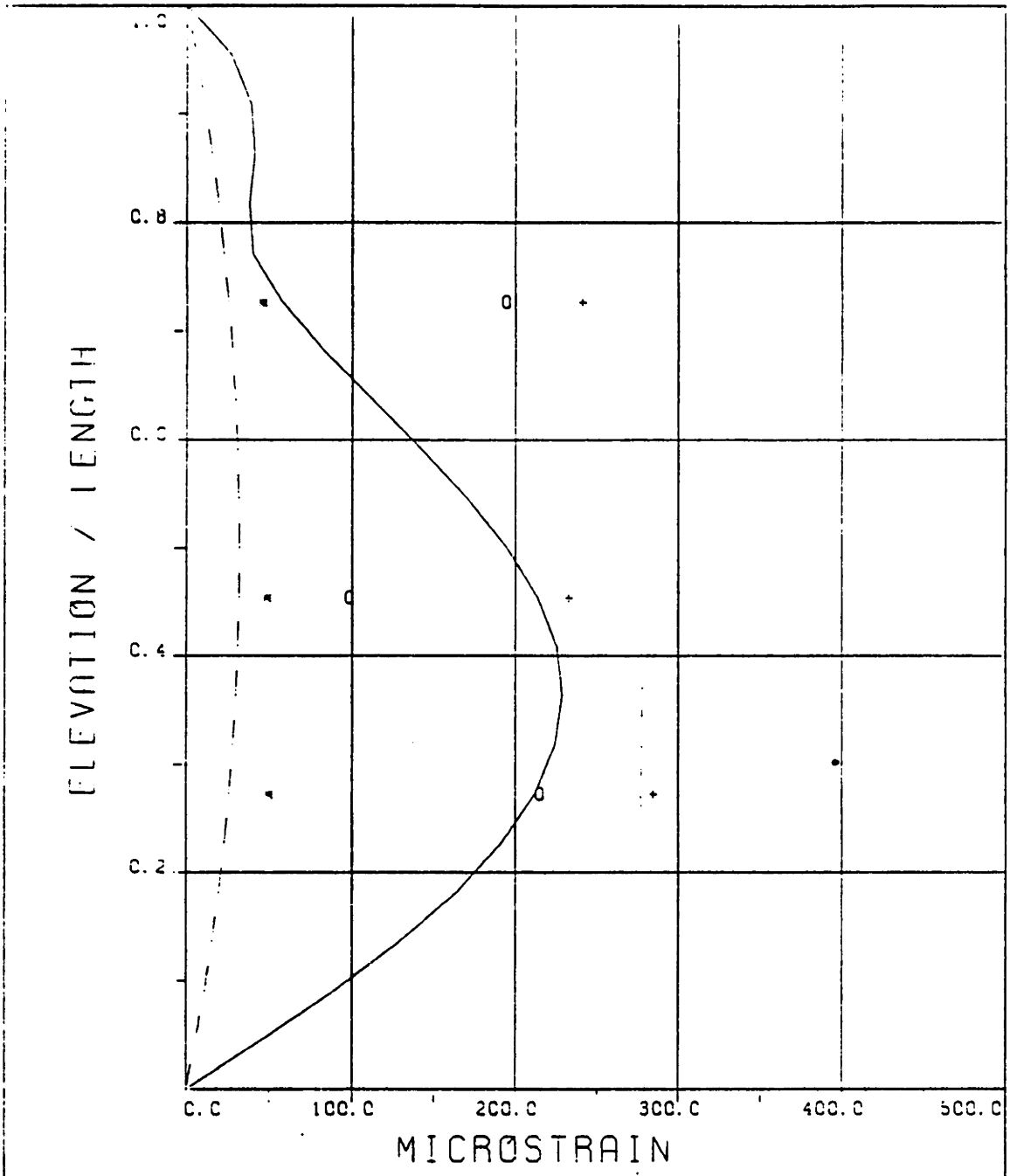

EXPERIMENT NUMBER 89

THETA=90 VC=120 FE=2.925 A/DE=1.94

STATIC RESPONSE IN PLANE A

----- THEORY * * * EXPERIMENT

MAXIMUM DYNAMIC RESPONSE IN PLANE A

o o o EXPERIMENT

MAXIMUM RESPONSE

_____ THEORY + + + EXPERIMENT

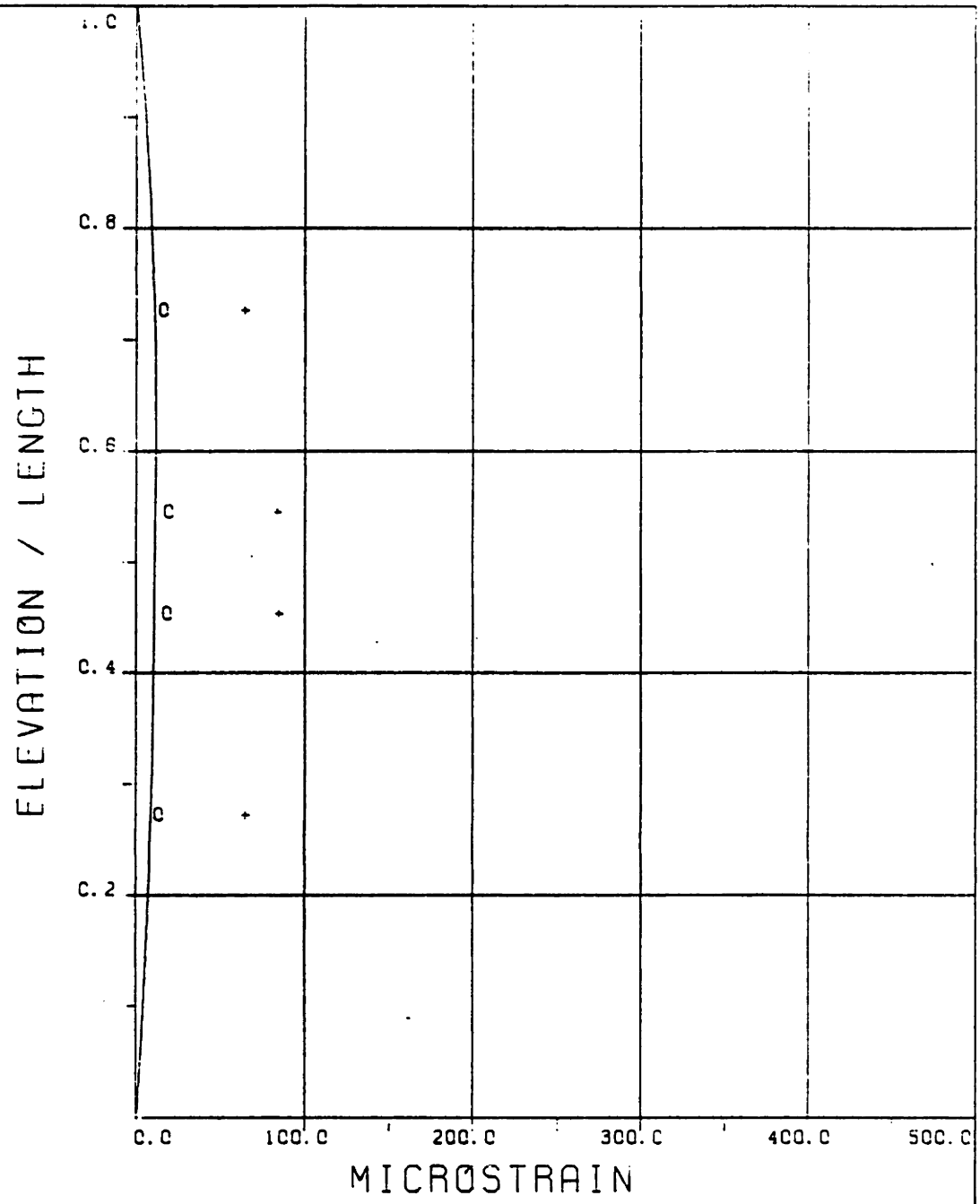

EXPERIMENT NUMBER 51

THETA=90 VC=240 FE=0.500 Q/DE=1.90

DYNAMIC RESPONSE AT F=FE IN PLANE B

_____ THEORY o o o EXPERIMENT

MAXIMUM DYNAMIC RESPONSE IN PLANE B

_____ THEORY + + + EXPERIMENT

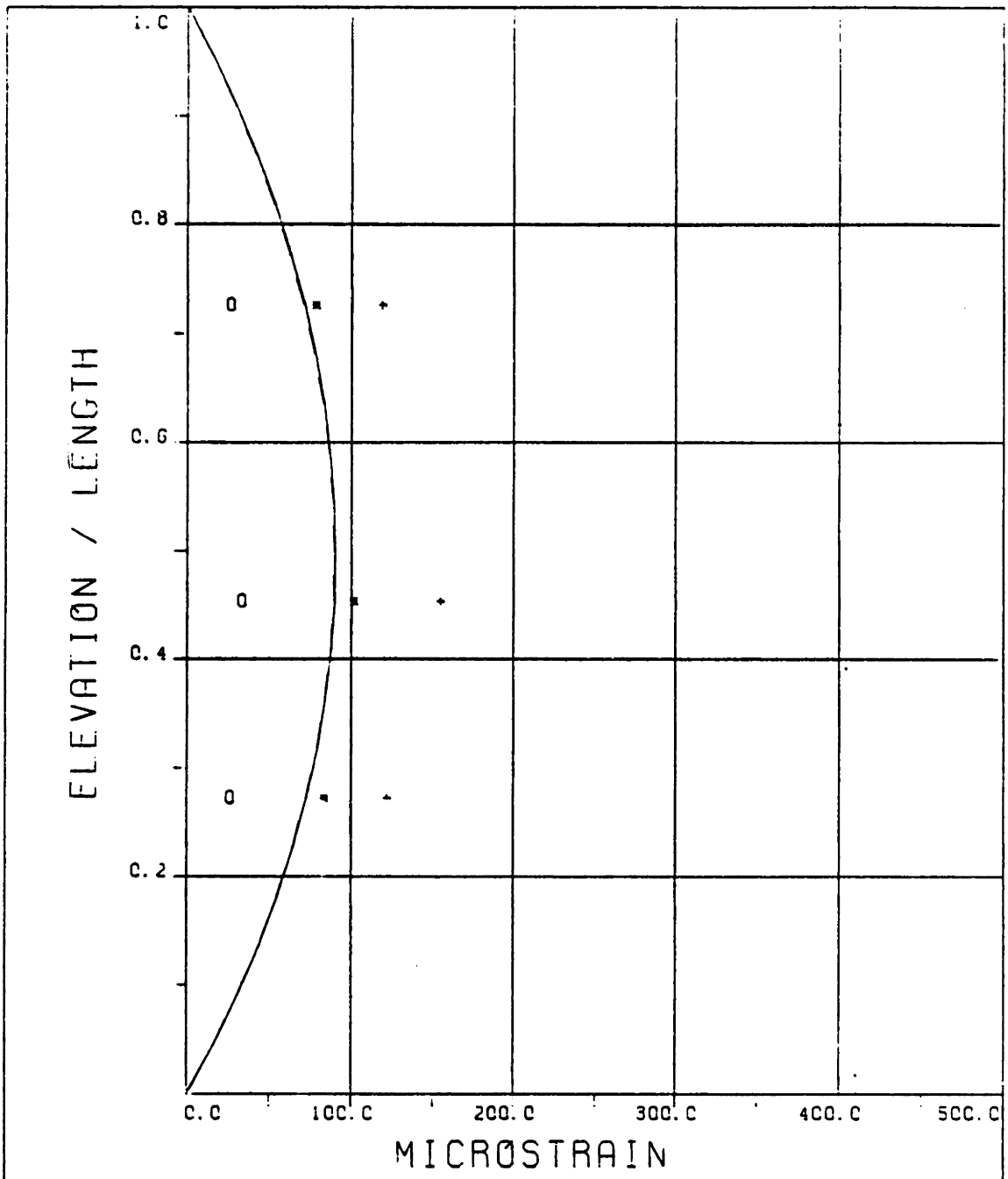

EXPERIMENT NUMBER 51

THETA=90 VC=240 FE=0.500 A/DE=1.90

STATIC RESPONSE IN PLANE A

----- THEORY * * * EXPERIMENT

MAXIMUM DYNAMIC RESPONSE IN PLANE A

o o o EXPERIMENT

MAXIMUM RESPONSE

_____ THEORY + + + EXPERIMENT

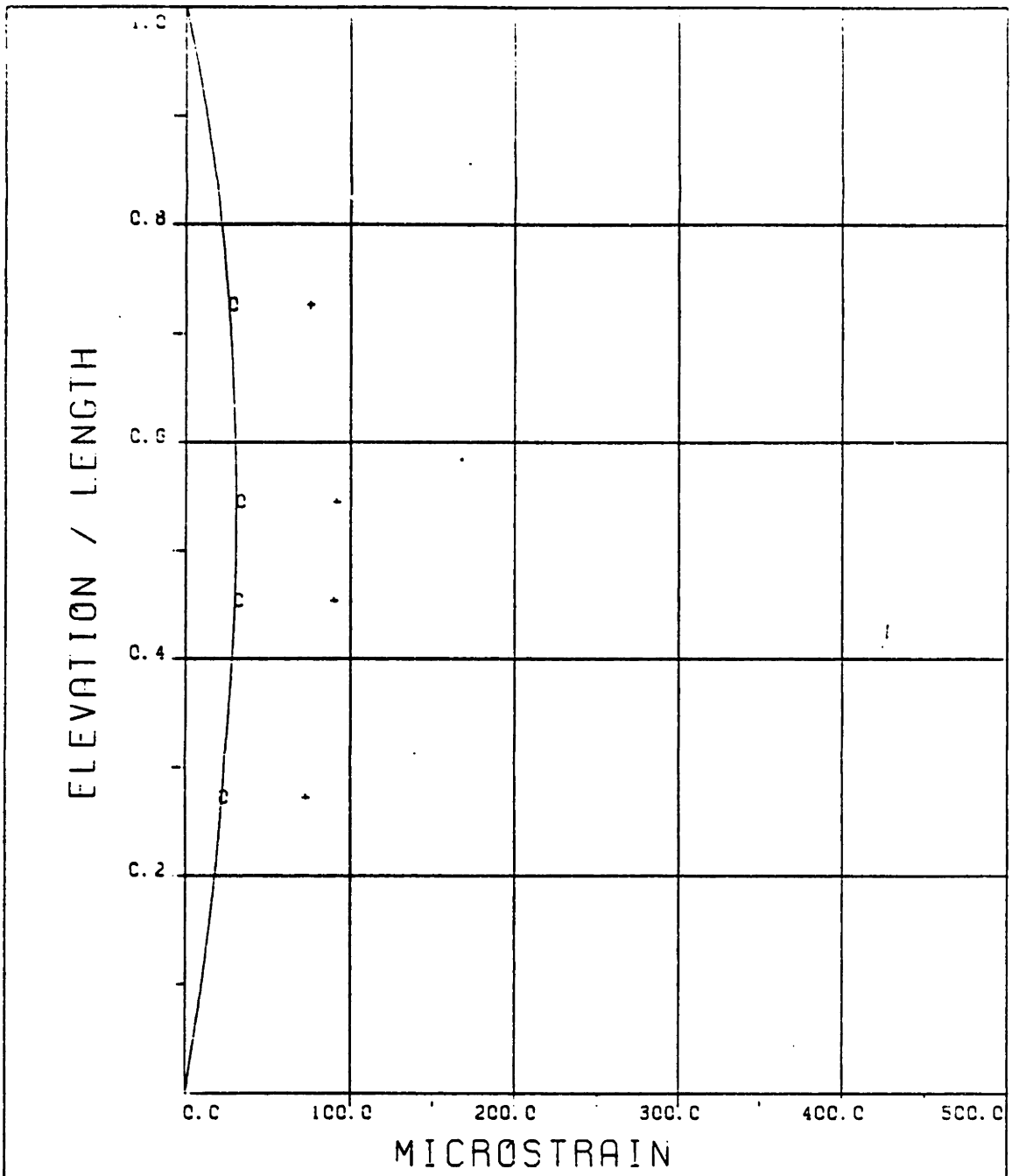

EXPERIMENT NUMBER 60

THETA=90 VC=240 FE=0.775 A/DE=1.90

DYNAMIC RESPONSE AT F=FE IN PLANE B

——— THEORY o o o EXPERIMENT

MAXIMUM DYNAMIC RESPONSE IN PLANE B

——— THEORY + + + EXPERIMENT

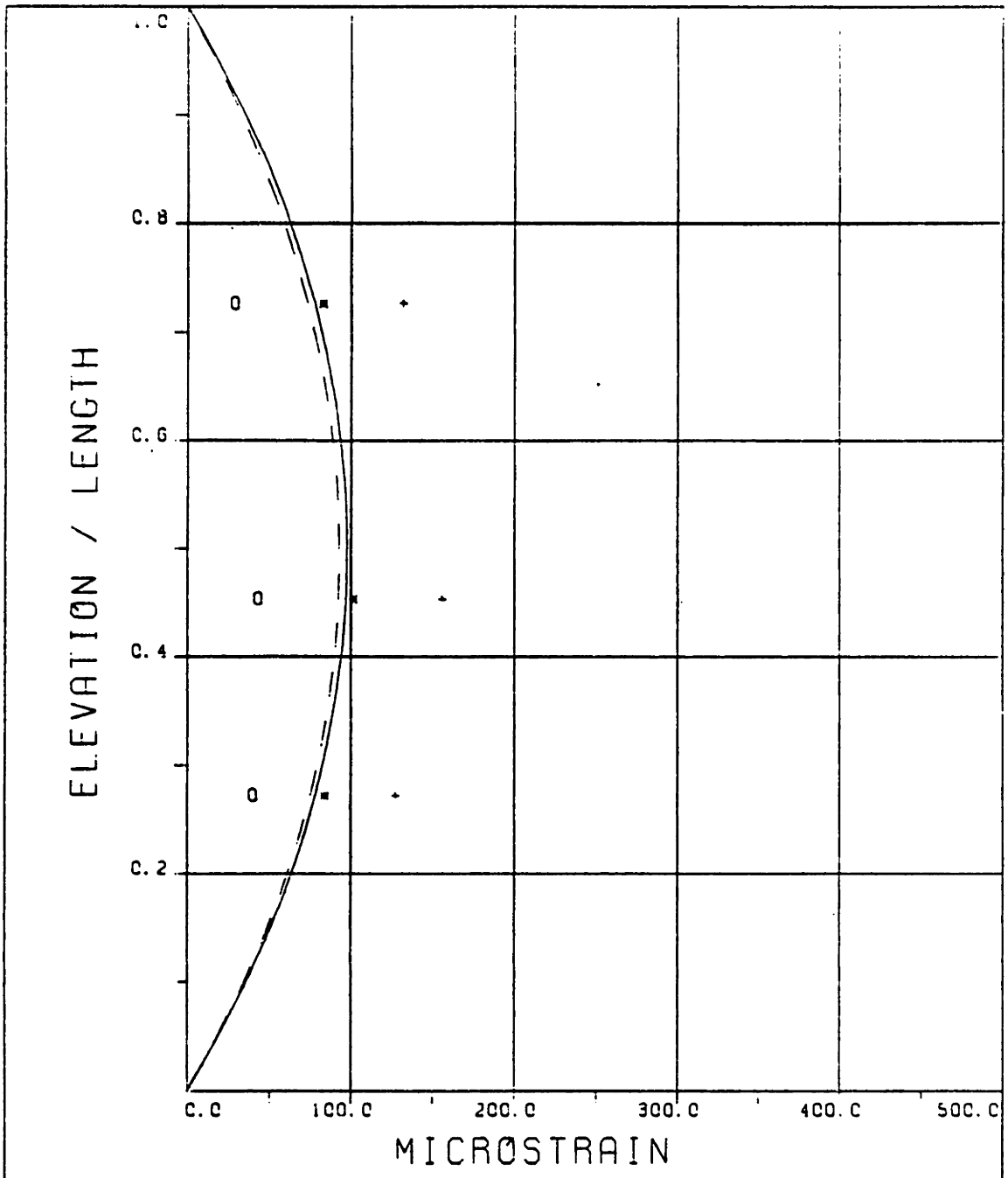

EXPERIMENT NUMBER 60

THETA=90 VC=240 FE=0.775 A/DE=1.90

STATIC RESPONSE IN PLANE A

----- THEORY * * * EXPERIMENT

MAXIMUM DYNAMIC RESPONSE IN PLANE A

o o o EXPERIMENT

MAXIMUM RESPONSE

_____ THEORY + + + EXPERIMENT

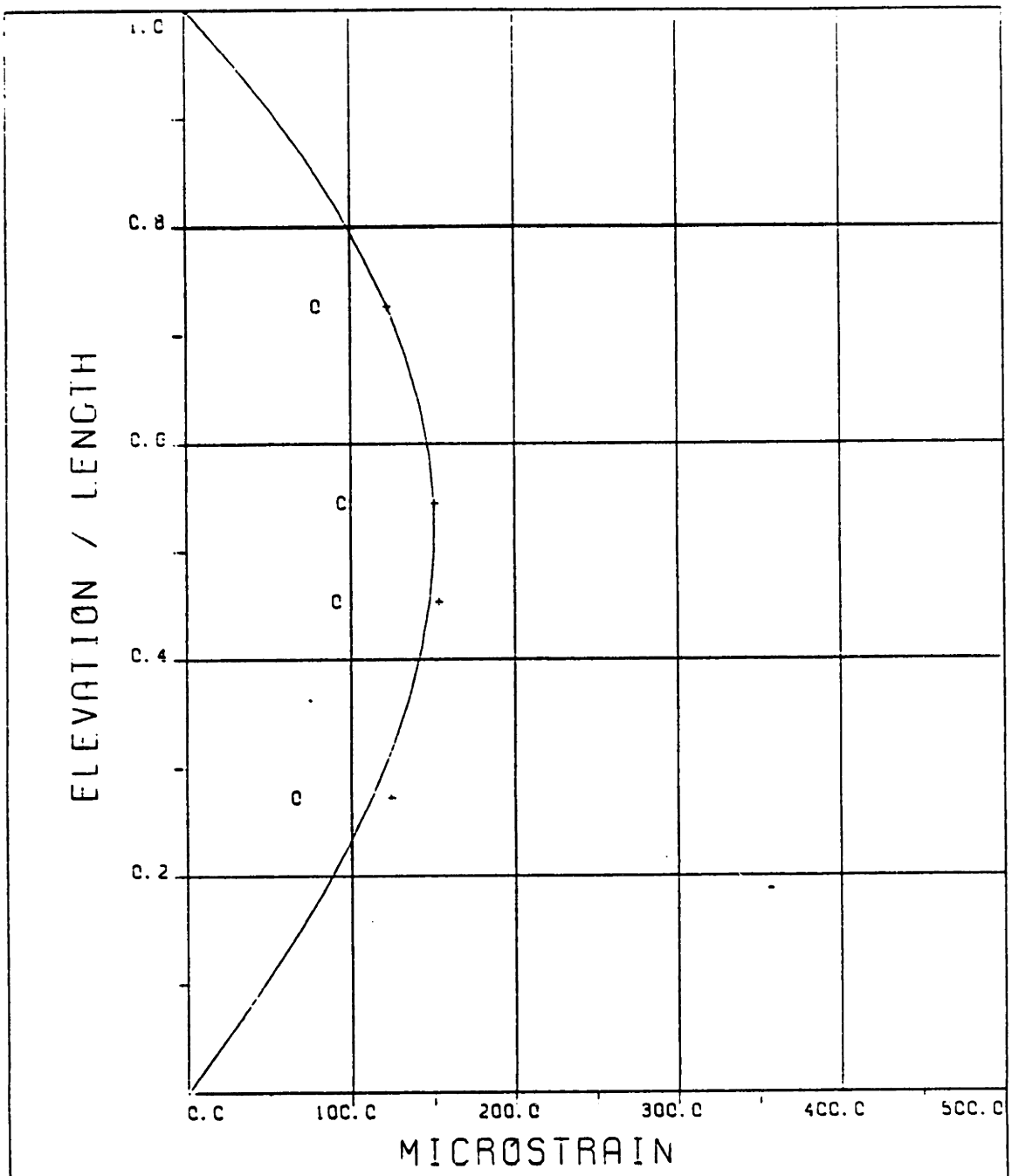

EXPERIMENT NUMBER 70

THETA=90 VC=240 FE=1.500 A/DE=1.91

DYNAMIC RESPONSE AT F=FE IN PLANE B

——— THEORY o o o EXPERIMENT

MAXIMUM DYNAMIC RESPONSE IN PLANE B

——— THEORY + + + EXPERIMENT

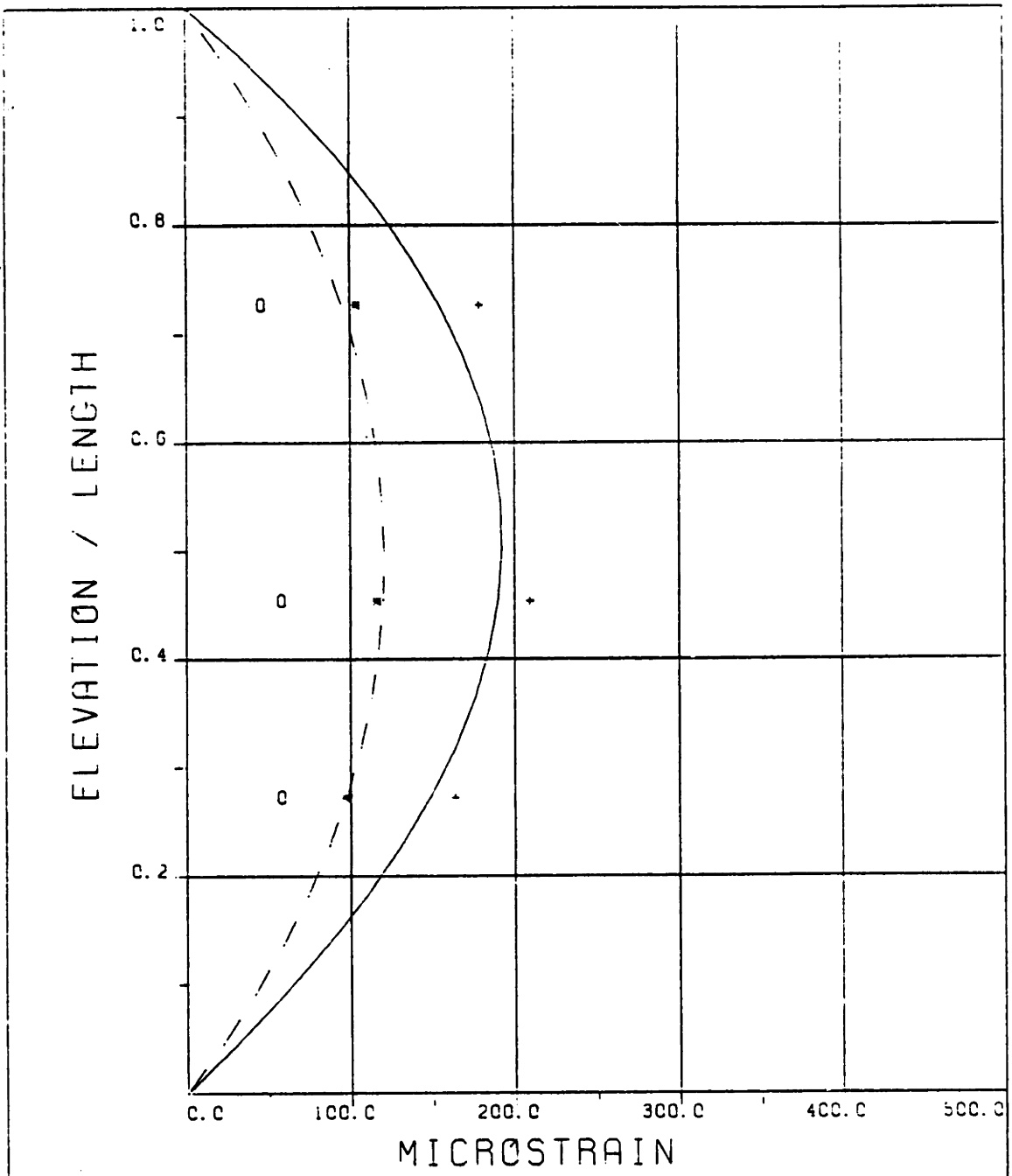

EXPERIMENT NUMBER 70

THETA=90 VC=240 FE=1.500 A/DE=1.91

STATIC RESPONSE IN PLANE 9

----- THEORY * * * EXPERIMENT

MAXIMUM DYNAMIC RESPONSE IN PLANE 9

o o o EXPERIMENT

MAXIMUM RESPONSE

_____ THEORY + + + EXPERIMENT

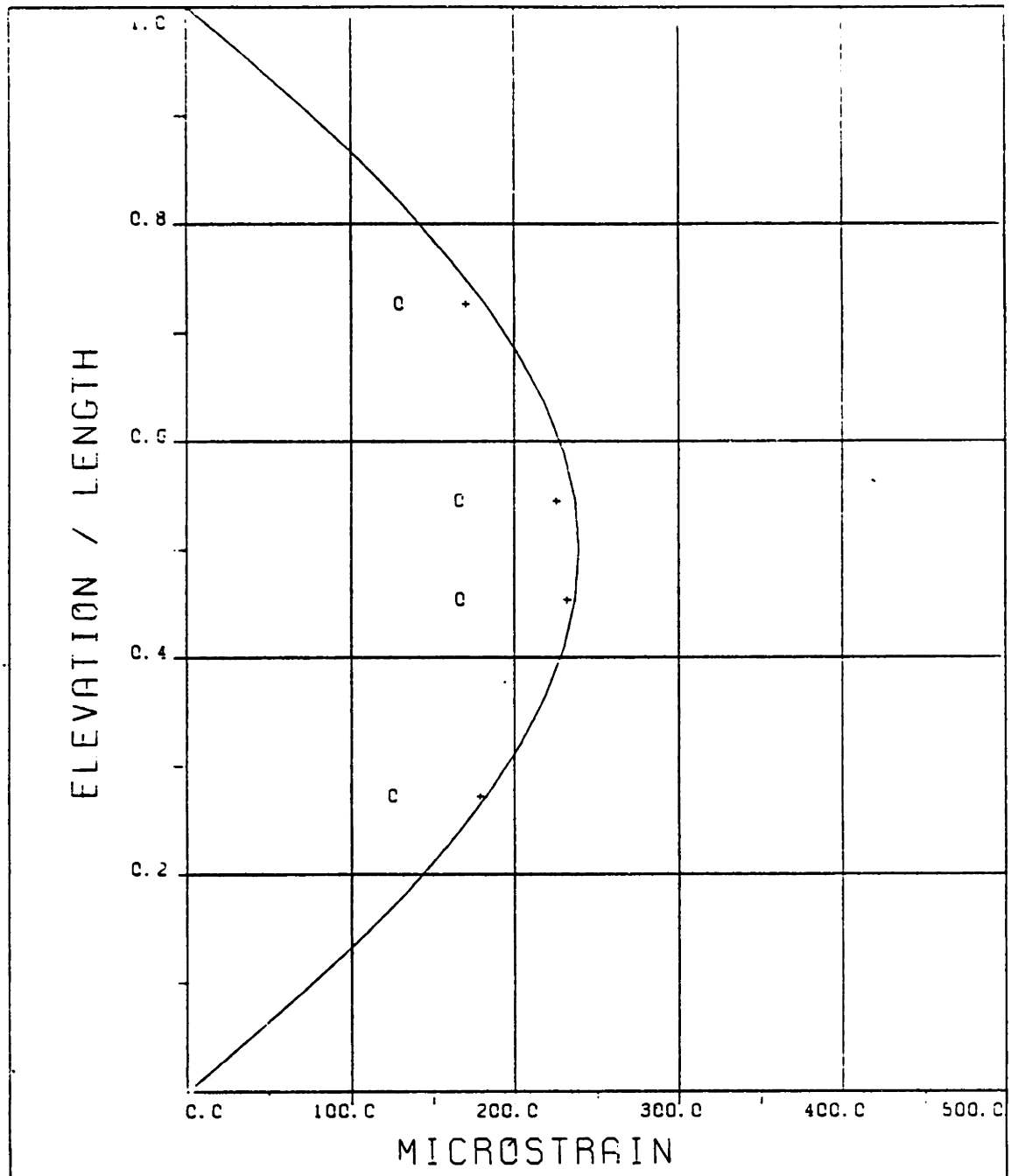

EXPERIMENT NUMBER 81

THETA=90 VC=240 FE=1.950 A/DE=1.92

DYNAMIC RESPONSE AT F=FE IN PLANE B

——— THEORY o o o EXPERIMENT

MAXIMUM DYNAMIC RESPONSE IN PLANE B

——— THEORY + + + EXPERIMENT

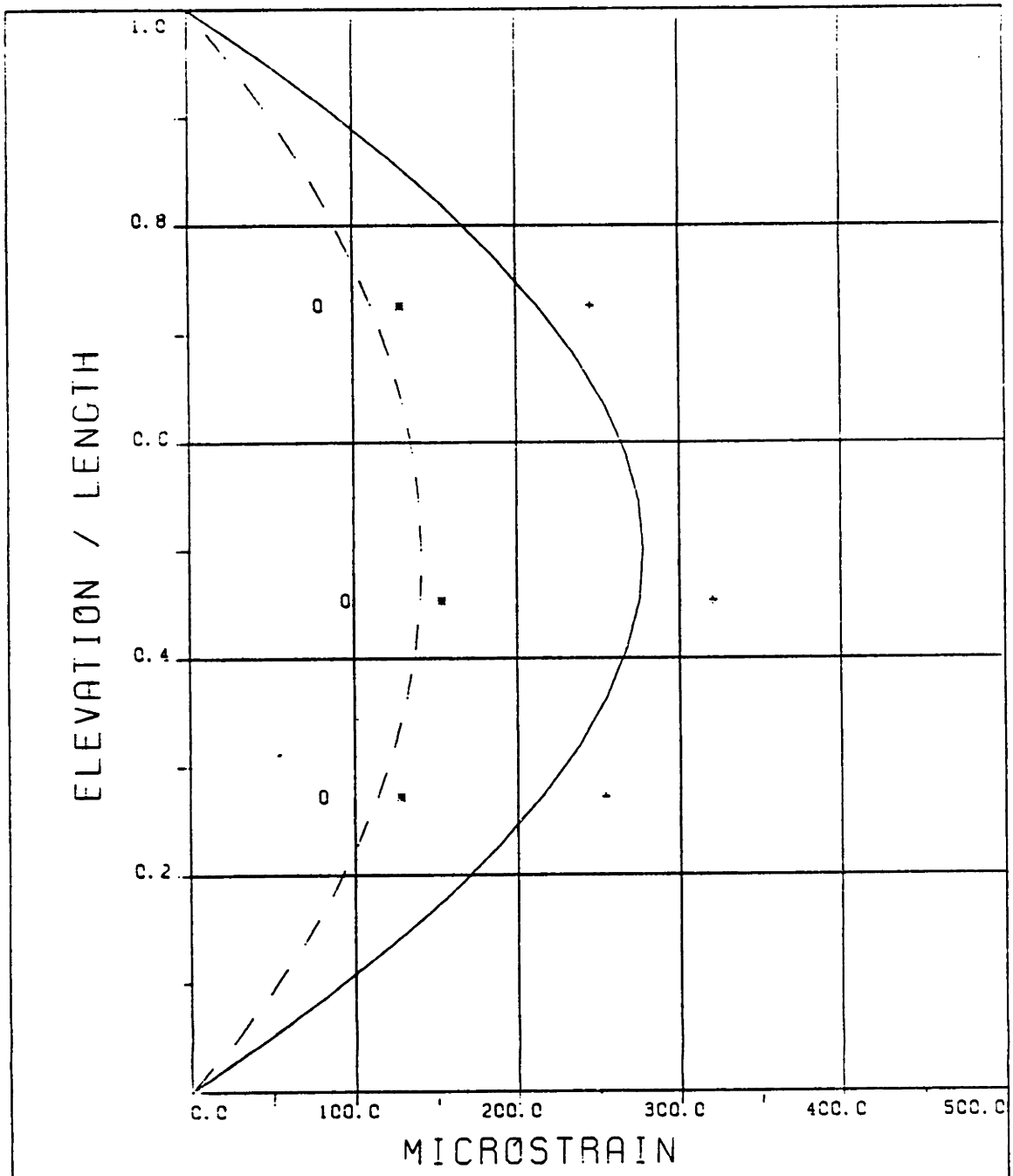

EXPERIMENT NUMBER 81

THETA=90 VC=240 FE=1.950 A/DE=1.92

STATIC RESPONSE IN PLANE A

----- THEORY * * * EXPERIMENT

MAXIMUM DYNAMIC RESPONSE IN PLANE A

c c c EXPERIMENT

MAXIMUM RESPONSE

_____ THEORY + + + EXPERIMENT

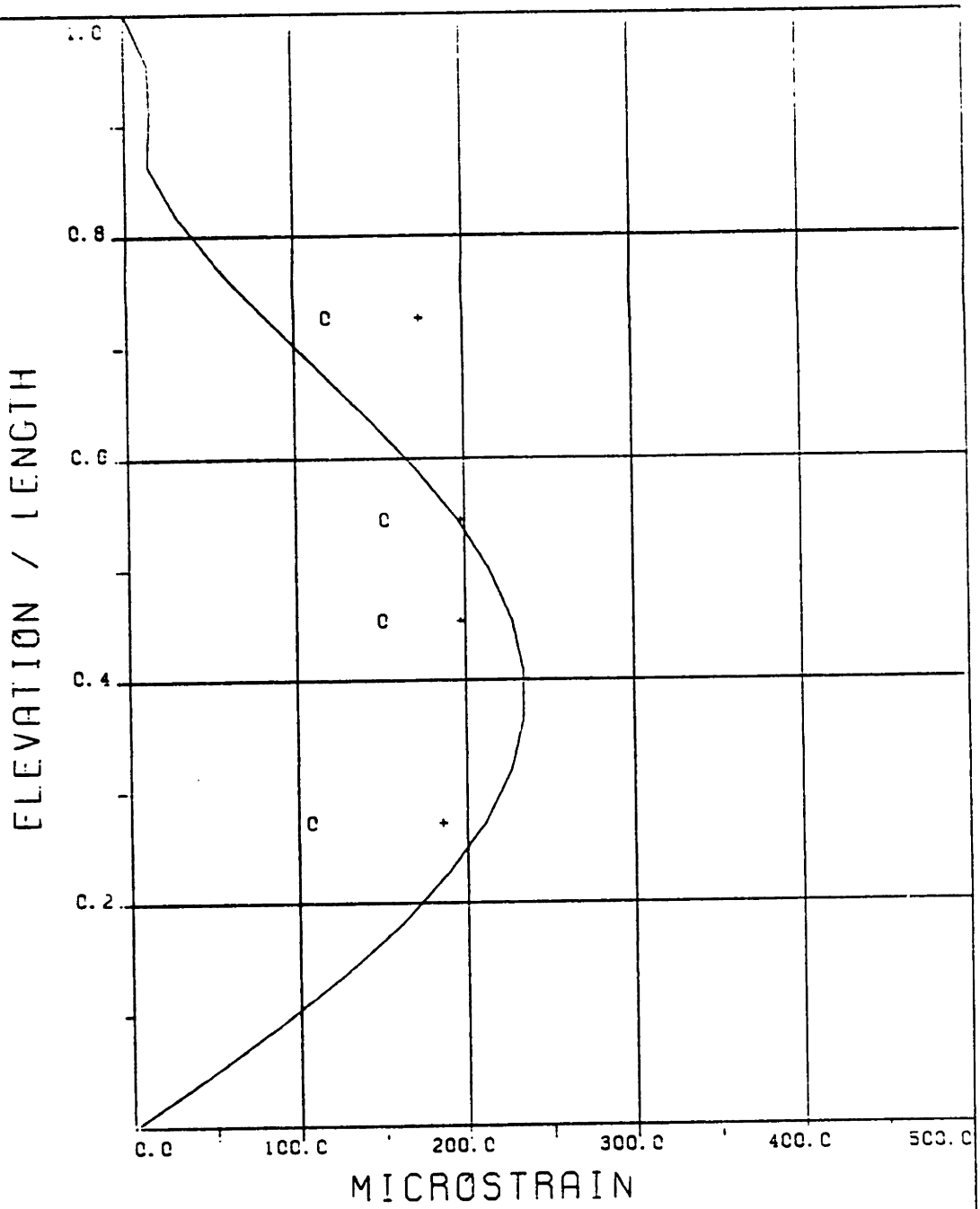

EXPERIMENT NUMBER 88

THETA=90 VC=240 FE=2.925 A/DE=1.94

DYNAMIC RESPONSE AT F=FE IN PLANE B

——— THEORY o o o EXPERIMENT

MAXIMUM DYNAMIC RESPONSE IN PLANE B

——— THEORY + + + EXPERIMENT

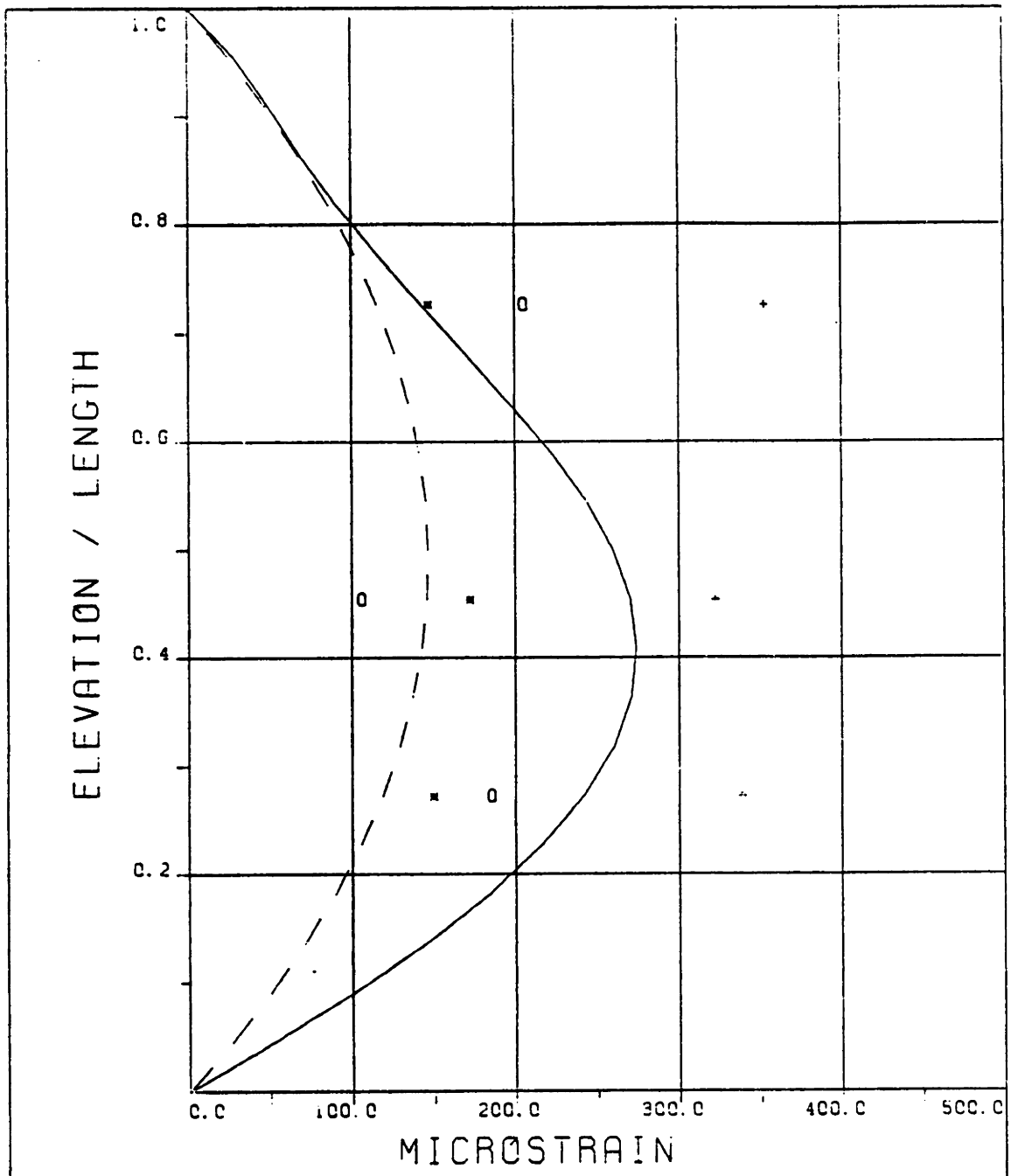

EXPERIMENT NUMBER 88

THETA=90 VC=240 FE=2.925 A/DE=1.94

STATIC RESPONSE IN PLANE A

----- THEORY * * * EXPERIMENT

MAXIMUM DYNAMIC RESPONSE IN PLANE A

c c c EXPERIMENT

MAXIMUM RESPONSE

_____ THEORY + + + EXPERIMENT

Chapter VI

CONCLUSIONS AND RECOMMENDATIONS

The overall objective of this thesis is to evaluate our theoretical ability to predict the global dynamic behavior of long tensioned flexible cylinders using information from available rigid cylinder experimental results. The example we chose to investigate in this work is a single tube marine riser.

The analysis of the second and third Chapter of this thesis leads to the conclusion that a linearized structural model of the riser idealized as a thin rod under tension, although not the most general model derived, provides a good description of the global dynamic behavior of the riser. These simplifications are possible because of the low excited flexural modes, the small transverse motions compared to the length and the presence of the slip joint. The solution of the resulting system of partial differential equations requires the modelling of the local hydrodynamic force. This became the central issue of this thesis.

The approach taken in this work is to employ available rigid cylinder experimental results for formulate an

approximate mathematical model for the local hydrodynamic force acting on the flexible cylinder, as shown in the fourth Chapter of this thesis. Rigid cylinder experiments are subdivided into two broad categories.

The first category involves measurements of the force acting on rigid cylinders in an a priori defined flow. As it is apparent from the definition of such experiments, a model for the local hydrodynamic force on a flexible cylinder derived on the basis of rigid cylinder experiments implies the following two assumptions:

1. Any force component measured in a rigid cylinder experiment which will make a flexible cylinder respond in a different form than the one used to conduct the rigid cylinder experiment must be neglected.

2. Rigid cylinder experiments cannot provide information on the spanwise correlation of local hydrodynamic forces.

The second catetory of rigid cylinder experiments involves cylinders which are mounted on elastic springs and dashpots. These experiments attempt to relate force to response of different form than the imposed motion by representing the flexible cylinder with an idealization

which has only a small number of degrees of freedom, and allowing the idealized system to respond to the force it experiences. The response in existing spring mounted rigid cylinder experiments is a one degree of freedom translation.

Therefore, the first task of this work was to provide a quantitative estimate of the significance of the above idealizations. The approach we selected was to construct a flexible cylindrical model and study its dynamic behavior in idealized excitation conditions for which rigid cylinder experimental data is available. The comparison between our experimental results and our theoretical prediction based on rigid cylinder experiments showed that our theoretical procedure permitted us to predict the important features of the response of our flexible model with confidence, provided us with estimates of the magnitude of the response and of the possible error in our response prediction for the flows examined.

The model employed in our experiments did not correspond to a specific prototype. Its non-dimensional parameters were, however, carefully selected so as to help us evaluate our theoretical capabilities to predict the dynamic behavior of a riser type structure using rigid cylinder results in a stripwise manner under conditions

likely to lead to pronounced violation of the assumptions necessary for our theoretical predictions. The experiments presented in this study correspond to harmonic excitation of the top end of the model at approximately two diameters. Experiments with and without current were conducted. The major observations made in the fifth Chapter of this thesis are summarized below.

1. The basic characteristics of the frequency decomposition of the response of the flexible cylinder can be explained from rigid cylinder experiments. At present, both categories of rigid cylinder experiments, namely rigid cylinders in a priori defined flows and spring mounted rigid cylinders, need to be employed to provide an explanation of the existence of various components of the response.

2. The measured response at the frequency of excitation f_e and parallel to the direction of motion of the top end is approximately within 30% of the corresponding theoretical estimate of the response. Part of this difference might be attributed to the fact that during our estimation we needed to use rigid cylinder data at Reynolds number higher than the one implied by our experiment. The trend of available results shows that if the correct data becomes available the difference reported above will reduce.

3. The prediction of the maxima in the direction of motion of the top end is good when there is no appreciable dynamic response at frequencies other than the frequency of excitation. The flexible riser responds primarily at one frequency when the frequency of imposed oscillation is close to a "natural frequency" of our flexible system and if the current does not introduce appreciable response in another frequency in the same direction as the imposed motion.

4. The prediction of the dynamic response orthogonal to the plane of excitation in the absence of a current and at one frequency based on flexibly mounted rigid cylinder results is encouraging although no definitive statements can be made because of the need to extrapolate existing flexibly mounted rigid cylinder experimental data to predict the response. When there is current, there is no data currently available to us to estimate the magnitude of the dynamic response orthogonal to the direction of motion of the top end. However, we expect we will be able to obtain an estimate of this response from suitably conducted flexibly mounted rigid cylinder experiments.

5. The theoretical estimate of the static response is at most within 40% of the corresponding measurement. No further statements can be made on this subject until the

controversy that exists with published data is resolved with independent experiments. The likelihood is that the difference reported above will reduce when the improved data becomes available.

6. The prediction of the maximum independent of plane does not contain any phase information between the responses in the planes parallel and orthogonal to the direction of motion of the top end. Our prediction of the maxima independent of plane provides an estimate of the upper bound of the maximum response likely to be encountered.

The above completes the discussion for the specific problem addressed in this thesis. Now we wish to address the more general problem of extending our research to provide information useful to the design of actual and proposed long flexible and tensioned cylindrical systems, such as risers. Such an extension we feel is possible because the system under investigation is highly damped and because the structural part of our problem is linear. These two conditions are likely to make our system's response shape similar to the shape of excitation. This similarity between the imposed excitation and the system response permit us to envision a finite set of rigid cylinder experiments describing more complicated excitations suitable for design.

The development of this approach requires the following additional work:

1) Perform an experiment using a flexible cylindrical model where the imposed excitation is some spectrum suitably selected to represent some environmental condition of interest to test the hypothesis of similarily between excitation and response shape.

2) Perform rigid cylinder experiments where the imposed excitation is described by the same spectrum used above. Repeat this experiment by keeping the area under the spectrum the same but altering the position of the peak of the spectrum. This will serve to quantify the effect of distortion in our results. Conduct experiments keeping the shape of the spectrum the same but proportionately vary its ordinates to cover the range of interest in system responses.

3) Use the experimental results obtained from the flexible model to evaluate theoretical predictions obtained using the rigid cylinder experiments described above.

It should be noted that the flexible model described in this thesis is representative of shallow water risers. The 10 m model described in Chryssostomidis and Patrikalakis (1982b) is typical of a deeper water riser. These two models allow us to test if our proposed method is extendable to deep water risers where the response is likely to be a superposition of more than one mode.

It might be of interest to note that if we decide that flexible cylinder experiments at higher Reynolds numbers are needed we feel that this can be accomplished by foregoing the outer geometric similarity between model and prototype. The disproportionate scaling of the diameter with respect to the length is not expected to substantially affect the results for low excited flexural modes, but it allows to increase Reynolds number. It is, however, recommended to verify the maximum allowable distortion experimentally.

Parallel research for a development of an efficient method of direct evaluation of the hydrodynamic force on circular cylinders primarily employing analytic and numerical techniques with possible assistance from experimental observations is also recommended. The development of such a method will permit us to expand our design capabilities without the limitations of our present

theoretical procedures for the prediction of the response of flexible cylinders. Work addressing this very subject is currently under way, see Faltinsen and Pettersen (1982) and (1983)*.

---

* Faltinsen, O. M. and Pettersen, B., 1982, "Vortex Shedding Around Two-Dimensional Bodies at High Reynolds Numbers," Proceedings of the 14th Symposium on Naval Hydrodynamics, The University of Michigan, Ann Arbor, August 1982.

Faltinsen, O. M., and Pettersen, B., 1983, "Separated Flow Around Marine Structures," SSPA Ocean Engineering Symposium, Gothenburg, March 1983 (To be presented).

REFERENCES

Achenbach, E., 1968, "Distribution of Local Pressure and Skin Friction Around a Circular Cyinder in Cross-Flow up to Rn $5x10^6$," Journal of Fluid Mechanics, Vol. 34, Part 4, pp. 625-639.

Achenbach, E., 1971, "Influence of Surface Roughness on the Cross-Flow around a Circular Cylinder," Journal of Fluid Mechanics, Vol. 46, Part 2, pp. 321-335.

Bender, C. M. and Orszag, S. A., 1978, Advanced Mathematical Methods for Scientists and Engineers, Mc-Graw Hill Co.

Berger, E. and Wille, R., 1972, "Periodic Flow Phenomena," Annual Review of Fluid Mechanics, Vol. 4, pp. 313-340. Palo Alto, CA: Annual Reviews, Inc.

Bernitsas, M. M., 1979a, "Analysis of The Hydrodynamic Forces Exerted on a Harmonically Oscillating Circular Cylinder in any Direction with Respect to A Uniform Current," Proceedings of the Second International Conference on the Behaviour of Off-Shore Structures, London, August 1979.

Bernitsas, M. M., 1979b, Contributions Towards the Solution of Marine Riser Design Problem, Ph.D. Thesis, Massachusetts Institute of Technology, Department of Ocean Engineering.

Bernitsas, M. M., 1980, "Riser Top Tension and Riser Buckling Loads," American Society of Mechanical Engineers, Winter Annual Meeting.

Bernitsas, M. M., 1982, "A Three-Dimensional Non-Linear Large-Deflection Model for Dynamic Behavior of Risers, Pipelines, and Cables," Journal of Ship Research, Vol 26, Number 1.

Bishop, R. E. D., and Hassan, A. Y., 1964a, "The Lift and Drag Forces on a Circular Cylinder in a Flowing Fluid," Proceedings of the Royal Society, Series A, Vol. 277, pp.32-50.

Bishop, R. E. D., and Hassan, A. Y., 1964b, "The Lift and Drag Forces on a Circular Cylinder Oscillating in a Flowing Fluid," Proceedings of the Royal Society, Series A, Vol. 277, pp. 51-75.

Boyce, T. M., 1975, "Internal Waves in the Straits of Gibraltar," Deep-Sea Research, Vol. 22, pp. 597-610.

Carrier, G. F., 1943, "On the Nonlinear Problem of the Elastic String," Quarterly of Applied Mathematics.

Carrier, G. F. and Pearson, C. E., 1968, Ordinary Differential Equations, Ginn (Blaisdell), Boston, Massachusetts.

Chen, Y. N., 1973, "60-Jahre Forschung über die Kármánschen Wirbelstrassen - Ein Rückblick," Schweizerische Bauzeitung, Vol. 91, Heft 44, Nov. 1, pp. 1079-1096.

Chryssostomidis, C., and Oakes, M. C., 1974, "Selection of Wave Spectra for Use in Ship Design," International Symposium on Ocean Wave Measurements and Analysis, New Orleans, Sept. 8-11, 1974.

Chryssostomidis, C., and Patrikalakis, N. M., 1982a, "An Experimental Procedure for the Prediction of the Dynamic Behavior of Riser Type Systems," Proceedings of the 3rd International Conference on the Behaviour of Off-Shore Structures, August 1982, Vol. 1, pp. 565-598, Hemisphere Publishing Co., New York.

Chryssostomidis, C., and Patrikalakis, N. M., 1982b, Experimental and Theoretical Prediction of the Response of a Marine Riser System Supported by a Tension Leg Platform Subjected to Surface Wave Excitation, Massachusetts Institute of Technology, Department of Ocean Engineering, Design Laboratory Report No. 82-1, September 1982.

Crandall, S. H., Karnopp, D. C., Kurtz, E. F., Pridmore-Brown, D.C., 1968, Dynamics of Mechanical and Electromechanical Systems, Mc-Graw Hill.

Dale, J. R., Menzel, H., and McCandless, J., 1966, Dynamic Characteristics of Underwater Cables: Flow-Induced Transverse Vibrations, U.S. Naval Air Development Center, Report NADC-AE-6620; AD640-593.

Dean, R. B., Milligan, R. W., and Wootton, L. R., 1977, An Experimental Study of Flow Induced Vibration, Atkins Research and Development, Epsom, Surrey, England, Report December 1977/1.

Dean, R. B., and Wootton, L. R., 1977, The Analysis of Vortex Shedding Problems in Offshore Engineering, Atkins Research and Development, Epsom, Surrey, England, Report September 1977/14.

Eisenhart, L. P., 1947, An Introduction to Differential Geometry, Princeton University Press.

Graham, C., 1966, A Survey of Correlation Length Measurements of the Vortex Shedding Process Behind a Circular Cylinder, MIT Department of Mechanical Engineering, Technical Report No. 76028-1, October 30, 1966.

Griffin, O. M., Skop, R. A., and Ramberg, S. E., 1975, "The Resonant, Vortex Excited Vibrations of Structures and Cable Systems," Offshore Technology Conference, Paper No. 2319, Dallas, Texas.

Griffin, O. M., 1981, "OTEC Cold Water Pipe Design for Problems Caused by Vortex-Excited Oscillations," Ocean Engineering, Vol. 8, No. 2, pp. 129-209, Pergamon Press.

Hogben, N. and Lumb, F. E., 1967, Ocean Wave Statistics, Her Majesty's Stationary Office, London, England.

Hogben, N., 1974, Ocean Wave Statistics - 'Five Minutes Slow' After Six Years, Technical Report, NPL SHIP 80, NMI.

Jones, G. W., Cincotta, J. J., Walker, R. W., 1969, Aerodynamic Forces on a Stationary and Oscillating Circular Cylinder at High Reynolds Numbers, NASA TR R-300.

Kármán, T. von, 1911, "Über die Formänderung Dünnwanndiger Rohre, Innsbesondere Federnder Ausgleichrohre," Zeitschrift des Vereines Deutscher Ingenieure, Vol. 55, pp. 1889-1895.

Keulegan, G. H., and Carpenter, L. H., 1958, "Forces on Cylinders and Plates in an Oscillating Fluid," Journal of Research of the U.S. National Bureau of Standards, Vol. 60, No. 5, May, pp. 423-440; U.S. National Bureau of Standards Research Paper RP-2857.

King, R., 1977a, "An Investigation of the Criteria Controlling Sustained Self-Excited Oscillations of Cylinders in Flowing Water," Proceedings, 4th Biennial Symposium on Turbulence in Liquids, University of Missouri - Rolla, Department of Chemical Engineering, 1975, pp. 179-191, Princeton, NJ: Science Press.

King, R., 1977b, "A Review of Vortex Shedding Research and Its Application," Ocean Engineering, Vol. 4, pp. 141-171. London: Pergamon Press.

Landau, L. D., and Lifshitz, E. M., 1959, Theory of Elasticity, Pergamon Press.

Lee, T. N., Brooks, I., Düing, W., 1977, The Florida Current; Its Structure and Variability, Technical Report 77003, July 1977, University of Miami, Rosenstiel School of Marine and Atmospheric Sciences, Miami, Florida.

Love, A. E. H., 1944, A Treatise on the Mathematical Theory of Elasticity, Dover, Fourth Edition.

McConnell, K. G., and Park, Y. S., 1982, "The Response and the Lift-Force Analysis of an Elastically-Mounted Cylinder Oscillating in Still Water," Proceedings of the Third International Conference on the Behaviour of Off-Shore Structures, August 1982, Vol. 2, pp. 671-680. New York: Hemisphere Publishing Co.

McGlothlin, J. C., 1982, Drag Coefficients of Long Flexible Cylinders Subject to Vortex Induced Oscillations, MS Thesis, Massachusetts Institute of Technology, Department of Ocean Engineering.

Mercier, J. A., 1973, Large Amplitude Oscillation of a Circular Cylinder in a Low Speed Stream, Ph.D. Thesis, Stevens Institute of Technology, Department of Mechanical Engineering. Ann Arbor, MI: University Microfilms Order No. UM74-884.

Moeller, M. J. and Leehey, P., 1982, "Measurement of Fluctuating Forces on an Oscillating Cylinder in a Cross Flow," Proceedings of the Third International Conference on the Behaviour of Off-Shore Structures, August 1982, Vol. 2, pp. 681-689. New York: Hemisphere Publishing Co.

Morison, J. R., O'Brien, M. P., Johnson, J. W., and Shaaf, S. A., 1950, "The Forces Exerted by Surface Waves on Piles," Petroleum Transactions, A.I.M.E., Vol. 189, pp. 149-154.

Osborne, A. R., Brown, J. R., Burch, T. L., and Scarlet, R. I., 1977, "The Influence of Internal Waves on Deepwater Drilling Operations," Proceedings of the Ninth Annual Offshore Technology Conference, Paper 2797, Vol. I, pp. 537-544, May 1977.

Park, Y. S., 1981, The Response and the Lift Force Analysis of a Cylinder Oscillating in Still Water, Ph.D. Thesis, Iowa State University, Department of Engineering Science and Mechanics.

Patel, M. H. and Sarohia, S., 1982, "On The Dynamics of Production Risers," Proceedings of the 3rd International Conference on the Behaviour of Off-Shore Structures, August 1982, Vol. 1, pp. 599-617. New York: Hemisphere Publishing Co.

Patrikalakis, N. M., 1980, A Review of Existing Experimental Results for the Forces Exerted on Circular Cylinders in Separated Flows, Massachusetts Institute of Technology, Department of Ocean Engineering, Design Laboratory Report No. 80-2.

Phillips, O. M., 1980, The Dynamics of the Upper Ocean, Second Edition, Cambridge University Press.

Richardson, W. S., Schmitz, W. J., Jr., Niiler, P. P, 1969, "The Velocity Structure of the Florida Current From the Straits of Florida to Cape Fear," Deep-Sea Research, Supplement to Vol. 16, pp. 225-231, Pergamon Press, England.

Roshko, A., 1953, On The Development of Turbulent Wakes from Vortex Streets, N.A.C.A. Technical Note 2913, March 1953.

Roshko, A., 1954, On the Drag and Shedding Frequency of Two-Dimensional Bluff Bodies, N.A.C.A. Technical Note 3169, July 1954.

Roshko, A., 1961, "Experiments on the Flow Past a Circular Cylinder at Very High Reynolds Number," Journal of Fluid Mechanics, Vol. 10, pp. 345-356.

Sarpkaya, T., 1975, "Forces on Cylinders and Spheres in a Sinusoidally Oscillating Fluid," Journal of Applied Mechanics, Transactions of ASME, pp. 32-37, March 1975.

Sarpkaya, T., 1977a, Transverse Oscillations of a Circular Cylinder in Uniform Flow, Naval Postgraduate School, Report No. NPS-69SL77071, Monterey, CA, July 1977.

Sarpkaya, T., 1977b, "In-Line and Transverse Forces on Cylinders in Oscillatory Flow at High Reynolds Numbers," Journal of Ship Research, Vol. 21, No. 4, pp. 200-216.

Sarpkaya, T., 1979, "Vortex Induced Oscillations," Journal of Applied Mechanics, Vol. 46, pp. 241-258, June 1979.

Sarpkaya, T., 1980, "Hydroelastic Response of Cylinders in Harmonic Flow," Naval Architect, No. 3, pp. 103-110.

Sarpkaya, T., Rajabi, F., and Zedan, M. F., 1981, "Hydroelastic Response of Cylinders in Harmonic and Wave Flow," Proceedings, 13th Offshore Technology Conference, Houston, Texas, Vol. I, Paper 3992.

Sawaragi, T., Nakamura, T., and Miki, H., 1977, "Dynamic Behavior of a Circular Pile due to Eddy Shedding in Waves," Coastal Engineering in Japan, Vol. 20, pp. 109-120.

Scruton, C., 1965, "On the Wind Excited Oscillations of Stacks, Towers, and Masts," Proceedings, 1st International Conference on Wind Effects on Buildings and Structures, National Physical Laboratory, Teddington, England, 1963, Vol. II, Paper 16, pp. 797-836, London: Her Majesty's Stationary Office.

Stcker, J. J. and Lubkin, S., 1943, "Stability of Columns and Strings Under Periodically Varying Loads," Quarterly of Applied Mathematics.

Triantafyllou, M. S., 1979, The Dynamic Positioning System of A Drilling Vessel, Sc.D. Thesis, Massachusetts Institute of Technology, Department of Ocean Engineering.

Triantafyllou, M. S., 1982, "The Preliminary Design of Mooring Systems," Journal of Ship Research, March 1982, Vol. 26, No. 1, pp. 25-35.

Verley, R. L. P. and Every, M. J., 1977, "Wave-Induced Vibrations of Flexible Cylinders," Proceedings, 9th Offshore Technology Conference, Houston, Texas, Vol. 3, Paper 2899.

Verley, R. L. P. and Moe, G., 1979, The Forces on a Cylinder Oscillating in a Current, Norwegian Institute of Technology, River and Harbour Laboratory, SINTEF Report Number STF60A79061.

Verley, R. L. P. and Johns, D. J., 1982, "Oscillations of Cylinders in Waves and Current," Proceedings of the Third International Conference on the Behavior of Offshore Structures, August 1982, Vol. 2, pp. 690-701, New York: Hemisphere Publishing Co.

Vickery, B. J., and Watkins, R. D., 1964, "Flow Induced Vibrations of Cylindrical Structures," Proceedings, 1st Australasian Conference on Hydraulics and Fluid Mechanics, University of Western Australia, pp. 213-241, London: Pergamon.

Wootton, L. R., 1968, "The Oscillations of Model Circular Stacks Due to Vortex Shedding at Reynolds Numbers in the Range 10^5 to 3×10^6," Proceedings, Symposium on Wind Effects on Buildings and Structures, Loughborough University of Technology, Department of Transport Technology, Vol. II, Paper 18.

Zedan, M. F. and Rajabi, F., 1981, "Lift Forces on Cylinders Undergoing Hydroelastic Oscillations in Waves and Two-Dimensional Harmonic Flow," Proceedings, Hydrodynamics in Ocean Engineering, August 1981, The Norwegian Institute of Technology, Trondheim, Norway.

Appendix A

BRIEF DESCRIPTION OF THE PHYSICAL SYSTEM

A typical offshore drilling system is shown in Figure 1 borrowed from Bernitsas (1979), where an extensive description of the physical system is given. As shown in the above Figure, the marine exploration riser is part of that system, which also includes the following additional elements:

a) The drill ship
b) The tensioning system
c) The upper slip joint
d) The upper ball joint
e) The tube connectors
f) The kill and choke lines
g) The lower ball joint
h) The marine connector
i) The blowout preventer
j) The well head
k) The buoyancy modules
l) The circulating mud
m) The drill string

For reasons of completeness, a brief description of the above items and their functions is presented below:

The marine riser itself consists of cylindrical steel tubes of average length of the order of 15 m, an outer diameter varying between 0.25 m and 0.65 m and a tube thickness between 1 and 2.5 cm.

The drill ship holds the top end of the riser and houses the tensioning system. It is controlled automatically so that excessive offsets from the vertical through the well head are avoided.

The upper slip joint practically eliminates the transmission of the vertical motion of the drill ship to the top end of the riser. This joint is designed to eliminate any static or dynamic tension variation at the top end of the riser due to its own motion and the vertical motion of the ship.

The upper ball joint eliminates excessive bending moments at the top end of the riser, at least within a range of top end slopes.

The marine riser connectors join the tubes together and are able to withstand large tensions.

The kill and choke lines are high pressure pipes controlling sudden variations of the well pressure. They are mounted directly on the riser connectors on the outside of the riser.

The lower ball joint has a similar function as the upper ball joint.

The marine connector connects the riser and the blow out preventer, which is attached rigidly to the well

head.

The buoyancy modules are distributed along the riser and decrease the required top end tension. This is done at the expense of larger hydrodynamic forces. The modules are usually made of synthetic materials and their outer diameter usually varies between 0.6 m and 0.8 m. The kill and choke lines are usually embedded in these modules.

The drilling mud is forced down the drill string and it returns to the surface through the space between the drill string and the marine riser. Due to its motion inside a deflected riser it exerts forces on the latter which can be shown to be very small compared to the static and/or dynamic forces acting on the riser. This happens because the mud speed is small.

The riser itself provides protection of the drill string from environmental excitations.

Appendix B

THE SELECTION OF THE HYDRODYNAMIC COEFFICIENTS

As we saw in Chapter IV, the proposed method of calculation of the local hydrodynamic force on a flexible cylinder is based on rigid cylinder results. Assumption 1 of Chapter IV implies that rigid cylinder results can provide information about the dynamic response parallel to the motion of the top end at the frequency of excitation alone. This means that the component of the dynamic response parallel to the motion of the top end that we can calculate on the basis of rigid cylinder results will be a standing wave of the form:

$$\sigma(Z,t) = R(Z) \cos(\omega t + \phi(Z)) \quad . \qquad (B.1)$$

where $R \geq 0$, $\sigma(0,t) = 0$ and $\sigma(L,t) = R(L)\cos(\omega t)$, where $R(L)$ and ω are given.

The integration of partial differential equations (III.87) and (III.88) in time with monochromatic excitation at Z=L leads to a steady state response which is almost exclusively determined from the fundamental harmonic alone. This observation is associated with the use of drag forces proportional to the square of local calculated relative velocity of the water with respect to the cylinder in the direction of dynamic motion of the

cylinder and having the sign of the above relative velocity. Typical calculations have shown that the response at 3ω is less than approximately 2% of the response at ω. This is due to the highly damped behavior of our system.

The theoretical predictions of Chapter V are based on the time integration of the above partial differential equations until steady state is reached. Furthermore, the integration was performed by selecting appropriate constant hydrodynamic coefficients along the length, $\hat{c}_d$, $\hat{c}_m$, for each iteration. Successive iterations were performed by adjusting the magnitude of $\hat{c}_d$, $\hat{c}_m$, on the basis of the variable local coefficients found from the calculated local motion and rigid cylinder results. The procedure for the selection of $\hat{c}_d$ for the nth iteration is based on the amplitudes R(Z) from the previous iteration and the drag coefficients obtained from rigid cylinder experiments on the basis of the local calculated amplitude R(Z) at iteration (n-1). The selection procedure is based on equating the overall energy dissipated in one cycle using the variable drag coefficients and the overall energy dissipated using $\hat{c}_d$. For the case of harmonic oscillations of the top end in the absence of current or for harmonic oscillations of the top end orthogonal to a current the drag force parallel to the imposed oscillation can be written as:

$$F_d(Z,t) = -0.5\rho D\, c_d[R(Z)/D,\ Re(Z),\ U^*(Z)]\sigma_t|\sigma_t|$$

where $\sigma(Z,t)$ is the dynamic motion parallel to the oscillation of the top end, $U^*(Z) = 2\pi|V_c(Z)|/\omega D$, and $Re(Z) = R(Z)\omega D/\nu$, when there is no current, or $Re(Z) = |V_c(Z)|D/\nu$, when there is current. The drag force is approximated by:

$$\hat{F}_d(Z,t) = -0.5\rho D\hat{c}_d\sigma_t|\sigma_t|$$

where $\hat{c}_d$ is determined from:

$$\int_0^L dZ \int_0^{2\pi/\omega} dt\ \hat{F}_d\sigma_t = \int_0^L dZ \int_0^{2\pi/\omega} dt\ F_d\sigma_t$$

This leads to:

$$\hat{c}_d = \int_0^L c_d(Z)R^3(Z)dZ \Big/ \int_0^L R^3(Z)dZ$$

For the case of harmonic excitation of the top end parallel to a current with the drag force written as:

$$F_d(Z,t) = 0.5\rho D\ c_d(R(Z)/D, Re(Z), U^*(Z))\ |V_c(Z)-\sigma_t|\ (V_c(Z)-\sigma_t)$$

where $Re(Z) = |V_c(Z)|\ D/\nu$, and using the same argument as before the expression for $\hat{c}_d$ is:

$$\hat{c}_d = \int_0^L c_d(Z)\psi(r(Z))R^3(Z)dZ \Big/ \int_0^L \psi(r(Z))R^3(Z)dZ$$

where $r(Z) = V_c(Z)/R(Z)\omega$ and

$$\psi(r) = \begin{cases} \pi r & r \geq 1 \\ 2[r\sin^{-1}r + \frac{1}{3}(2+r^2)(1-r^2)^{1/2}] & 1 \geq r \geq 0 \end{cases}$$

Note that phase $\phi(Z)$ defined in equation (B.1) does not affect any of the results derived above.

The added mass force is written as:

$$M_a(Z,t) = -\rho A_o c_m(R(Z)/D,\ U^*(Z),\ Re(Z))\sigma_{tt}$$

and is approximated by:

$$\hat{M}_a(Z,t) = -\rho A_o \hat{c}_m \sigma_{tt}$$

so that:

$$E = \int_0^L dZ \int_0^{2\pi/\omega} dt\ [M_a - \hat{M}_a]^2$$

is minimum. This leads to:

$$\hat{c}_m = \int_0^L c_m(Z)R^2(Z)dZ \Big/ \int_0^L R^2(Z)dZ$$

The convergence of the above procedure is very rapid. For a reasonable initial guess, performed by inspection of the appropriate rigid cylinder results, two iterations are usually adequate.

The above procedure after convergence is expected to provide good initial estimates of the response if

variable coefficients are to be used. We feel that such a procedure will not yield appreciably different estimates of the response than the procedure used here. For oscillations orthogonal to a current and for the range of U* for which rapid variation of c_d, c_m is found, somewhat larger differences might arise. This cannot be estimated until the controversy of existing rigid cylinder data for this case is resolved with independent experiments and larger amplitudes of oscillation orthogonal to current are investigated.